Cenozoic basin evolution and petroleum system characterization within the Tangier 3D Seismic Survey, central Scotian Slope, Canada

by

John Mishael Garcia Dooma

A Thesis Submitted to

Saint Mary's University, Halifax, Nova Scotia

In Partial Fulfillment of the Requirements for

The Degree of Master of Science in Applied Science

September 2023, Halifax, Nova Scotia

Approved: Dr. G. Todd Ventura
Supervisor

Approved: Dr. R. Andrew MacRae
Committee Member

Approved: Dr. Shawna White
Committee Member

Approved: Mr. Adam MacDonald
Committee Member

Approved: Dr. Mark Deptuck
External Reviewer

Date: September 6th, 2023

Abstract

Cenozoic basin evolution and petroleum system characterization within the Tangier 3D Seismic Survey, central Scotian Slope, Canada

By John Mishael G. Dooma

Undiscovered hydrocarbon reservoirs potentially exist in the deep-water regions of the Scotian Margin off the coast of Nova Scotia. The deep-water environments can involve major challenges with high exploration risk because the presence, quality, size, and distribution of source and reservoir rocks are still relatively unknown for many areas. Using the Tangier 3D Seismic Survey, seismic interpretation and attribute analysis within the Cenozoic was conducted. The results show the region hosts a complex subsurface geology with modern-day and paleo-channels and canyons, contourite sediment drifts, slope failure complexes, and proglacial slope drapes. Salt-related structural features, which occur deeper than 3 km in the basin, include welds, wings, feeders, pedestals, rollers, withdrawal minibasins, rafted overburden, and growth and crestal faults. Also observed within the Tangier 3D area are three shallow-level amplitude anomalies interpreted to be direct hydrocarbon indicators (DHIs). The DHIs situated above diapirs and a salt canopy strongly indicate the presence of migrating fluids. The architectural investigation of these DHIs provides evidence of a working petroleum system governed by salt mobility, which provides migration pathways for the more deeply sourced fluids. However, further study is needed to determine if the fluids filling these DHIs are thermogenic hydrocarbons that escaped from deeper Jurassic or Cretaceous sources and breached reservoirs.

September 6th, 2023

Acknowledgments

I would like to express my gratitude to Dr. G. Todd Ventura for the opportunity that he gave to work on this graduate research project. His ability to encourage excellence, endless support and his inputs to this project have been highly valuable through the completion of this thesis. I would like to extend my gratitude to my supervisors in the Nova Scotia Department of Natural Resources and Renewables (NSDNRR), Mrs. Natasha MacAdam and Mr. Adam MacDonald, for welcoming me in the department and for providing me a workstation. Their inputs and insights to this project are highly valuable and greatly appreciated. I would like to thank Dr. R. Andrew MacRae for his valuable inputs about the interpretation of my results based on his in-depth knowledge on seismic stratigraphy and salt tectonics, which was integral for my thesis. I would also like to extend thanks to Dr. Shawna White for her time on my committee, for providing valuable feedback and suggestions. Lastly, I would like to express my gratitude to Dr. Mark Deptuck of Canada-Nova Scotia Offshore Petroleum Board (CNSOPB) for providing valuable and critical feedback. Thank you all for taking your time for helping me shape this project as best as possible.

This project is the result under the Genome Application Partnership Program (GAPP) and would not have been possible without the funding provided by Mitacs, NSERC through Canada Graduate Scholarships, and Saint Mary's University. I would like to thank BP Exploration Canada Ltd., TGS, and Schlumberger for providing necessary seismic dataset and software licenses for data collection, analysis, and interpretation.

Finally, I would like to extend thanks to my comrades at Organic Geochemistry Lab (esp. Elish and Nikita) and my fellow graduate students in the Geology Department. Most importantly, I would like to express my immense gratitude to my family – especially my parents, my dad Jeffrey

and my mom Sally, for supporting and helping me throughout this journey. A deep thank you goes out to my brothers, Jeriel and Joshua, to whom I am always annoyed with – daily. You, guys, have served as an inspiration to me. I dedicate this work to all of you. None of this would have been worthwhile without you and I thank you from the bottom of my heart.

Table of Contents

List of Figures

Chapter 1

Chapter 2

Chapter 3

Chapter 5

Appendix

List of Abbreviations

2D – Two-dimensional

3D – Three-dimensional

AA – Amplitude Anomaly

AVO – amplitude-versus-offset

AI – Acoustic Impedance

AUV – Autonomous Underwater Vehicle

Bbbl – Billion Barrels

BP – British Petroleum

BSS – Basal Shear Surface

BSW – Banquereau Synkinematic Wedge

CDP – Common Depth Points

CCGS – Canadian Coast Guard Ships

CMP – Common Mid Points

CNSOPB – Canada-Nova Scotia Offshore Petroleum Board

DHI – Direct Hydrocarbon Indicator

EL – Exploration License

GAPP – Genomic Application Partnership Program

GR – Gamma Ray

IL – In-lines

ka – kilo-annum

KPSDM – Kirchoff Pre-Stack Depth Migration

Ma – Mega-annum

MFS – Maximum Flooding Surface

MTD – Mass Transport Deposit

NAZ – Narrow Azimuth

NSDNRR – Nova Scotia Department of Natural Resources and Renewables

NSERC – Natural Sciences and Engineering Research Council

OERA – Offshore Energy Research Association

OETR – Offshore Energy Technical Research

PFA – Play Fairway Atlas

RC – Reflection Coefficient

RMS amplitude – root-mean square amplitude

ROV – Remotely Operated Vehicle

RTM – Reverse Time Migration

SP – Sub-Province

Tcf – trillion cubic feet

TD – Total Depth

TTI – Tilted Transverse Isotropic

TVT – True Vertical Thickness

TWT – Two-Way Time

WATS – Wide Azimuth Towed Survey

WAZ – Wide Azimuth

XL – Cross-lines

Chapter 1. Introduction

1.1. Research motivation

The 2011 Play Fairway Analysis (OETR, 2011) predicts an estimated 120 trillion cubic feet (Tcf) of natural gas and 8 billion barrels (Bbbl) of oil remains undiscovered along the Scotian Margin. Much of this is anticipated to derive from deep-water environments. However, exploration in these areas is challenging and the geological risks associated with the presence, quality, size, and distribution of source and reservoir rocks is high. To help constrain these issues, new data are needed to de-risk offshore exploration to achieve the next generation of potential discoveries.

Hydrocarbon seep sites have been investigated since 2015 by the Piston Coring Geochemistry Program (Fowler et al., 2016; 2017; 2017; 2019) conducted by the Offshore Energy Research Association (OERA), Nova Scotia Department of Natural Resources and Renewables, and Geological Survey of Canada. This seep characterization program involved different sampling cruises conducted using Canadian Coast Guard Ships (CCGS) spanning from 2015, 2016, 2018 (CCGS Hudson), 2017 (CCGS Coriolis II), 2020 (Pacific Constructor – no sampling; only AUV Multibeam), and 2021 (Atlantic Condor). Some of these cruises (2018, 2020, 2021) also involved the surveying of seep sites using an Autonomous Underwater Vehicle (AUV) and a Remotely Operated Vehicle (ROV) to help position piston core samples.

The Genomic Application Partnership Program (GAPP) is a collaboration between several academic and governmental institutions across Canada. The program's goal is to confirm the presence of an active working petroleum system in deeper waters that involves integrated application of microbiological, geochemical, and geoscience investigative techniques. This thesis will mainly focus on a portion of the geophysical aspect of the GAPP program.

1.2. Hypothesis and theory of methodology

The working hypothesis of this thesis is that most fluid-related shallow amplitude anomalies (or direct hydrocarbon indicators; DHIs) are expected to occur above salt diapirs because the structural deformation caused by vertical salt movement produces conduits (e.g., faults or breaches in otherwise impermeable strata) that can facilitate hydrocarbon migration from underlying source or reservoir rocks to the more permeable, shallow strata. The domal structure of many salt diapirs also establishes localized relief thereby controlling the hydrocarbon drainage system by funnelling fluid flow from the surrounding area.

This thesis aims to achieve two overarching outcomes through the integration of geophysical techniques such as horizon mapping, seismic attribute extractions, and the generation of isochore maps. The first is to describe the subsurface central Scotian Slope geology of BP's Tangier 3D Seismic Survey (e.g., Fig. 2.1) by characterizing seismic facies and the stratal deformation history associated with salt tectonism. The second aim of this thesis is to locate shallow seismic amplitude anomalies, investigate their subsurface architecture, and resolve the possible migration pathways that may have produced them.

1.3. Research questions and objectives

The research questions and objectives for this thesis follows several themes.

Theme 1 – Cenozoic basin evolution

Questions: What important subsurface seismic stratigraphic and structural features are present in this part of the slope that reflect the Cenozoic basin evolution and what sedimentary slope-related processes were responsible for developing such features?

Objectives: (a) map seven seismic horizons within the Tangier 3D Seismic Survey and correlate these to Cenozoic stratigraphy based on available well log information; (b) to use the resulting seismic stratigraphy to characterize the Cenozoic basin evolution.

Theme 2 – Salt tectonic characterization

Question: What types of salt structures are present in this part of the slope and how does its mobility affect the deformation of the sediments from the Paleogene to the Neogene?

Objective: To assess how salt mobility has structurally impacted the Cenozoic strata using isochore maps.

Theme 3 – DHI occurrences and distributions

Questions: Are there amplitude anomalies in the Tangier 3D Seismic Survey? If so, do they have a definable spatial distribution? Can any detected anomalies be reasonably interpreted as fluid-generated (e.g., hydrocarbons) features known as DHIs? Can identified DHIs be structurally and stratigraphically linked to deeper reservoir or source rocks? Is the evidence of DHIs associated with identified ocean floor cold seep sites?

Objectives: (a) to locate amplitude anomalies that could be fluid-hosted features through seismic interpretation and horizon or interval amplitude extractions and evaluate the strength and validity of these prospective DHIs; (b) to incorporate available autonomous underwater vehicle (AUV) data (multibeam bathymetry) for selected DHIs, when available, to understand the surrounding seafloor morphology; (c) to map the 3D architecture of selected DHIs to identify possible fluid migration pathways by linking structural features (i.e., faults and salt diapirism) from potential

underlying Mesozoic source/reservoir rock intervals (mapped based on existing deeper seismic horizons from the PFA and well log information) up to where the DHIs are residing in the Cenozoic strata.

Theme 4 – Comparisons to other seismic surveys

Questions: How does the abundance and distribution of DHIs in the Tangier 3D Seismic Survey compare to the adjacent Shelburne 3D survey (e.g., Owino, 2022; Fig. 2.1) on the Scotian Slope and what are the main reasons for any difference between the two seismic surveys?

Objective: To compare the abundance and distribution of shallow amplitude anomalies between the Tangier 3D and Shelburne 3D surveys (e.g., Fig. 2.1) using RMS amplitude maps from this thesis and Owino (2022).

1.4. Thesis organization

This thesis has five chapters. Chapter 1 introduces the research motivation, hypotheses, research questions and objectives, regional geology of the study area, and relevant background literature. Chapter 2 discusses methodological information about the dataset and interpretative strategies used for Chapters 3 and 4. Chapter 3 provides a comprehensive interpretation and analysis of the Paleogene to Neogene seismic stratigraphy from the Tangier 3D Seismic Survey located on the central Scotian Slope. Chapter 4 encompasses a detailed investigation of selected amplitude anomalies, which are thought to be fluid related. This chapter investigates the stratigraphic and structural architecture, possible underlying reservoir and source rock intervals, and migration pathways that may have led to the formation of the amplitude anomalies. Lastly, Chapter 5 offers

key conclusions, including general recommendations and suggested directions of future research of the Scotian Slope.

1.5. Scotian Margin regional stratigraphy

1.5.1. Mesozoic stratigraphy

Rifting of the supercontinent Pangaea initiated the opening of the Atlantic Ocean that led to the formation and development of the Scotian Margin. In the Middle Triassic, rifting created a series of intricately linked and contemporaneous asymmetric rift basins (e.g., half-grabens) that were filled with sediments from the adjacent Appalachian terranes. These rift basins were filled by the continental red beds of the Eurydice Formation and the evaporite deposits of the Argo Formation (Fig. 1.1) from the eventual Tethys paleo-ocean incursion in the late Triassic to Early Jurassic (Wade and MacLean, 1990; Wade et al., 1995).

In the Early Jurassic, restricted marine conditions of the developing Scotian Margin resulted in deposition of dolomites and clastic sediments of the Iroquois Formation (Fig. 1.1). A laterally equivalent, shallow water sequence consisting of coarser grained siliciclastics and shales of the Mohican Formation was also deposited on parts of the margin affected by elevated fluvial sediment transport (Fig. 1.1; McIver, 1972; Wade and MacLean, 1990; Wade et al., 1995).

In the latter part of the Jurassic, the Abenaki Formation was deposited over the Iroquois and Mohican Formations, which are carbonates accumulated along more slowly subsiding parts of the margin that mainly reside along the western to central parts of the Scotian Shelf, in areas far removed from fluvial sediment input. The Abenaki Formation is divided into the Scaterie, Misaine and Baccaro Members (Fig. 1.1; Wade et al., 1989; Kidston et al., 2005). Starting with

the lowermost member, the Scaterie Member is characterized as deposits of margin and platform limestones. Deposited on top of the Scaterie Member is the Misaine Member, which is characterized as carbonate-rich shales corresponding to rising sea level. The Baccaro Member marks a final succession of carbonate reef, bank, and platform setting deposits (McIver, 1972; Wade and MacLean, 1990; Kidston et al., 2005; Wierzbicki et al., 2006).

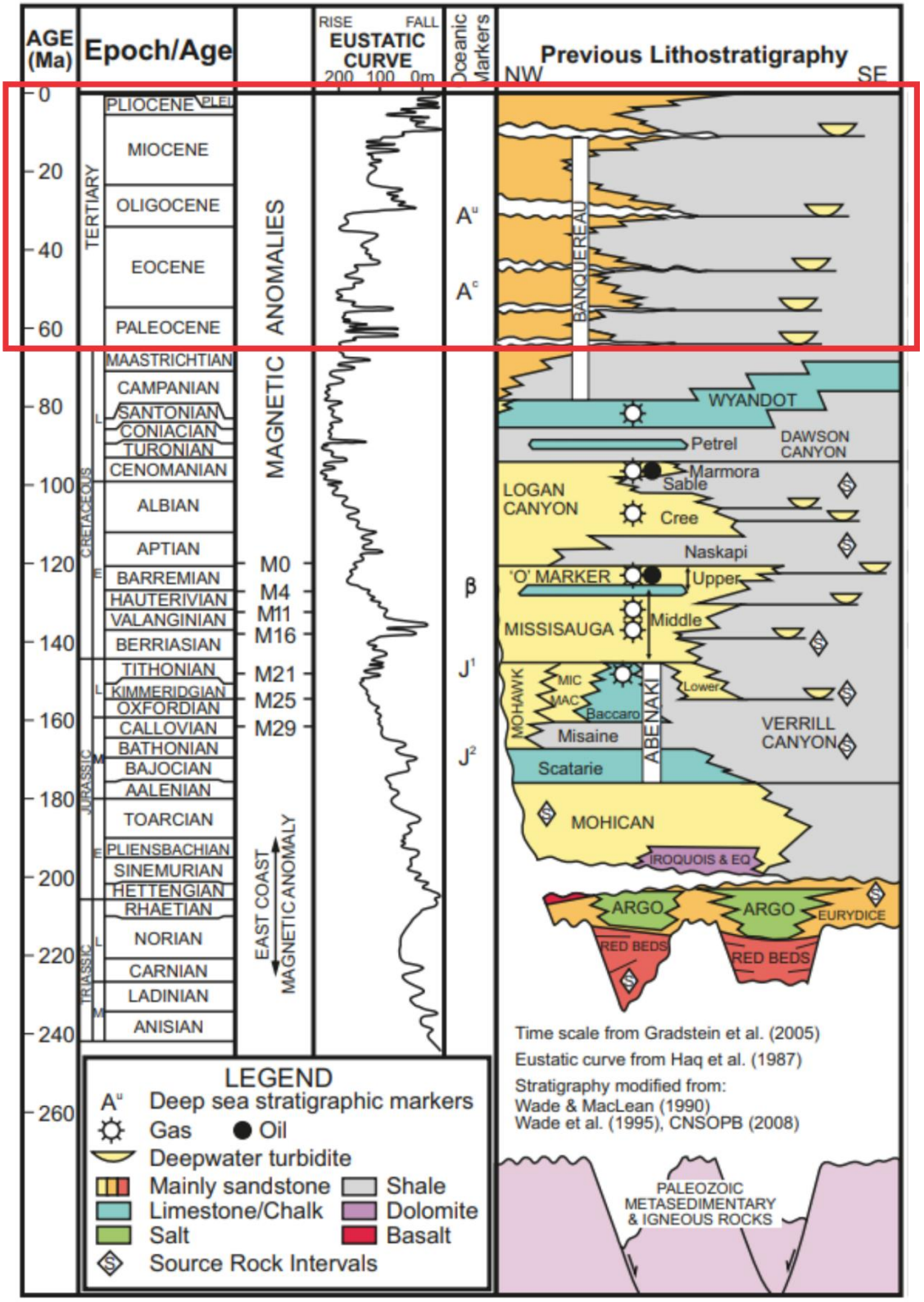

Figure 1.1. Lithostratigraphy of the Scotian Margin correlated to geologic ages, eustatic sea level, and regional seismic markers (from Weston et al., 2012). The red box highlights the Cenozoic as the study interval for this thesis.

Landward and towards the northeast, the Abenaki Formation grades laterally into the Mic Mac and Mohawk Formations, which are co-equivalent siliciclastic deposits of continental origin (Fig. 1.1). Moreover, limestone intervals of the Abenaki Formation are interbedded with deeper water basinal shales and siliciclastic units of the Verrill Canyon Formation. The Verrill Canyon Formation extends into younger Early Cretaceous stratigraphic sections as siliciclastic lateral equivalents (Fig. 1.1.; Wade and MacLean, 1990).

Middle to Late Jurassic Mohawk, Mic Mac, and Abenaki Formations are overlain by Early Cretaceous siliciclastic sediments of the Missisauga and Logan Canyon Formations (Fig. 1.1). The Missisauga Formation was deposited in a fluvio-deltaic system and is further divided into three members: Upper, Middle, and Lower Members, which are separated by the O-Marker (Fig. 1.1; (Cummings and Arnott, 2005; Cummings et al., 2006), a temporary transition to carbonate deposition interpreted to be caused by a transgression in the Early Cretaceous (Hauterivian). Carbonate sedimentation was followed by the Upper Member of the Missisauga Formation then by the deposition of the thick, shaly interval of the Naskapi Member of the Logan Canyon Formation due to a major marine transgression marked by the Aptian Maximum Flooding Surface (Chavez et al., 2016; Chavez et al., 2018). The Naskapi Member is overlain by cyclic estuarine and shallow marine coarse-grained sediment successions of the Logan Canyon Formation, in the form of the Cree, Sable, and Marmora Members (Fig. 1.1). The Early Cretaceous was heavily influenced by the sediment deposition of the Sable Delta.

Following deposition of the Logan Canyon Formation, sedimentation changed from dominantly clastic to mixed carbonate-siliciclastic due to the deposition of the Dawson Canyon Formation (Fig. 1.1; Wade and MacLean, 1990). Within the Dawson Canyon Formation, a deep-water limestone unit known as the Petrel Member was also deposited. This unit is overlain by deep-

water chalk of the Wyandot Formation (Fig. 1.1; Wade and MacLean, 1990; Hansen et al., 2004).

1.5.2. Cenozoic stratigraphy

The Mesozoic strata is dominated by siliciclastic deposits with sandstone in shallow water parts of the basin and shale in deep water regions, mainly as the Banquereau Formation. This formation is composed of mudstones interbedded with a mixture of sandstones, conglomerates, and notable chalk units. The deposition of the Banquereau Formation persisted from the Late Cretaceous to Neogene (Fig. 1.1). The progradation of the Banquereau Delta started in the Campanian – Maastrichtian to the shelf edge of the central Scotian Margin. At the start of Tertiary, the margin experienced a phase of regression and progradation coupled with a series of smaller scale transgression and regression cycles likely a result of global sea level changes (Wade and MacLean, 1990; Zachos et al., 2001). The Banquereau Delta later shifted to eastern portions of the Scotian Margin in the Paleocene (Fensome et al., 2008).

Within the period in which the formation was deposited, at ~51 Ma, a marine bolide impact created an impact crater on the southwestern Scotian Margin, known as the Montagnais impact crater, that triggered margin-wide mass transport and slope failure processes in the down-slope direction (Deptuck and Campbell, 2012). Following the marine bolide impact, chalk units were deposited in the Eocene because of a period of sea-level rise, with the most notable widespread chalk deposits being Ypresian in age, known informally as the Ypresian Chalk unit (Weston et al., 2012).

During the Oligocene a major period of regression ensued from a global cooling that caused expansion of the Antarctic ice sheet (Zachos et al., 2001). This initiated widespread canyon formation across the margin (Wade and MacLean, 1990). The Oligocene also marks a dramatic enhancement of the Deep Western Boundary Current in the North Atlantic (Hutchinson et al., 2019). This resulted in large-scale erosion and along-slope sedimentation that overprinted gravity-induced mass transport deposition from the upper shelf to produce large contourite deposits along the slope (MacDonald, 2006; Campbell, 2011; Campbell and Deptuck, 2012; Campbell et al., 2015; Campbell and Mosher, 2016). These contourites are widely recognized in seismic profile as low to moderate amplitude, parallel to sub-parallel, coherent, wavy reflections, and in map view dune-like bedforms and linear scours are visible (discussed in Chapter 3).

During the late Middle Miocene, a second significant sea level fall further destabilized the shelf break, resulting in additional erosion of the shelf edge as well as dramatic, margin-wide canyon incision down the slope (Wade and MacLean, 1990; MacDonald, 2006). The resulting change in sedimentation patterns led to the formation of thick, widespread contourite deposits, known as the Shubenacadie Drift. These drift deposits diverted around topographic highs (e.g., salt structures) to fill bathymetric lows such as minibasins and paleocanyons along the Scotian Slope (Campbell, 2011; Campbell and Mosher, 2016; Deptuck and Kendell, 2020).

Three lowstand system tracts on the central Scotian Slope are recognized during the Middle to Late Pliocene (Piper et al., 1987; MacDonald, 2006). These are thought to be related to eustatic sea level fluctuations associated with changing insolation caused by Milankovich cyclicity that triggered glacial-interglacial climate cycles (Zachos et al., 2001). The first lowstand is marked by an erosion of a paleo-valley, the second comprises a series of small-scale gullies, and the third is marked by more widespread gully erosion at the Pliocene-Pleistocene boundary (Piper et al.,

1987; MacDonald, 2006). These lowstand system tracts were followed by increased sedimentation in the Early Pleistocene confined to the upper slope and possibly sourced from ice margin settings (Piper et al., 1987; Piper, 2000; Piper et al., 2002).

The final phase of the Neogene and Quaternary deposition along the Scotian Margin was dominantly related to the Laurentide ice sheet glaciation. The last glaciation in North America (Quaternary Period; ~20 ka) influenced sedimentation in the Scotian Margin by depositing hundreds of meters of glacio-marine till and dropstones (Amos and Knoll, 1987; Piper et al., 1987; Amos and Miller, 1990; Gipp, 1994; Piper, 2000; Piper et al., 2002).

Today, the central Scotian Slope hosts several large-scale canyons, slides, slumps, scarps, and downslope mass transport deposits that are possibly related to previous glaciations. Reworking of continental shelf and slope sediments persisted through the Cenozoic up to recent. This involves down- or along-slope sediment transportation into the deeper parts of the slope via turbidity/contour currents and mass transport processes.

1.6. Salt tectonics of the Scotian Margin

Salt tectonic deformation commonly occurs in salt-dominated, passive margin, sedimentary systems (e.g., the Gulf of Mexico and offshore Brazil, West Central Africa, Morocco, and Nova Scotia) that are driven by salt mobility, gravity and differential sediment loading (Hudec and Jackson, 2006; 2007; 2011; Jackson and Hudec, 2017).

The movement of salt bodies results produces various recuring morphologies. Vertical salt structures can be characterized as stocks, diapirs, walls, pillows, and anticlines. (Fig. 1.2) Horizontal to sub-horizontal slabs of salt are often described as salt stock canopy, wall canopy,

glacier, sheet, and rollers (Fig. 1.2). The classification of these salt structures can lead to the distinction of salt provinces in a passive margin.

Salt provinces are highly dynamic with many types of autochthonous and allochthonous structures. Autochthonous salt is defined as salt layers resting in-situ, such that younger strata overlie it. Allochthonous salt bodies are described as subhorizontal, moderately dipping, or sheet-like salt bodies (e.g., diapirs and canopies; Fig. 1.2) that have intruded younger stratigraphic levels (Hudec and Jackson, 2007; 2011).

Salt tectonics has been proven to be a critical component of many active petroleum systems (e.g., Geletti et al., 2008; Wenau et al., 2015) for several reasons including: (1) the capacity of allochthonous salt bodies to change the geothermal gradient due to salt's high thermal conductivity relative to the surrounding bedrock, (2) deformation structures formed during salt movement generates migration pathways for fluid flow, (3) the impermeability of salt allows it to act as and create hydrocarbon seals, and (4) the deformation of the overlying sediments may produce structural traps (Hudec and Jackson, 2006; 2007; 2011; Jackson and Hudec, 2017).

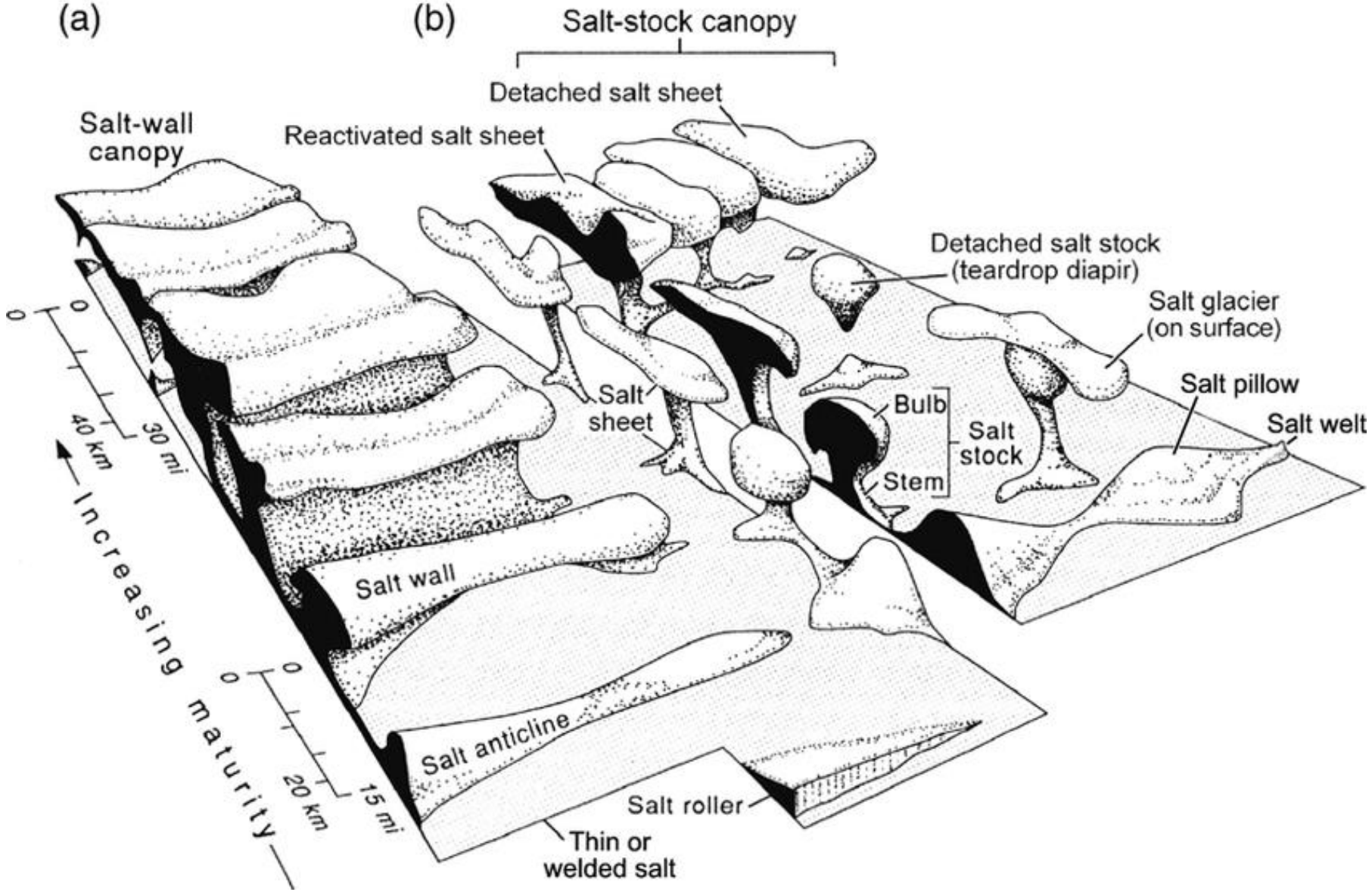

Figure 1.2. Structural geometry of common allochthonous salt bodies such as salt sheets, salt-stock canopy, and salt stocks/diapirs (from Hudec and Jackson, 2007). Some of these salt structures are found on the Scotian Margin (Shimeld, 2004; Ings and Shimeld, 2006; Albertz et al., 2010; Deptuck, 2010; 2011; Deptuck et al., 2014; 2020; Christians, 2015; Deptuck and Kendell, 2017; 2020). Investigation of allochthonous salt bodies in the Tangier 3D area is discussed in detail in Chapter 3.

Several earlier studies have been completed to investigate salt tectonism and the resulting structural deformation along the Scotian Margin (Shimeld, 2004; Ings and Shimeld, 2006; Albertz et al., 2010; Deptuck, 2010; 2011; Deptuck et al., 2014; 2020; Christians, 2015; Deptuck and Kendell, 2017; 2020). Five distinct tectonostratigraphic sub-provinces are defined on the Scotian Margin (subprovinces I to V), based on the structural geometry of salt bodies related to salt expulsion due to consequent overburden deformation (Fig. 1.3; Shimeld, 2004; Ings and Shimeld, 2006; Albertz et al., 2010; Adam and Krezsek, 2012; Kendell, 2012).

The salt bodies in the Scotian Margin are autochthonous and allochthonous in nature (Shimeld, 2004; Ings and Shimeld, 2006; Albertz et al., 2010; Deptuck, 2010; 2011; Deptuck et al., 2014; 2020; Christians, 2015; Deptuck and Kendell, 2017; 2020).

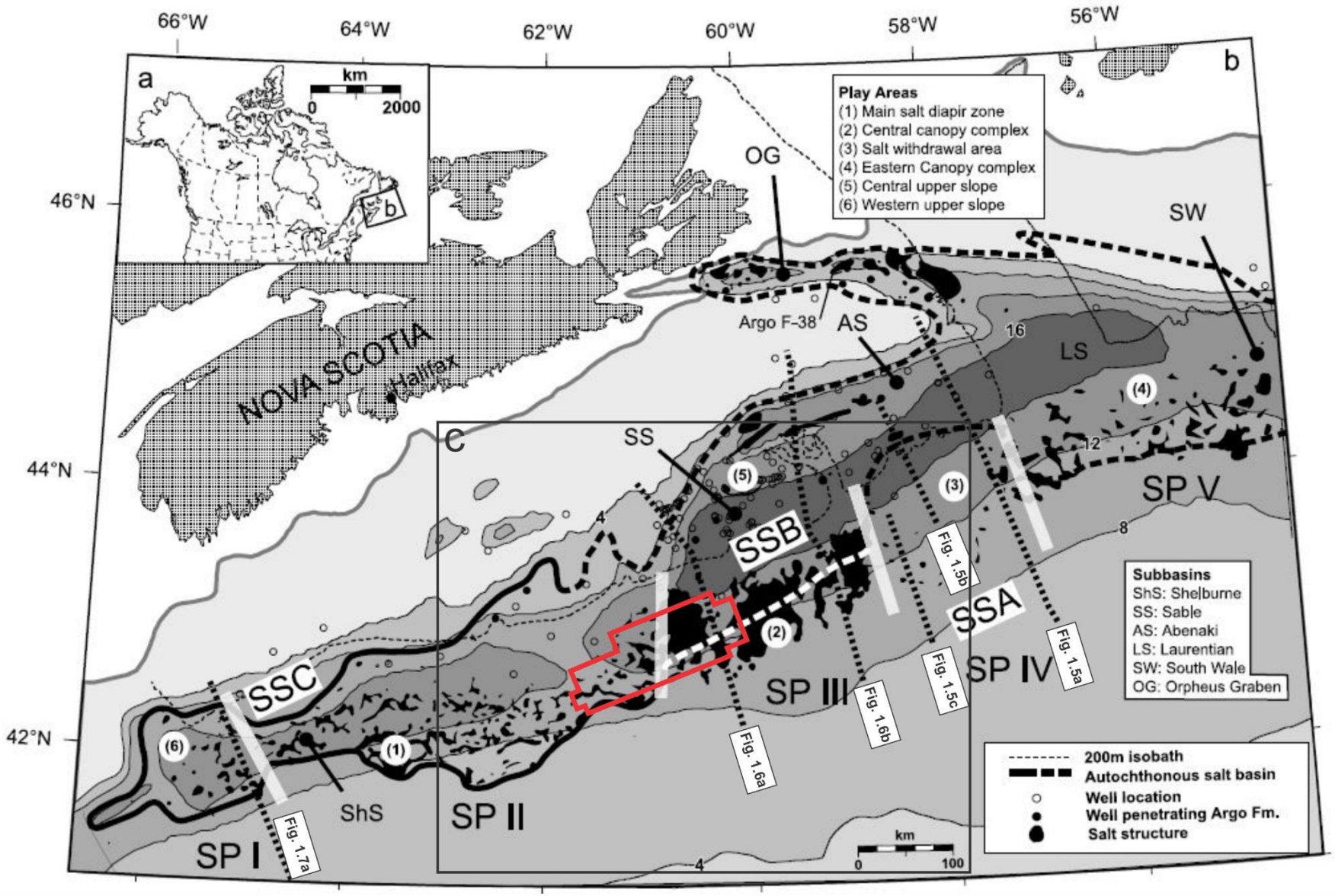

Figure 1.3. (a) Inset map of mainland and offshore Nova Scotia; (b) A close-up map of different salt bodies on the Scotian Margin (shaded regions) with black dashed lines determining the boundaries of five tectonostratigraphic provinces, highlighted in thick white lines, based on different salt bodies and related structures to salt deformation in various subbasins (from Ings and Shimeld, 2006; map modified from Albertz et al., 2010). The study area, Tangier 3D Seismic Survey, for this thesis is highlighted in red (close-up in c; discussed in Chapter 3).

1.6.1. Tectonostratigraphic provinces

There are five distinct salt-related tectonostratigraphic provinces (SP I to SP V; Fig. 1.3) defined for the Scotian Margin (Ings and Shimeld, 2006).

Subprovince I (SP I), is described as a region with salt diapirs and walls (Figs. 1.3). The growth and development of diapirs started in the Jurassic and Cretaceous, concurrent with mixed carbonate-siliciclastic sedimentation (Shimeld, 2004; Kidston et al., 2002; Deptuck and Kendell, 2017). The presence of concordant strata, mainly above the Upper Cretaceous Wyandot Formation, suggests that there was more limited movement of salt during the Cenozoic. In the deeper water settings, an allochthonous salt canopy complex is observed on top of Middle Jurassic and older rocks (Shimeld, 2004; Ings and Shimeld, 2006; Deptuck, 2011). The development of SP 1 has been linked to progradation of the Shelburne Delta across Georges Bank. SP I differs from SP II as it is a gravity spreading system, in contrast to the sediment starved gravity gliding system that makes up most of the Shelburne Subbasin in SP II.

Subprovince II (SP II) is defined as a salt diapiric region (Figs. 1.3). Apparent in the eastern part of SP II are highly squeezed, most likely detached, and still recently moving diapirs that show bathymetric relief (Shimeld, 2004). Other characteristics of SP II are mainly vertical salt diapirs and sediment starved minibasins. Sediment loading occurred into the primary salt basin with salt bodies sitting immediately above the primary salt layer that supplied them, in contrast to the eastern part of the Sable Canopy or the Banquereau Synkinematic Wedge, which is in contrast to the salt bodies that are now sitting seawards of the primary salt basin.

Subprovince III (SP III) differs from SPs I and II by its extensive allochthonous salt canopy complexes that overlie Lower Cretaceous and older rocks below (Fig. 1.3). The canopy complexes also indicate translation of salt deposits likely due to the deposition of the Sable Delta

during the Middle Jurassic to Early Cretaceous (Shimeld, 2004; Ings and Shimeld, 2006; Albertz et al., 2010).

Subprovince IV (SP IV) is characterized by the near lack of salt bodies (i.e., salt withdrawal area; Fig. 1.3) suggesting that the salt has been almost fully expelled. SP IV has extensive landward-dipping reflections (Ings and Shimeld, 2006) located above a widespread salt-based detachment formed above salt that was originally expelled from landward salt basins (Huron and to a lesser extent, Laurentian) (Deptuck et al., 2014). The Banquereau synkinematic wedge, is the name given to the structure located underneath SP IV (Shimeld, 2004).

Lastly, **subprovince V (SP V)** is the least understood region because of poor seismic imaging, a thick sediment cover, and limited data coverage (Fig. 1.3). However, Shimeld (2004) and Ings and Shimeld (2006) interpret that salt bodies in this region were possibly influenced by extension in the Early Cretaceous and contraction in the Late Cretaceous to Neogene. (Shimeld, 2004; Ings and Shimeld, 2006; Albertz et al., 2010; Deptuck, 2011; Deptuck et al., 2014).

1.7. Source rocks of the Scotian Margin

The source rock for most of the hydrocarbons found on the Scotian Margin, aside from the Pre-Tithonian-aged oil in Mic Mac J-77, is thought to be the Upper Jurassic are the Upper Jurassic (Tithonian) shales of the Mic Mac/Verrill Canyon Formations (Fig. 1.1), which are responsible for generation of most gas and light oils/condensates on the Scotian Shelf (deriving from Type II-III kerogens) (Fowler, 2020). Based on the Play Fairway Analysis (2011), technical reports and studies (CNSOPB, 2000; Kidston et al., 2002; Mukhopadhyay et al., 2003; Mukhopadhyay,

2006; Kidston et al., 2007; Silva et al., 2015; Fowler et al., 2016), there are several other potential source rock intervals, including:

a) Upper Triassic early syn-rift to post-rift clastic succession of the Eurydice Formation that has the potential of hosting Type I lacustrine source rocks.
b) Lower Jurassic (Sinemurian-Pliensbachian-Toarcian) for potential earliest post-rift marine (Type II) clastic succession of the Mohican Formation.
c) Middle Jurassic (Callovian) Misaine Member Type II-III carbonates of the Abenaki Formation that formed after the rifting in the Triassic during the transition from hypersaline to carbonate marine setting.
d) Lower Cretaceous (Berriasian – Valangianian) sandstones and shales of the Missisauga/Verrill Canyon Formations were deposited in a deltaic setting and present evidence of widespread occurrence on the margin (host Type III kerogen).
e) Lower Cretaceous (Aptian) shales in the Naskapi Member of the Logan Canyon Formation were deposited during the Intra-Aptian MFS in a deltaic depositional setting (Type III kerogens).
f) Middle to Upper Cretaceous (Albian to Turonian) sandstones and shales in the Dawson Canyon Formation, which are not present on the shelf, but may possibly exist in deep waters (e.g., slope).

At present, strong evidence for these potential older source rock intervals such as Upper Triassic to Lower Jurassic in the offshore of Nova Scotia is lacking because they have not been penetrated by any well to date (OETR, 2011). Additionally, there are deepwater wells through Middle Jurassic and younger intervals that also have not found robust source rocks. These predicted source rocks may be volumetrically significant in deeper-water settings on the Scotian

Slope that has been tested in only a small number of wells. Additionally, these predicted source rocks (e.g., Upper Triassic to Middle Jurassic) may indicate the existence of similar style petroleum systems on the conjugate margin (Morocco) (Fowler, 2020).

In addition, Powell and Snowdon (1979), Powell (1982), and Mukhopadhyay et al. (2003) concluded that there are four geochemical hydrocarbon families. These families originated from different source/reservoir rock intervals. Based on organic geochemical evidence, the first family was produced from the shale interbeds within both Missisauga and Mic Mac sandstone reservoirs and laterally equivalent Verrill Canyon Formation. The light oil/condensates from this family are Type II-III to Type III kerogen derived from terrigenous organic matter.

The second family was discovered in Cohasset, Panuke, and Balmoral Fields from Logan Canyon and upper Missisauga Formation reservoirs (Fig. 1.1). The hydrocarbon from this family might have originated from early syn-rift (Late Triassic) to Eurydice, Mohican, or Iroquois Formations (Early Jurassic), characterized as possibly forming from Type I to Type II source rocks (i.e., sourced from a lacustrine or restricted marine setting).

The third family of hydrocarbons on the shelf contains condensates from the Banquereau and Citnalta wells produced from the Missisauga Formation reservoir (Fig. 1.1). The kerogen type is Type II-III sourced from marine and terrestrial organic matter from the Verrill Canyon and Mic Mac Formations.

Lastly, the fourth family of hydrocarbons are light oils/gas/condensate discovered on the Primrose field, also a region associated with intervening salt diapir structures. The reservoirs discovered on the Primrose field are the limestones of the Wyandot Formation and the

sandstones of the Logan Canyon Formation of the Early Cretaceous (Fig. 1.1; Kidston et al., 2002; Mukhopadhyay et al., 2003; Fowler, 2020).

1.7.1. Hydrocarbon occurrences and discoveries

Offshore hydrocarbon exploration of Nova Scotia started in 1959. To date, there have been 130 exploration wells including 78 development wells since exploration started (CNSOPB, 2000). There have also been 25 significant hydrocarbon discoveries on the shelf and slope (Fig. 1.4) that mostly are geographically located within the Sable Subbasin (Fig. 1.3; Wade et al., 1989). Only a few of these prospects have been put into production.

According to Cummings and Arnott (2005), the occurrence of growth-faulted shelf deltas or delta complexes that formed at the paleoshelf edge during periods of low sea level (i.e., during lowstand tracts systems tracts) are the most important known hydrocarbon reservoirs in offshore Nova Scotia or in any offshore passive margin sedimentary systems globally. Such delta complexes are targeted for exploration because of the lateral extent of overlying shale acting as seals and expanded sandstone reservoirs, which are commonly associated with growth fault structures (Cummings and Arnott, 2005). Several petroleum fields on the shelf were mainly gas discoveries. The Venture field contained at least 50% of gas in the region (Mukhopadhyay et al., 2003; Cummings and Arnott, 2005) and together with the smaller Alma, North Triumph, South Venture, Thebaud, Deep Panuke (Fig. 1.4) were put into production in the Sable Offshore Energy Project from 1999 to 2018. Several slope wells such as Annapolis, Newburn, and Tantallon encountered gas/condensate reservoirs. Additional slope wells such as Crimson, Aspy, and Balvenie encountered gas-charged siltstones. The trapping features in these regions are

rollover anticlinal structures in association with salt-related listric growth faults (Cummings and Arnott, 2005).

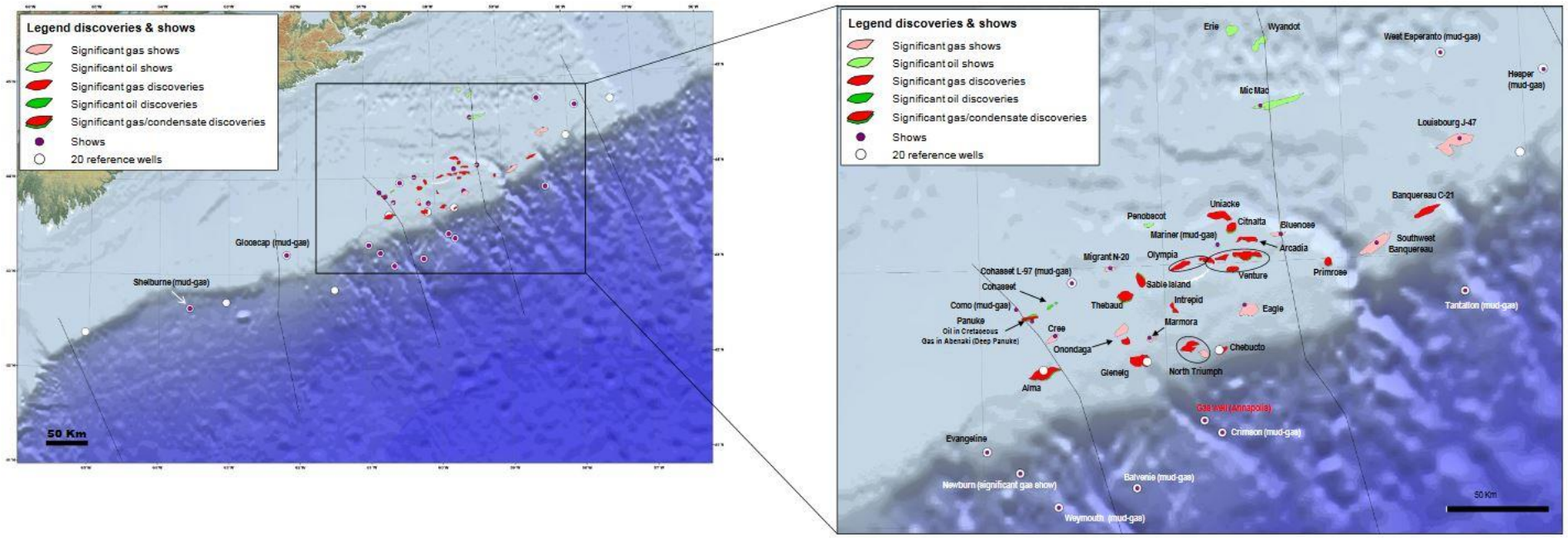

Figure 1.4. The locations of significant hydrocarbon field discoveries on the Scotian Shelf near Sable Island (from OETR, 2011).

1.8. Overview of reflection seismology and its data interpretation

1.8.1. Marine seismic reflection data

In reflection seismology, seismic profiles are generated by seismic waves reflected at boundaries between rocks with different density and velocity characteristics. These variations are quantified by the acoustic impedance (AI) contrast across a boundary (Eq. 1; Fig. 1.5), resulting as the seismic wave passes between units with different physical properties. The magnitude of contrast is controlled by the change of acoustic impedance between two units. Therefore, the larger the contrast, the stronger (brighter) the amplitude of the seismic reflection (Eq. 2; Yilmaz, 1987; 2001; Herron, 2011; Zhao et al., 2018).

$$(1) AI = V\rho$$

where AI is calculated by the product of compressional-wave velocity V and bulk density ρ (Yilmaz, 1987; Herron, 2011).

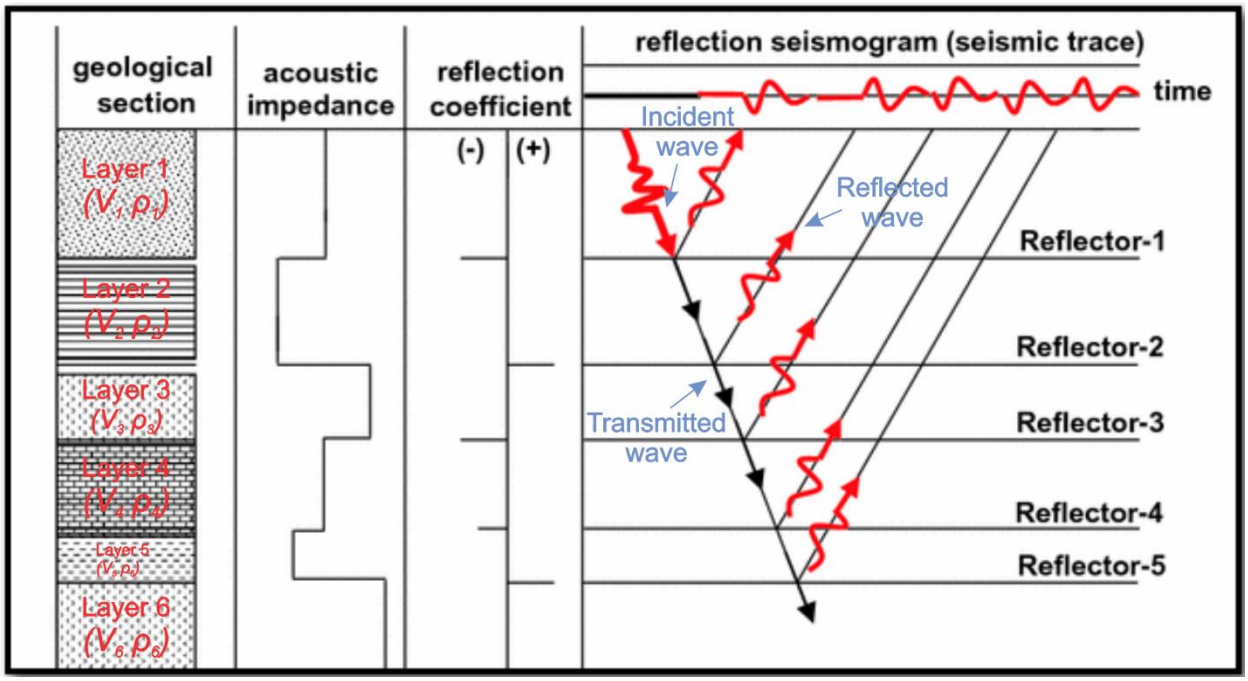

Figure 1.5. Simplified schematic depicting principle of reflection seismology. Lithologic thickness and density (ρ) variations impact the velocity (V) seismic wave energy causing impedance contrasts that result in unique reflection coefficients between stratal layers. No depth and time scales are implied for the hypothetical geological section and reflection seismogram, respectively (modified from Alsadi, 2017).

Reflection coefficient (RC; Eq. 2) is defined by the ratio of the amplitude of the reflected wave to the amplitude of the incident wave (i.e., how much energy is reflected at the interface boundary). The RC is commonly convolved with a model of a sound source wavelet to stimulate reflection amplitude in the form of a synthetic seismogram (Yilmaz, 1987; 2001; Herron, 2011; Alsadi, 2017). The magnitude of the reflection is directly proportional to the reflection coefficient (Yilmaz, 1987; 2001; Herron, 2011; Brown, 2011).

$$(2) RC = \frac{V_2\rho_2 - V_1\rho_1}{V_2\rho_2 + V_1\rho_1} = \frac{AI_2 - AI_1}{AI_2 + AI_1}$$

The RC is calculated by the ratio of subtracted acoustic impedances over added acoustic impedances of layers 1 and 2 (Fig. 1.5; Yilmaz, 1987; Herron, 2011; Brown, 2011).

The principles of reflection seismology have been applied in subsurface exploration since the 1950s. In two-dimensional (2D) reflection seismic surveying, both the acoustic source (e.g., airgun) and the receivers (e.g., geophones) are within a single line. Moreover, 2D lines are collected during a single pass of a ship that tows the source and receivers behind it. The resulting seismic profile is a single vertical cross-section of the reflections produced at boundaries with the subsurface beneath the survey line, which is constructed by compressional wave reflections from the airgun and the detected reflected waves by the receivers (Fig. 1.6; Yilmaz, 1987; 2001; Alsadi, 2017).

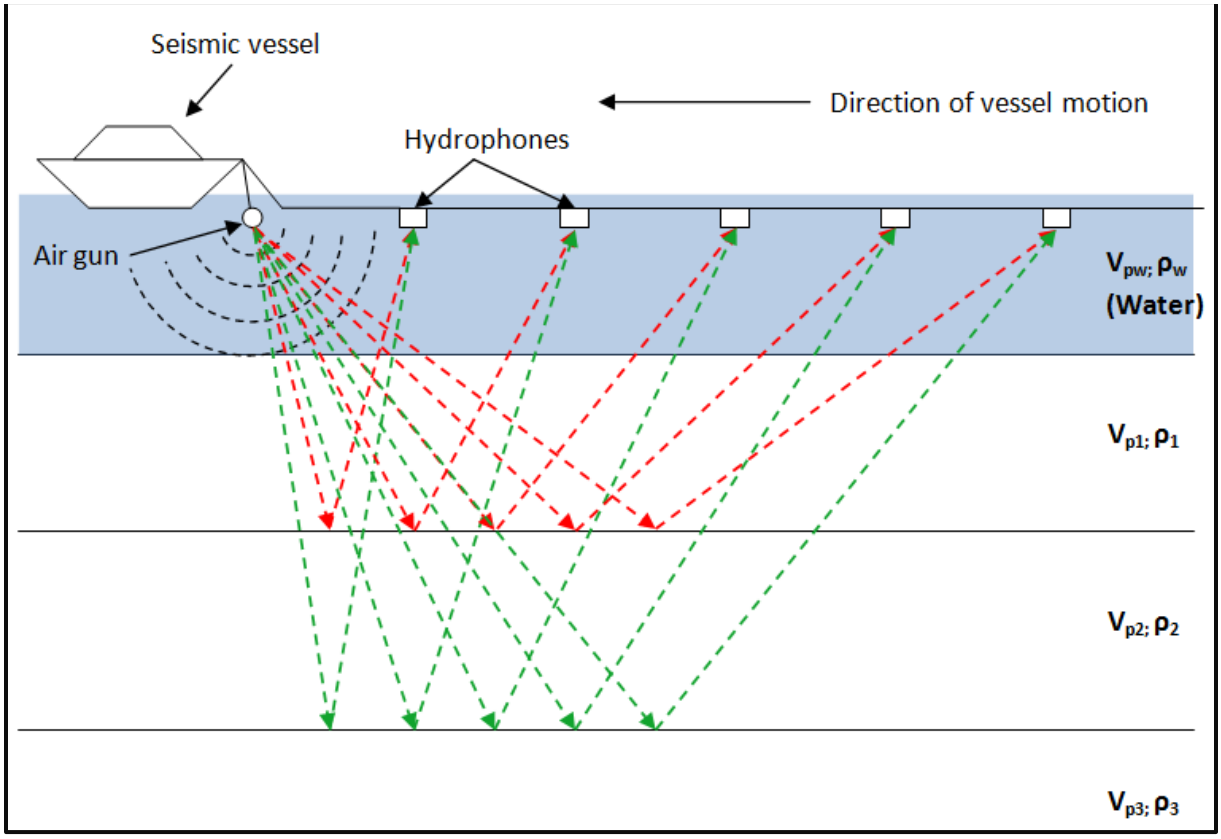

Figure 1.6. Conventional set-up of marine 2D seismic reflection surveying (not to scale; Alsadi, 2017).

In contrast, the acquisition of three-dimensional (3D) seismic surveys uses multiple acoustic sources (e.g., airguns) and receivers (e.g., geophones or hydrophones), commonly attached to a series of evenly spaced streamers spread out over an area by the ship steaming back and forth across the survey area to form a dense grid, where a volume of data is collected.

For marine 3D seismic surveys, the streamers, depending on the direction of the recording vessel, are defined to have in-lines (IL) and cross-lines (XL) (Fig. 1.8). In-line is a seismic line within a 3D seismic survey that is parallel to the direction of the recording vessel that tows the streamer, and cross-lines are perpendicular. The resulting product can be thought of as a seismic cube, where seismic reflectors are visualized and observed in three-dimensions and geologic structures can be interpreted. 2D or 3D lines can follow strike orientation of the regional bedding and can then be called strike-oriented lines, versus dip-oriented lines that are perpendicular to the regional strike (Yilmaz, 1987; 2001; Galbraith, 2001; Howard, 2007; Alsadi, 2017).

During single-channel seismic data acquisition, seismic waves generated by each source point images one subsurface location only resulting to one seismic trace. Multichannel 2D and 3D seismic surveys commonly use multi-channel data acquisition that requires receiving information from any one subsurface point multiple times from the hydrophones that are progressively further away from the sound source (Yilmaz, 1987; 2001; Herron, 2011; Brown, 2011). The stacking of these data into common-mid-points (CMP) improve the signal-to-noise ratio after applying normal/dynamic moveout to account for the time lag from increasingly further hydrophones. The acquisition of multi-channel seismic data can be done by conventional narrow azimuth (NAZ) and by wide azimuth (WAZ) surveys (Fig. 1.7), where the azimuth angle is the angle between the source-receiver direction and the survey direction that also represent the direction of seismic illumination within the area of interest. If the number of sources and

receivers is increased, it is called a wide azimuth (WAZ) survey with the purpose of increasing azimuth coverage resulting to increased seismic illumination, thus, improving subsurface imaging.

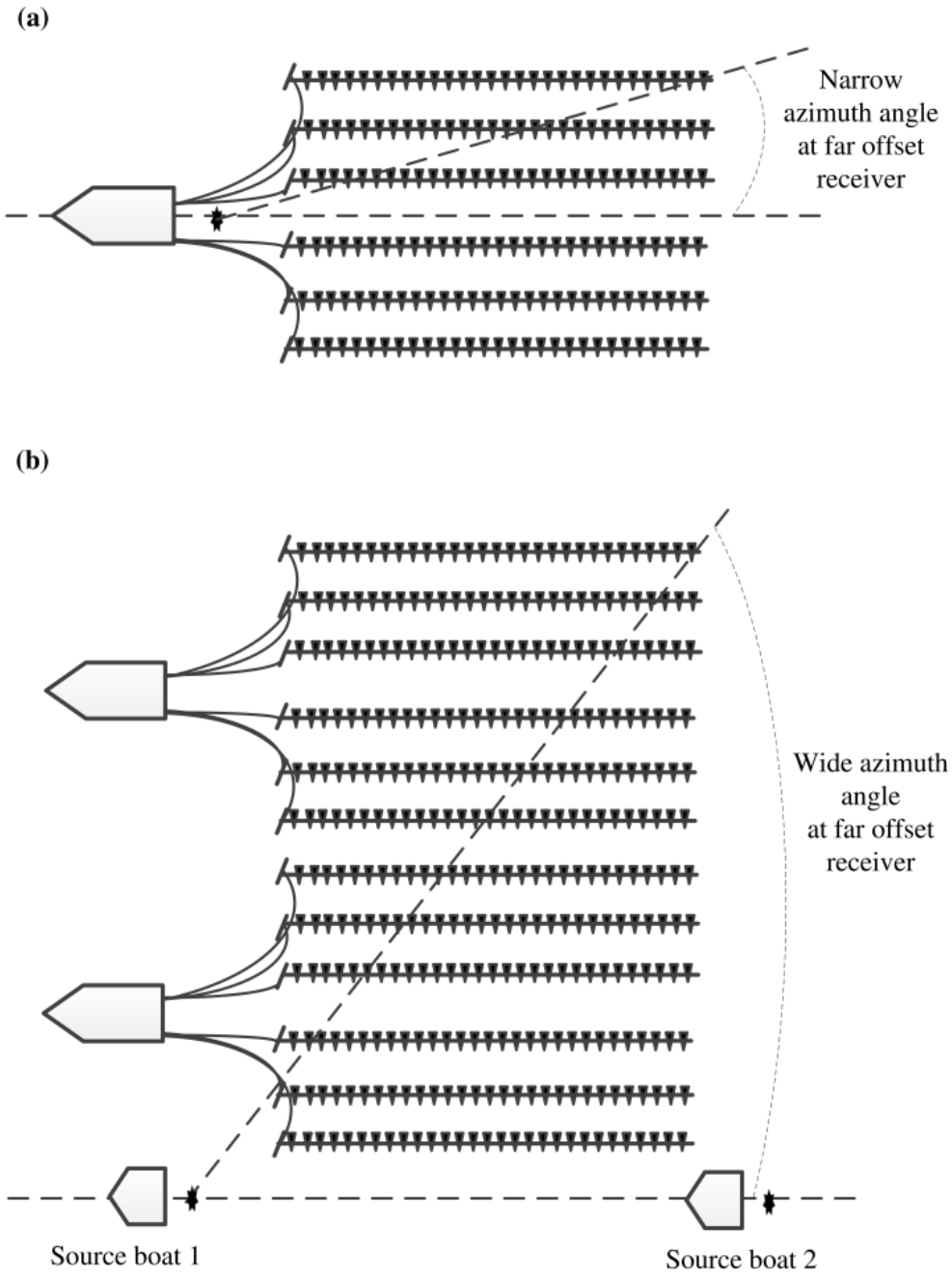

Figure 1.7. (a) Conventional narrow azimuth (NAZ) streamer survey; (b) Wide azimuth (WAZ) streamer survey with two source boats (Ibrahim, 2015).

The processing of acquired multi-channel seismic data either from NAZ or WAZ surveys include migration. Migration of seismic data is the process that converts seismic traces collected from a function of recording time to features in the subsurface as a function of depth. Migration is used to further improve signal-to-noise ratio, resolution, and imaging by moving dipping reflections into the correct position (Yilmaz, 1987; 2001; Herron, 2011; Brown, 2011). In 3D seismic surveys, out-of-plane artifacts are reduced in migration in areas of complex structure, such as areas of salt structures. Longer streamer lengths are also used to improve imaging of steeply dipping layers (e.g., flanks of salt diapirs). This can be followed by filtering, which is a process to remove undesirable portions of seismic data during processing to increase the signal-to-noise ratio. Filtering can eliminate certain frequencies, amplitudes, or any other information related to seismic data (Yilmaz, 1987; 2001; Herron, 2011; Brown, 2011).

In general, 3D seismic surveys usually provide a greater resolution and better imaging of the subsurface compared to 2D seismic surveys since more reflections are stacked at each common-mid-points (CMPs). The net result is a greatly improved resolution of subsurface features.

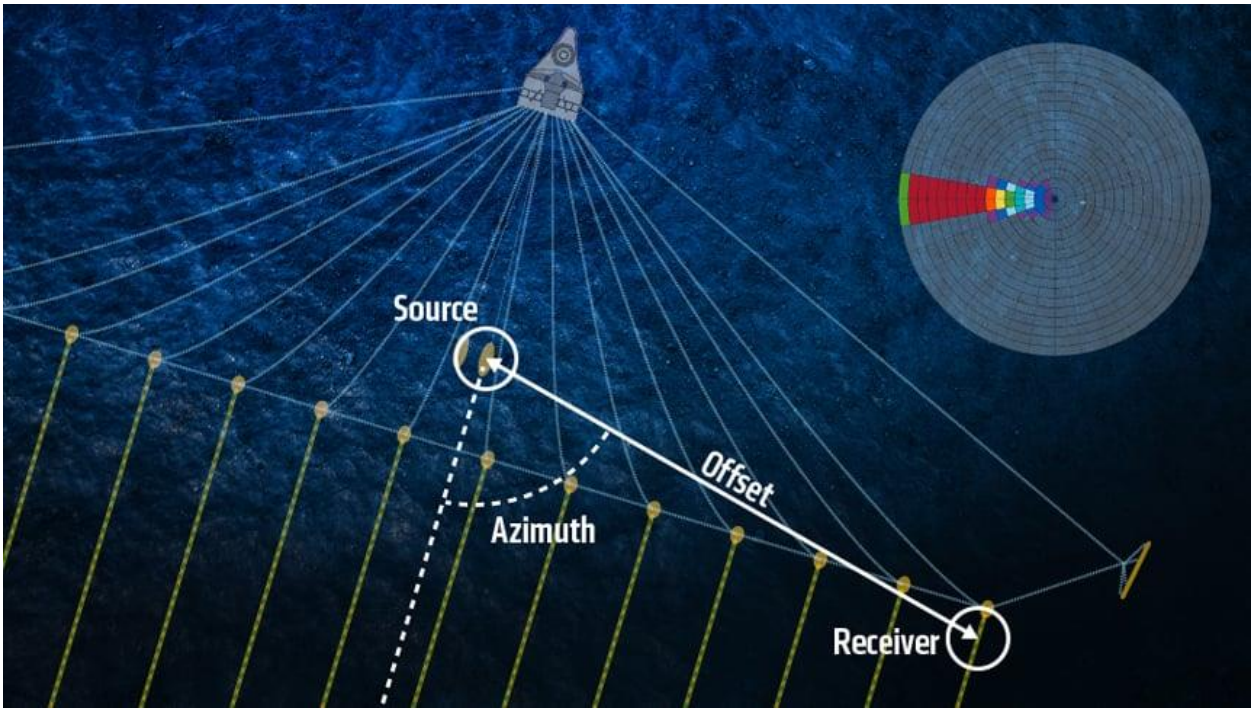

Figure 1.8. General framework design of marine 3D seismic surveying using Wide Azimuth (not to scale; from Vermeer, 2012). Streamers are highlighted in yellow in the direction of the in-lines.

1.8.2. Seismic stratigraphy

Identification of seismic facies is based on the reflection geometry or configuration, continuity, amplitude and frequency, and bounding relationships (Mitchum et al., 1977a; 1977b; Vail et al., 1977; Vail 1987). Investigation of stratigraphy in seismic data is commonly performed by the analysis and the identification of seismic intervals defined by distinctive seismic facies. Individual mapped reflections are known as seismic horizons, between which a generalized seismic unit or interval can be recognized. A seismic sequence is a specific type of interval defined by stratal patterns and/or geometries indicating a conformable succession bounded by unconformities or their correlative bounding surfaces (Posamentier and Kolla, 2003; Posamentier et al., 2007). Seismic stratigraphy is the interpretation of stratigraphy, sedimentary facies, and geological history from seismic reflection data, which leads to better understand depositional

systems (Mitchum et al., 1977a; 1977b; Vail et al., 1977; Vail 1987; Bertram and Milton, 1996; Xu et al., 2022). Catuneanu et al. (2009) further stated that the analysis of stratal stacking patterns in rocks corresponds with the interplay of changes in sedimentation rates that reflect combinations of depositional trends such as progradation, retrogradation, aggradation, downcutting, and other geometrical patterns which can also be recognized in seismic.

Seismic reflections can have multiple geometries within a sedimentary basin (Fig. 1.9). The common reflection geometries are concordant (parallel to subparallel), hummocky, chaotic, deformed, reflection blanking, wavy, granular, divergent, convergent, and progradational reflections (sigmoid, oblique, shingled). These reflection geometries can be indicators of basinward migration of sediments or other situations with lateral migration. In the study area, most of these reflection geometries are observed and analyzed. Additionally, channel infill reflections are limited to several paleocanyons and paleochannels in the study area.

There are four main reflection terminations that can be observed in the stratigraphy, that may also correspond to a sequence boundary: onlap, downlap, toplap, and truncation (Fig. 1.10).

Onlap is the termination of low-angle reflections against steeper reflections. Downlap is the termination of steeply dipping overlying reflections against the underlying strata that are inclined or horizontal. Toplap is the gently oblique termination of reflections against overlying strata or boundary. Truncation is the abrupt and angular termination of reflections below an unconformity (Mitchum et al., 1977a; 1977b; Vail et al., 1977; Vail 1987; Bertram and Milton, 1996; Catuneanu et al., 2009; Xu et al., 2022).

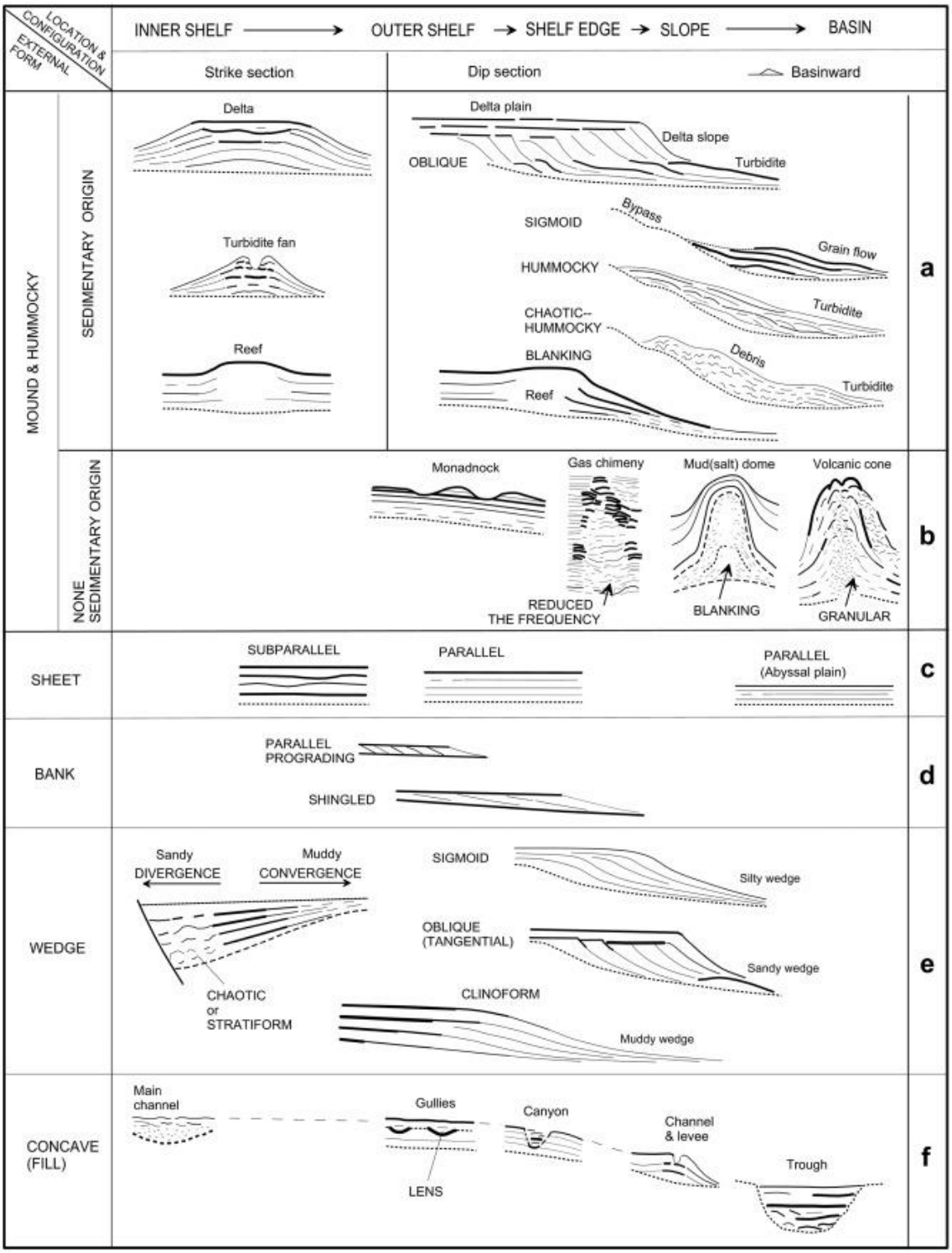

Figure 1.9. Common examples of seismic reflection configurations or geometry and facies distribution patterns in an offshore sedimentary basin (dotted lines = sequence boundaries; solid lines = reflection features; lines with greater width = strong reflection amplitude; solid and dashed lines = continuity; from Xu et al., 2022).

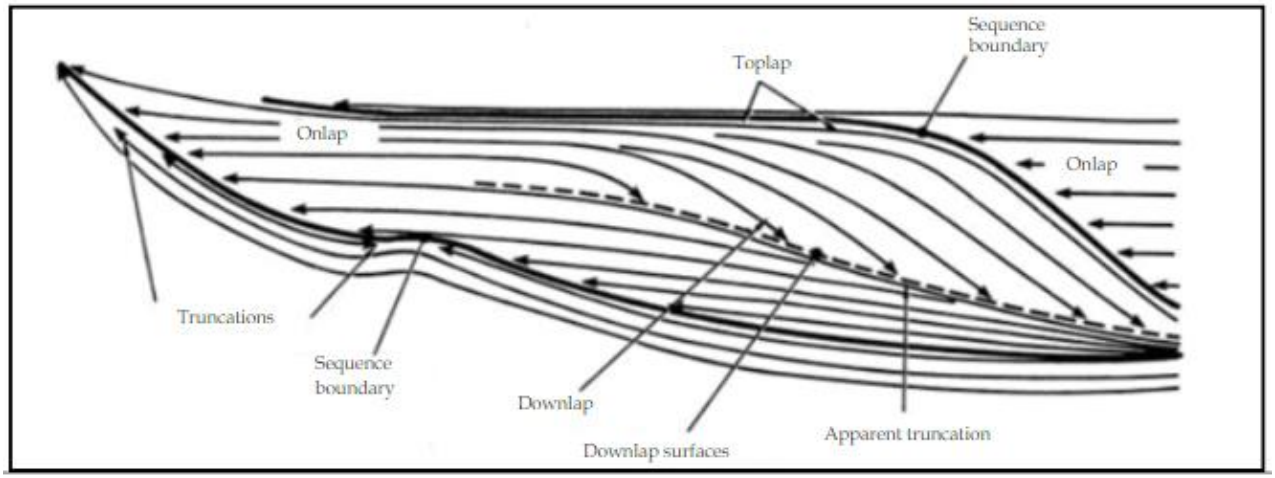

Figure 1.10. Main stratal and reflection termination patterns in a sequence stratigraphic and seismic framework. The reflection terminations within this sequence suggest different sedimentary processes in association with sedimentation rates, tectonism, and sea-level changes (from Vail, 1987).

1.9. Overview of marine hydrocarbon seeps

Natural marine hydrocarbon seeps are areas where fluids from the subsurface naturally escape to the seafloor from a leaking reservoir. Seeps are common occurrences in passive sedimentary margins and may indicate the presence of active petroleum systems from the deep subsurface (Ma et al., 2021). Hydrocarbon seeps and their relation to basin morphology and architecture have been well documented in several sedimentary basins in the world (Cunningham et al., 2000; Chapman et al., 2004; Geletti et al., 2008; Crutchley et al., 2010; Andresen et al., 2011; de Mahiques et al., 2017; Serié et al. 2017; Razaz et al., 2020; Cox et al., 2021; Römer et al. 2021). The fluid sources of seeps generally comprise either deeply sourced thermogenic fluids driven by temperature-induced chemical cracking of organic matter (kerogen) in rocks or shallow biogenic fluids formed from the microbial communities present within the shallow sediments. In some cases, a mix of thermogenic and biogenic fluids can occur (e.g., Scotian Margin; Fowler et al., 2017; 2017; 2019). Thermogenic gas is sourced from source rock intervals in a basin, migrating

along available permeable pathways. These can include the interface between a salt body such as a diapir and the surrounding sediments or through related faults. The classification of thermogenic and biogenic hydrocarbons in the Scotian Margin is based on methane carbon ($\delta^{13}C$) and hydrogen (δD) isotopic signatures (Fowler et al., 2017; 2017; 2019). The challenges with the distinction between two types of fluids are biodegradation and if relevant microbes prefer to use thermogenic hydrocarbons as energy source to produce biogenic hydrocarbons that may overprint thermogenic signatures (Fowler et al., 2017; 2017; 2019).

Hydrocarbon seeps can be classified as micro- and macro-seepage. Macroseepage refers to large-scale, visible fluids escaping the subsurface. Macroseepage sites are localized areas where significant concentrations of fluids (e.g., hydrocarbons) that commonly migrate within the constraints of porous, permeable damage zones around large faults, fractures, or vents from the reservoir to the near surface (Fig. 1.11; Boruah et al., 2022; Argentino et al., 2021). Macroseepage sites have been widely documented and are known indicators of active petroleum systems from deep subsurface. They have been used to aid the identification of some of the largest discoveries of hydrocarbon-producing areas in the world (Link, 1952; Perrodon, 1983; Macgregor, 1993).

In contrast, microseepage sites are areas with small-scale fluid migration from the subsurface to the seafloor. This type of seepage occurs when fluids have sufficient fluid overpressure to invade the overlying seal but not enough to create major faulting and fracturing. They can migrate vertically through the sediment succession and possibly reach the near surface, in the form of gas chimneys (Fig. 1.11; Tedesco, 1995; Chen et al., 2019; Ma et al., 2021). Microseepage sites do not provide massive leakage of fluids in significant concentrations. It is only an indication that fluids can migrate and diffuse through sealing layers in slow manner.

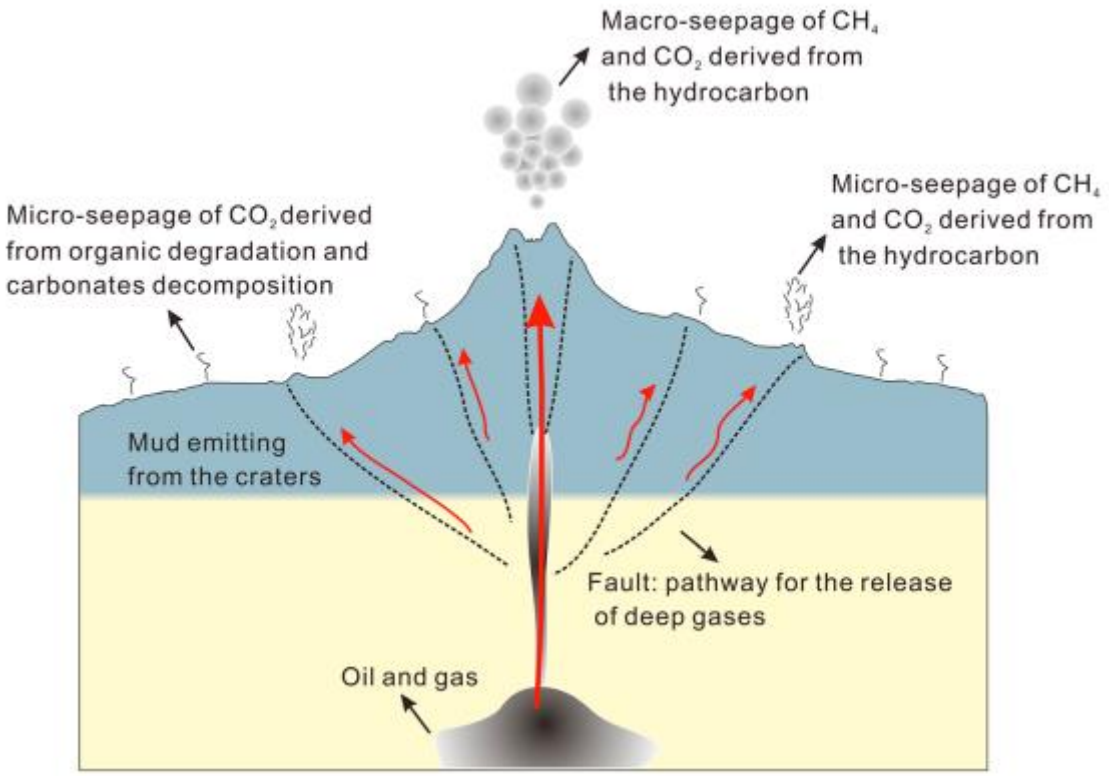

Figure 1.11. Simplified conceptual model (not to scale) depicting source of migrating subsurface fluids and migration pathways for the occurrences of macro- and micro-seeps in sedimentary basins (from Chen et al. 2019).

Once the fluids reach the near surface, there will be localized changes on the seafloor morphology. Some of the examples of seep-related features are pockmarks, gas chimneys, and mud diapirs and mud volcanoes (Figs 1.11-1.14). When geological conditions are favourable, these seep-related features may occur and dominate the seafloor where active seeps are occurring because such features are the conduits for fluid flow from the subsurface reservoir and disrupt the seafloor and near seafloor sediments in the process of fluid expulsion.

Pockmarks are defined as crater-like or cone-shaped depressions on the seafloor occurring in soft, fine-grained surface sediments, which are commonly characterized by U- or V-shaped geometry in seismic and bathymetric images. These pockmarks vary in sizes that can be

characterized as “unit pockmark” (1-10 m wide, <0.6 m deep) to “normal pockmark” (10 to 700 m wide, up to 45 m deep) (Fig. 1.12; King and MacLean, 1970; Hovland and Judd, 1988; Hovland et al., 2002; Duarte et al., 2017; de Prunelé et al., 2017). Pockmarks can be strong indicators of gas that can be related to depressurization of gas hydrates from the subsurface caused by overpressure and sediment collapse (Serié et al., 2012; 2017). Deeply rooted gas chimneys are commonly found beneath pockmarks, which indicate leaking reservoir.

Gas chimneys commonly appear to have columnar or conic geometry and are recognized as acoustic blank zones, amplitude blanking, turbulent zones, ambiguous zones, with sometimes notable pull-up or push-down reflections, which possibly indicate gas-saturated sediments or free gas occurrence that generate localized velocity anomalies (Gay et al., 2006b; Dixit and Mandal, 2020; Ma et al., 2021). Gay et al. (2007) provided evidence of fluid flow by investigating pockmarks that are related to tectonic features (e.g., faults and salt diapirs), erosional surfaces (e.g., active canyons and paleocanyons), and buried sedimentary bodies (e.g., shallow- and deep-buried paleochannels) in the Lower Congo Basin. They also concluded that these are fluid related pockmarks and found that such erosional surfaces may have allowed fluids to migrate laterally and vertically. In addition, they found that shallow- and deep-buried turbiditic channels may also have acted as conduits or as intermediate reservoir that focused fluid flow before seeping through the seafloor (Fig. 1.14).

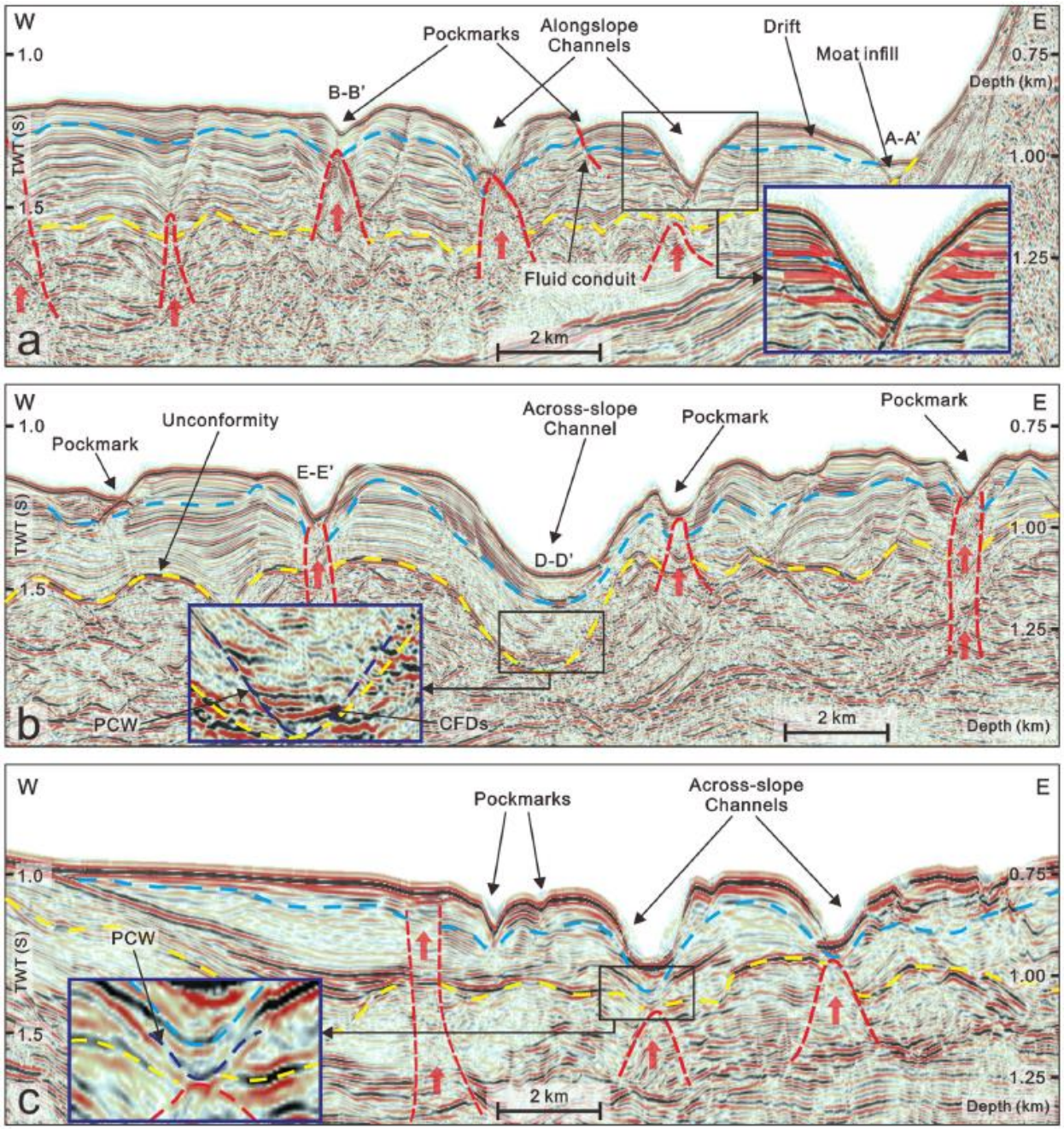

Figure 1.12. Interpreted representative seismic profiles from two-dimensional seismic data acquired from the western South China Sea. These profiles show the architecture of investigated pockmarks and several features related to slope-processes such as along-slope channels, sediment drift, and moat infill. Blue and yellow dashed lines represent base of Quaternary and Pliocene strata, respectively. Several fluid migration conduits are also interpreted in red dashed lines and red vertical arrows. PCW = Paleo-channel wall; CFDs = Channel-fill deposits (from Yu et al., 2021).

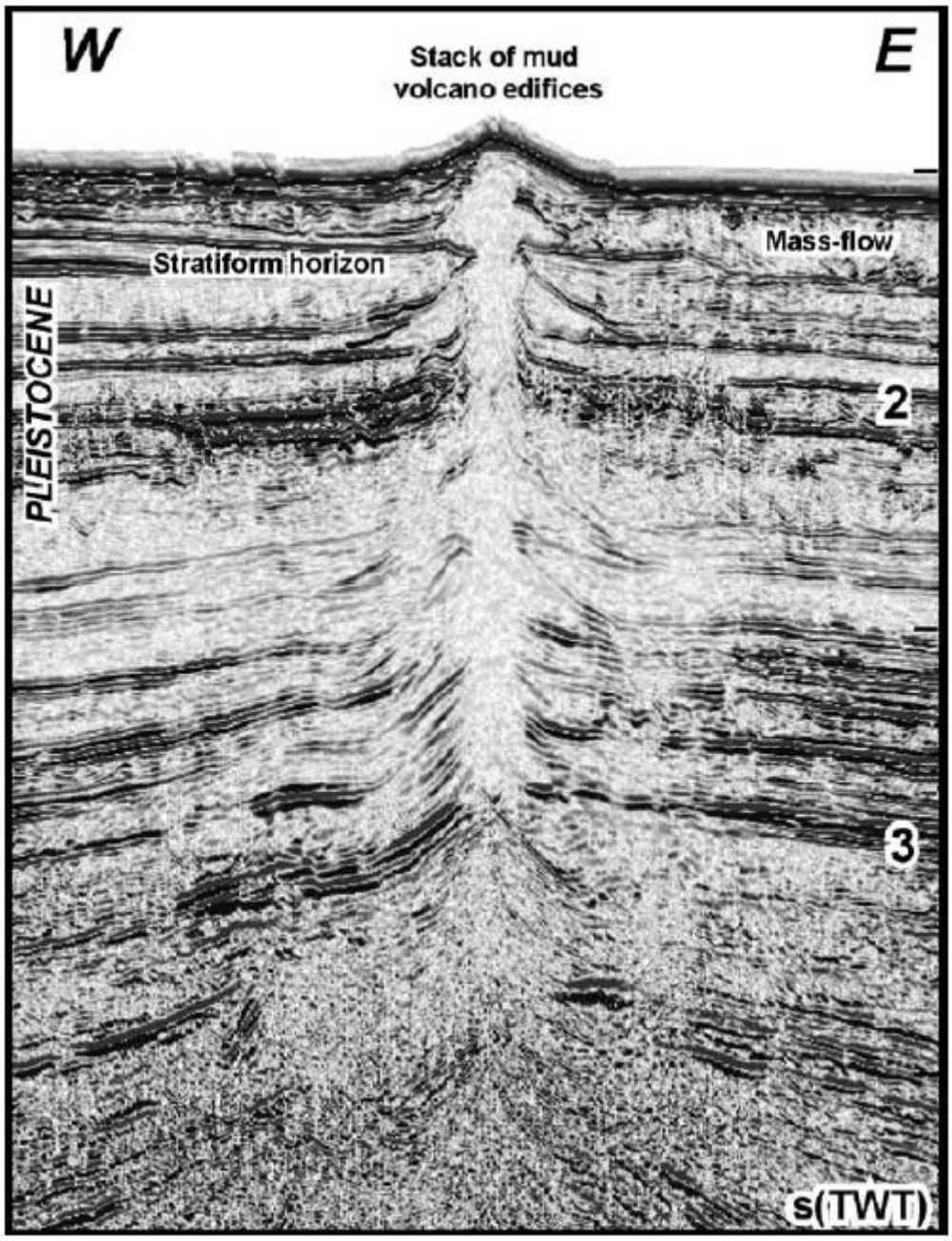

Figure 1.13. Example of mud volcano shown in seismic profile situated in the eastern offshore Trinidad. Migration of fluids is illustrated in low amplitude, semi-transparent, weakly chaotic reflectors, forming a mound at the seafloor. Velocity pull-ups are apparent that also suggest vertical fluid migration. The mud volcano is draped by the surrounding Pleistocene sediments and notable mass transport flows (from Deville et al., 2006).

Mound features such as mud diapirs and mud volcanoes are also common seep-type related features (Figs. 1.13-1.14). Significant quantities of discharging methane through unconsolidated,

fine-grained sediments such as mud will result in decreased mud density, increased buoyancy forces within the structure of the diapirs and increased entraining of sediments that will eventually result in the formation of mud diapirs and mud volcanoes. A mud diapir does not protrude through overburden to be exposed on the seafloor. Instead, a mud volcano occurs when shallow mud layers are saturated with fluids that are migrating upward, then commonly erupt on the seafloor. After the eruption on the seafloor by the seeping fluids, the muddy sediments get deposited. Both features appear to have dome-like or mound structure on and underneath the seafloor (Reed et al., 1990; Kopf, 2002; He et al., 2016).

However, other mechanism also play a role in mud diapirsm and mud volcanism, such as existence of tectonic faults that constitute preferential migration pathways for the subsurface fluids (Hovland and Curzi, 1989; Brown, 1990; Reed et al., 1990; Kopf, 2002; Talukder et al., 2007; Chen et al., 2010). All the mentioned structures can be presently active or can be inactive and buried in the subsurface, recording past activity (e.g., paleo-pockmarks).

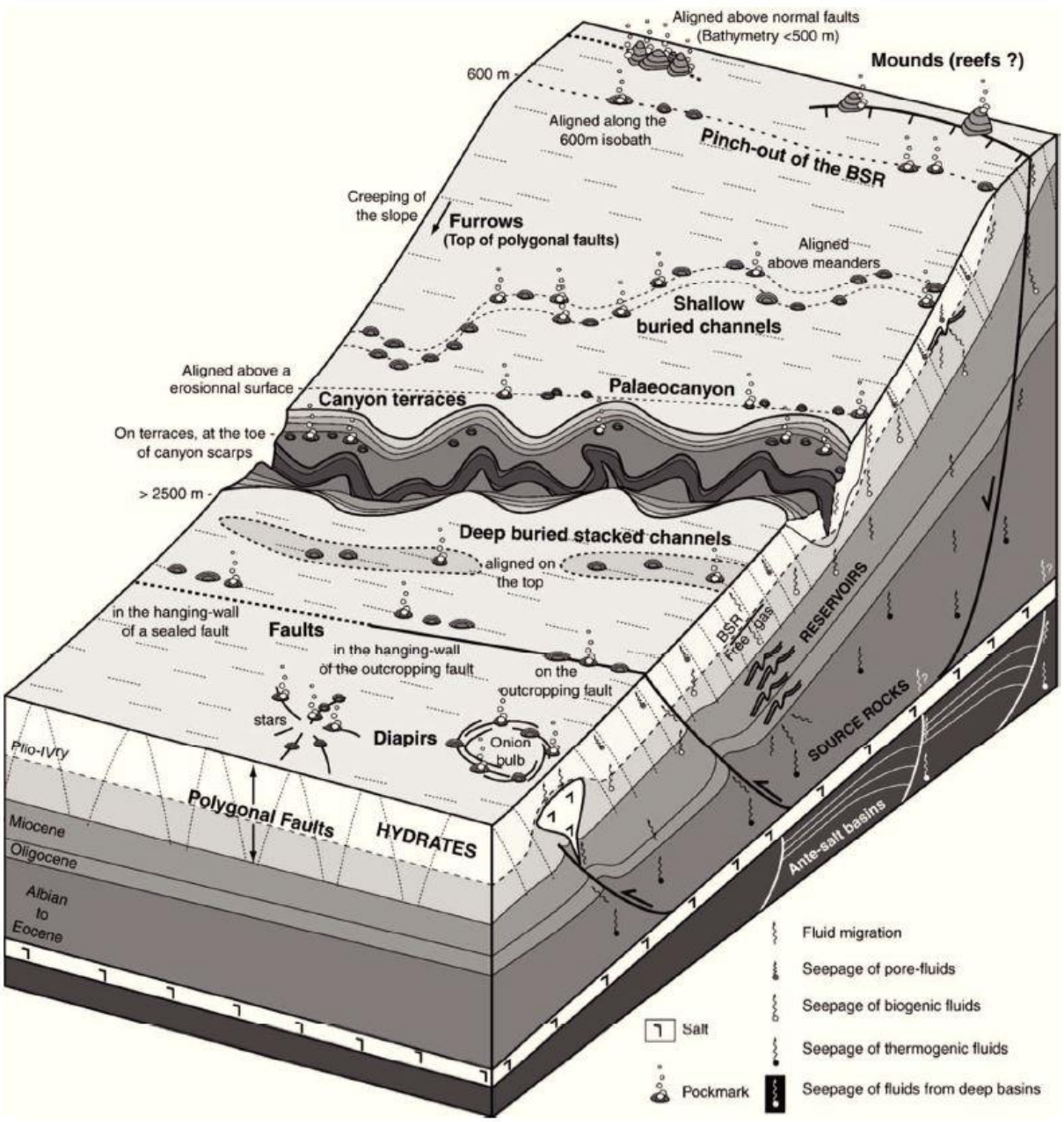

Figure 1.14. Simplified conceptual 3D diagram showing common features of seep-related seafloor morphology such as pockmarks related to tectonic features (faults and salt diapirs), pockmarks related to erosional surfaces (active canyons and paleocanyons), and pockmarks related to buried sedimentary bodies (shallow- and deep-buried paleochannels). This diagram also shows major migration pathways and erosional features. This diagram shows possibly source and reservoir rocks, which are contributing to the flow of fluids to the surface (from Gay et al., 2007).

1.10. Works cited

Adam, J., and Krezsek, C. (2012). Basin-scale salt tectonic processes of the Laurentian Basin, Eastern Canada: insights from integrated regional 2D seismic interpretation and 4D physical experiments. *The Geological Society of London, 363*, 331–360.

Albertz, M., Beaumont, C., Shimeld, J. W., Ings, S. J., and Gradmann, S. (2010). An investigation of salt tectonic structural styles in the Scotian Basin, offshore Atlantic Canada: 1. Comparison of observations with geometrically simple numerical models. *Tectonics, 29*, 1–29.

Alsadi, H. N. (2017). The Seismic Reflection Signal. In R. Swennen and K. U. Leuven (Eds.), Advances in Oil and Gas Exploration & Production. Springer, Cham. Retrieved from https://link.springer.com/chapter/10.1007/978-3-319-40436-3_6#citeas.

Amos, C. L., and Knoll, R. G. (1987). The Quaternary sediments of Banquereau, Scotian Shelf. *Geological Society of America Bulletin,* 244–260.

Amos, C. L., and Miller, A. A. L. (1990). The Quaternary stratigraphy of southwest Sable Island Bank, eastern Canada. *Geological Society of America Bulletin, 102*, 915–934.

Andresen, K. J., Huuse, M., Schødt, N. H., Clausen, L., and Seidler, L. (2011). Hydrocarbon plumbing systems of salt minibasins offshore Angola revealed by three-dimensional seismic analysis. *American Association of Petroleum Geologists Bulletin, 95*, 1039–1065.

Argentino, C., Waghorn, K. A., Vadakkepuliyambatta, S., Polteau, S., Bünz, S., and Panieri, G. (2021). Dynamic and history of methane seepage in the SW Barents Sea: new insights from Leirdjupet Fault Complex. *Scientific Reports, 11 (4373)*, 1–13.

Bertram, G. T., Milton, N. J. (1996). Seismic stratigraphy. In D. Emery and K. J. Meyers (Eds.), Sequence stratigraphy: Blackwell Scientific, 45–60.

Boruah, A., Verma, S., Rasheed, A., Gairola, G. S., and Gogoi, A. (2022). Macro-seepage based potential new hydrocarbon prospects in Assam-Arakan Basin, India. *Scientific Reports, 12 (2273)*, 1–15.

Brown, A. R. (2011). Interpretation of three-dimensional seismic data. *AAPG Memoir, 42*, 1–309.

Brown, K. M. (1990). The Nature and Hydrogeologic Significance of Mud Diapirs and Diatremes for Accretionary Systems. *Journal of Geophysical Research, 95 (B6)*, 8969–8982.

Campbell, D. C. (2011). *The Late Cretaceous and Cenozoic Geological History of the Outer Continental Margin off Nova Scotia, Canada: Insights into Margin Evolution from a Mature Passive Margin* (PhD thesis). Dalhousie University, Halifax, NS.

Campbell, D. C. and Deptuck, M. E. (2012). Alternating bottom-current-dominated and gravity-flow-dominated deposition in a lower slope and rise setting – Insights from the seismic geomorphology of the western Scotian Margin, Eastern Canada. *Applications of the Principles of Seismic Geomorphology to Continental-Slope and Base-of-Slope Systems: Case Studies from Seafloor and Near-Seafloor Analogues.* SEPM, Special Publication No. 99, 329–346.

Campbell, D. C. and Mosher, D. C. (2016). Geophysical evidence for widespread Cenozoic bottom current activity from the continental margin of Nova Scotia, Canada. *Marine Geology,* 237–260.

Campbell, D. C., Shimeld, J., Deptuck, M. E., and Mosher, D. C. (2015). Seismic stratigraphic framework and depositional history of a large Upper Cretaceous and Cenozoic depocenter off southwest Nova Scotia, Canada. *Marine and Petroleum Geology, 65*, 22-42.

Canada-Nova Scotia Offshore Petroleum Board. (2000). *Technical Summaries of Scotian Shelf* (Significant and Commercial Discoveries status offshore Nova Scotia Resource Assessment Report), 1–212.

Catuneanu, O., Abreu, V., Bhattacharya, J. P., Blum, M. D., Dalrymple, R. W., Eriksson, P. G., Fielding, C. R., Fisher, W. L., Galloway, W. E., Gibling, M. R., Giles, K. A., Holbrook, J. M., Jordan, R., Kendall, C. G. St. C., Macurda, B., Martinsen, O. J., Miall, A. D., Neal, J. E., Nummedal, D., Pomar, L., Posamentier, H. W., Pratt, B. R., Sarg, J. F., Shanley, K. W., Steel, R. J., Strasser, A., Tucker, M. E., and Winker, C. (2009). Towards the standardization of sequence stratigraphy. *Earth-Science Reviews, 92*, 1–33.

Chapman, R., Pohlman, J., Coffin, R., Chanton, J., and Lapham, L. (2004). Thermogenic gas hydrates in the northern Cascadia margin: *Eos, Transactions, American Geophysical Union, 85 (38)*, 361–368.

Chavez, I., Piper, D. J. W., and Pe-Piper, G. (2018). Correlation of the Aptian Naskapi Member of the Scotian Basin and its regional implications. *Canadian Journal of Earth Sciences, 55 (5)*, 514–535.

Chavez, I., Piper, D. J. W., Pe-Piper, G., and Zhang, Y. (2016). North Atlantic climatic events recorded in Aptian Naskapi Member cores, Scotian Basin. *Cretaceous Research, 60*, 297–307.

Chen, S-C., Hsu, S-K., Tsai, C-H., Ku, C-Y., Yeh, Y-C., and Wang, Y. (2010). Gas seepage, pockmarks and mud volcanoes in the near shore of SW Taiwan. *Marine Geophysical Research, 31*, 133–147.

Chen, Z., Li, Y., Liu, Z., Zheng, G., Xu, W., Yan, W., and Yi, L. (2019). CH_4 and CO_2 Emissions From Mud Volcanoes on the Southern Margin of the Junggar Basin, NW China: Origin, Output, and Relation to Regional Tectonics. *Journal of Geophysical Research: Solid Earth, 124*, 5030–5044.

Chopra, S., and Murfurt, K. J. (2007). Seismic attributes for prospect identification and reservoir characterization: SEG Geophysical Developments No. 11.

Christians, A. (2015). *Late Cretaceous to Cenozoic Reactivation of Central Scotian Slope Salt Bodies and the Impact on Slope Depositional Systems* (MSc thesis). Dalhousie University. Halifax, NS.

Cox, D. R., Huuse, M., Newton, A. N. W., Sarkar, A. D., and Knutz, P. C. (2021). Shallow gas and gas hydrate occurrences on the northwest Greenland shelf margin. *Marine Geology, 432*, 1–21.

Crutchley, G.J., Pecher, I. A., Gorman, A. R., Henrys, S. A., and Greinert, J. (2010). Seismic imaging of gas conduits beneath seafloor seep sites in a shallow marine gas hydrate province, Hikurangi Margin, New Zealand. *Marine Geology*, *272*, 114–126.

Cummings, D. I., and Arnott, R. W. C. (2005). Growth-faulted shelf-margin deltas: a new (but old) play type, offshore Nova Scotia. *Bulletin of Canadian Petroleum Geology, 53 (3),* 211–236.

Cummings, D. I., Hart, B. S., and Arnott, R. W. C. (2006). Sedimentology and stratigraphy of a thick, areally extensive fluvial-marine transition, Missisauga Formation, offshore Nova Scotia, and its correlation with shelf margin and slope strata. *Bulletin of Canadian Petroleum Geology, 54 (2),* 152–174.

Cunningham, R., and Lindholm, R. M. (2000). Seismic evidence for widespread gas hydrate formation, offshore west Africa. In M. R. Mello, and B. J. Katz (Eds.), *Petroleum Systems of South Atlantic Margins*. American Association of Petroleum Geologists Memoir 73, pp. 93–105.

de Mahiques, M. M., Schattner, U., Lazar, M., Sumida, P. Y. G., de Souza, L. A. P. (2017). An extensive pockmark field on the upper Atlantic margin of Southeast Brazil: spatial analysis and its relationship with salt diapirism. *Heliyon, e00257*, 1–21.

de Prunelé, A., Ruffine, L., Riboulot, V., Peters, C. A., Croguennec, C., Guyader, V., Pape, T., Bollinger, C., Bayon, G., Caprais, J-C., Germain, Y., Donval, J-P., Marsset, T., Bohrmann, G., Géli, L., Rabiu, A., Lescanne, M., Cauquil, E., and Sultan, N. (2017). Focused hydrocarbon migration in shallow sediments of a pockmark cluster in the Niger Delta (Off Nigeria). *Geochemistry, Geophysics, Geosystems, 18*, 93–112.

Deptuck, M. E. (2010). The "slope detachment zone" on the western Scotian Slope, offshore Nova Scotia: Structural style, timing, and implications for margin evolution. *Central and North Atlantic Conjugate Margins, IV*, 87–95.

Deptuck, M. E. (2011). *Proximal to distal postrift structural provinces of the western Scotian Margin, offshore Eastern Canada: Geological context and parcel prospectivity for Call for Bids NS11-1* (CNSOPB Geoscience Open File Report, 2011-001MF, 42 p.). Halifax, NS: Canada Nova Scotia Offshore Petroleum Board.

Deptuck, M. E., and Campbell, D. C. (2012). Widespread erosion and mass failure from the ~51 Ma Montagnais marine bolide impact off southwestern Nova Scotia, Canada. *Canadian Journal of Earth Sciences, 49*, 1567–1594.

Deptuck, M. E., and Kendell, K. L. (2017). A Review of Mesozoic-Cenozoic Salt Tectonics Along the Scotian Margin, Eastern Canada. In J. Soto, J. F. Flinch, and G. Tari (Eds.), *Permo-Triassic Salt Provinces of Europe, North Africa, and the Atlantic Margins* (Ch. 13, pp. 287–312). Amsterdam, Netherlands: Elsevier.

Deptuck, M. E., Kendell, K., Brown, D. E., and Smith, B. M. (2014). *Seismic stratigraphic framework and structural evolution of the eastern Scotian Slope: geological context for the NS14-1 Call for Bids area, offshore Nova Scotia* (CNSOPB Geoscience Open File

Report, 2014-001MF, 58 p.). Halifax, NS: Canada-Nova Scotia Offshore Petroleum Board.

Dixit, A., and Mandal, A. (2020). Detection of gas chimney and its linkage with deep-seated reservoir in poseidon, NW shelf, Australia from 3D seismic data using multi-attribute analysis and artificial neural network approach. *Journal of Natural Gas Science and Engineering, 83 (10356)*, 1–18.

Duarte, D., Magalhães, V. H., Terrinha, P., Ribeiro, C., Madureira, P., Pinheiro, L. M., Benazzouz, O., Kim, J-H., and Duarte, H. (2017). Identification and characterization of fluid escape structures (pockmarks) in the Estremadura Spur, West Iberian Margin. *Marine and Petroleum Geology, 82*, 414–423.

Fowler, M., Webb, J., Obermajer, M., Monnier, F., Mort, A., Luheshi, M., and MacDonald, A. (2016). Petroleum Systems of the Scotian Basin. *AAPG Annual Convention and Exhibition, Oral Presentation*. Calgary, Alberta: Canada.

Fowler, M., Webb, J., Olsen, H., Ashraf, F., and Guldbrandsen, S. (2017). Geochemistry Data Report for 2016 Scotian Slope Piston Coring Program. *Applied Petroleum Technology*, 1-310. APT Canada Ltd.

Fowler, M. (2017). Piston Core Geochemistry – Final Report. *Applied Petroleum Technology*, 1-4. APT Canada Ltd.

Fowler, M., Webb, J., Gulbrandsen, S., Austnes, L-K, and Ashraf, F. (2019). Geochemistry Data Report for 2018 Scotian Slope Coring Program. *Applied Petroleum Technology*, 1-306. APT Canada Ltd.

Fowler, M. (2020). Geochemical Evidence for Multiple Source Rocks on the Scotian Shelf. *Applied Petroleum Technology*, 1-254. APT Canada Ltd.

Galbraith, M. (2001). 3D Seismic Surveys – Past, Present and Future. *CSEG Recorder, 26 (6)*, 1-9.

Gay, A., Lopez, M., Berndt, C., and Séranne, M. (2007). Geological controls on focused fluid flow associated with seafloor seeps in the Lower Congo Basin. *Marine Geology, 244*, 68–92.

Gay, A., Lopez, M., Cochonat, P., Séranne, M., Levaché, D., and Sermondadaz, G. (2006b). Isolated seafloor pockmarks linked to BSRs, fluid chimneys, polygonal faults and stacked Oligocene–Miocene turbiditic palaeochannels in the Lower Congo Basin. *Marine Geology, 226*, 25–40.

Geletti, R., Del Ben, A., Busetti, M., Ramella, R., and Volpi, V. (2008). Gas seeps linked to salt structures in the Central Adriatic Sea. *Basin Research, 20*, 473–487.

Gipp, M. R. (1994). Late Wisconsinan deglaciation of Emerald Basin, Scotian Shelf. *Canadian Journal of Earth Sciences, 31*, 554-566.

Hansen, D. M., Shimeld, J. W., Williamson, M. A., and Lykke-Andersen, H. (2004). Development of a major polygonal fault system in Upper Cretaceous chalk and Cenozoic mudrocks of the Sable Subbasin, Canadian Atlantic margin. *Marine and Petroleum Geology, 21*, 1205–1219.

Haq, B. U., Hardenbol, J., and Vail, P. R. (1987). Chronology of Fluctuating Sea Levels Since the Triassic. *Science, 235 (4793)*, 1156–1167.

He, J., Wang, S., Zhang, W., Yan, W., and Lu, Z. (2016). Characteristics of mud diapirs and mud volcanoes and their relationship to oil and gas migration and accumulation in a marginal basin of the northern South China Sea. *Environmental Earth Science, 75 (1122)*, 1–12.

Herron, D. A. (2011). First Steps in Seismic Interpretation. *Geophysical Monograph Series No. 16*, Society of Exploration Geophysicists.

Hovland, M., and Curzi, P. V. (1989). Gas seepage and assumed mud diapirism in the Italian central Adriatic Sea. *Marine and Petroleum Geology, 6*, 161–169.

Hovland, M., and Judd, A. G. (1988). Seabed Pockmarks and Seepages: Impact on Geology, Biology, and the Marine Environment. Graham and Trotman, London, U. K. Retrieved from http://dx.doi.org/10.13140/RG.2.1.1414.1286.

Hovland, M., Gardner, J. V., and Judd, A. G. (2002). The significance of pockmarks to understanding the fluid flow processes and geohazards. *Geofluids, 2*, 127–136.

Howard, M. (2007). Marine seismic surveys with enhanced azimuth coverage: Lessons in survey design and acquisition. *The Leading Edge, 26 (4)*, 480-493.

Hudec, M. R., and Jackson, M. P. A. (2006). Growth of allochthonous salt sheets in passive margins and orogens. *AAPG Bulletin, 90*, 1535–1564.

Hudec, M. R. and Jackson, M. P. A. (2007). Terra infirma: Understanding salt tectonics. *Earth Science Reviews, 82*, 1–28.

Hudec, M. R. and Jackson, M. P. A. (2011). The Salt Mine: a Digital Atlas of Salt Tectonics. *AAPG Memoir, 99*, 305.

Hutchinson, D. K., Coxall, H. K., O'Regan, M., Nilsson, J., Caballero, R., and de Boer, A. M. (2019). Arctic closure as a trigger for Atlantic overturning at the Eocene-Oligocene Transition. *Nature Communications, 10 (3797)*, 1-9.

Ibrahim, A. A. M. (2015). *Separating Simultaneous Seismic Sources using Robust Inversion of Radon and Migration Operators* (PhD thesis). University of Alberta, Edmonton, AB.

Ings, S. J., and Shimeld, J. W. (2006). A new conceptual model for the structural evolution of a regional salt detachment on the northeast Scotian margin, offshore eastern Canada. *The American Association of Petroleum Geologists Bulletin, 90 (9)*, 1407–1423.

Jackson, M. P. A., and Hudec, M. R. (2017). Salt Tectonics: Principles and Practice (Part II), 1-498. Cambridge, UK: Cambridge University Press.

Jackson, M. P. A., Vendeville, B. C., and Schultz-Ela, D. D. (1994). Structural dynamics of salt systems. *Annual Review of Earth Planet Science, 22*, 9–117.

Kendell, K. L. (2012). Variations in salt expulsion style within the Sable Canopy Complex, central Scotian margin. *Canadian Journal of Earth Sciences, 49*, 1504–1522.

Kidston, A. G., Brown, D. E., Altheim, B., and Smith, B. M. (2002). Hydrocarbon potential of the deep-water Scotian slope. *Canada-Nova Scotia Offshore Petroleum Board Open Report*, 1–111.

Kidston, A. G., Brown, D. E., Smith, B. M. and Altheim, B. (2005). *The Upper Jurassic Abenaki Formation, Offshore Nova Scotia: A Seismic and Geologic Perspective*. (CNSOPB Open Report, 168 p.). Halifax, NS: Canada-Nova Scotia Offshore Petroleum Board.

Kidston, A. G., Smith, B. M., Brown, D. E., Makrides, C., and Altheim, B. (2007). Nova Scotia deepwater post-drill analysis 1982-2004. *Canada-Nova Scotia Offshore Petroleum Board Open Report*, 1–182.

King, L. H., and MacLean, B. (1970). Pockmarks on the Scotian Shelf, *Geological Society of America Bulletin, 81*, 3141–3148.

Kopf, A. J. (2002). Significance of mud volcanism. *Reviews of Geophysics, 40 (2)*, 1-52.

Link, W. K. (1952). Significance of oil and gas seeps in world oil exploration. *AAPG Bulletin, 36*, 1505–1541.

Ma, G., Zhan, L., Lu, H., and Hou, G. (2021). Structures in Shallow Marine Sediments Associated with Gas and Fluid Migration. *Journal of Marine Science and Engineering, 9 (396)*, 1–26.

MacDonald, A. W. (2006). *Cenozoic seismic stratigraphy of the Central Nova Scotian Continental Margin: The interplay of erosion, deposition, and salt tectonics* (MSc thesis). Saint Mary's University, Halifax, NS.

Macgregor, D. S. (1993). Relationships between seepage, tectonics, and subsurface petroleum reserves. *Marine and Petroleum Geology, 10 (6)*, 606–619.

Mauduit, T., Gaullier, V., and Brun, J. P. (1997). On the asymmetry of turtle-back growth anticlines. *Marine and Petroleum Geology, 14 (7/8)*, 763–771.

McIver, N. L. (1972). Cenozoic and Mesozoic Stratigraphy of the Nova Scotia Shelf. *Canadian Journal of Earth Sciences, 9 (1)*, 54–70.

Miller, K. G., Kominz, M. A., Browning, J. V., Wright, J. D., Mountain, G. S., Katz, M. E., Sugarman, P. J., Cramer, B. S., Christie-Blick, N., and Pekar, S. F. (2005). The Phanerozoic Record of Global Sea-Level Change. *Science, 310 (5752)*, 1293–1298.

Mitchum, R. M., Vail, P. R., Sangree, J. B. (1977a). Seismic stratigraphy and global changes of sea level, part 6: stratigraphic interpretation of seismic reflection patterns in depositional sequences. *AAPG Memoir, 26*, 117–135.

Mitchum, R. M., Vail, P. R., Thompson III, S. (1977b). Seismic stratigraphy and global changes of sea level, part 2: the depositional sequence as a basic unit for stratigraphic analysis. *AAPG Memoir, 26*, 53–63.

Mukhopadhyay, P. K. (2006). *Evaluation of the petroleum systems by 1D and 2D numerical modeling and geochemical analysis in the area of most recent exploration wells on the deepwater Scotian Slope, offshore Nova Scotia*. (NSDoEM Final Report 60127404, 485 p.). Halifax, NS: Nova Scotia Department of Energy and Mines.

Mukhopadhyay, P. K., Brown, D. E., Kidston, A. G., Bowman, T. D., Faber, J., and Harvey, P. J. (2003). Petroleum Systems of Deepwater Scotian Basin, Eastern Canada: Challenges for Finding Oil versus Gas Provinces. *Offshore Technology Conference (OTC 15304)*, 1–11.

Offshore Energy Research Association. (2011). *Play Fairway Analysis Atlas*. Retrieved from https://oera.ca/research/play-fairway-analysis-atlas.

Peel, F. J. (2014). How do salt withdrawal minibasins form? Insights from forward modelling, and implications for hydrocarbon migration. *Tectonophysics, 630*, 222–235.

Perrodon, A. (1983) Dynamics of oil and gas accumulations. *Bull. Centre Expl. Prod. Res., Elf Aquitaine, Mem. 5*.

Piper, D. J. W. (2000). Pleistocene ice outlets on the central Scotian Slope, offshore Nova Scotia. Geological Survey of Canada, Current Research 2000-D7, 1–8.

Piper, D. J. W., and Aksu, A. E. (1987). The Source and Origin of the 1929 Grand Banks Turbidity Current Inferred from Sediment Budgets. *Geo-Marine Letters, 7*, 177–182.

Piper, D. J. W., Mosher, D. C., and Newton, S. (2002). Ice-margin seismic stratigraphy of the central Scotian Slope, eastern Canada. Geological Survey of Canada, Current Research 2002-E16, 1–16.

Piper, D. J. W., Normark, W. R., and Sparkes, R. (1987). Late Cenozoic stratigraphy of the central Scotian Slope, Eastern Canada. *Bulletin of Canadian Petroleum Geology, 35*, 1–11.

Posamentier, H. W., Davies, R. J., Cartwright, J. A., and Wood, L. (2007). Seismic geomorphology – an overview. In R. J. Davies, H. W. Posamentier, L. J. Wood, and J. A. Cartwright (Eds.), *Seismic Geomorphology* (vol. 277, pp. 1–14). Geological Society of London Special Publication.

Posamentier, H. W. and Kolla, V. (2003). Seismic geomorphology and stratigraphy of depositional elements in deep-water settings. *Journal of Sedimentary Research, 73 (3)*, 367–388.

Powell, T. G. (1982). Petroleum geochemistry of the Verrill Canyon Formation: A source for Scotian Shelf hydrocarbons. *Bulletin of Canadian Petroleum Geology, 30*, 167-179.

Powell, T. G., and Snowdon, L. R. (1979). Geochemistry of crude oils and condensates from the Scotian Basin, Offshore eastern Canada. *Bulletin of Canadian Petroleum Geology, 27*, 453-466.

Tedesco, S.A. (1995). Concepts of Microseepage. In: Surface Geochemistry in Petroleum Exploration. Springer, Boston, MA. Retrieved from https://doi.org/10.1007/978-1-4615-2660-5_4.

Razaz, M., Iorio, D. D., Wang, B., Asl, S. D., and Thurnherr, A. M. (2020). Variability of a natural hydrocarbon seep and its connection to the ocean surface. *Scientific Reports, 10 (12654)*, 1–13.

Reed, D. L., Silver, E. A., Tagudin, J. E., Shipley, T. H., and Vrolijk, P. (1990). Relations between mud volcanoes, thrust deformation, slope sedimentation, and gas hydrate, offshore north Panama. *Marine and Petroleum Geology, 7*, 44–54.

Römer, M., Blumenberg, M., Heeschen, K., Schloemer, S., Müller, H., Müller, S., Hilgenfeldt, C., Barckhausen, U., and Schwalenberg, K. (2021). Seafloor Methane Seepage Related to

Salt Diapirism in the Northwestern Part of the German North Sea. *Frontiers in Earth Science, 9 (556329)*, 1–19.

Schenk, P. E. (1971). Southeastern Atlantic Canada, Northwestern Africa, and Continental Drift. *Canadian Journal of Earth Sciences, 8*, 1218–1251.

Schlumberger. (2015). Recommended Seismic Volume Attributes. Retrieved from https://www.software.slb.com/-/media/software-media-items/software/documents/external/product-sheets/petrel_recommended_seismic_volume_attributes_2015_poster.pdf

Serié, C., Huuse, M., and Schødt, N. H. (2012). Gas hydrate pingoes: Deep seafloor evidence of focused fluid flow on continental margins. *Geology, 40 (3)*, 207–210.

Serié, C., Huuse, M., Schødt, N. H., Brooks, J. M., and Williams, A. (2017). Subsurface fluid flow in the deep-water Kwanza Basin, offshore Angola. *Basin Research, 29*, 149–179.

Shimeld, J. (2004). A Comparison of Salt Tectonic Subprovinces Beneath the Scotian Slope and Laurentian Fan. In P. J. Post, D. L. Olson, K. T. Lyons, S. L. Palmes, P. F. Harrison, and N. C. Rosen (Eds.), *Salt Sediment Interactions and Hydrocarbon Prospectivity Concepts, Applications and Case Studies for the 21st Century*. SEPM Society for Sedimentary Geology.

Silva, R. L., Wong, C., and Wach, G. (2015). Source Rocks and Petroleum Systems of the Scotian Basin. *CSEG Recorder, 40 (8)*, 22–27.

Talukder, A. R., Bialas, J., Klaeschen, D., Buerk, D., Brueckmann, W., Reston, T., and Breitzke, M. (2007). High-resolution, deep tow, multichannel seismic and sidescan sonar survey of the submarine mounds and associated BSR off Nicaragua pacific margin. *Marine Geology*, *241*, 33–43.

Vail, P. R. (1987). Seismic Stratigraphy Interpretation Procedures. In A. W. Bally (Ed.), *Atlas of Seismic Stratigraphy*, AAPG Studies in Geology, Vol. 1, No. 27, 1–10.

Vail, P. R., Todd, R. G., and Sangree, J. B. (1977). Stratigraphic interpretation of seismic reflection patterns in depositional sequences. In C. E. Payton (Ed.), *Seismic stratigraphy – Applications to hydrocarbon exploration*. AAPG Memoir 26, 99–116.

Vermeer, G. J. O. (2012). 3D Seismic Survey Design (2nd edition). Society of Exploration Geophysicists. Retrieved from https://doi.org/10.1190/1.9781560803041.

Wade, J. A., Campbell, G. R., Procter, R. M., and Taylor, G. C. (1989). Petroleum Resources of the Scotian Shelf. *Geological Survey of Canada (Paper 88-19)*, 1–26.

Wade, J. A., and MacLean, B. C. (1990). The geology of the southeastern margin of Canada. In M. J. Keen and G. L. Williams (Eds.), *Geology of the continental margin of eastern Canada* (Ch. 5, pp. 167–238). Canada: Geological Survey of Canada.

Wade, J. A., MacLean, B. C., and Williams, G. L. (1995). Mesozoic and Cenozoic stratigraphy, eastern Scotian Shelf: new interpretations. *Canadian Journal of Earth Sciences, 32*, 1462–1473.

Wenau, S., Spiess, V., Pape, T., and Fekete, N. (2015). Cold seeps at the salt front in the Lower Congo Basin II: The impact of spatial and temporal evolution of salt-tectonics on hydrocarbon seepage. *Marine and Petroleum Geology, 67,* 880–893.

Weston, J. F., MacRae, R. A., Ascoli, P., Cooper, M. K. E., Fensome, R. A., Shaw, D., and Williams, G. L. (2012). A revised biostratigraphic and well-log sequence-stratigraphic framework for the Scotian Margin, offshore eastern Canada. *Canadian Journal of Earth Science, 49,* 1417–1462.

Wierzbicki, R., Dravis, J. J., Al-Aasm, I., and Harland, N. (2006). Burial dolomitization and dissolution of Upper Jurassic Abenaki platform carbonates, Deep Panuke reservoir, Nova Scotia, Canada. *The American Association of Petroleum Geologists Bulletin, 90 (11),* 1843–1861.

Withjack, M. O., Schlische, R. W., and Olsen, P. E. (2012). Development of the passive margin of Eastern North America: Mesozoic rifting, igneous activity, and breakup. In D. G. Roberts and A. W. Bally (Eds.), *Phanerozoic Rift Systems and Sedimentary Basins* (Ch. 13, pp. 301–335). Amsterdam, Netherlands: Elsevier.

Xu, G., and Haq, B. U. (2022). Seismic facies analysis: Past, present, and future. *Earth-Science Reviews, 224*, 1–30.

Yilmaz, Ö. (1987). Seismic Data Processing. *Investigations into Geophysics, No. 2*. Society of Exploration Geophysicists, Tulsa, Oklahoma.

Yilmaz, Ö. (2001). Seismic data analysis. *Investigations into Geophysics, No. 10.* Society of Exploration Geophysicists, Tulsa, Oklahoma.

Yu, K., Miramontes, E., Alves, T. M., Li, W., Liang, L., Li, S., Zhan, W., and Wu, S. (2021). Incision of submarine channels over pockmark trains in the South China Sea. *Geophysical Research Letters, 48*, 1–13.

Zachos, J., Pagani, M., Sloan, L., Thomas, E., and Billups, K. Trends, Rhythms, and Aberrations in Global Climate 65 Ma to Present. (2001). *Science, 292 (5517),* 686-693.

Zhao, H., Gao, J., and Peng, J. (2018). Properties of seismic absorption induced reflections. *Journal of Applied Geophysics, 152,* 118–128.

Chapter 2. Methodology

2.1. Tangier 3D Seismic Survey

BP Exploration Ltd. acquired four exploration licenses (Parcels 5 to 8; EL 2431-2434) from the Nova Scotia Call for Bids NS12-1 in the deep-water Scotian Slope. The data set used for this study was made available to the Nova Scotia Department of Natural Resources and Renewables (NSDNRR), following the data collection and processing by BP Exploration Ltd. in 2014. The 3D Tangier Wide Azimuth Towed Survey (WATS) was gathered with two streamer vessels, each towing twelve streamers that are 8 km long. The streamers were towed at a water depth of 15 m. 5085 in^3 airgun source arrays were towed by the other four source vessels at a 10 m water depth. The output grid/CDP bin spacing for the survey is 25 m × 25 m. Data were recorded at a 4 ms time sampling rate. The water depth within the survey area ranges from 1,540 m to 3,730 m.

Upon its completion, the 3D Tangier WATS (NS24-B71-1E; BP Tangier 3D WATS Final Report, 2014) covers ~ 8000 km^2 of area within the southwestern – central Scotian Slope. The seismic data was then processed with Tilted Transverse Isotropic (TTI) Reverse Time Migration (RTM) and Kirchhoff Pre-Stack Depth Migration (KPSDM) by Schlumberger Ltd. as a final deliverable (BP Data Processing Report, 2016; BP Tangier 3D Interpretation Report, 2016). The data were processed to zero-phase, with positive impedance contrast corresponding to a hard over soft reflection, which in the present work is rendered as black (positive peak) over white (negative trough).

The advantages of the Tangier 3D Seismic Survey versus the overlapping, older Thrumcap and Weymouth 3D surveys, which were collected and processed in the time domain, are improved imaging of salt and subsalt features, steeply inclined strata, and increased seaward coverage.

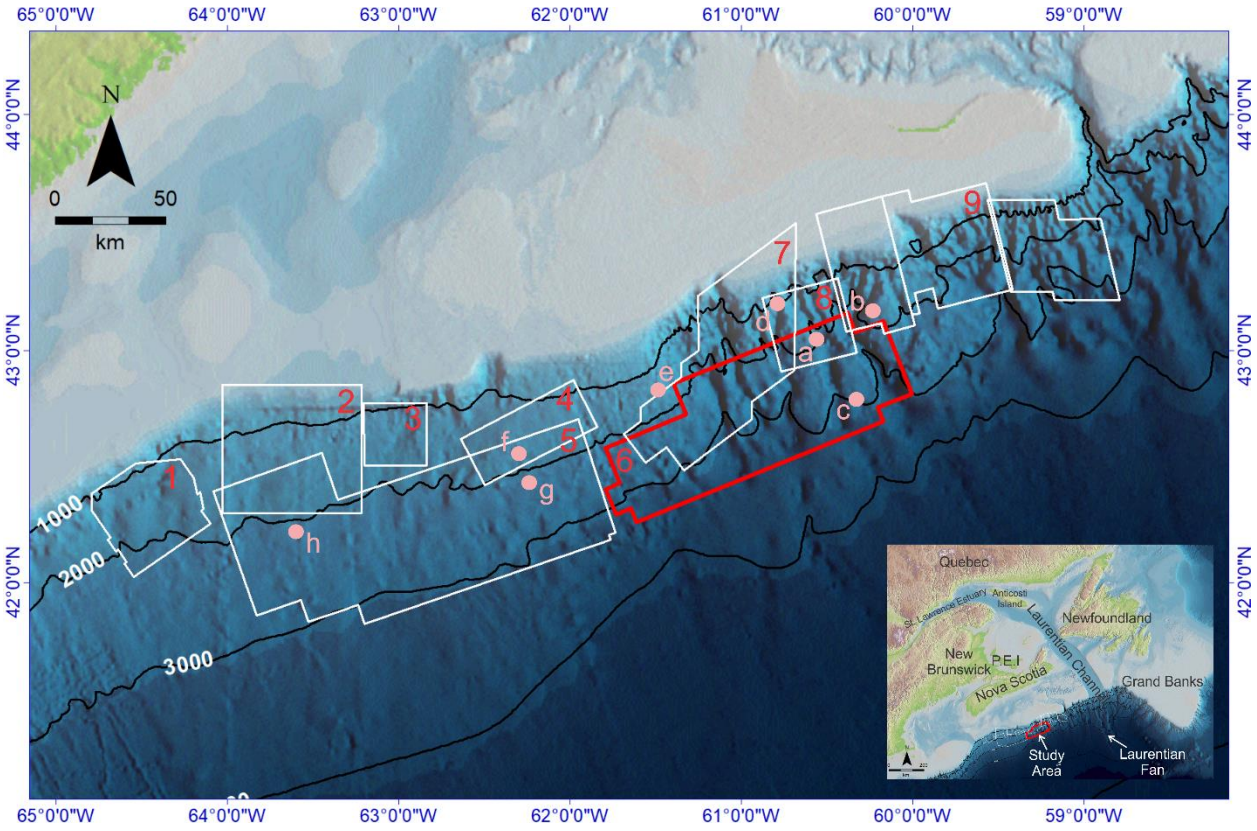

Figure 2.1. Close-up view of the geographical location of Tangier 3D area located on the Scotian Slope with an inset map showing the Tangier 3D area (red) relative to mainland Nova Scotia and the adjacent provinces. Scotian Slope seismic surveys: (1) Barrington 3D; (2) WG 3D; (3) Mamou 3D; (4) Torbrook 3D; (5) Shelburne 3D; **(6) Tangier 3D (study area)**; (7) Thrumcap 3D; (8) Weymouth 3D; (9) Veritas 3D. Locations of exploration wells near/within Tangier 3D: (a) Weymouth A-45; (b) Balvenie B-79; (c) Aspy D-11/D-11A; (d) Newburn H-23; (e) Shubenacadie H-100; (f) Torbrook C-15; (g) Cheshire L-97/L-97A; (h) Monterey Jack E-43/E-43A.

2.2. Well ties

Exploration wells provide ground-truthing of lithostratigraphy and allow production of geochemical and micropaleontological (biostratigraphy) surveys and geophysical logs, which collectively facilitate the reconstruction of depositional environments and age within penetrated rock intervals. When tied to geophysical surveys, these evaluations can be spatially extrapolated over larger areas to provide insight and context to the general regional subsurface geology of the

sedimentary basin. In this way, exploration wells allow for improved insight into the regional geology to thereby reduce exploration uncertainty. Several wells were incorporated in this thesis to track geologic ages based on biostratigraphy observations and lithological changes across the shallow buried strata of the Scotian Slope (Fig. 2.1).

For this thesis, the closest wells to the Tangier 3D Seismic Survey (e.g., Weymouth A-45, Balvenie B-79, Aspy D-11/D-11A) are presented to help tie to seismic. Other slope wells (e.g., Shubenacadie H-100, Newburn H-23, Torbrook C-15, Cheshire L-97/L-97A) were also used to confirm biostratigraphic ages where the mapped horizons lie at an approximate correlative stratigraphic level. Biostratigraphic ages were generally limited for Cenozoic strata for some wells due to limited study and lack of sample recovery of the rocks at the targeted depths during drilling (OERA, 2011; Weston et al., 2012; Campbell et al., 2015).

Wells located within the Tangier 3D area are discussed in detail in Chapter 3 along with their corresponding synthetic seismograms, well seismic sections, and lithology. Since the Tangier 3D Seismic Survey is already depth-converted data, the correlation of horizons to the well is relatively straightforward at shallow depths above the salt that are most relevant to this thesis. However, the processing velocities used in the original Tangier 3D volumes were clearly incorrect beneath the salt (e.g., at the Aspy D-11/D-11A area; BP Data Processing Report, 2016) due to incorrect assumptions about compaction and overpressure, which would result to a complex correlation at deeper depths. Moreover, since Balvenie B-79 is outside of the survey boundary by at least 100 m, it was projected inside the survey area for generating a seismic section where the well is penetrating (Fig. 3.3). The estimated uncertainty of the well ties is approximately ±50 m. All mapped horizons are shown in the well synthetic seismograms (Figs. 3.2-3.4).

2.3. Seismic interpretation and mapping

Mapping and interpretation of the survey for this study was accomplished at the NSDNRR using Schlumberger's Petrel E&P Software Platform v2019.1©. The workstation has basic specifications such as 96 GB RAM with an additional 3 TB Hard Drive. The Tangier 3D Seismic Survey is in SEG-Y format and its uncompressed format is 427 GB in size.

All generated maps and calculations were carried out on grids. Grid size and position was set as automatic from the input boundary, with a grid increment of 50m × 50m in the X and Y direction (Fig. 2.2). For local interpolation, ½ cell was set as influence radius with average of points as interpolation method, and point weighting. For global extrapolation, minimum curvature was set (Fig. 2.2).

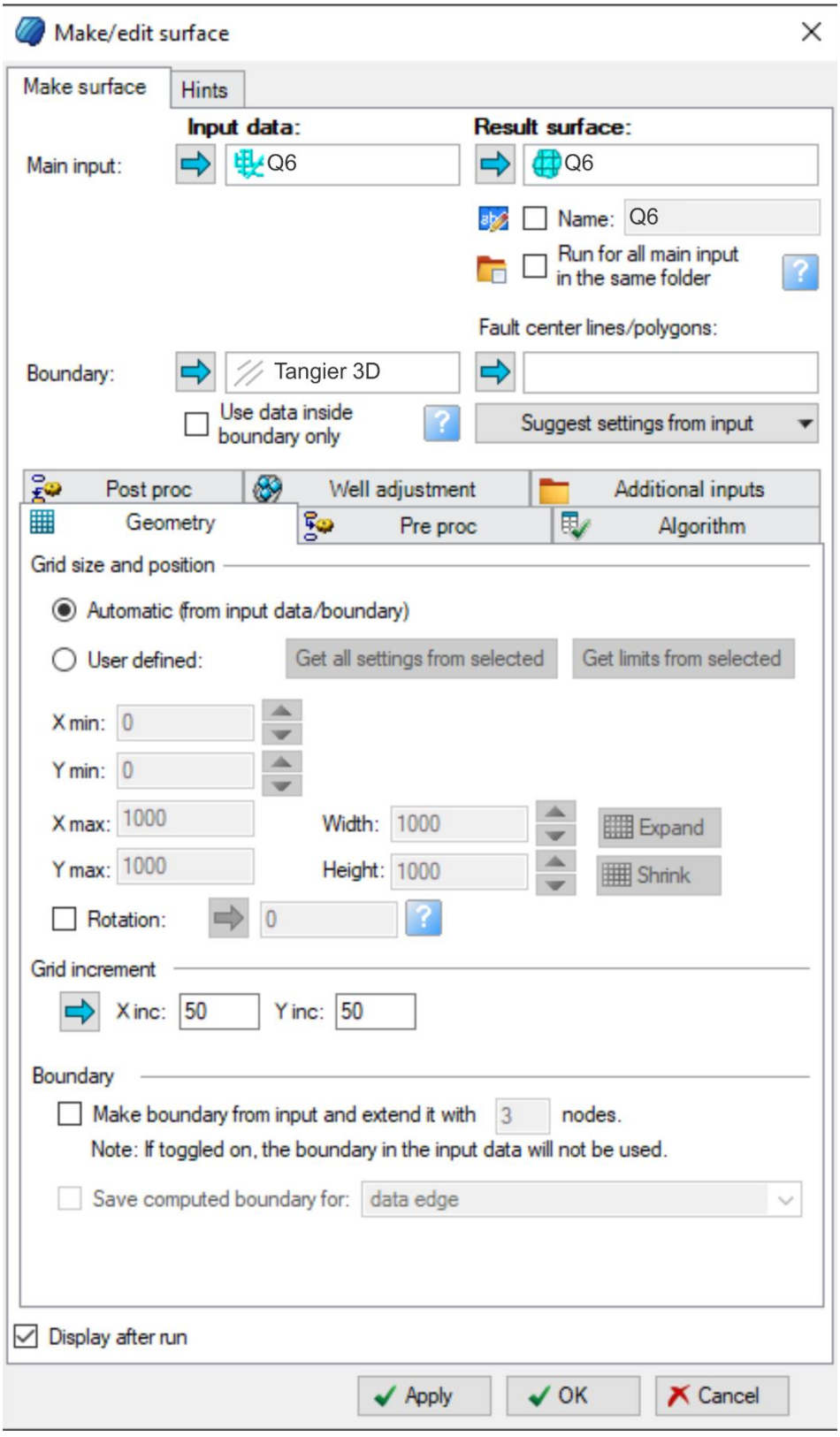
Make/edit surface
Make surface
Hints
Input data:
Result surface:
Main input:
Q6
Q6
Name:
Q6
Run for all main input in the same folder
Fault center lines/polygons:
Boundary:
Tangier 3D
Use data inside boundary only
Suggest settings from input
Post proc
Well adjustment
Additional inputs
Geometry
Pre proc
Algorithm
Grid size and position
Automatic (from input data/boundary)
User defined:
Get all settings from selected
Get limits from selected
X min:
0
Y min:
0
X max:
1000
Width:
1000
Expand
Y max:
1000
Height:
1000
Shrink
Rotation:
0
Grid increment
X inc:
50
Y inc:
50
Boundary
Make boundary from input and extend it with
3
nodes.
Note: If toggled on, the boundary in the input data will not be used.
Save computed boundary for:
data edge
Display after run
Apply
OK
Cancel

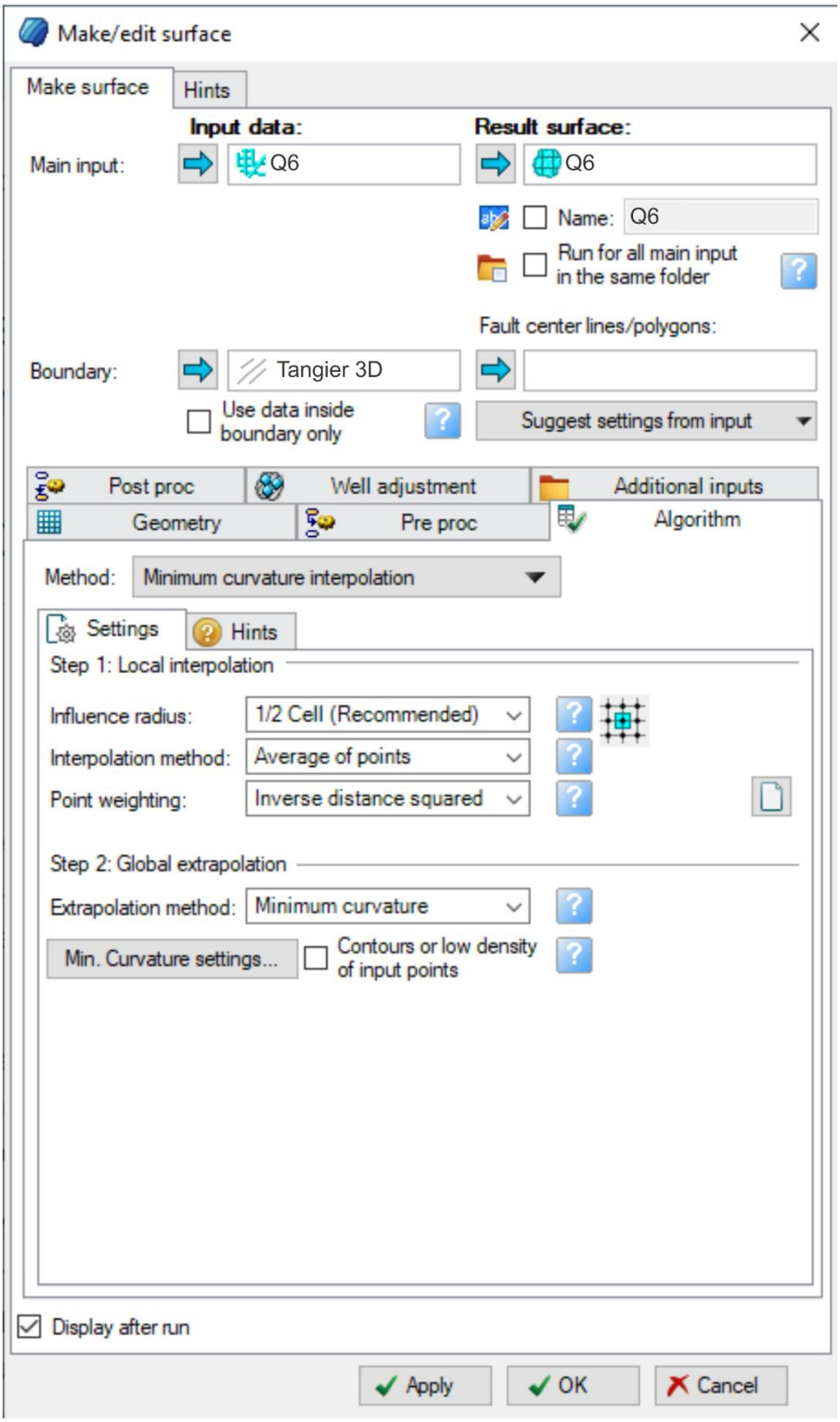

Figure 2.2. Gridding parameters for generation of surface maps for each horizon.

In Chapter 3, seismic horizons (labelled from P1 to N6) were mapped by the author based on regionally pervasive reflections with strong amplitude and later correlated to exploration wells (e.g., Balvenie B-79; Figs. 2.1; 3.3) to generate seven depth-structure maps from the Paleogene to the Neogene using the Kirchhoff Pre-Stack Depth Migration (KPSDM) volume for regional area mapping (up to 5000 mbsf), which will be discussed in detail in Chapter 3. KPSDM volume is known to be excellent in imaging complex structural areas, especially at shallow depths.

Seismic interpretation was based on a stratigraphic framework developed in this thesis for the Cenozoic by manually picking distinct reflections and then extending these surfaces laterally across the Tangier 3D volume and describing seismic facies units in between horizons.

Seismic facies classification involves the observational and interpretative analysis of seismic reflection parameters in terms of reflection configuration, geometry, continuity, amplitude, and frequency (Vail et al., 1977; Vail, 1987; Bertram and Milton, 1996). Coupled with the bounding relationships between seismic packages, such analysis permits the separation of a stratigraphic succession into logical units. The purpose of seismic facies analysis is to relate the changing appearance of seismic reflection packages to temporal changes in geology and depositional setting.

In this thesis, the seismic sequences bounded by mapped horizons were further classified into seismic units based on seismic facies (labelled Unit 1 to Unit 6). Chapter 4 features the Reverse Time Migration (RTM) volume, that is used for interrogation of deeper stratigraphic intervals (up to 10 km) of selected DHIs based on type of amplitude anomalies (e.g., bright spots, dim spots, flat spots, and gas chimneys) and their possible relation to the elements of a petroleum system. RTM volume has been known to be excellent data for imaging in and below areas with great structural and velocity complexities (e.g., areas with steep salt inclusions).

Deeper seismic horizons were correlated from existing studies to the Tangier 3D volume (e.g., OETR, 2011; Deptuck and Kendell, 2020) to find prospective source and reservoir rock intervals. The methodology in this chapter follows Chapter 3's seismic interpretation and seismic attribute analysis. However, Chapter 4 focuses more on the investigation of DHIs and their vicinity from the possible deeper source or reservoir rock intervals in order to track possible migration pathways and interpret trap and sealing mechanisms. To compliment the interpretation of possible migration pathways, a seismic section in TWT (s) (e.g., Figs. 4.11; 4.16) was also used from the Weymouth 3D survey (Fig. 2.1) for a DHI is at the edge of the Tangier 3D survey, where the imaging of the salt canopy was cut-off (e.g., Figs. 4.10; 4.15).

2.4. Seismic attribute analysis

Careful picking of reflections, in addition to automatic tracking of horizons (Herron, 2000), was performed where possible to ensure that the picked reflections yielded consistent and accurate representations of the horizons throughout the survey. Seismic attributes were then subsequently generated to enhance the visualization of the shallow subsurface stratigraphy and architectural features.

Amplitude attributes reflect the changes in geology because such attributes correspond to acoustic impedance (AI) contrasts that measure rock and fluid properties (Herron, 2011). The RMS amplitude is an attribute of reflection seismic that is based on the calculation of the square root of the sum of squared amplitudes divided by the number of samples within a specified window. This attribute is effective for detecting variations in amplitude, which could indicate lithological changes, presence of fluid overpressure, porosity, tuning effects of thinning beds. In slope environments, several sedimentary features such as turbidite channels and buried and

modern canyons can be revealed effectively by RMS amplitude (Brown, 1999; Chopra and Murfurt, 2007; Herron, 2011).

In Chapter 3, seven RMS amplitude maps were generated from mapped Paleogene (P1) and Neogene (N1-N6) horizons (see Appendix III). The horizons are named from stratigraphically oldest to youngest starting from P1 (~2000 mbsf), N1 (~1700 mbsf), N2 (~1500 mbsf), N3 (~1000 mbsf), N4 (~700 mbsf), N5 (~500 mbsf), and N6 (seafloor). These depths vary from the upper to the lower slope. A ±25 m search window interval was used for RMS amplitude calculation for each horizon.

For example, RMS extraction of the surface map of P1 on the depth of 2000 mbsf was produced by adding and subtracting 25 m above and below P1, creating a search window. This allows the algorithm to calculate amplitude values above and below a picked horizon. If anomalous amplitude values are within the given search window, it will appear on the generated RMS amplitude map. RMS amplitude maps are an excellent tool to reveal amplitude anomalies in seismic data such as shallow sands, buried channels, contourites, mass transport deposits (turbidites and slumps), and direct hydrocarbon indicators (DHIs; see Chapter 4) (Brown, 1999; Chopra and Murfurt, 2007; Herron, 2011).

Coherence attribute is an attribute of reflection seismic that is based on the continuity measurement between adjacent seismic traces in a specified window. High coherence values result from the similarity of amplitude and polarity of a seismic trace to its surroundings. Low coherence values are calculated when it is dissimilar. Coherence calculations (inverse or variance) enhance discontinuous features such as faults and fractures in the map extracted from the seismic volume. This attribute is also excellent for imaging channels, canyons, slope failure

scarps, growth faults, and other discontinuities. (Yilmaz, 1987; 2001; Brown, 1999; Chopra and Murfurt, 2007; Herron, 2011).

Contrary to RMS amplitude extraction, the search window interval for extracting coherence maps for each horizon was set to 0 m. This is to ensure that discontinuity features such as faulting are only highlighted on surface maps generated from horizons at depth and not from a window of amplitude values like in RMS amplitude. In this thesis, seven coherence slices were generated and produced from the interpreted horizons (P1 to N6; see Appendix IV) to understand and map different structural features within the survey at given approximate depths, as well as to identify faults (e.g., polygonal, radial, and crestal faults) caused by salt tectonics that could be potential migration pathways for deeply sourced fluids (see Chapter 4).

2.5. Isochore maps

Isochore maps depict thickness variations between seismic markers in the subsurface. An isochore map illustrates lines of equal thickness between seismic units, where the thicknesses are measured vertically between two acoustic boundaries (i.e., horizons). Isochore maps are also referred to as True Vertical Thickness (TVT) maps, as generation of isochore maps does not account for the dip angle of the bedding within the area of interest.

In this thesis, six isochore maps were generated and produced from the established seismic units by subtracting Z values from surfaces generated from each horizon (e.g., Unit 1 = $Z_{N1} – Z_{P1}$; see Appendix V). These isochore maps were primarily used for the purpose of tracking and characterizing salt deformation history and its influence on associated subsurface seismic stratigraphic and structural features of the Cenozoic within the study area.

2.6. Works cited

Bertram, G. T. and Milton, N. J. (1996). Seismic stratigraphy. In D. Emery and K. J. Meyers, eds., Sequence stratigraphy: Blackwell Scientific, 45–60.

Bondurant, C. (2014). Tangier 3D WATS Program Report, Offshore Nova Scotia. BP Canada Exploration Ltd.

Bondurant, C. (2016). Tangier 3D Interpretation Report, Offshore Nova Scotia. BP Canada Exploration Ltd.

Brown, A. R. (1999). Reservoir Identification. In A. R. Brown (Eds.), Interpretation of Three Dimensional Seismic Data (Ch. 5, pp. 147–187). AAPG Memoir, 42; SEG Investigations in Geophysics, 9.

Campbell, D. C., Shimeld, J., Deptuck, M. E., and Mosher, D. C. (2015). Seismic stratigraphic framework and depositional history of a large Upper Cretaceous and Cenozoic depocenter off southwest Nova Scotia, Canada. *Marine and Petroleum Geology, 65*, 22-42.

Chopra, S. and Murfurt, K. J. (2007). Seismic attributes for prospect identification and reservoir characterization: SEG Geophysical Developments No. 11.

Government of Canada. *The BASIN Database*. Retrieved from https://basin.marine-geo.canada.ca/wells/index_e.php.

Herron, D. A. (2000). Horizon autopicking. *The Leading Edge*, *19*, 491–492.

Herron, D. A. (2011). First Steps in Seismic Interpretation. *Geophysical Monograph Series No. 16*, Society of Exploration Geophysicists.

Leon, L., and Guirguis, S. (2016). *Data Processing Report for BP Exploration Canada Limited*. Houston, TX: Schlumberger.

Offshore Energy Research Association. (2011). *Play Fairway Analysis Atlas*. Retrieved from https://oera.ca/research/play-fairway-analysis-atlas.

Vail, P. R. (1987). Seismic Stratigraphy Interpretation Procedures. In A. W. Bally, ed., *Atlas of Seismic Stratigraphy*, AAPG Studies in Geology, Vol. 1, No. 27, 1–10.

Vail, P. R., Todd, R. G., and Sangree, J. B. (1977). Stratigraphic interpretation of seismic reflection patterns in depositional sequences. In C. E. Payton, ed., Seismic stratigraphy – Applications to hydrocarbon exploration: AAPG Memoir 26, 99–116.

Weston, J. F., MacRae, R. A., Ascoli, P., Cooper, M. K. E., Fensome, R. A., Shaw, D., and Williams, G. L. (2012). A revised biostratigraphic and well-log sequence-stratigraphic framework for the Scotian Margin, offshore eastern Canada. *Canadian Journal of Earth Science, 49*, 1417–1462.

Yilmaz, Ö. (1987). Seismic Data Processing. *Investigations into Geophysics, No. 2*. Society of Exploration Geophysicists, Tulsa, Oklahoma.

Yilmaz, Ö. (2001). Seismic data analysis. *Investigations into Geophysics, No. 10.* Society of Exploration Geophysicists, Tulsa, Oklahoma.

Chapter 3. Basin Evolution and Salt Tectonic Related Stratal Deformation in the Tangier 3D Seismic Survey, Central Scotian Slope

3.1. Introduction

The Scotian Margin began to form with the rifting of Pangaea in the Late Triassic to Early Jurassic (ca. 250 to 190 Ma), eventually leading to formation of the Atlantic Ocean. Oceanic break-up began in the offshore of Nova Scotia by the Early Jurassic. This was followed by younger North Atlantic Ocean spreading in Early to mid Cretaceous in offshore the eastern Grand Banks and a offshore Labrador separation during the Late Cretaceous. The Scotian Margin is now marked by a variety of subbasins, platforms, and depocentres separated by half-grabens and fault-bounded major basement ridges (Wade and MacLean, 1990; Piqué and Laville, 1996; Brown, 2008; Adam and Krezsek, 2012; Withjack et al., 2012). These subbasins host post-rift rocks ranging from the Lower Jurassic to Neogene that are eventually overlain by unconsolidated sediments (See Ch. 1.5 for a summary).

This chapter discusses the evolution of the Cenozoic stratigraphy and salt-related structures in the Tangier 3D area (Fig. 3.1), central Scotian Slope. However, the mobilization of the salt of the Argo Formation has played a large role in the stratal deformation style since the Lower Jurassic. Several studies have been conducted on the location of salt bodies and their associated structures in the Scotian Margin (e.g., Jansa and Wade, 1975; Wade and MacLean, 1990; Shimeld, 2004; Ings and Shimeld, 2006; Albertz et al., 2010; Deptuck, 2011; OETR, 2011; Christian, 2015; Deptuck and Kendell, 2017; 2020). Vertical salt diapirs and salt canopy complexes are common features in the study area. The majority of the diapirs are found on the western portion of the survey, whereas salt canopy complexes dominate the eastern end with some minor diapirism. In the Tangier 3D survey, the top salt horizon is observed as a positive

high amplitude reflector due to the increase in velocity below the top of the salt (4450 m/s; BP Data Processing Report, 2016) relative to the surrounding sediment. When resolvable, the base of the salt horizon appears to be a negative low amplitude reflector. However, due to the long history of salt mobility and stratal deformation, the analysis of seismic reflection profiles is made complicated by diffraction and multiples that commonly appear at deeper depths due to overlying salt (>6 km).

As discussed in Chapter 1 (section 1.6.2), the Tangier 3D Seismic Survey straddles structural subprovinces II and III (Fig. 3.1). The western part of the study area, that generally contains vertical salt bodies, is found within subprovince II, whereas the allochthonous salt canopy is in subprovince III (Kidston et al., 2002; 2007; Shimeld, 2004; Ings and Shimeld, 2006; Albertz et al., 2010).

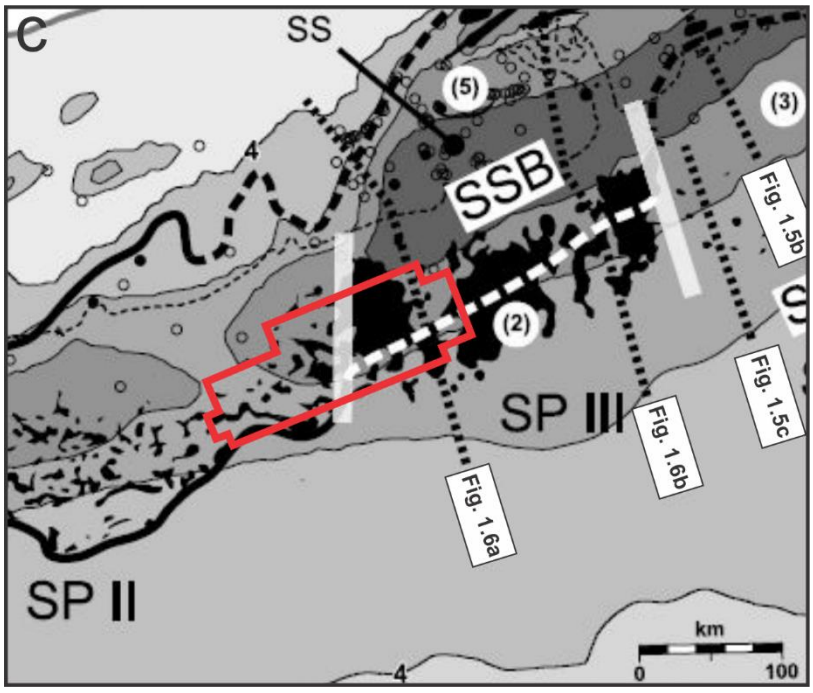

Figure 3.1. Close-up view of the Tangier 3D Seismic Survey, where the survey boundary straddles two salt structural subprovinces (as discussed in Chapter 1; map cropped from Fig. 1.3).

The main objective of this chapter is to define and map seven key horizons through the upper one to three kilometres of BP's Tangier 3D Seismic Survey, to characterize subsurface seismic structural and stratigraphic features, and to study how salt mobility influenced Cenozoic sedimentation and slope evolution. Specifically, the aim is to answer the following questions:

a) What important subsurface seismic stratigraphic and structural features are present in this part of the slope that could describe the Cenozoic basin evolution? What sedimentary slope-related processes were responsible for developing such features?
b) What types of salt structures are present in this part of the slope? How does salt mobility affect the deformation of sediments from the Paleogene to the Neogene?

3.2. Dataset and Methodology

In this chapter, well calibration, seismic facies analysis, attribute-based extractions, and isochore maps were used to characterize seismic facies, subsurface seismic stratigraphic and structural features, and the stratal deformation history resulting from salt tectonism (see Chapter 2 for more details about these approaches).

3.2.1. Well calibration

3.2.1.1. Weymouth A-45

Weymouth A-45 is located at the northeastern part of the study area within the western Sable Subbasin (Fig. 2.1; 43.06697° N; 60.604671° W (NAD27)). This exploration well was drilled by Ovintiv (former EnCana) and Shell in 2004. The primary target was a predicted Early Cretaceous

Middle to Lower Missisauga Formation turbidite fan within a subsalt anticline (Kidston et al., 2007). Van Helden et al. (2004) performed palynological analysis on the recovered samples from the section between 4395 m to 6525 m (TD). There is no available biostratigraphic age data for Cenozoic strata (above ~2800 m) for Weymouth A-45. However, a surficial geology and seafloor topography map of the modern-day Verrill Canyon (Campbell et al., 2005) confirms that the sediments dominating the shallow strata where Weymouth A-45 penetrates are mostly proglacial muds with sand and silts deposited from subsequent erosion and turbidity currents in the proximity of canyons that have exposed Middle Pleistocene and older sediments.

This well penetrates an allochthonous salt canopy. More importantly, interpreted Ypresian chalk (Weston et al., 2012) and marls and possibly chalks from the Late Cretaceous Wyandot Formation (K78) are observed at the top of the allochthonous salt canopy. The observed lithostratigraphy suggests the Shortland Shale (Aptian-Albian) underlies the salt canopy with several important formations such as the Naskapi Member of the Logan Canyon Formation, and mostly mudstone-dominated equivalents of the Upper, Middle, and Lower Members of the Missisauga Formation with minor siltstone and sandstone beds. The well also reached the top of the equivalent of the O-Marker (OERA, 2011; BP Tangier 3D Interpretation Report, 2016). Based on palynological evidence from Weymouth A-45, van Helden et al. (2004) interpreted a gradual change in the paleoenvironment from inner to middle neritic (shallow to near-shore marine) in Hauterivian – Early Barremian to middle-outer neritic (shallow open marine) from in Early Aptian – Late Albian or Early Cenomanian. All mapped horizons for this study intersect this well (Fig. 3.2).

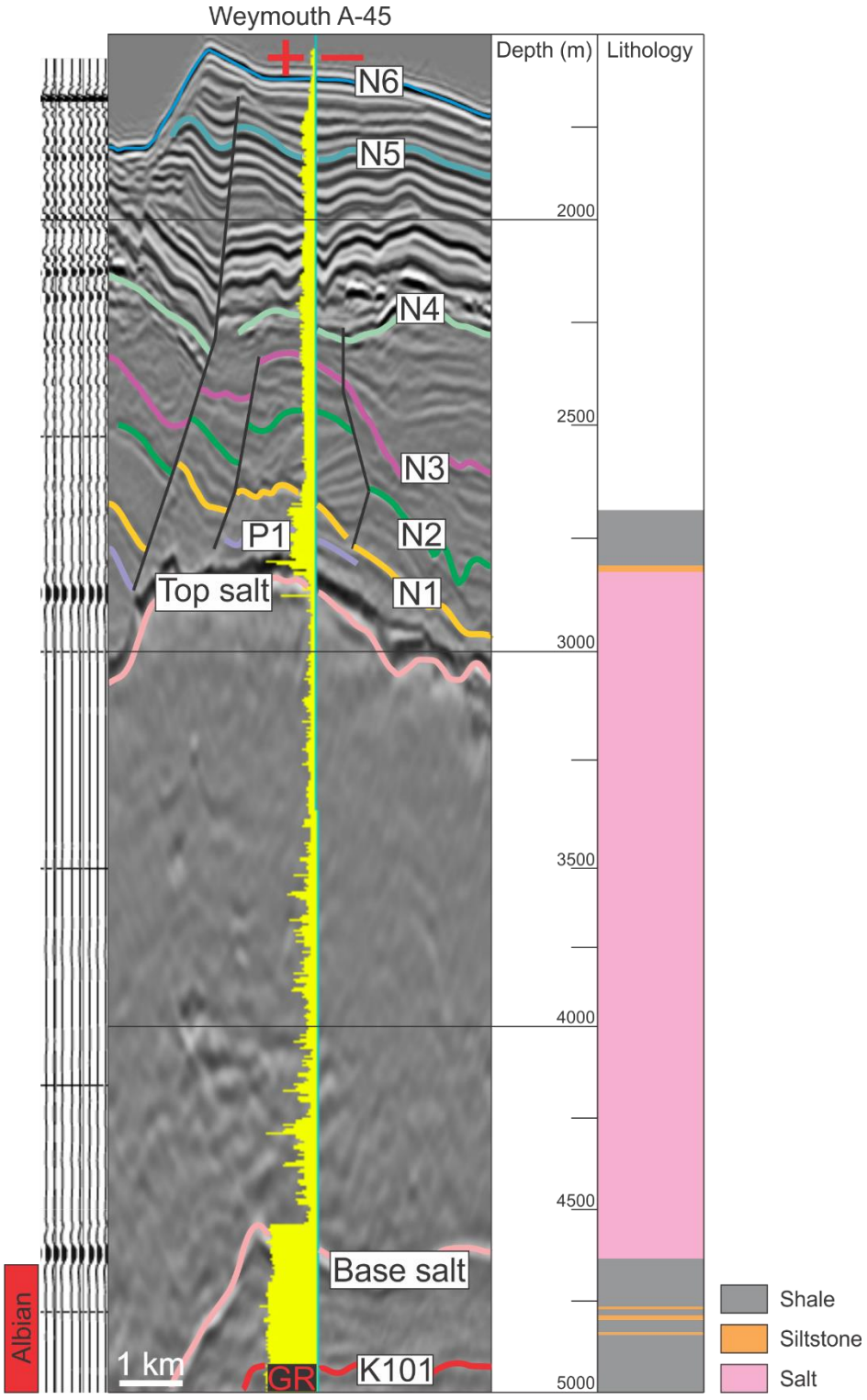

Figure 3.2.Well information of the upper part of Weymouth A-45 including seismic horizons for this thesis from P1 to N6, gamma-ray (GR) log (values increasing to the left), lithology track from rock cuttings, biostratigraphic age, and well seismic location from the Tangier 3D Seismic Survey (Cretaceous marker: K101; derived from OERA, 2011; Campbell et al., 2015). Data courtesy of Ovintiv (formerly EnCana) (2004) via NSDNRR and the BASIN Database.

3.2.1.2. Balvenie B-79

Balvenie B-79 is located on the easternmost part (western Sable Subbasin) outside of the Tangier 3D area (Fig. 2.1; 43.133692° N; 60.182456° W (NAD27)) and projected by at least 50 m from its initial position. The drilling operation was completed by Imperial Oil in 2003. The primary reservoir objective was at the Albian level, where several amplitude anomalies with modest amplitude-versus-offset (AVO) response were observed (Kidston et al., 2007). All mapped horizons in this thesis were resolvable and correlated with the Cenozoic biostratigraphic ages from Fenton and Pardon (2003), OETR (2011), and Weston et al. (2012) (Fig. 3.3).

Several thin, tight, gas-charged siltstones were encountered by the well in the Albian target with thicknesses ranging from 1 to 8 m producing a considerable mud-gas show (CNSOPB, 2016). Several Cretaceous intervals (K70 to K113 seismic markers of OETR, 2011) were also penetrated. The Early (Aptian – Albian) to Middle Late Cretaceous (Cenomanian – Turonian) comprises bedded shale with small amounts of siltstone in the Logan Canyon and Dawson Canyon formations. The upper part of the Late Cretaceous (Santonian – Maastrichian) represents a start of change in the depositional system by the abundance of marlstone and limestone intervals form the Wyandot Formation. Tertiary sediments are mostly mud interbedded with siltstone and sandstone including several marlstone, with limestone beds from the interpreted Ypresian chalk (OERA, 2011; Weston et al., 2012; Campbell et al., 2015).

The interpreted paleoenvironment of the Balvenie well based on palynological evidence suggests that there is a gradual change from middle-outer neritic (Middle to Late Albian) to outer neritic-bathyal starting from Turonian – Maastrichtian to Late Miocene (OETR, 2011).

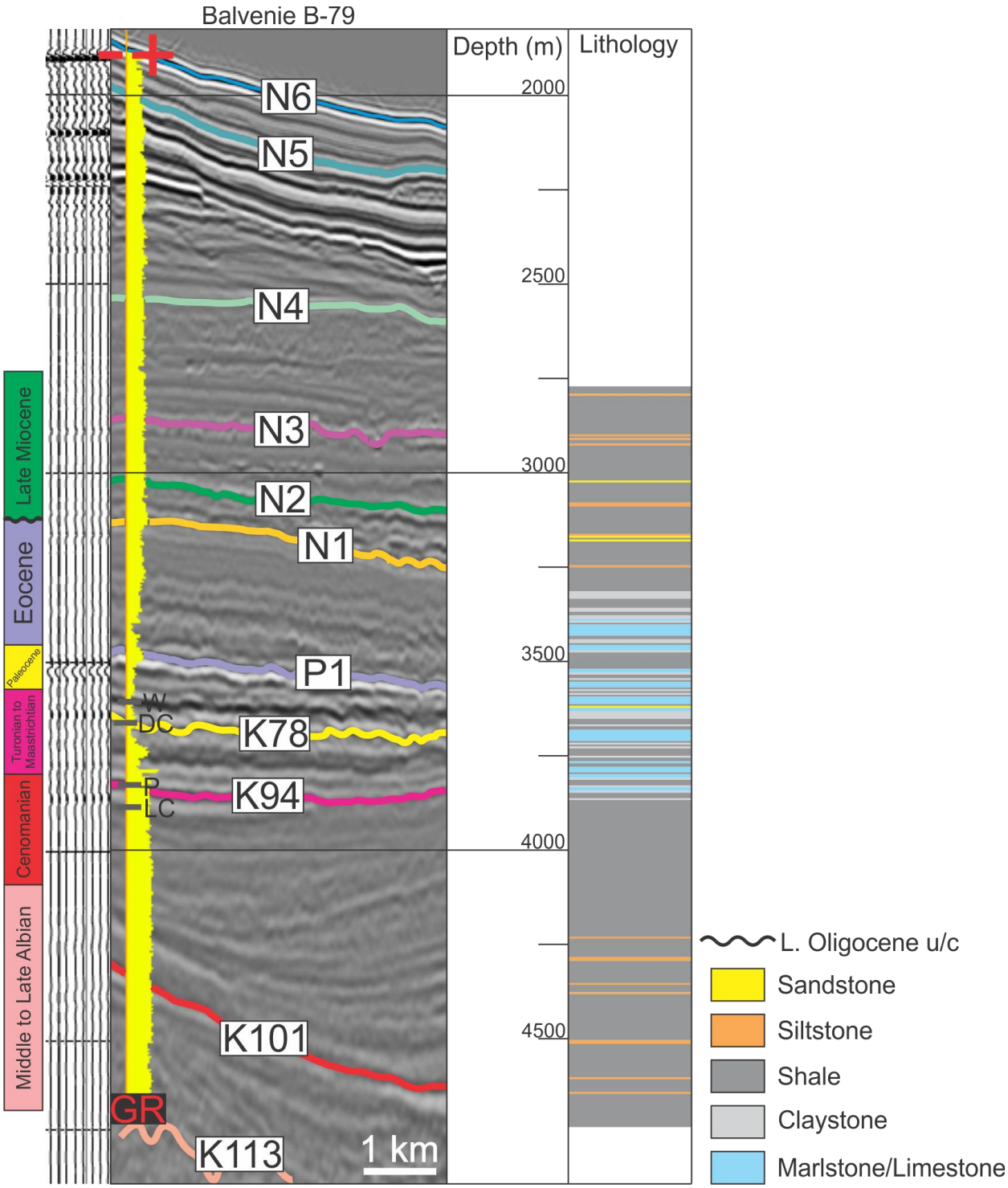

Figure 3.3. Well information of Balvenie B-79 including seismic horizons for this thesis from P1 to N6, gamma ray (GR) log (values increasing to the right), lithology track from rock cuttings, well seismic location, and biostratigraphic ages within the Tangier 3D area (Formation tops: W = Wyandot; DC = Dawson Canyon; P = Petrel; LC = Logan Canyon; Cretaceous markers: K78 to K113; derived from OERA, 2011; Campbell et al., 2015). Data courtesy of Imperial Oil (2003) via NSDNRR and the BASIN Database.

3.2.1.3. Aspy D-11/D-11A

BP Canada Energy Group, ULC, drilled the Aspy D-11 exploration well within the exploration licenses as part of their Scotian Basin Exploration Drilling Project. Aspy D-11 is located at the lower part of the Scotian Slope (Fig. 2.1; 42.833427° N, 60.297825° W (NAD27)). There are no biostratigraphic data available for the Cenozoic strata in this well, but some lithostratigraphic data is present for the Paleogene and earliest Neogene (Fig. 3.4). All the mapped horizons were penetrated in this well.

The primary targets were Early Cretaceous siliciclastic mid to lower slope turbidite lobes and channel complexes. A sidetrack occurred (Aspy D-11A) due to technical problems within the Argo allochthonous salt above the primary target intervals. The distal equivalent of the Missisauga and Logan Canyon formations make up most of the sub-salt stratigraphy. It is predicted that the major Early Cretaceous paleo-Laurentian depositional system drained sediments from the southeastern Canadian Shield that resulted in the deposition of a large deltaic sequence on the shelf and deep-water rocks on the slope (BP Subsurface Well History Report, 2019). Initial interpretation suggested that there were shelf penetrations of quality Cretaceous reservoirs during activity of the Sable Delta and that the Missisauga and Logan Canyon formations prograded on the Scotian Slope over the top of underlying Jurassic source rocks (BP Subsurface Well History Report, 2019).

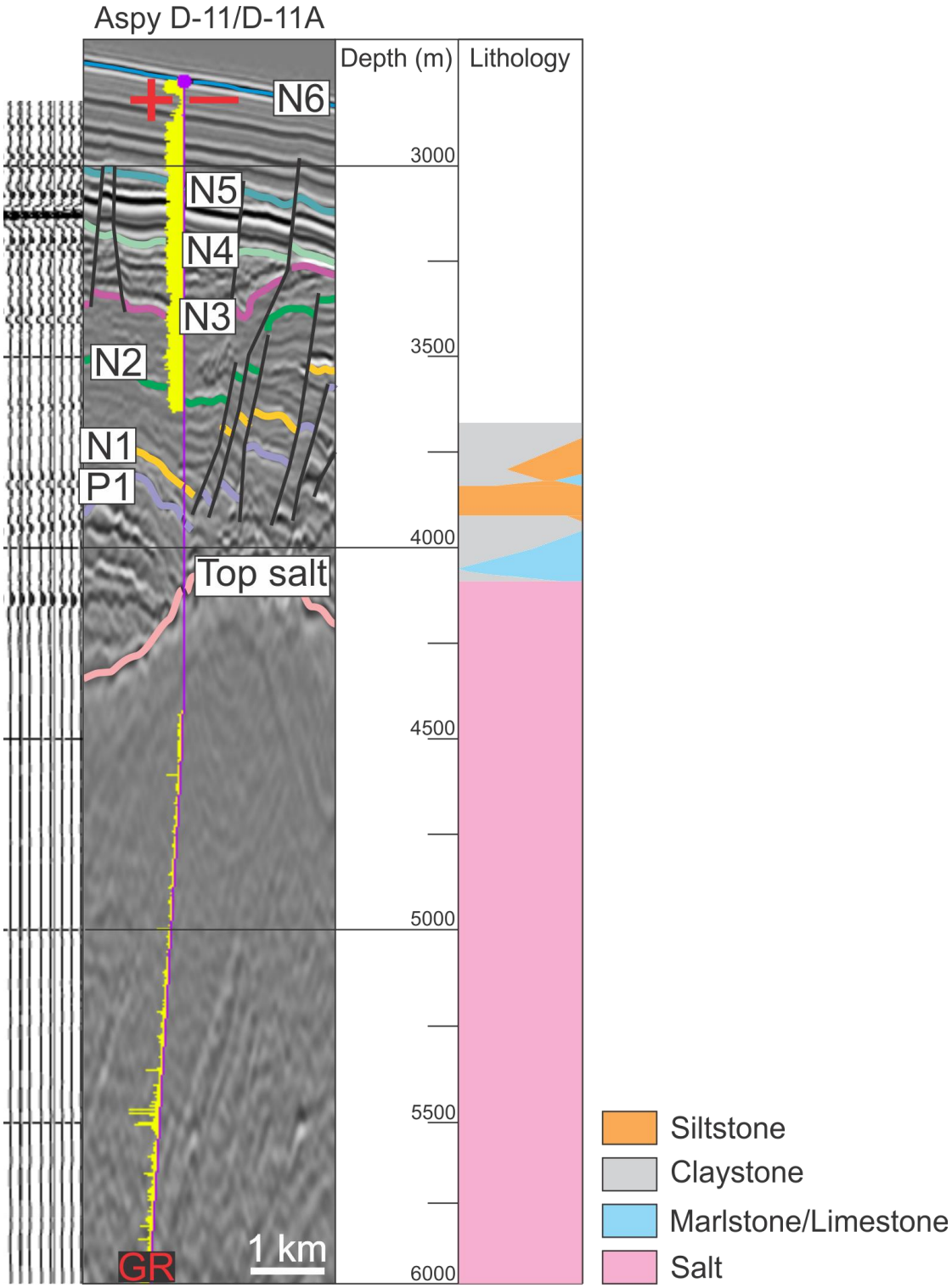

Figure 3.*4*. Well information of the upper part of Aspy D-11/D-11A including seismic horizons for this thesis from P1 to N6, gamma ray (GR) log (values increasing to the left), lithology track from rock cuttings, and well seismic location within the Tangier 3D area (derived from BP Subsurface Well History Report, 2019). Data courtesy of BP Canada Exploration Ltd (2018) via NSDNRR and the BASIN Database.

3.2.2. Seismic facies analysis

3.2.2.1. Recognition of shelf to slope facies

This section provides an overview of the methodology used in recognizing shelf and slope facies including seismic units and bounding horizons, which are thoroughly discussed in section 3.3 onwards (refer to section 3.3.1.1.). The Cenozoic section is subdivided into 6 seismic units across the shelf and slope. These seismic units are defined in between a pair of horizons and are named, from oldest to youngest, Unit 1 to Unit 6 (Fig. 3.7).

Shelf facies

Seismic facies on the central Scotian Shelf are observed from a regional 2D seismic line (in Two Way Travel Time in seconds) acquired by TGS (Figs. 3.5-3.6). The seafloor horizon corresponds to a strong peak-trough pair. It is underlain by an interval of well-stratified reflectors. High amplitude, well-stratified reflectors are observed in the upper shelf from 1 to 3 s (Fig. 3.5). These reflectors have parallel to sub-parallel orientation, are continuous, and mostly concordant. On the shelf break, high to moderate amplitude, prograding clinoform-like reflectors are present, suggesting basinward sediment deposition from the shelf from 1 to 3 s. The shelf break reflector's geometry seems to be sigmoidal and oblique and appears to be relatively continuous, but the detailed reflection geometry is partly obscured by interfering multiples from the seafloor reflector.

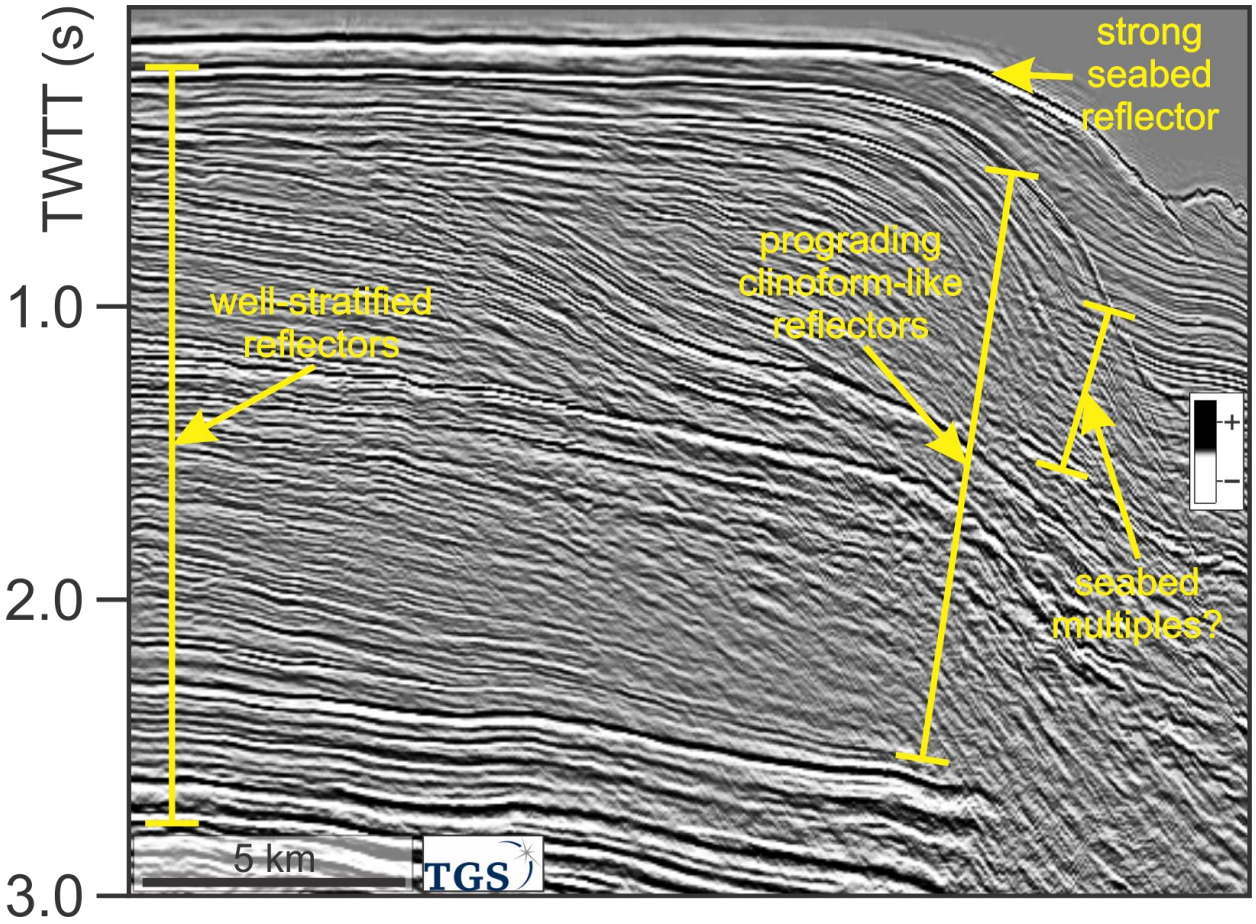

Figure 3.5. Representative seismic profile of a part of the central Scotian Shelf, cropped from profile A-A' (Fig. 3.6). This section provides an overview of the common seismic facies in the shelf transitioning to the shelf break. Data courtesy of TGS via NSDNRR.

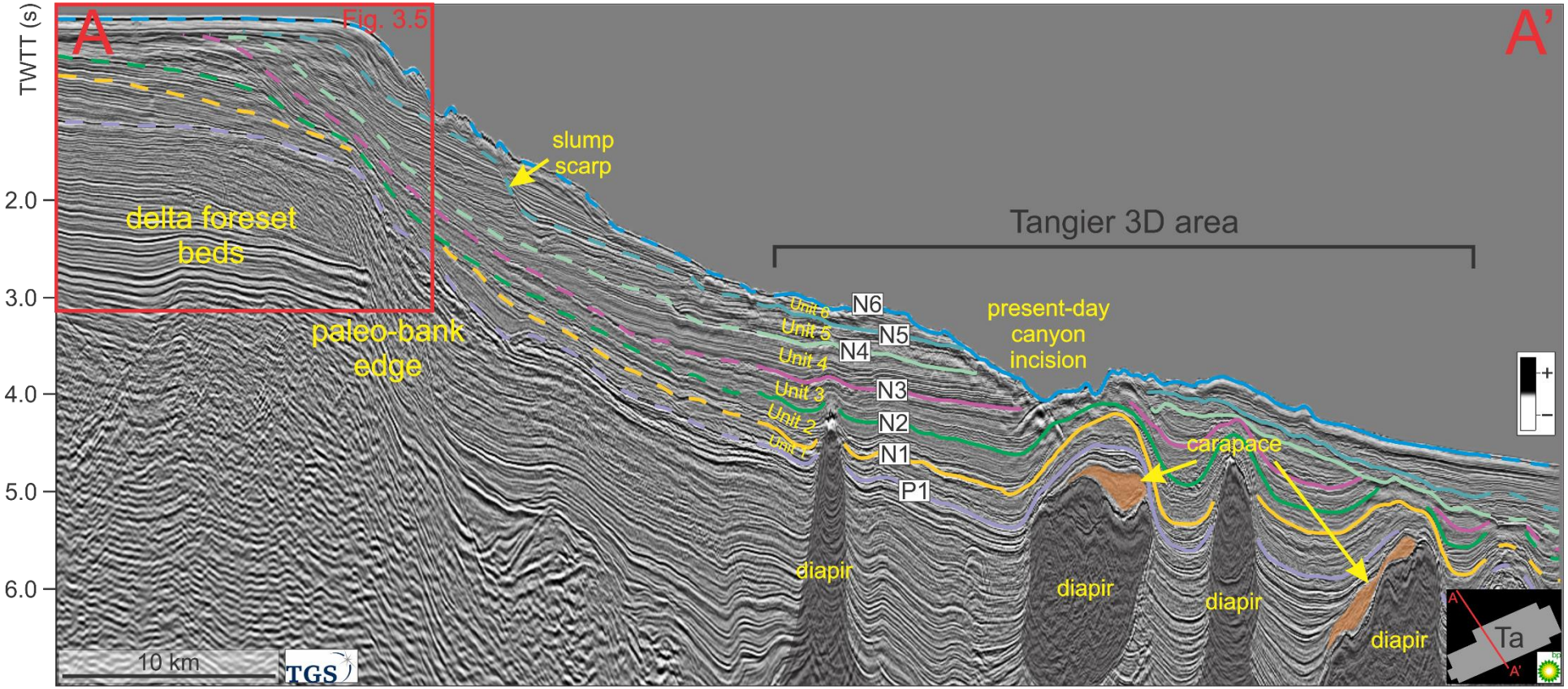

Figure 3.6. Representative dip-oriented profile (A to A'; see Appendix VI for uninterpreted version) showing the seven horizons mapped (i.e., Tangier 3D area) with the labelled seismic units (U1 to U6) to exhibit the transition of seismic facies from the shelf to the slope. This includes features such as delta foreset beds and paleo-bank edge (i.e., Jurassic carbonate reef build-up) represented by well-stratified, layered, high amplitude, and prograding clinoform-like reflectors, respectively. The common slope facies are represented by mixture of parallel to subparallel, high amplitude, weakly chaotic, low to moderate amplitude, wavy, coherent, moderate to high amplitude reflectors, and reflection blanking (see Fig. 3.7). Carapace blocks are marked by orange highlights. Data courtesy of TGS via NSDNRR.

Slope facies

On the slope within the Tangier 3D area (in True Vertical Depth in m; Fig. 3.7), a strong peak-trough pair reflector is present, considered as the seafloor (Fig 3.7). Well-stratified, high amplitude reflectors are also present below the seafloor in Unit 5 to Unit 6. An interval of well-stratified, low to moderate amplitude reflectors is observed at depth of ~800 to ~1100 m below seafloor (mbsf) in Unit 1 to Unit 3. Moreover, at depth of ~1600 to ~1800 mbsf, series of high amplitude reflectors in Unit 1 are observed and interpreted to be related to the Paleocene to Eocene chalks based on the lithology information from Balvenie B-79 (Figs. 3.3; 3.7).

Structurally deformed, semi-transparent, weak chaotic to moderate chaotic reflectors in Unit 1, Unit 4 to Unit 5 are also observed in the slope and are commonly semi-continuous to discontinuous in terms of reflection continuity. Two generations of this facies are highlight in Fig. 3.7, the deformed reflectors at ~800 mbsf and the reflectors at ~1300 mbsf appear to have been structurally deformed because of polygonal faulting. Seismic examples are highlighted in the subsequent sections.

Reflection blanking with strong reflections at the top boundary is common on the slope due to the presence of salt bodies and their large impedance contrast with surrounding sediments, which strongly reflects seismic energy and masks underlying reflections (Fig. 3.8A-3.8B). The salt bodies appear to have little or no sign of stratigraphic bedding internally, except in Aspy D-11/D-11A, where internal reflections in salt bodies correspond to intervals of carnalite and basalt (Deptuck and Kendell, 2020). Vertical salt diapirs and salt canopy often have signs of onlapping reflections on their flanks (Fig. 3.8A-3.8B).

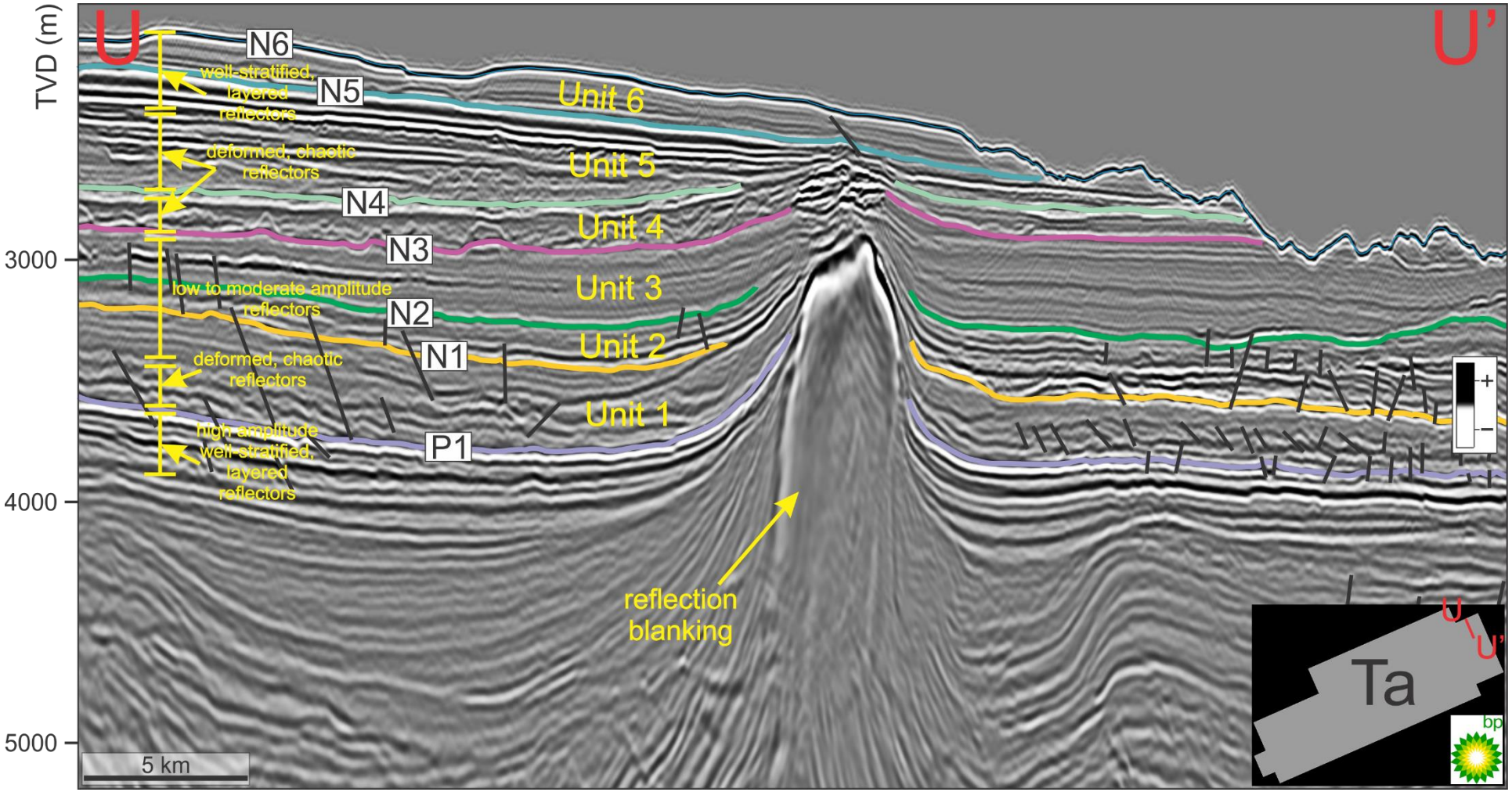

Figure 3.7. Seismic section cropped from profile U-U' (discussed in detail in Chapter 4; see Appendix VI for uninterpreted version) to characterize seismic facies and represent a geologic type section of the Tangier 3D Seismic Survey located on the central Scotian Slope. Data courtesy of BP Canada Exploration Ltd via NSDNRR.

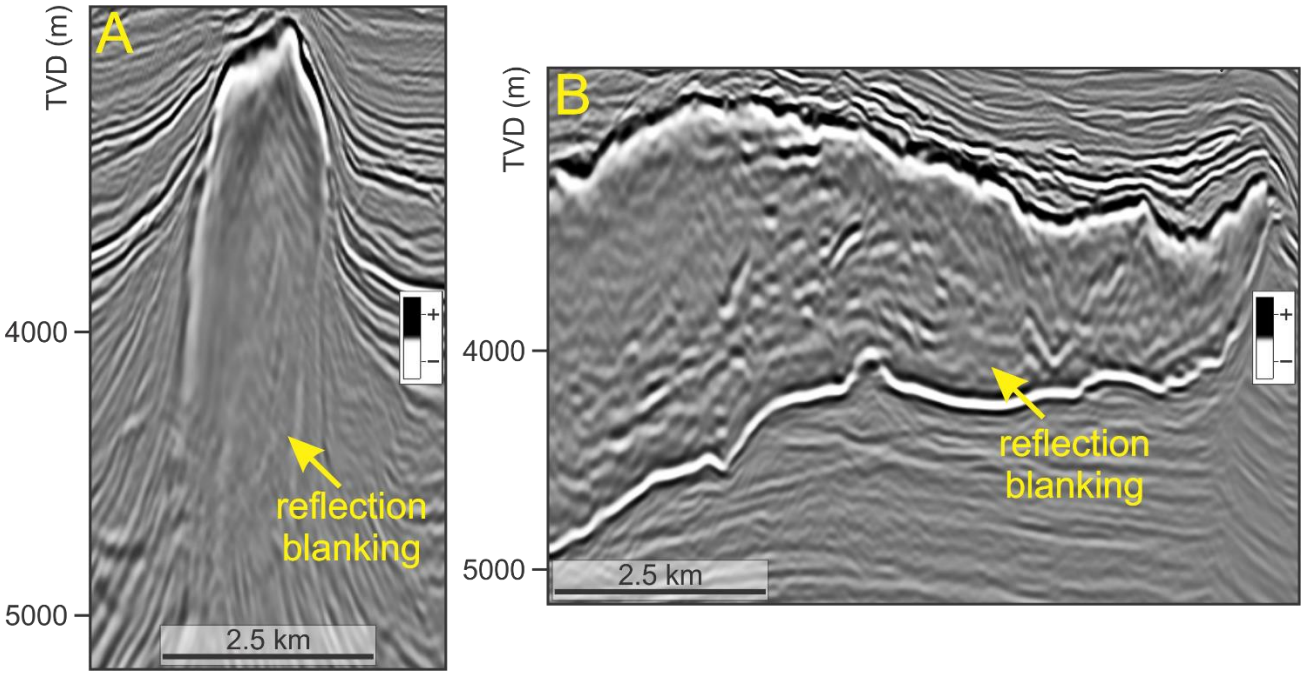

Figure 3.*8*A and 3.8B. Examples of reflection blanking (salt bodies from Figs. 4.3 and 4.7, respectively; salt bodies are discussed in detail in Chapters 3 and 4) observed from the Tangier 3D area. Data courtesy of BP Canada Exploration Ltd via NSDNRR.

3.3. Results

3.3.1. Seismic stratigraphy

3.3.1.1. Seismic stratigraphic framework

Slope stratigraphy

Seven horizons were correlated from the Paleogene to Neogene succession in the study area. Each horizon was mapped as either distinct reflection at boundaries between facies that have their own distinct seismic characteristics in terms of reflection continuity and geometry. The oldest horizon (basal) in the study area is the P1 horizon. In terms of naming horizons, "P" represents Paleogene strata; and horizons beginning with "N" are found within the Neogene strata:

- P1 horizon is picked as a peak reflector. P1 coincides as the base of the Early Eocene (Ypresian) chalk unit (McIver, 1971; Given, 1977; Weston et al., 2012), resulting in a strong reflection because of changing acoustic impedance with the lithological change (Fig. 3.3). P1 closely coincides with the T50 marker mapped by OETR (2011), Deptuck and Campbell (2012), Campbell et al. (2015), and Deptuck and Kendell (2020), as well as the P2 marker in Christians (2015).
- N1 horizon is picked as a peak reflector. The age assignment for N1 is interpreted to be related to the Late Oligocene Unconformity of Weston et al. (2012) with variation of the age of the strata below being due to different levels of canyon development in the Oligocene (with the age of the canyon infill as young as the Miocene; Fig., 3.3; OETR, 2011; Campbell et al., 2015; Deptuck and Kendell, 2020). In the eastern part of the Tangier survey, N1 corresponds to a truncating reflector at the base of a canyon (e.g., Fig. 3.21; Oligocene Wenonah Canyon) showing a strong contrast in reflection geometry versus the onlapping reflectors above. In some parts of the survey, N1 is locally discontinuous and observed with weakly chaotic reflections. Deptuck and Kendell (2020) also suggested that mass transport complexes are common features above N1 horizon (i.e., corresponding to their T25 marker). N1 locally corresponds to T29 of OETR (2011), and the P4 marker of Christians (2015).
- N2 horizon is picked as a peak reflector. N2 is interpreted to be within the Late Miocene (Fig. 3.3; OETR, 2011; Campbell et al., 2015; Deptuck and Kendell, 2020). This horizon is mapped below a unit of high amplitude, continuous, parallel to subparallel reflections with occasional weakly chaotic reflectors in some parts of the survey, possibly erosion

character down-slope. In Fig. 3.7, N2 appears to be a high amplitude, erosive-like reflector due to its uneven geometry that the reflections above N2 appear to be onlapping.

- N3 horizon is picked as a peak reflector. There is no definitive age assignment for this horizon in Balvenie B-79 (Fig. 3.3). However, looking at Figure 3.3 for Balvenie, N3 horizon coincides within the upper part of the Late Miocene. At the correlative stratigraphic level in Shubenacadie H-100 (Fig. 2.1), Campbell et al. (2015) determined that the age is approximately within the Tortonian (Late Miocene). N3 locally corresponds to the T13 marker of Campbell et al. (2015) and the N5 marker of Christians (2015).
- N4 horizon is picked as a peak reflector. There is no definitive age assignment for this horizon in Balvenie B-79 (Fig. 3.3). At the correlative stratigraphic level in Shubenacadie H-100 (Fig. 2.1), Campbell et al. (2015) stated that the age is approximately within the Messinian (Late Miocene). N4 is mapped at the base of a unit of moderate to low amplitude, weakly chaotic reflections. N4 locally corresponds to the T7 marker of Campbell et al. (2015) and the N7 marker of Christians (2015).
- N5 horizon is picked as a peak reflector. There is no definitive age assignment for this horizon in Balvenie B-79 (Fig. 3.3) or in other wells in the area. N5 is anticipated to correspond to the Pliocene to younger and is mapped below of a unit of high amplitude, layered reflections. N5 locally corresponds to the T3 marker of Campbell et al. (2015) and the N8 marker of Christians (2015).
- N6 horizon is picked as a peak reflector. The age is Holocene as it is the modern seafloor. N6 is the seafloor as represented by its strong impedance contrast.

All horizons were mapped throughout the Tangier 3D area. Furthermore, these horizons were extrapolated to the shelf using 2D seismic data.

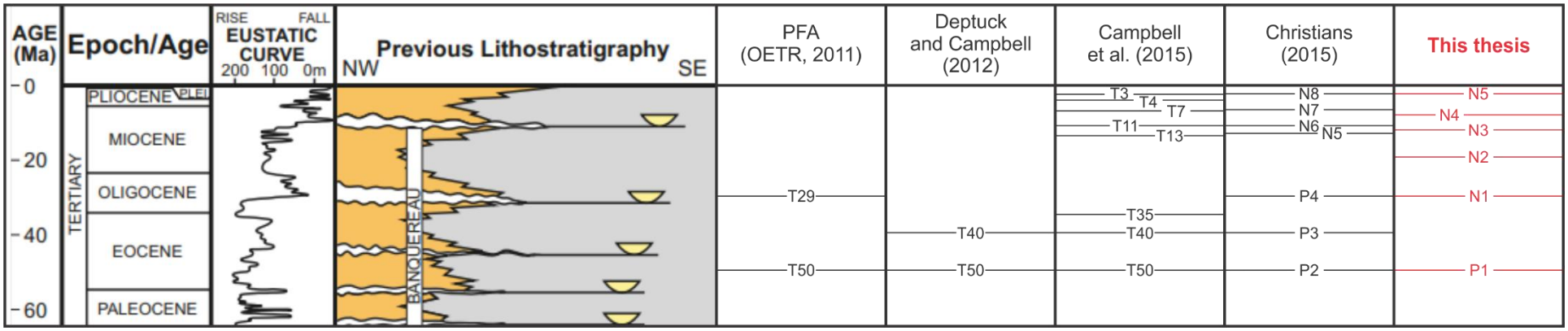

Figure 3.9. Seismic horizons from P1 to N6 (this thesis) correlating to relative ages and lithostratigraphy of the Scotian Margin (derived from Weston et al., 2012). Other horizons are also included from previous studies (e.g., OETR, 2011; Deptuck and Campbell, 2012; Campbell et al., 2015; Christians, 2015).

P1 to N1: Unit 1 (U1)

Unit 1 is recognized and mapped across the paleo-shelf and the slope (Figs. 3.6-3.7). Unit 1 is up to 650 m thick (Fig. 3.10; Appendix V) and is bounded below by the P1 marker and above by the N1 marker. This unit is composed of deformed chaotic reflectors near P1 and high to low amplitude reflectors near N1 (sub-units 1b and 1c of Deptuck and Campbell, 2012; Fig. 3.7). There is a set of well-stratified, layered, high amplitude reflectors below P1 that is concordant in nature, which correspond to chalk deposits (Fig. 3.7; Fig. 3.3 from Balvenie B-79). Reflectors that are tructurally deformed by faults above P1 appear to terminate via downlap onto the P1 marker. Unit 1 commonly thins and onlaps above salt bodies (Figs. 3.7; 3.10). The upper bounding N1 horizon is mapped as a set of low to moderate amplitude reflectors that concordantly drapes over underlying truncated reflections. In terms of sediment thickness, this unit appears to vary spatially, which can be observed by comparing the sediment thickness variations in the east (e.g., <100 m) versus the thickness in the central and western parts of the survey (Fig. 3.10), reaching up to 600 m, but there is little to no variation in thickness from up-slope to down-slope within the study area.

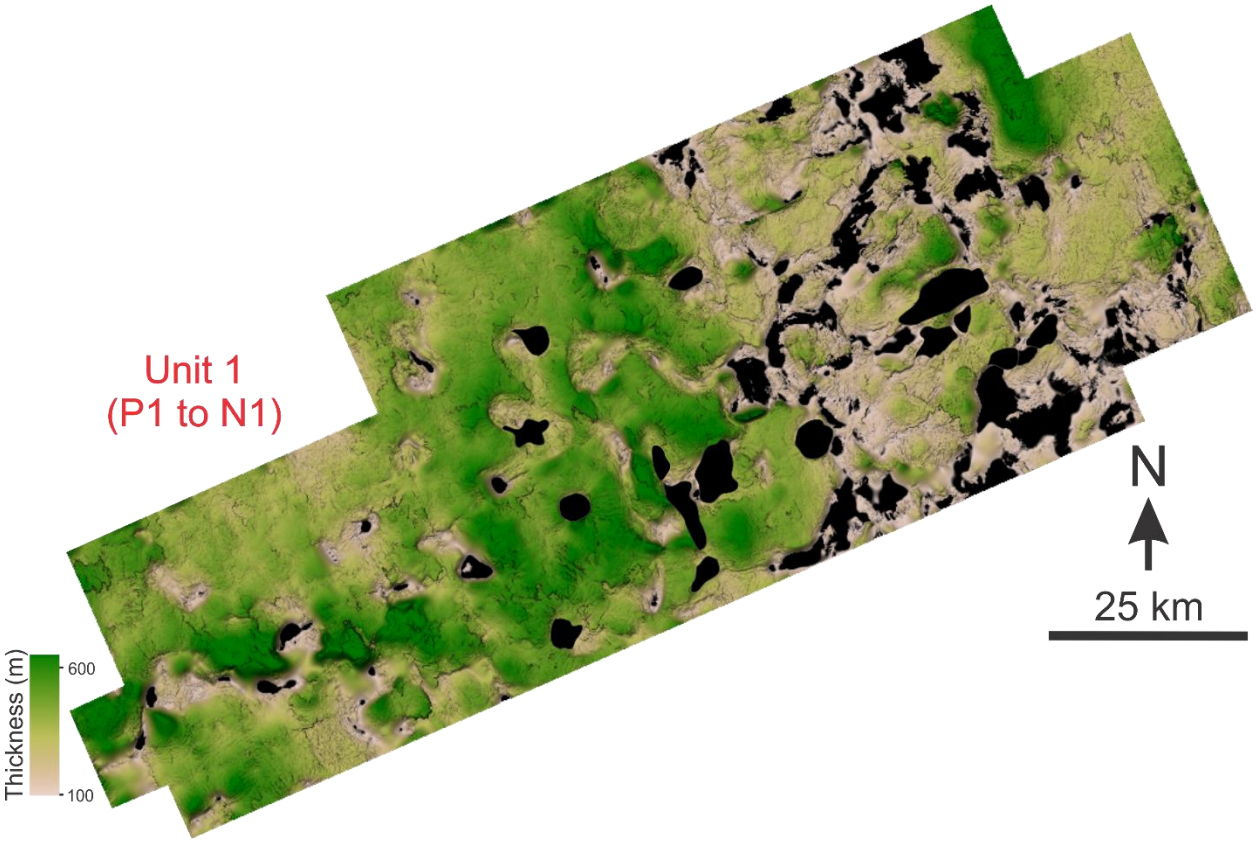

Figure 3.10. Isochore map of Unit 1.

N1 to N2: Unit 2 (U2)

Above N1, in Unit 2, another set of concordant low to moderate amplitude reflectors draping underlying parallel reflectors are present. Unit 2 (Figs. 3.6-3.7) is up to 700 m thick (Fig. 3.11; Appendix V) and is bounded by the N1 marker below and the N2 marker above. This unit is composed of low to moderate amplitude well-stratified reflections in the landward parts of the survey. Unit 2 is more structurally deformed by small polygonal faults moving down the slope, where it also contains high amplitude reflections (Fig. 3.7). These reflections are mainly concordant with markers beneath the N1 horizon, but some reflectors do terminate via downlap onto Unit 1 (Fig. 3.7). Unit 2 commonly thins and onlaps salt bodies in the study area (e.g., Fig.

3.7). The sediment thickness of Unit 2 varies spatially as observed by the more varying sediment thickness in the east versus to a more uniform sediment thickness variation in the central and western part (Fig. 3.11) but there is little to no variation from up-slope to down-slope.

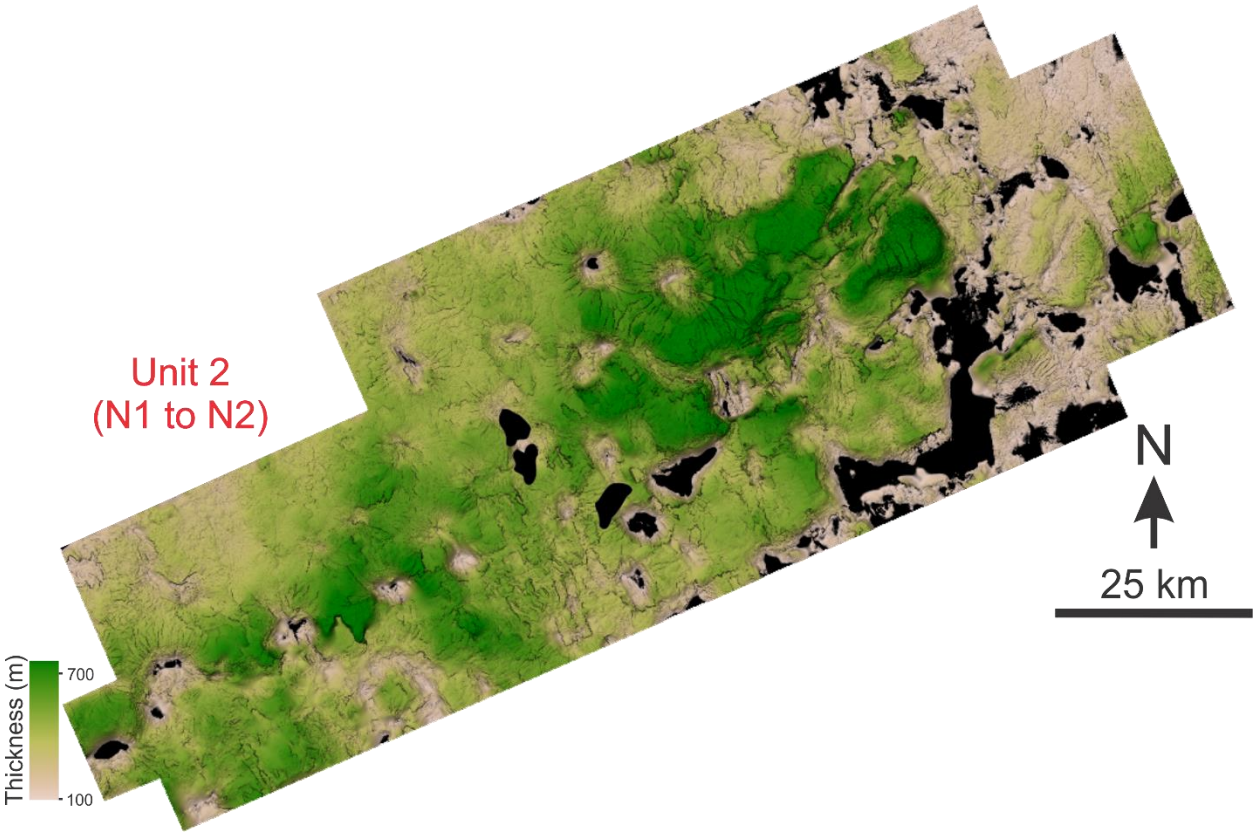

Figure 3.11. Isochore map of Unit 2.

N2 to N3: Unit 3 (U3)

Unit 3 (Figs. 3.6-3.7) is up to 350 m thick (Fig. 3.12; Appendix V) and is bounded by the N2 marker below and the N3 marker above. This unit is composed of low to moderate amplitude well-stratified reflections draping a set of subparallel reflectors (Fig. 3.7). Unit 3 commonly onlaps and thins above salt bodies in the study area, especially in the down-slope region (Fig. 3.7). The thickness of Unit 3 varies spatially as more regions with sediment thicks are apparent

in the east and more uniform thinning occurs in the central and western part of the survey (Fig. 3.12). There is also thickness difference from landward to seaward direction where the unit is thinning down-slope, from as thick as 350 up-slope to as thin as 50 m down-slope. Unit 3 is truncated by modern day canyons as shown in Figure 3.7, indicated by the jagged map geometry of the Unit 6 horizon due to erosion.

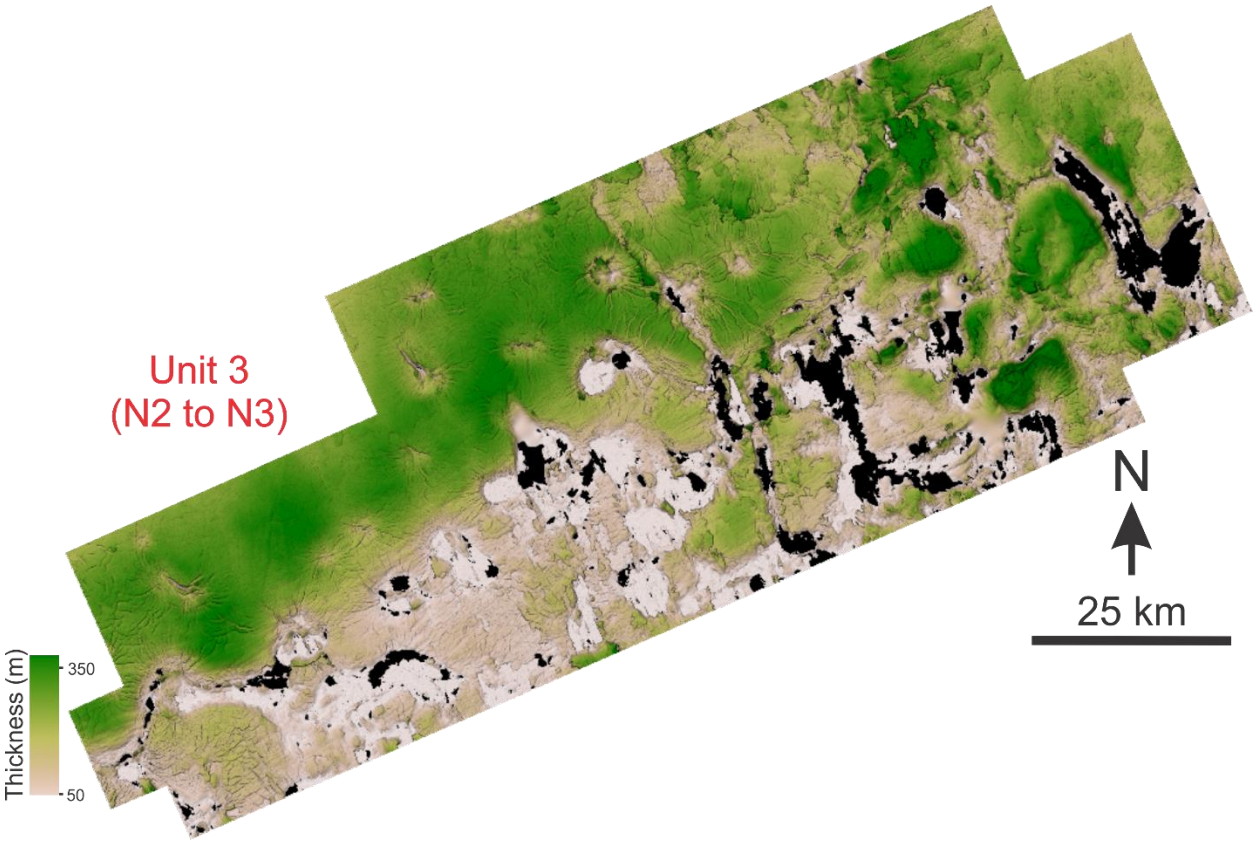

Figure 3.12. Isochore map of Unit 3.

N3 to N4: Unit 4 (U4)

Unit 4 is bounded below by the N3 marker and above by the N4 horizon (Fig. 3.7). The total thickness of Unit 4 is up to 450 m (Fig. 3.13; Appendix V). There is a significant change in reflection geometry from well-stratified, draping reflections of Unit 3 to chaotic reflections of

Unit 4. This possibly suggests presence of mass transport deposits in this interval. Unit 4 is described as weak, coherent, chaotic, low to moderate amplitude reflections. Unit 4 downlaps on the N3 horizon, while it concordantly bounds a high amplitude, continuous, stratified reflector of N4 horizon (Fig. 3.7). Unit 4 commonly onlaps and thins above salt bodies in the study area (Fig. 3.13). The unit thickness of Unit 4 varies spatially as in the east, there are some areas of sediment thicks, in the central and west, there are regions of sediment thicks including above the canyon in the central Tangier (see section 3.3.2.2). There is also thickness difference from landward to seaward direction where the unit is thinning down-slope, from as thick as 450 m up-slope to as thin as 50 m down-slope. This unit shows obvious erosion from modern day canyons based on uneven slope geometry due to slope failure escarpments in N6 horizon (Fig. 3.13).

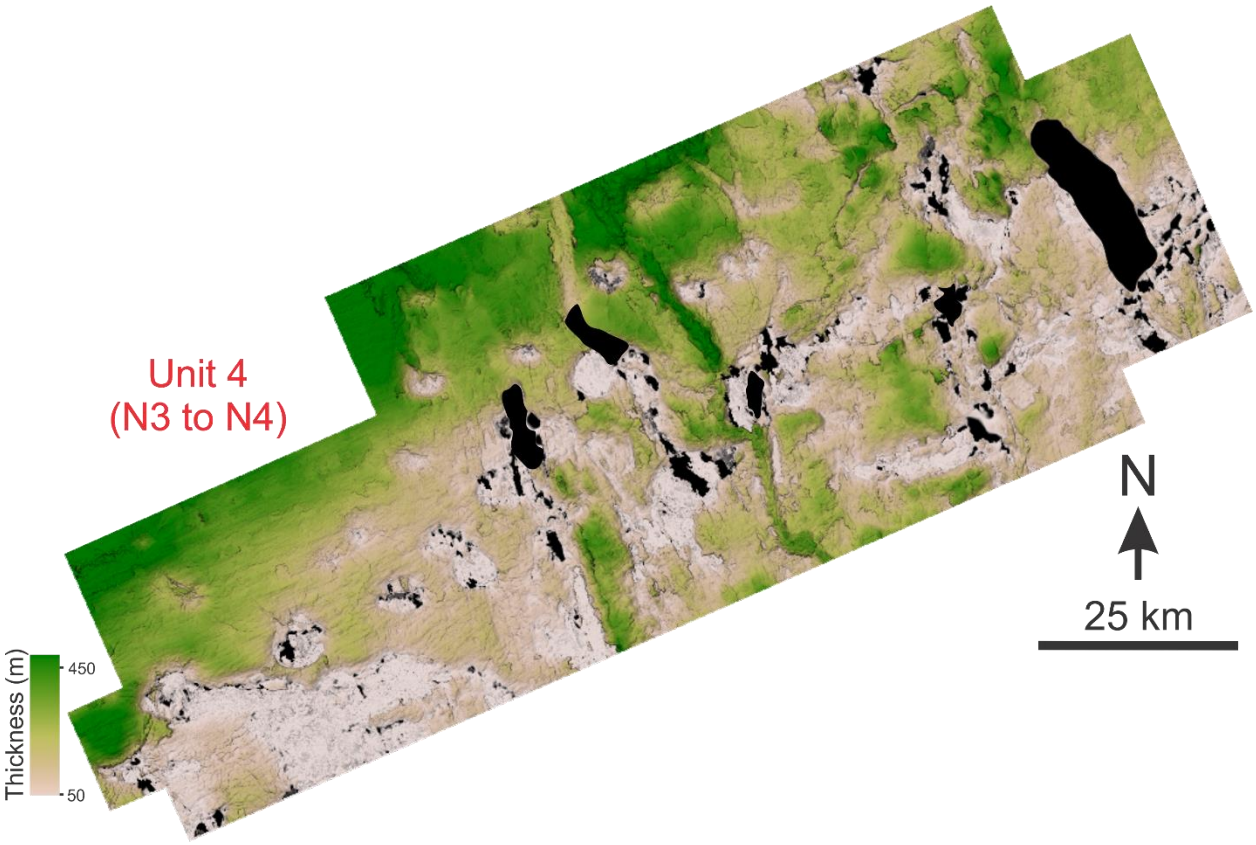

Figure 3.13. Isochore map of Unit 4.

N4 to N5: Unit 5 (U5)

Unit 5 is bounded below by the N4 and above by the N5 horizons (Fig. 3.7). Unit 5 is up to 500 m thick (Fig. 3.14; Appendix V). This unit is characterized as weak, chaotic, low to moderate amplitude reflections at the base (close to N4) with changing reflection geometry to well-stratified, layered, coherent, moderate to high amplitude reflectors near N5. The chaotic reflections of the lower part of Unit 5 concordantly bounds at the base at N4 horizon. The well-stratified reflectors at the top of Unit 5 that are concordantly bounding against N5. There is little to no variation of unit thickness between the east and the central and western parts of the survey. However, there is a thickness difference from landward to seaward direction where the unit thins down-slope, from as thick as 550 up-slope to as thin as 50 m down-slope (Fig. 3.14). This unit is truncated by modern day canyon based on the uneven slope geometry caused by failure escarpments in N6 suggesting erosion occurred (Fig. 3.7).

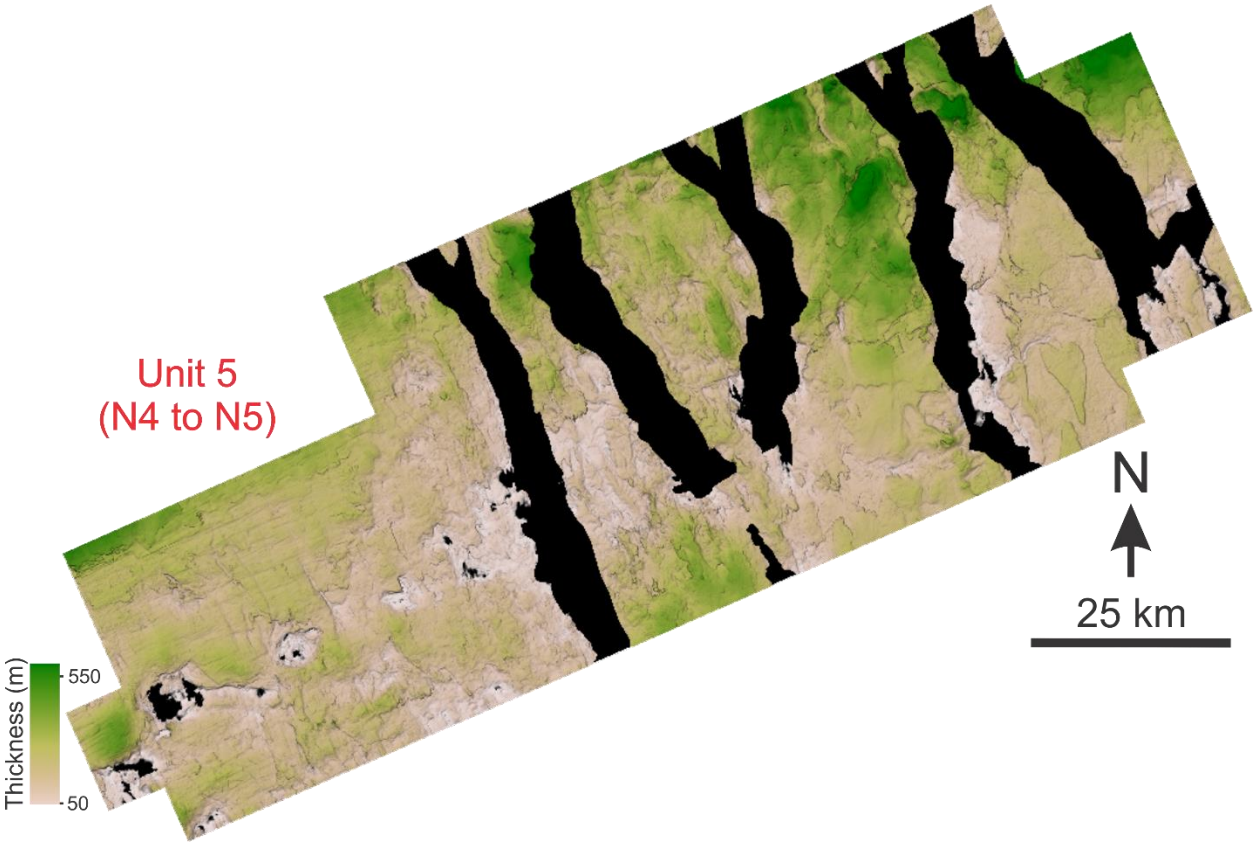

Figure 3.14. Isochore map of Unit 5.

N5 to N6: Unit 6 (U6)

Unit 6 is recognized and mapped across the shelf and the slope. The total thickness of Unit 6 is up to 300 m (Fig. 3.15; Appendix V). Unit 6 is bounded by the lower N5 and upper N6 horizons. Unit 6 comprises moderate to high amplitude, well-stratified reflections. Further downslope (Fig. 3.7), this unit is truncated by modern day canyons, which produce the uneven seafloor geometry due to failure escarpments in N6 horizon. There is also thickness difference from landward to seaward direction where the unit is thinning down-slope, from as thick as 550 up-slope to as thin as 50 m down-slope (Fig. 3.15) with exception in some areas (e.g., eastern part).

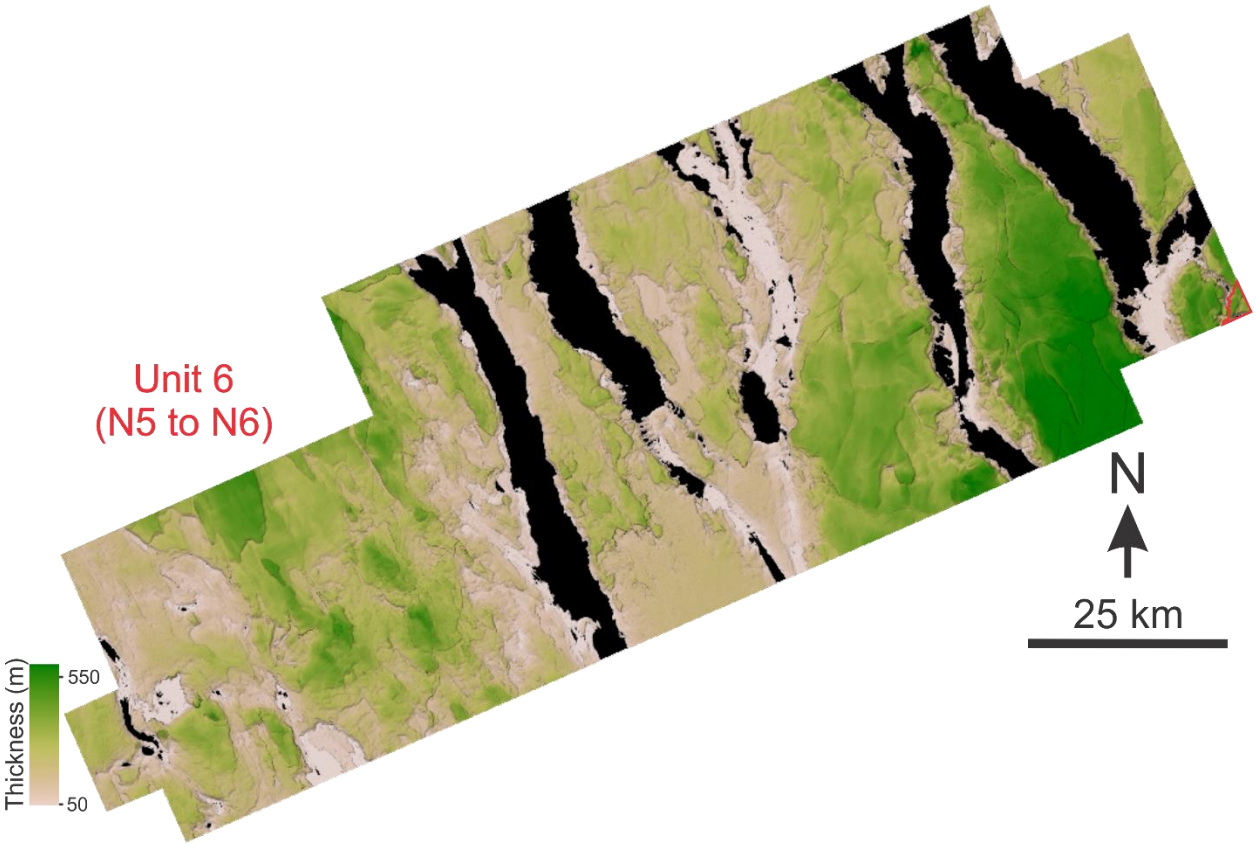

Figure 3.15. Isochore map of Unit 6.

3.3.2. Subsurface seismic stratigraphic features

3.3.2.1. Contourite sediment drifts

The identification of sediment drifts in seismic reflection data used in this thesis was based on other studies on sediment drifts on the Scotian Margin previously done by MacDonald (2006), Campbell (2011), Campbell and Deptuck (2012), and Campbell and Mosher (2016) on the Scotian Slope. Most sediment drifts commonly have either mounded (e.g., Fig. 3.20B), sheeted, or elongated morphology (e.g., Fig. 3.17) (Faugères and Stow, 1993; Stow and Faugères, 1998; Faugères et al., 1999; Rebesco and Stow, 2001; Stow et al., 2002; Posamentier et al., 2007; Faugères and Stow, 2008; Campbell, 2011; Campbell and Mosher, 2016).

Faugères and Stow (2008) suggested that the distinct features of contourite depositional systems are:

- the internal reflections of sediment drifts appear weaker than the bounding reflectors (e.g., unconformity or erosional truncation surface; Figs. 3.16; 3.18),
- locally thicker sediment thickness of drift packages than the surrounding sedimentary cover (e.g., Figs.3.17; 3.19),
- sediment drifts are commonly thicker on the drift axis, then thin landward and basinward, possibly forming as lens-shaped package of sediments,
- sediment drifts often have sigmoidal reflectors in cross section (e.g., Figs. 3.16; 3.18), and arcuate or linear ridges or more subtle amplitude anomalies in map view.

Large-scale sediment drifts can cover an area on the order of >1000 km^2 in map view (Faugères and Stow, 2008; e.g., Fig. 3.17). Small-scale sediment drifts are typically elongate in down-slope direction and extend for 10 km or more down-slope (e.g., Fig. 3.19). These small-scale sediment drifts are typically hosted within channels (Fig. 3.22A; Campbell, 2011; Campbell and Mosher, 2016).

Sediment drifts are recognized on the slope above P1 and below N1 horizons in Unit 1, above N2 and below N3 horizons in Unit 3 by wavy, sigmoidal, coherent, low to high amplitude reflections from the upper slope, and between N3 and N4 in Unit 4. On the middle to lower slope, a mass transport deposit (~2 to 5 km long) is observed on top of the contourite deposit and is deformed by two salt diapirs (Fig. 3.16). A dip-oriented seismic profile (Fig. 3.16) shows that this Eocene-aged contourite deposit is in Unit 1.

A Late Miocene contourite deposit is observed and recognized by sigmoidal reflections in Unit 3. The thickness of this drift can reach up to 400 m and forms an elongated morphology along-slope (NW-SE direction) in the Unit 3 isochore and mounded in some parts of the survey creating sediment thicks, as depicted in Figure 3.17. This is the younger Late Miocene Shubenacadie Drift (Campbell and Mosher, 2016 and Deptuck and Kendell, 2020) bounded by N2 and N3 horizons (Fig. 3.16).

Another sediment drift is recognized in Late Miocene by the presence of wavy, sigmoidal, coherent reflections in Unit 4. This drift is located only infilling an N3 paleocanyon, that appears to be relatively small-scale and localized compared to the large-scale Shubenacadie Drift (Fig. 3.19).

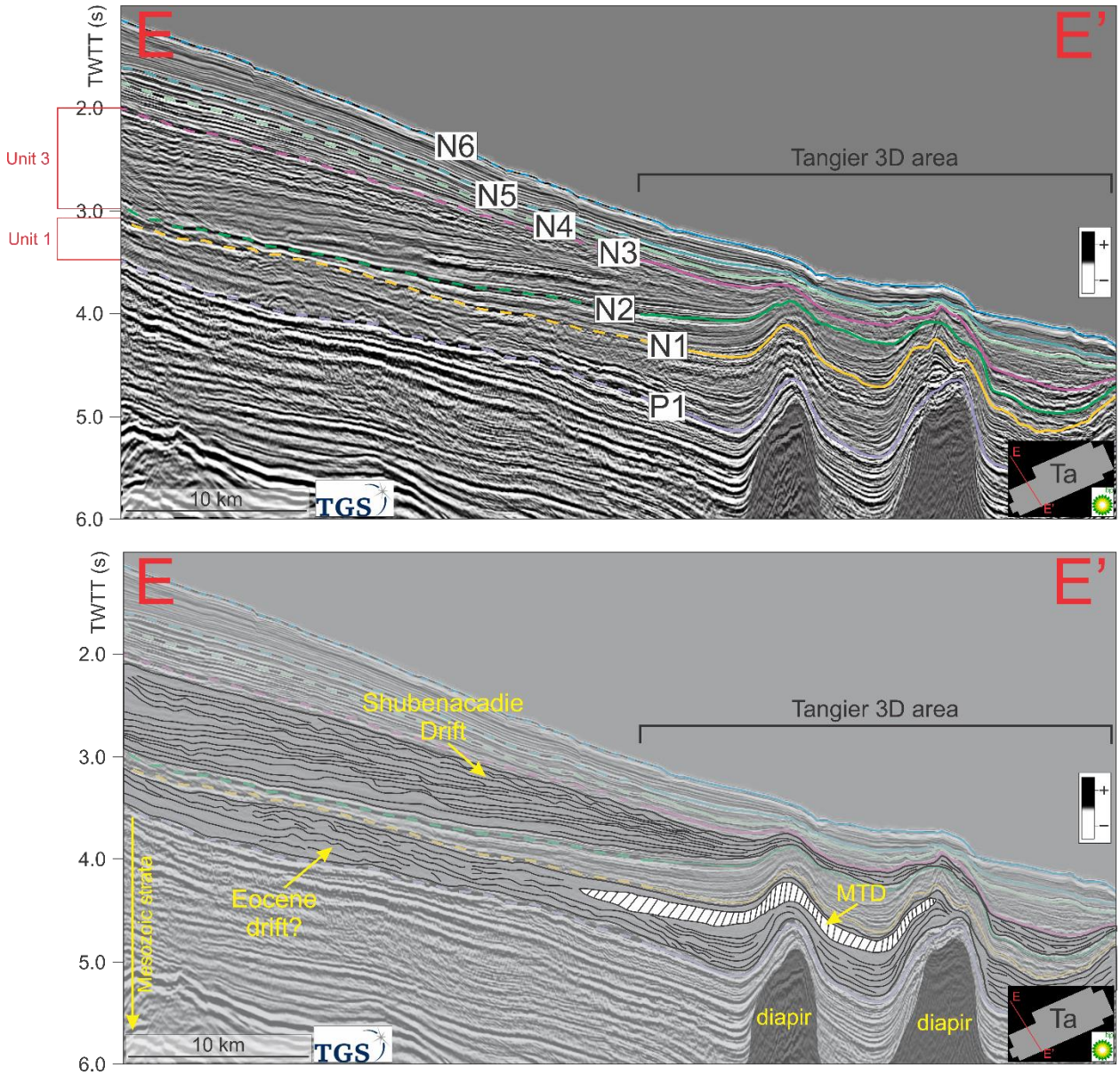

Figure 3.16. Interpreted 2D seismic line (E to E', location also in Fig. 3.17; see Appendix VI for uninterpreted version) illustrating sediment drift deposits found between P1 and N1 horizons (mainly Eocene-aged drift?), and between N2 and N3 horizons (Shubenacadie Drift in Campbell and Mosher, 2016 and Deptuck and Kendell, 2020) across the slope.

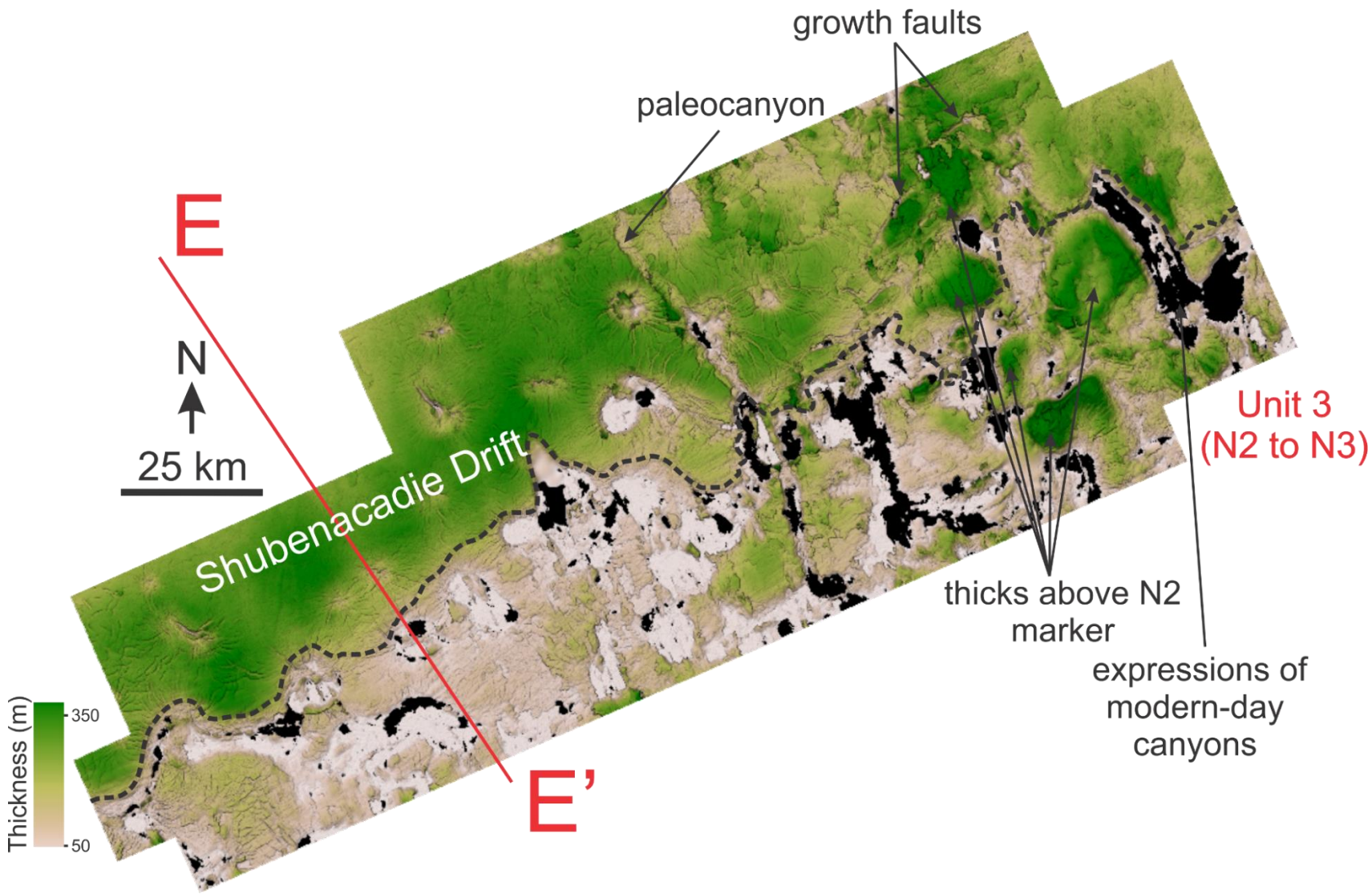

Figure 3.17. Isochore map of Unit 3 (N1 to N2; see Appendix V for uninterpreted version) showing the thickness of Shubenacadie Drift (Campbell and Mosher, 2016 and Deptuck and Kendell, 2020) across the Tangier 3D area with other stratigraphic features such as paleocanyons, stratal thinning where the salt diapirs are located (black boxes), and thicks above the developing minibasins on the eastern part of the study area. The extent of the Shubenacadie Drift is highlighted in dashed lines (derived from Deptuck and Kendell, 2020). Black regions represent areas where one or the other horizons is non-existent.

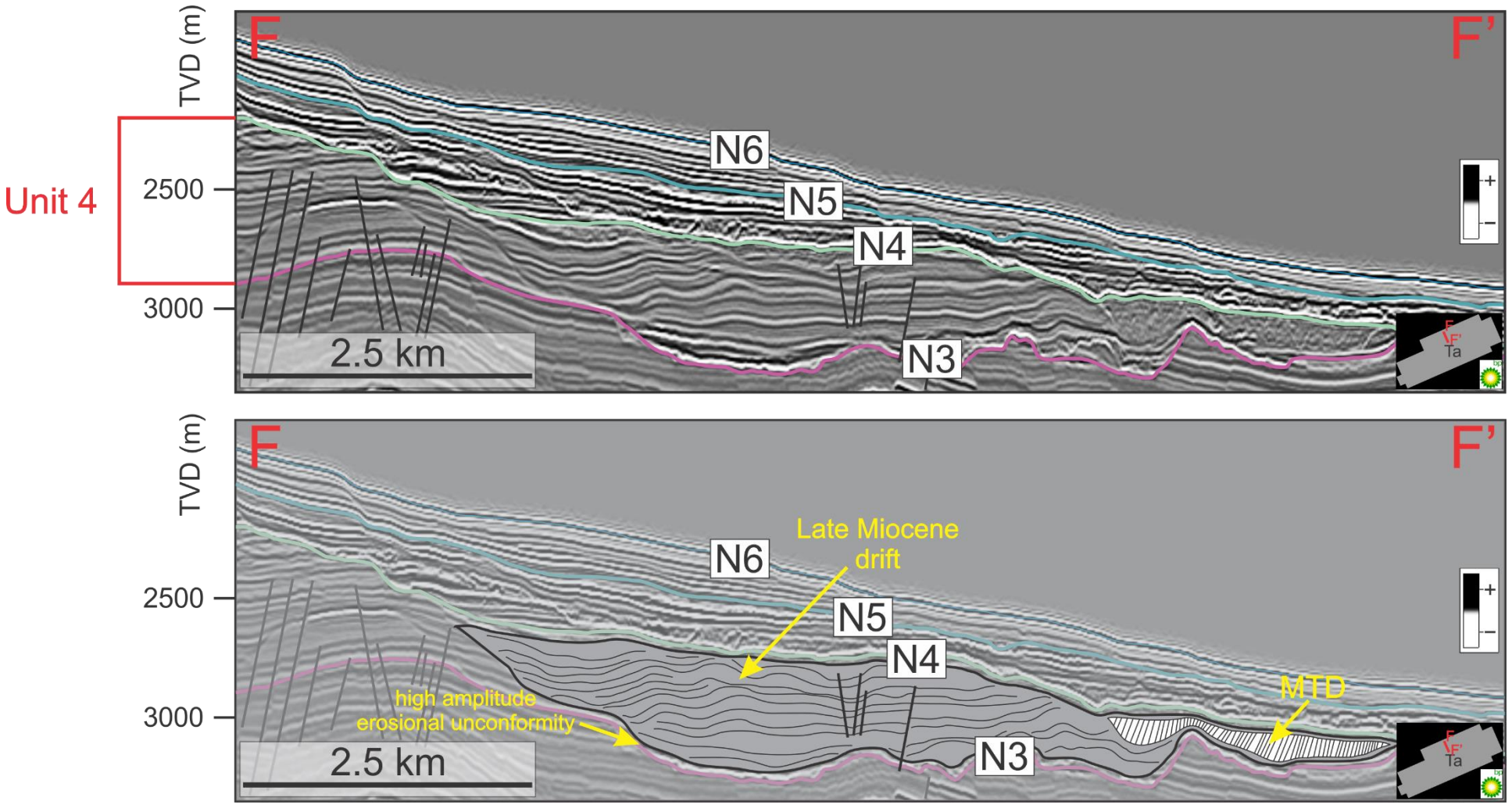

Figure 3.18. Interpreted dip-oriented seismic profile (F to F', location also in Fig. 3.19; see Appendix VI for uninterpreted version) is showing a small-scale Late Miocene drift (Unit 4, between N3 and N4 horizons) above a high amplitude erosive unconformity with associated mass transport deposit. The Late Miocene drift is only observed infilling an N3 paleocanyon, and this suggests strong influence of ocean bottom currents causing along-slope redistribution of sediments during this time. Data courtesy of BP Canada Exploration Ltd via NSDNRR.

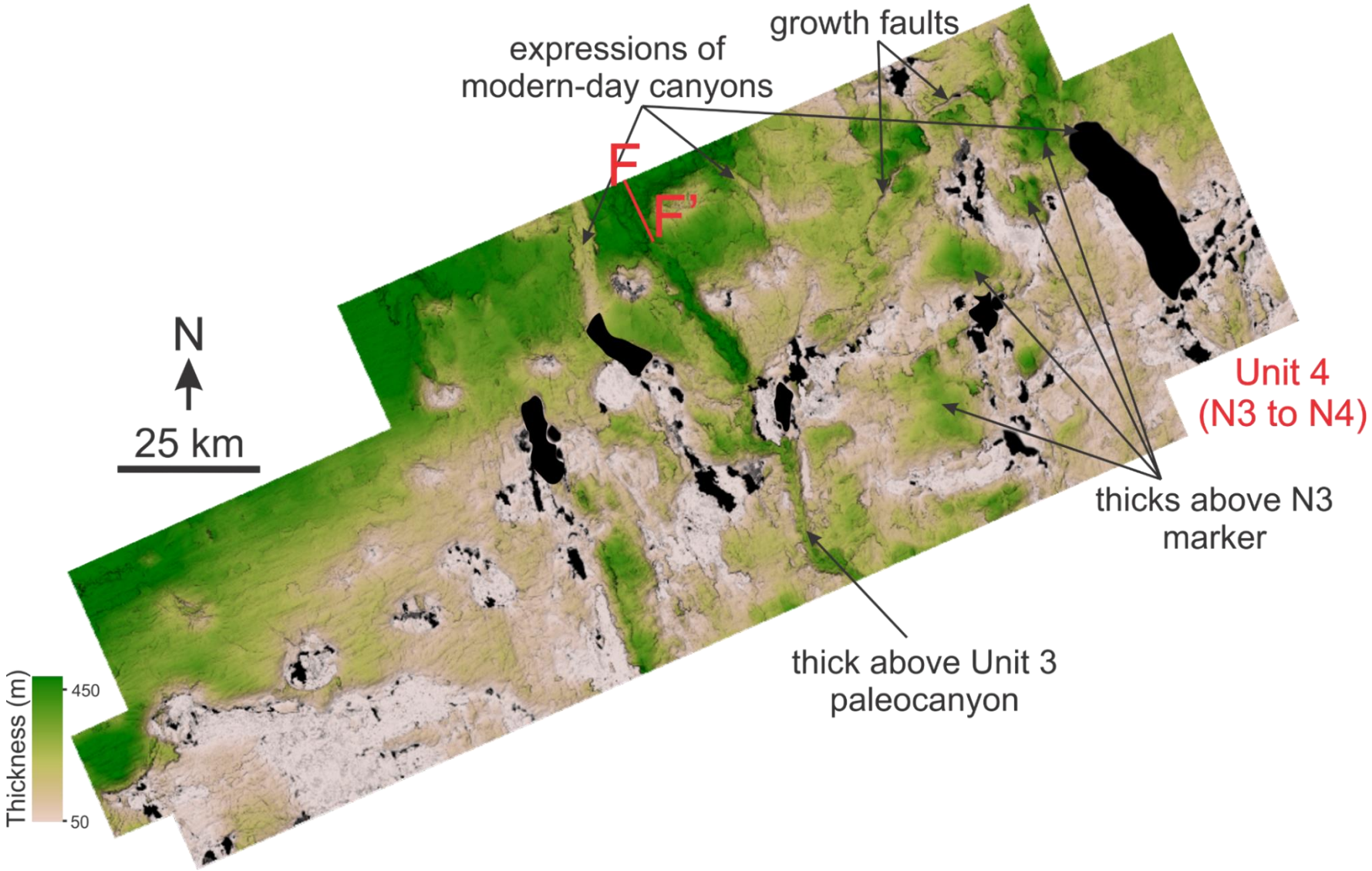

Figure 3.19. Isochore map of Unit 4 (N3 to N4; see Appendix V for uninterpreted version) showing the thickness of a small-scale Late Miocene drift across the Tangier 3D area with other stratigraphic features such as paleocanyons, stratal thinning where the salt diapirs are located (black boxes), and thicks above the developing minibasins on the eastern part of the study area. Black regions represent areas where one or the other horizons is non-existent.

3.3.2.2. Paleocanyons

The defined seismic facies of paleochannels are commonly expressed by a series of high amplitude seismic reflections with their base in a u- or v-shaped geometry in seismic sections and meander-like corridors with topographical lows in map view (Posamentier and Kolla, 2003; MacDonald, 2006; Posamentier et al., 2007). The paleochannel infill corresponds to high amplitude, high frequency, continuous reflectors onlapping the margins of the channels. In some cases, infill has asymmetrical facies onlapping the margin of the channel in seismic section (Fig. 3.22A) with moderate to high amplitude, wavy, coherent, continuous reflectors. (Posamentier and Kolla, 2003; MacDonald, 2006; Posamentier et al., 2007). Canyons are recognized on a larger scale (~5 to ~10 km wide in map view) than paleochannels with flat and wide high-amplitude reflectors recognized as canyon floors. Canyon fill can locally drape the base of the canyon (Figs 3.20A-3.21A) or aggrade as reflectors discordant to the surface (Fig. 3.21A) or in some cases, some canyon infills have wavy, reflectors (Fig. 3.22A).

Paleogene canyons

In Unit 1, there are u-shaped base features and onlapping reflections of the infills in the southwest part of the study area including at the level of the P1 horizon (Fig. 3.20B). These Unit 1 canyons are 5 km wide, and 2 km deep, and have a length that extends for at least 20 km down-slope, across the western part of the study area. These canyons were observed at a depth of ~2000 mbsf. These canyons have moderate RMS amplitude values in canyon floors as seen from RMS map using horizon extractions (Fig. 3.20C) with apparent lateral migration (Campbell et al., 2015; Deptuck and Kendell, 2020).

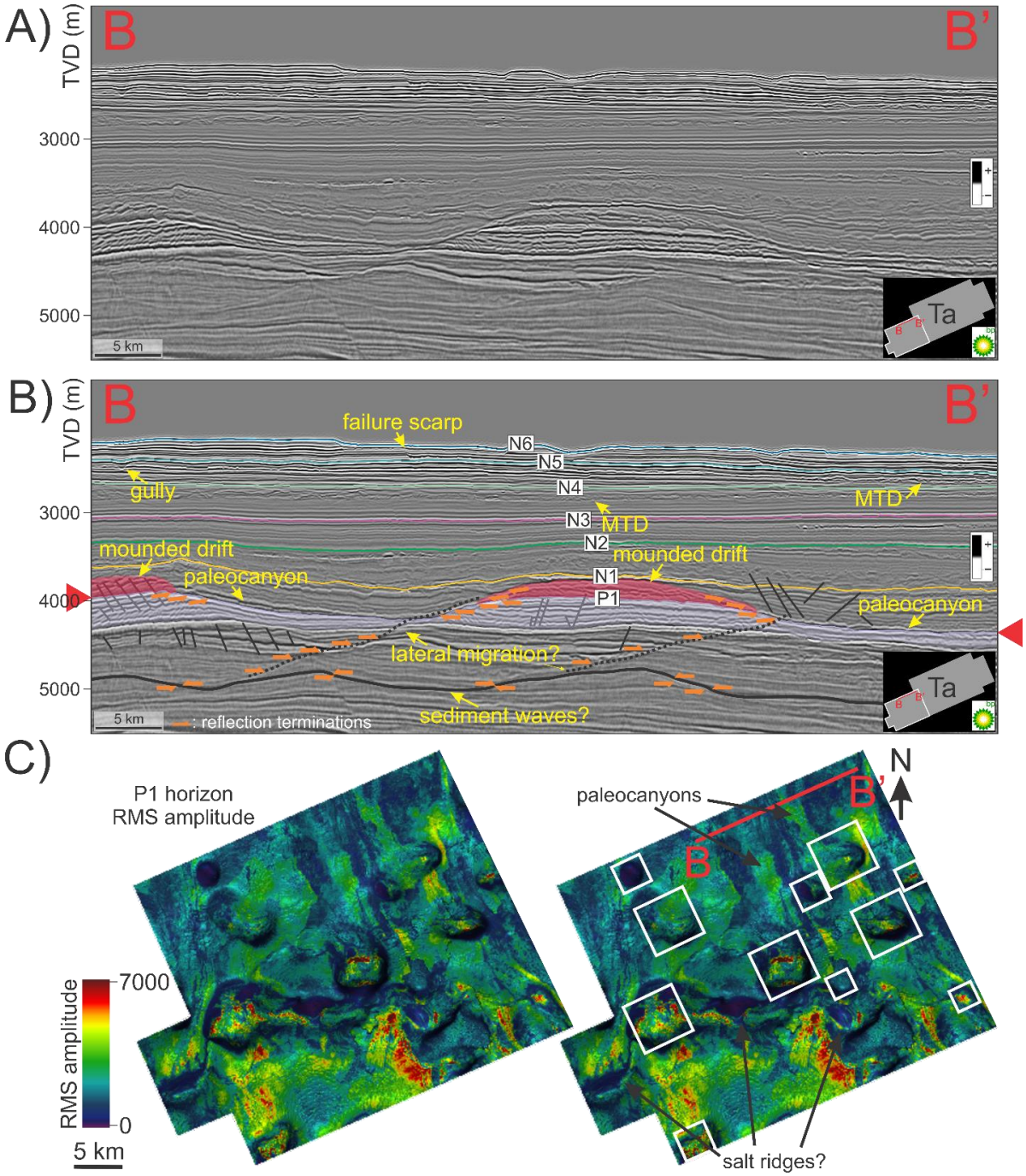

Figure 3.20. A) Strike-oriented section situated on the western part of the Tangier 3D area showing the uninterpreted, original seismic profile (B to B'); B) interpreted strike-oriented section (B to B') highlighting P1 horizon's paleocanyons and other sedimentary features such as underlying sediment waves (Campbell et al. 2015; Rodrigues et al., 2022) and overlying mounded sediment drift. C) An uninterpreted and interpreted portion of an RMS amplitude map (outlined in white from the inset map in A and B; see Appendix III for uninterpreted version) from P1 horizon in the Tangier 3D area showing the paleocanyons, salt diapirs (white boxes), and salt ridges. Data courtesy of BP Canada Exploration Ltd via NSDNRR.

Neogene canyons

Unit 2 contains a moderate amplitude, wide, u-shaped erosional feature that is 7 km wide, 2 km deep, and with a length that extends for at least 30 km down-slope, across the eastern part of the study area (Fig. 3.21B). Much of its fill onlaps the flanks of the structure and is composed of low to moderate amplitude reflections. This canyon is observed at a depth of ~1500 mbsf (Fig. 3.21A) in the Oligocene (e.g., Thomas, 2004). In RMS amplitude map (Fig. 3.21B), this canyon is manifested as moderate to high amplitude reflections at the base and floored with moderate to high amplitude reflections. In coherence map (Fig. 3.21B), the canyon is affected by a topographic high (e.g., salt diapir) suggesting salt diapir was moving at the time.

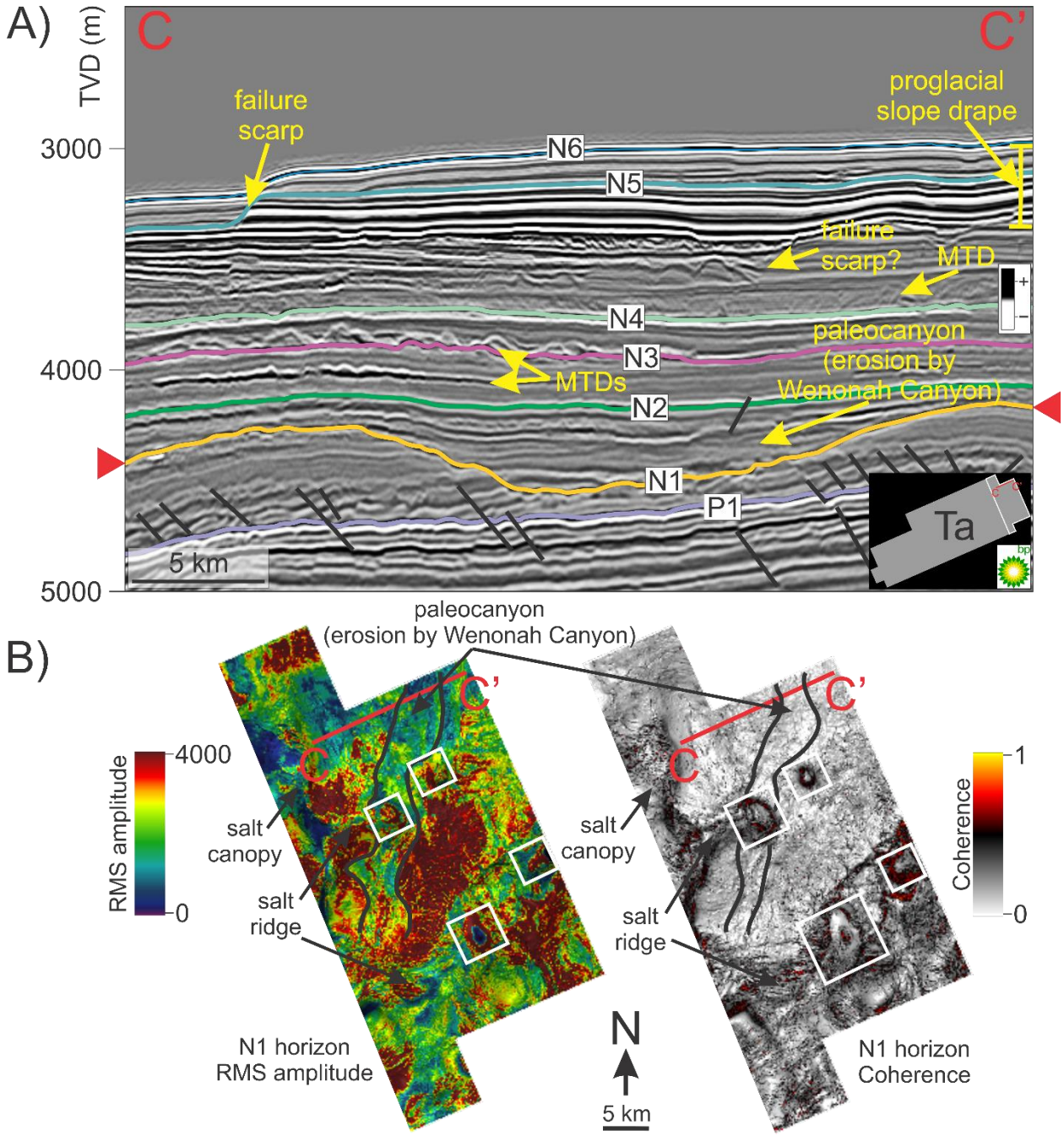

Figure 3.21. A) Strike-oriented section located on the eastern part of the Tangier 3D area showing interpreted seismic profile (C to C'; see Appendix VI for uninterpreted version) highlighting a paleocanyon mapped at the N1 horizon. B) A section of RMS amplitude and coherence maps from the N1 horizon in the Tangier 3D area (outlined in white in the inset map in A; see Appendix III for uninterpreted version) showing the paleocanyons, salt diapirs (white boxes), salt canopy, and salt ridges. Data courtesy of BP Canada Exploration Ltd via NSDNRR.

Unit 3 contains a clear erosional feature that is 5 km wide, and 2 km deep, and a length that extends for at least 35 km down-slope, across the eastern part of the study area. This conduit likely continues both landward (e.g., Deptuck, 2008) and seaward of the study area. It is floored by sinuous channels that have elevated amplitude near the floor of the incision (Fig. 3.22B). Much of its fill, however, is sigmoidal, comprising low to moderate amplitude reflections with the maximum thickness of successive fill packages migrating to the northeast, like representing contourite processes. The depth where the N3 canyon was found estimated at ~500 to ~700 m below seafloor (Fig. 3.22A). This canyon seems to wind around salt diapirs, implying there was relief on the diapirs at the time.

U-shaped erosional features originating from the seafloor (Fig. 3.23) cutting down to Units 5 and 6. These conduits also likely continue both landward and seaward of the study area. The extracted RMS amplitude maps of the canyons demonstrate high values of RMS amplitude. Areas with low amplitude suggest that these are regions of sediments with low impedance contrast, whereas areas with high amplitude suggest regions with high impedance contrast.

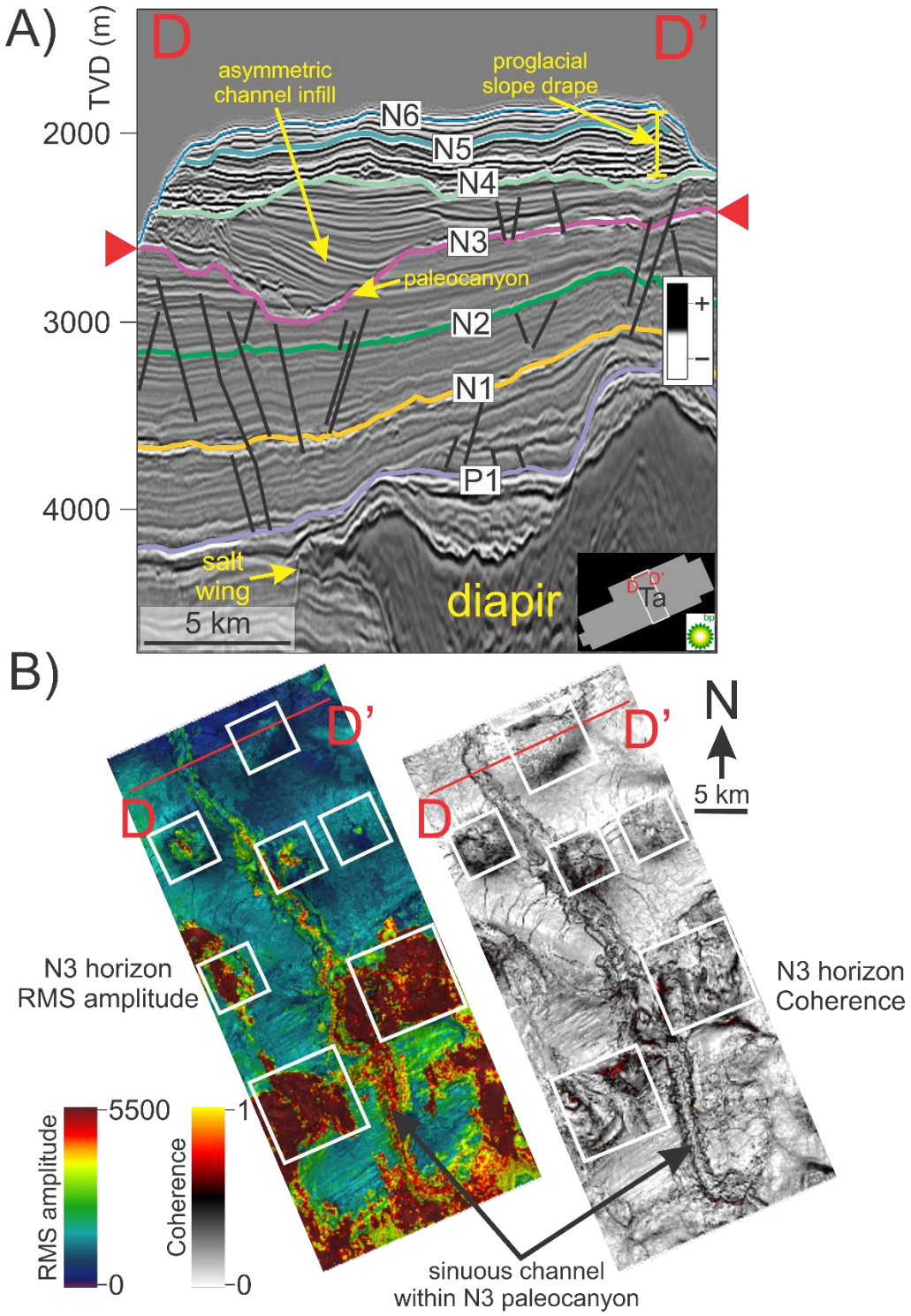

Figure 3.22. A) Strike-oriented section located on the central part of the Tangier 3D area showing interpreted seismic profile (D to D'; see Appendix VI for uninterpreted version) highlighting a notable paleocanyon mapped by N3 horizon. B) A section of RMS amplitude and coherence maps from N3 horizon in the Tangier 3D area (outlined in white in the inset map from A; see Appendix III for uninterpreted version) showing the paleocanyons, salt diapirs (white boxes) with polygonal and radial faults around the diapirs. Data courtesy of BP Canada Exploration Ltd via NSDNRR.

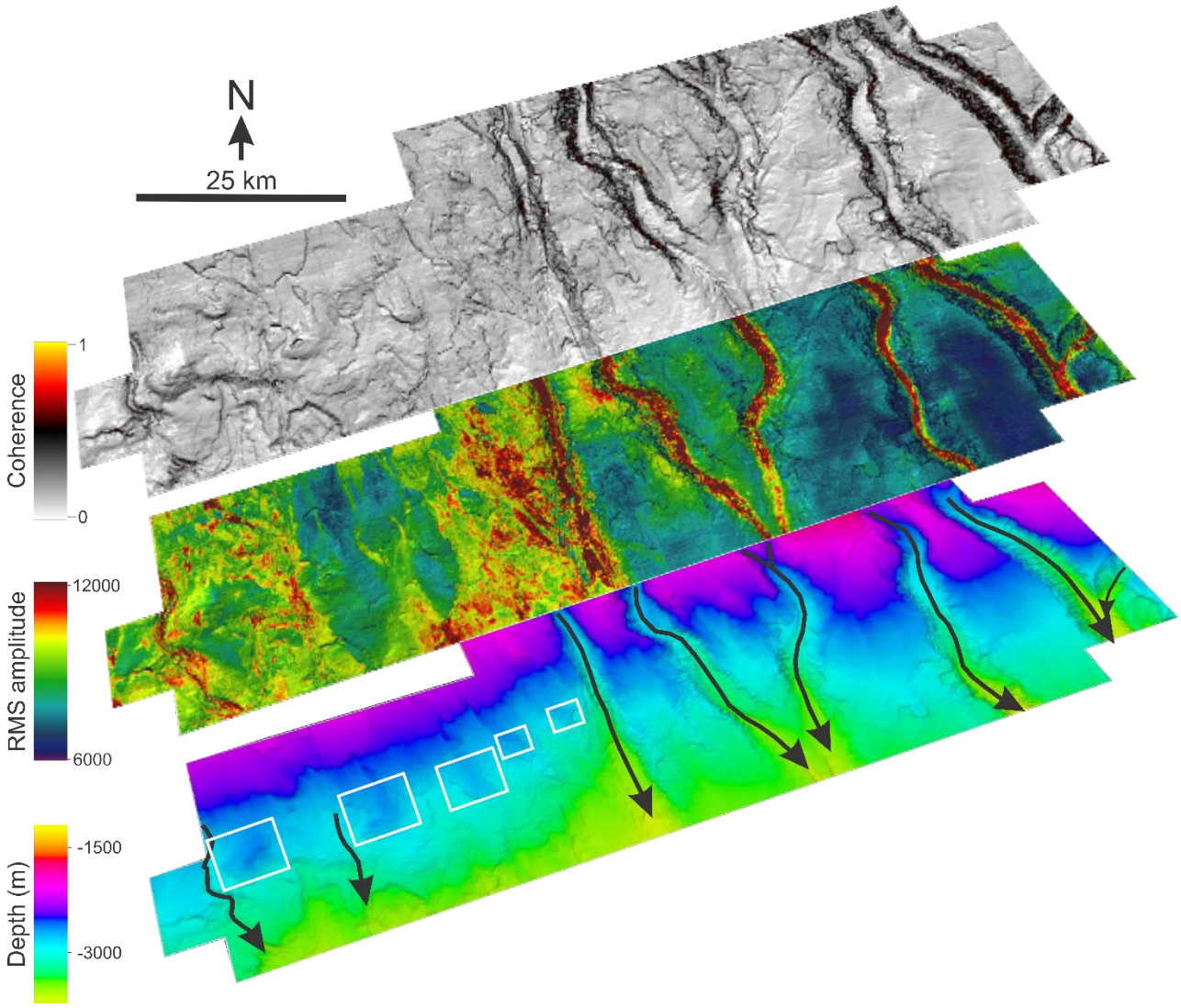

Figure 3.23. Generated depth-structure map of the N6 (seafloor) horizon with extracted RMS amplitude (see Appendix III for uninterpreted version) and coherence maps (see Appendix IV for uninterpreted version) to emphasize features such as submarine paleocanyons. The RMS amplitude map variations likely represent lithological changes between the canyon floor sediments and the surrounding areas that affect acoustic impedance contrast. The coherence map shows several slope failure scarps. The flow direction is indicated with black arrows. The white boxes highlight subtle expression of salt diapirs indicating that a limited degree of salt motion persists into near-modern times.

3.3.2.3. Slope drape

The recognition of slope draping horizons is based on commonly undisturbed, continuous to semi-continuous, moderate to high amplitude well-bedded reflectors with consistent thickness throughout the slope (Posamentier and Kolla, 2003; MacDonald, 2006; Posamentier et al., 2007). Slope draping units also occur in pre- and post-glacial periods. In addition, MacDonald (2006) suggested that proglacial slope draping units have excellent reflection continuity with distinct units of high- and low-amplitude coherent, well-stratified reflectors compared to non-glacial slope draping units as examples shown in Figures 3.24-3.25 and 3.28-3.32, usually occurring at the shallowest part of the strata.

Intervals of draping reflectors are recognized across the study area, where the draping reflectors maintain a consistent appearance due to their reflection continuity and low to moderate amplitude in Unit 1 to Unit 2 and in Unit 3 to Unit 4. It is also notable that the sediment thicknesses of these slope drapes broadly thin seaward and adjacent to and over paleobathymetric highs such as above salt diapirs. The slope draping units are commonly affected by faults caused by salt bodies and occasionally truncated by N4 horizon.

There are also well-stratified draping reflectors at the shallowest part of the Cenozoic in Unit 5 and Unit 6 (Figs. 3.21A; 3.22A). In terms of sediment thickness, these shallow draping horizons thin seaward and within areas of interpreted paleobathymetric highs such as salt diapirs. In some parts of the survey, modern-day canyon incisions commonly truncate these shallow slope draping facies (Figs. 3.28-3.32).

3.3.2.4. Slope failure complexes

Recognition of mass transport complexes is based on distinct features such as complex reflection characteristics with an underlying high amplitude erosional unconformity or the basal shear surface (Figs. 3.24-3.25) with the material translated and internally jumbled or deformed to become the overlying mass transport deposits (MTDs). The MTD facies type is described as commonly low amplitude with weak, chaotic, incoherent internal reflections (Varnes, 1978; Posamentier and Kolla, 2003; Posamentier et al., 2007; Bull et al., 2009).

In the Tangier 3D area, most of the mass transport deposits conform and onlap the flanks of salt structures on the lower parts of the slope (Figs. 3.24-3.25) within mass transport corridors (e.g., as defined by the map distribution of basal shear surface). MTD corridors are geographically confined zones of repeated mass failure events (Mosher et al., 2004; Campbell, 2005).

Above the N1 horizon in Profile G to G' (Fig. 3.24), an MTD unit is recognized with a recognizable basal shear surface (BSS) and possibly sections of BSS such as ramp and flat within the otherwise well-stratified, concordant, low to moderate amplitude reflectors of Unit 2. A ramp is defined as a segment of a basal shear surface that cuts up or down discordantly across bedding or to a new stratigraphic level (Bull et al., 2009). A flat is defined as the parallel segment of the basal shear surface on the newly cut stratigraphic level and is connected by ramps (Fig., 3.24; Bull et al., 2009). The Unit 2 MTD thickens seaward towards a ramp and then starts to thin due to widespread erosion that occurred in N4 horizon.

An observed mass transport deposit is also mapped in Unit 4 (between N3 and N4 horizons), that can be traced by the basal shear surface within the well-stratified, concordant, low to moderate amplitude reflectors of Unit 4 (Figs. 3.24-3.25). The Unit 4 MTD differs from the MTD observed from Unit 2 in terms of reflection characteristics and thickness. Unit 4 MTD appears

weakly chaotic, wavy, low to moderate amplitude reflectors, whereas Unit 2 MTD appears to have chaotic, fragmented, moderate to high amplitude reflectors. In terms of thickness, Unit 4 MTD thins basinward, whereas Unit 2 MTD thickens basinward. However, both MTDs are truncated by Unit 5 and are affected by structural relief caused by salt diapirs. There are also several patches of Unit 5 MTDs (Figs., 3.24-3.25) possibly originated from the mass transportation of slope drape units.

Multiple occurrences of MTD of various scales and intervals are recognized within the Tangier 3D area by using coherence maps. MTDs are recognized in coherence maps by appearing to have an irregular, granular variability in coherence maps (Fig. 3.26).

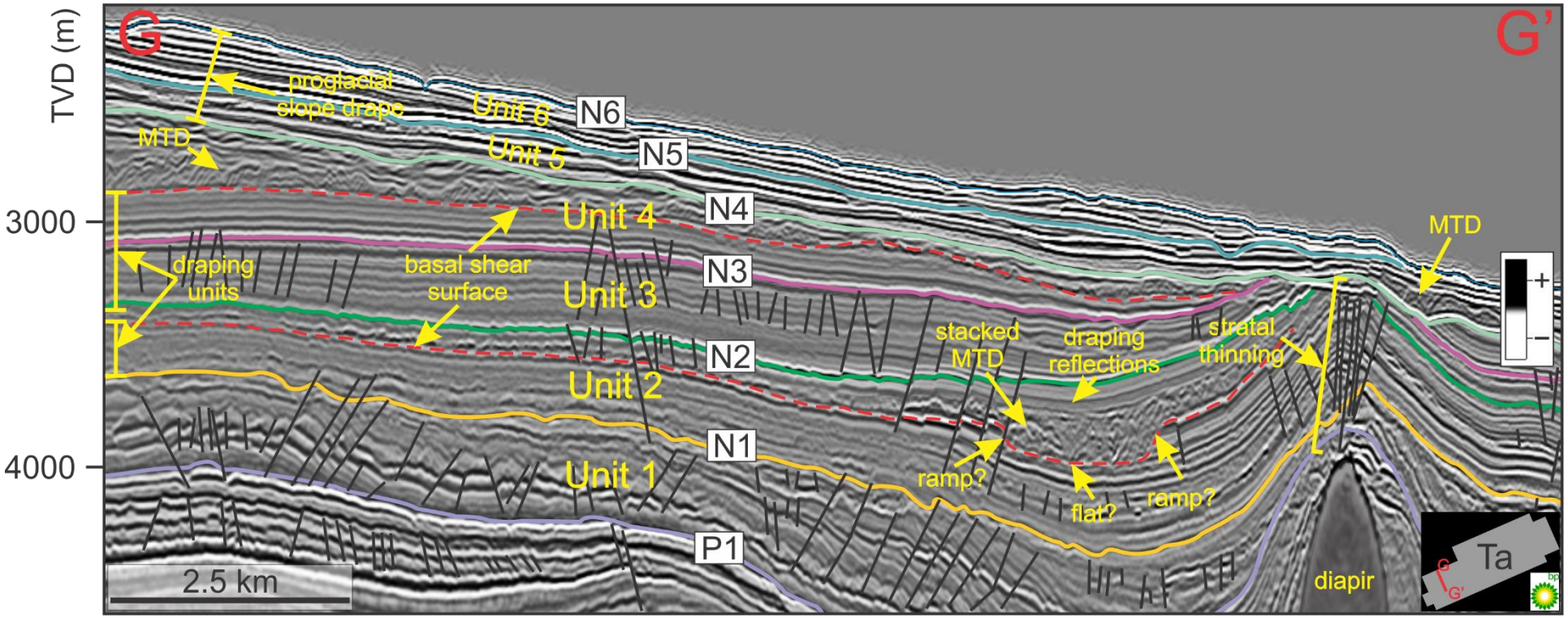

Figure 3.24. Representative dip-oriented section (G to G', location in Fig. 3.26; see Appendix VI for uninterpreted version) of slope failure deposits in different periods mapped between N1 and N2, and N3 and N4 horizons with associated structural architecture. The observed MTDs have weak, incoherent, seismic reflectors with low to moderate internal reflections. These occur on basal shear surfaces (BSS) for both MTDs, which truncate underlying well-stratified, low to moderate amplitude reflectors. A recognizable basal shear surface ramp is found in the Unit 2 MTD. Both MTDs thin towards the salt diapir due to paleo-seafloor relief related to salt movement. Data courtesy of BP Canada Exploration Ltd via NSDNRR.

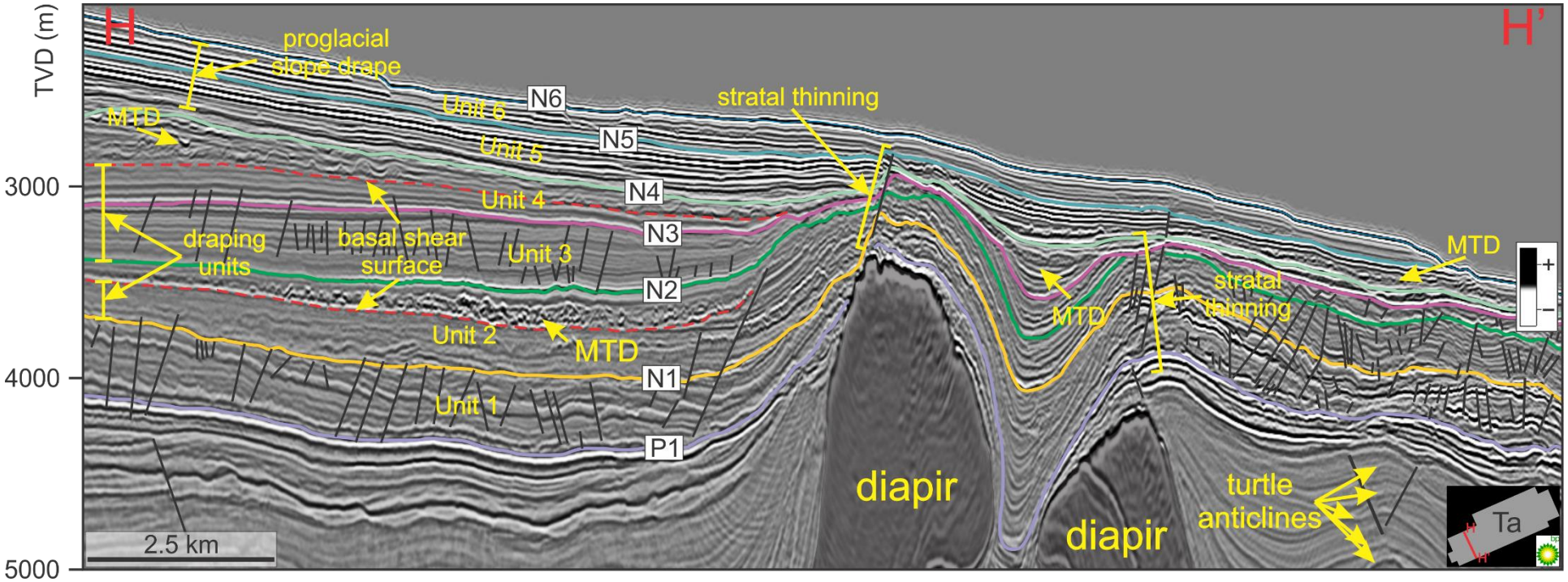

Figure 3.25. Representative dip-oriented section (H to H', location in Fig. 3.26; see Appendix VI for uninterpreted version) of another occurrence of slope failure deposits situated in Units 2 (between N1 and N2 horizons) and 4 (between N3 and N4 horizons). The observed MTD in Unit 2 demonstrates excellent low- to high-amplitude, chaotic reflectors compared with the recognized MTD in Unit 4 that shows more weak, incoherent, chaotic reflections. Both MTDs have recognizable basal shear surfaces (BSS) that are situated within the underlying, more concordant, well-stratified, low to moderate amplitude reflectors. Data courtesy of BP Canada Exploration Ltd via NSDNRR.

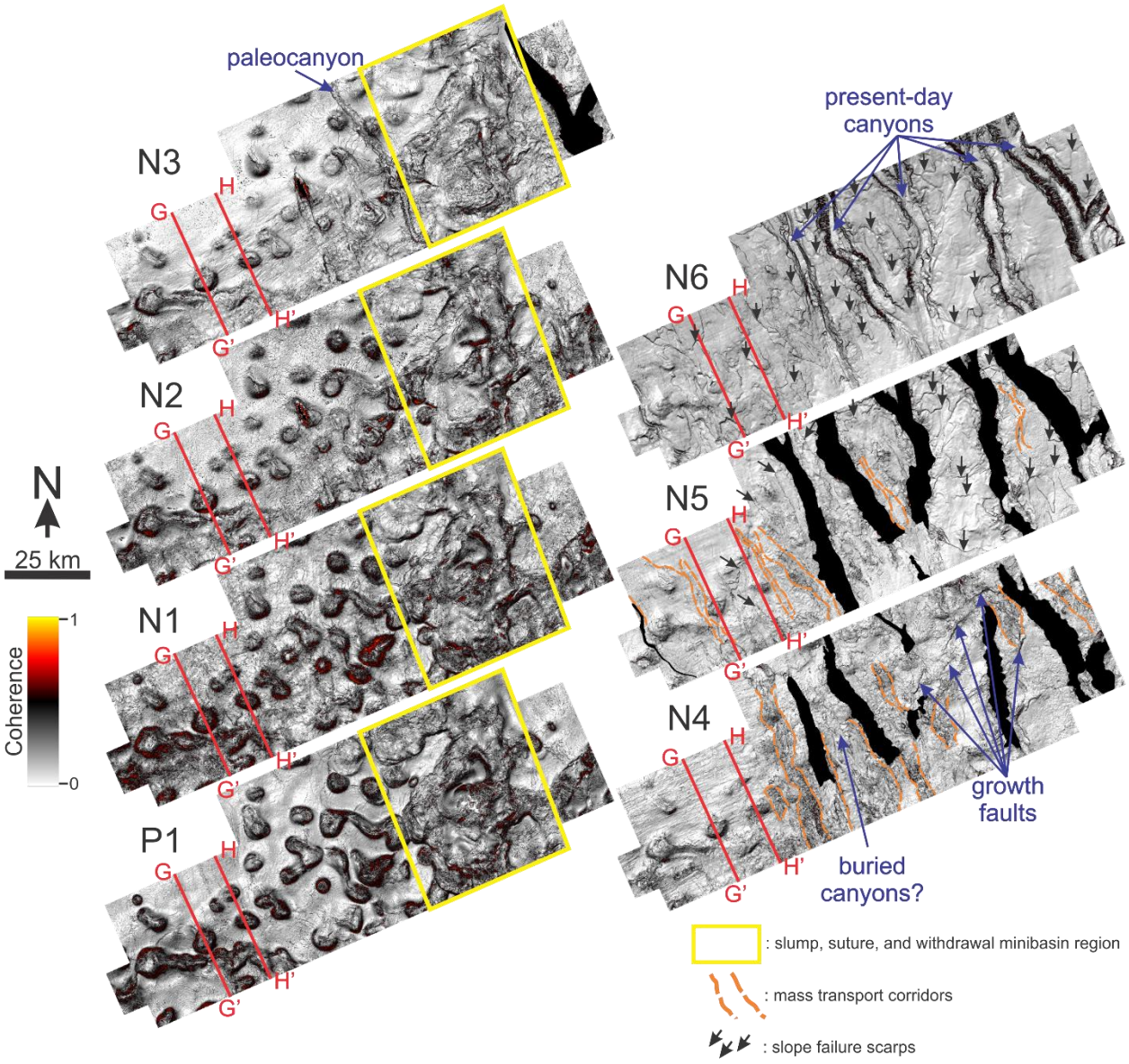

Figure 3.26. Extracted coherence maps from the seven key horizons (P1 to N6 horizons; see Appendix IV for uninterpreted version) showing slumps and withdrawal minibasins within the canopy complex during the Paleogene with increasing evidence of deposits from mass transport processes with accompanying slope failure scarps towards the Neogene. Black regions represent areas where horizons are non-existent (e.g., removed by modern seafloor canyons).

3.3.2.5. Distribution of salt bodies

Salt bodies in the study area were recognized as either vertical or horizontal slabs bounded by high amplitude reflections with reflection or amplitude blanking inside (e.g., Fig. 3.8A-B). In isochore maps (e.g., Figs. 3.10-3.15), salt bodies are recognized as such create a contrast in subsurface structural relief as salt bodies compress associated units at their crest, creating areas of thinning or areas of high sediment thickness in adjacent withdrawal minibasins.

Allochthonous salt bodies

Salt diapirs

Vertical salt diapirs in the study area typically appear elliptical in map view (Fig. 3.27) oriented with their long axis in the NW-SE direction. In seismic profiles, these diapirs typically are recognized to be vertical bodies with reflection blanking inside, bounded by high amplitude reflections. Diapirs also have a rounded bulb and pinched stems when resolvable (Fig. 3.31). In some parts of the survey, some diapirs have salt wings, which are defined as having high amplitude reflectors with pinch-out-like geometry concordant to the adjacent strata.

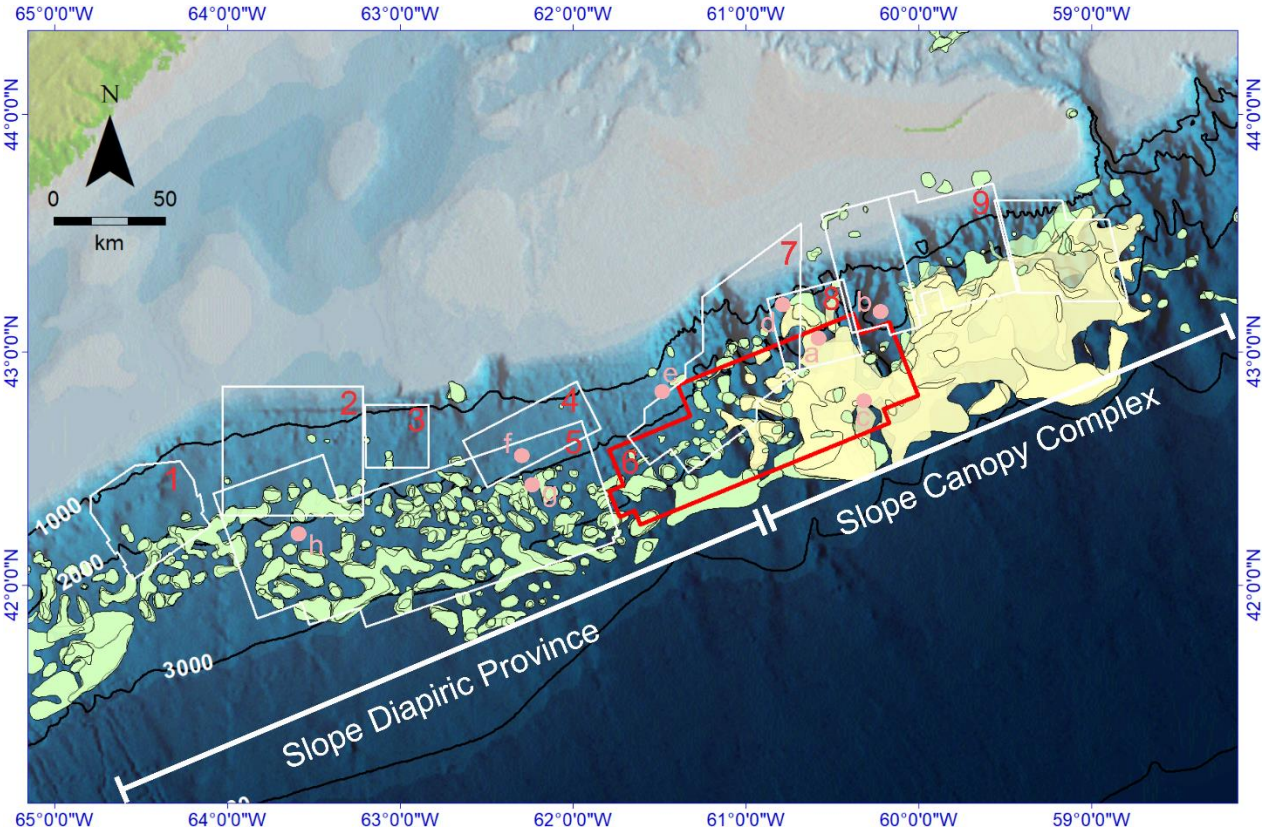

Figure 3.27. Map showing the location of the Tangier 3D area (red polygon), the Slope Diapiric Province (green) and the Slope Canopy Complex (yellow) (salt outline from OERA, 2011; labelled after Wade and MacLean, 1990 and Kendell, 2012). Scotian Slope seismic surveys: (1) Barrington 3D; (2) WG 3D; (3) Mamou 3D; (4) Torbrook 3D; (5) Shelburne 3D; **(6) Tangier 3D (study area)**; (7) Thrumcap 3D; (8) Weymouth 3D; (9) Veritas 3D. Locations of exploration wells near/within Tangier 3D: (a) Weymouth A-45; (b) Balvenie B-79; (c) Aspy D-11/D-11A; (d) Newburn H-23; (e) Shubenacadie H-100; (f) Torbrook C-15; (g) Cheshire L-97/L-97A; (h) Monterey Jack E-43/E-43A.

Salt canopy

The salt canopy body dominates the eastern part of the study area, which is part of the Sable Canopy Complex on the Scotian Margin (Deptuck and Kendell, 2020). In seismic profiles, salt canopy bodies are recognized as horizontal slabs with reflection blanking inside, bounded by high amplitude reflections (e.g., Figs. 3.28; 3.32). In map view, salt canopy bodies are massive

that could extend kilometres, with no distinct geometry, in the eastern part of the study area (Fig. 3.27).

Distinctive structural features are present in the canopy area such as withdrawal minibasins on top of the canopy (Figs. 3.21–3.22; 3.25–3.27), rafted overburden (highlighted in orange in Figs. 3.28; 3.32–3.33), and salt walls and ridges (Fig. 3.26).

Overburden

All observed salt bodies in the study area are buried by Paleogene to Neogene rocks and sediments (Figs. 3.28-3.32). Overburden thicknesses range from 200 m to <1 km in the distal areas in Tangier 3D (Figs. 3.28; 3.32). In some cases, shallow buried diapirs and canopies are in areas where present-day canyons are locally incising the materials above the salt crests (Figs. 3.29-3.32), focusing erosion on the overburden, or recent expulsion/movement of salt bodies, where even the seafloor horizon shows subtle expression of salt mobility due to sea floor relief (Deptuck and Kendell, 2020).

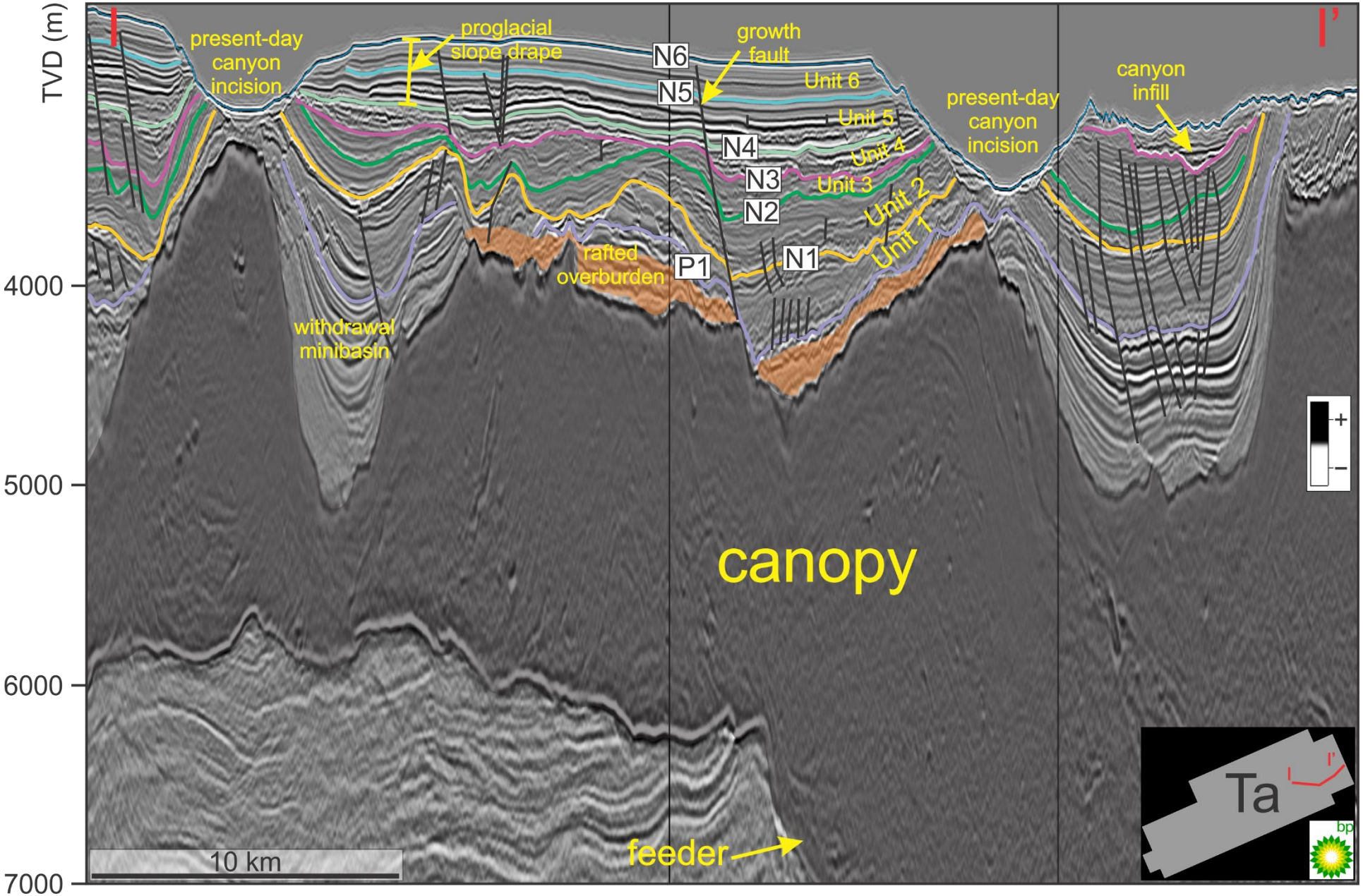

Figure 3.28. Representative strike-oriented section (I to I'; see Appendix VI for uninterpreted version) showing incising modern-day canyons resulting to low overburden thickness above a salt body. Data courtesy of BP Canada Exploration Ltd via NSDNRR.

Other salt-related structures

Crestal faults are any type of faults situated above a crest of a salt body. Radial faults are the most common fault networks that are associated with salt diapirism in the area. These are normal faults that extend radially from the salt body into the salt flanks (Carruthers et al., 2013; Coleman et al., 2018). Polygonal faults do not necessarily require salt deformation to be developed. Polygonal faults are a network of normal faults that are layer-bounded, argued to be formed by compaction and dewatering, which is common in fine-grained sediments (Figs. 3.24-3.25; 3.34; Cartwright and Lonergan, 1996; Carruthers et al., 2013; Li et al., 2020). Most of the salt bodies in the study area are overlain by crestal faults, recognized as displacement features of low to high amplitude reflectors.

Several salt-related structures such as carapaces and rafted overburden are observed in the study area. Carapaces are salt-related structures commonly defined as older hemipelagic-pelagic sediments that have been uplifted and detached from older strata due to the movement of salt bodies. Usually, the seismic character of carapaces is low amplitude internal reflections with discordant facies (e.g., Christians, 2015; Jackson and Hudec, 2017). On the slope, these blocks of hemipelagic-pelagic sediments are found above the crests of some salt diapirs and are commonly bounded by faults (Figs. 3.29-3.30). Rafted overburden is associated with older strata that was displaced by the allochthonous salt canopy (Fig. 3.32-3.33) and is commonly faulted. Rafted overburden and carapaces are deforming the underlying salt diapirs (highlighted in orange in seismic sections in the study area).

Several vertical salt diapirs show salt stems in the study area (Fig. 3.31). In addition, several salt diapirs appear to be completely detached from the salt feeders, leaving the bulb and an underlying salt weld. Interpretation of salt feeders are important in terms of locating the potential

source of allochthonous salt bodies feeding the salt canopy complexes. In the study area, salt feeders are located on top of structural highs (e.g., salt highs) and sometimes on paleobathymetric lows (e.g., withdrawal minibasins; Figs. 3.28; 3.31-3.32), when resolvable.

Additional seismic structural observation shows the presence of turtle structures (Fig. 3.25). These structures are recognized by their low to high amplitude reflections with turtle-back geometry (dome or anticline) in the study area. The presence of turtle anticlines is common in the Late Cretaceous (Fig. 3.25; Fig. 4.15). From the Paleogene to the Neogene, these turtle anticlinal structures are not pronounced based on the geometry of the reflectors.

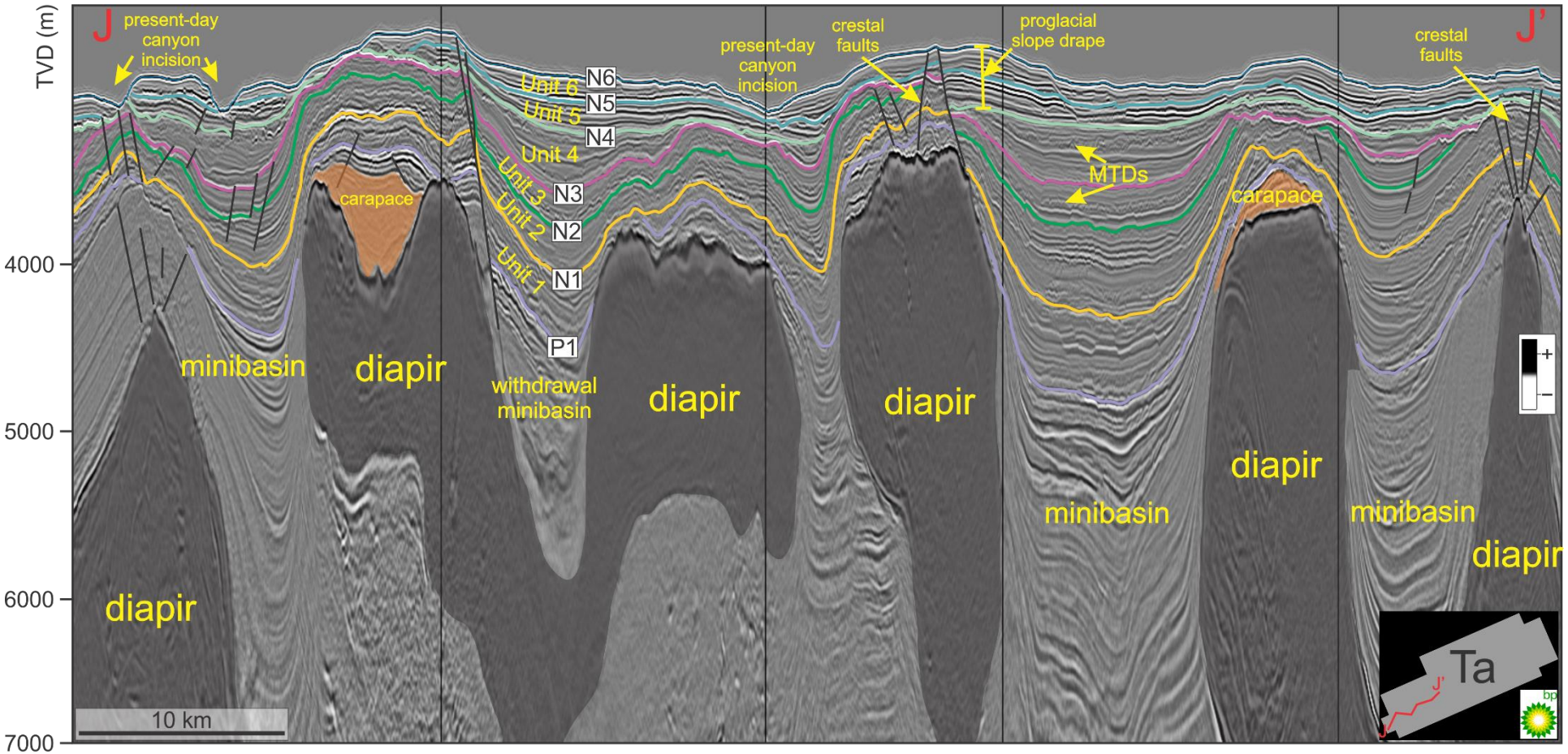

Figure 3.29. Representative strike-oriented section (J to J'; see Appendix VI for uninterpreted version) showing different diapirs with associated features such as carapaces, minibasins, and crestal faults along with the presence of erosion from the modern-day canyons. Data are courtesy of BP Canada Exploration Ltd via NSDNRR.

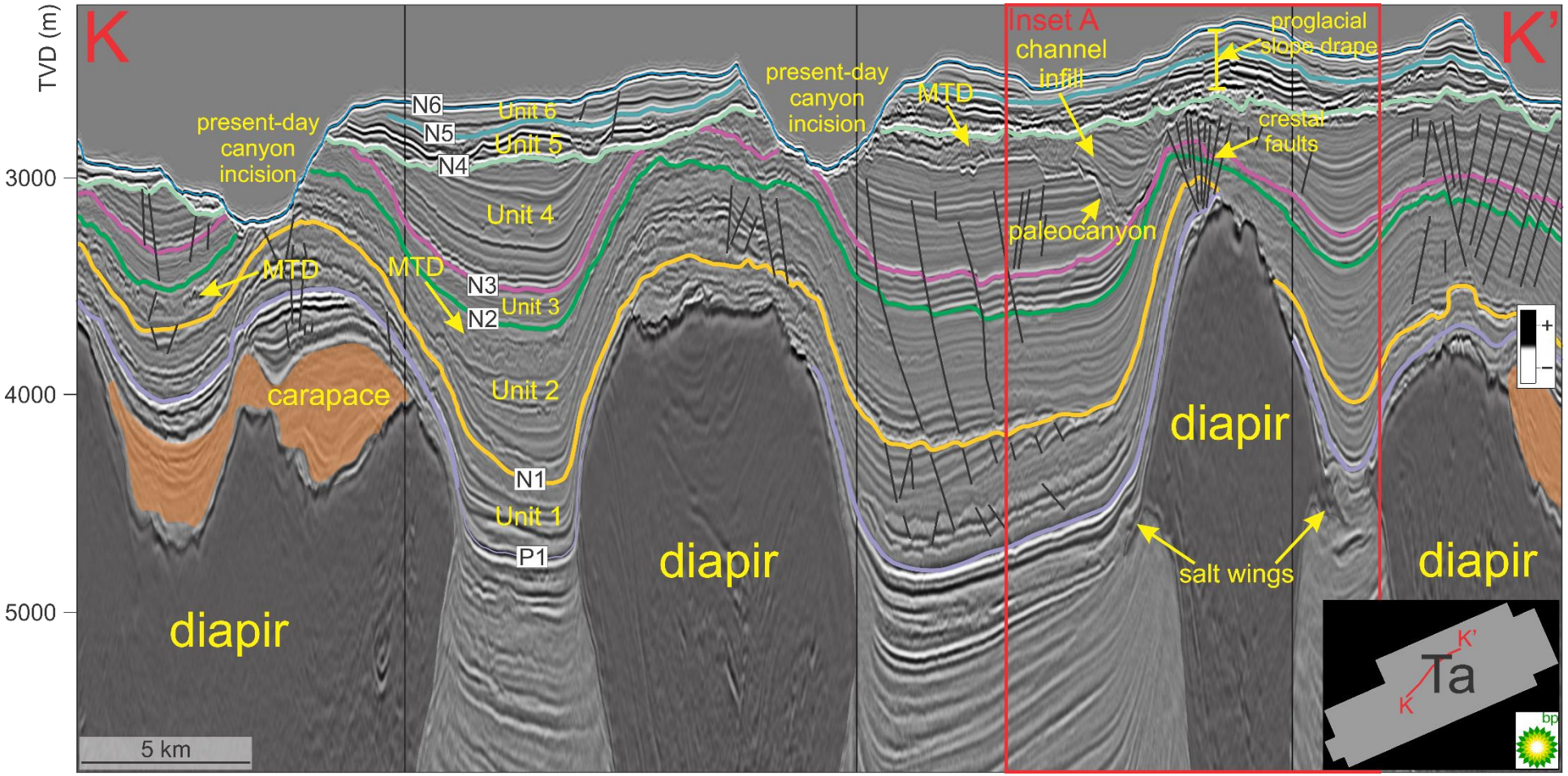

Figure 3.30. Interpreted strike-oriented section (K to K'; see Appendix VI for uninterpreted version) showing other salt-related features such as rafted overburden, salt wings, paleochannel infill, and notable mass transport deposit above a diapir. Data courtesy of BP Canada Exploration Ltd via NSDNRR.

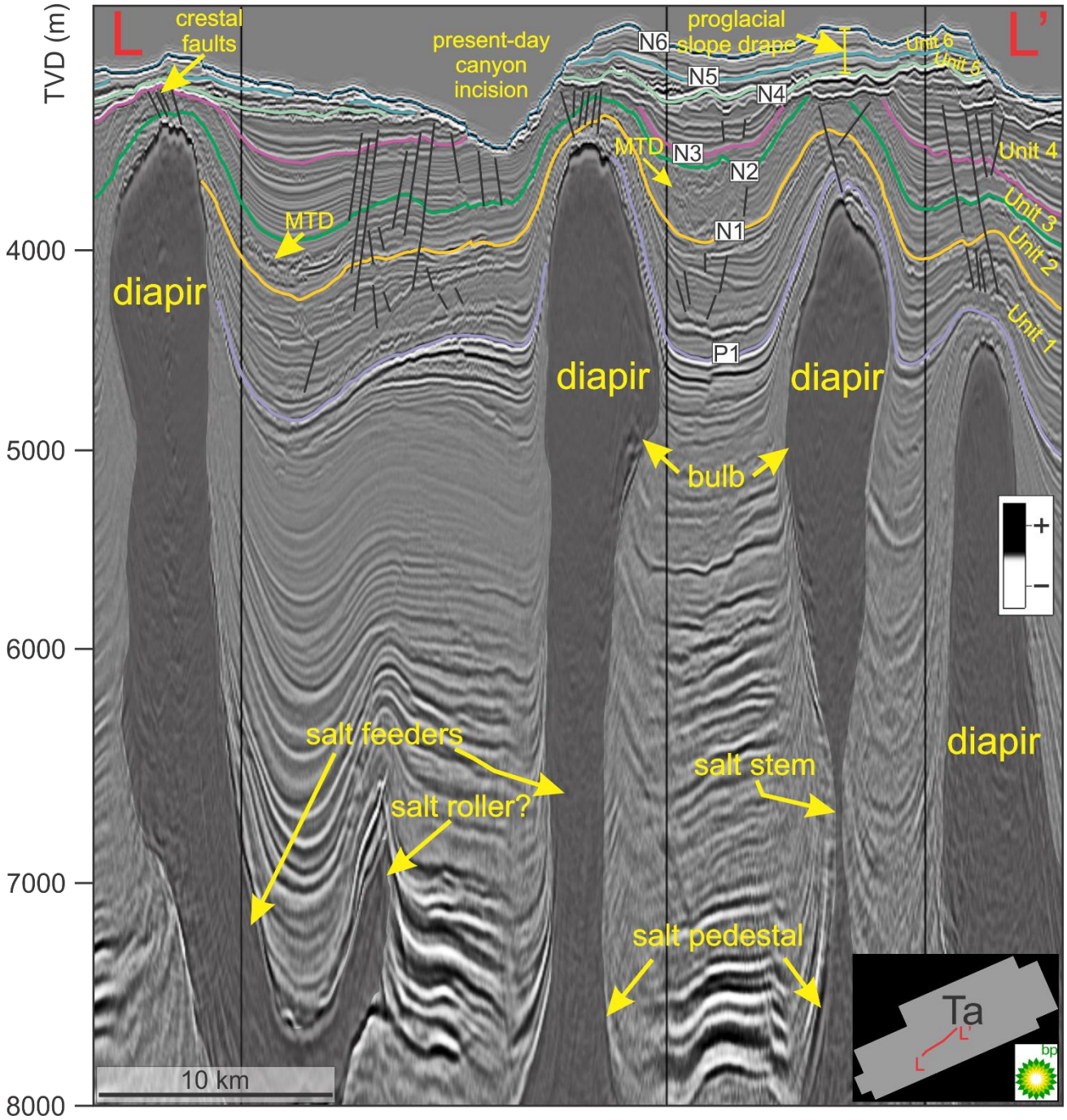

Figure 3.31. Representative strike-oriented section (L to L'; see Appendix VI for uninterpreted version) showing diapirs with salt pedestals, salt roller, stems, and bulbs. Data courtesy of BP Canada Exploration Ltd via NSDNRR.

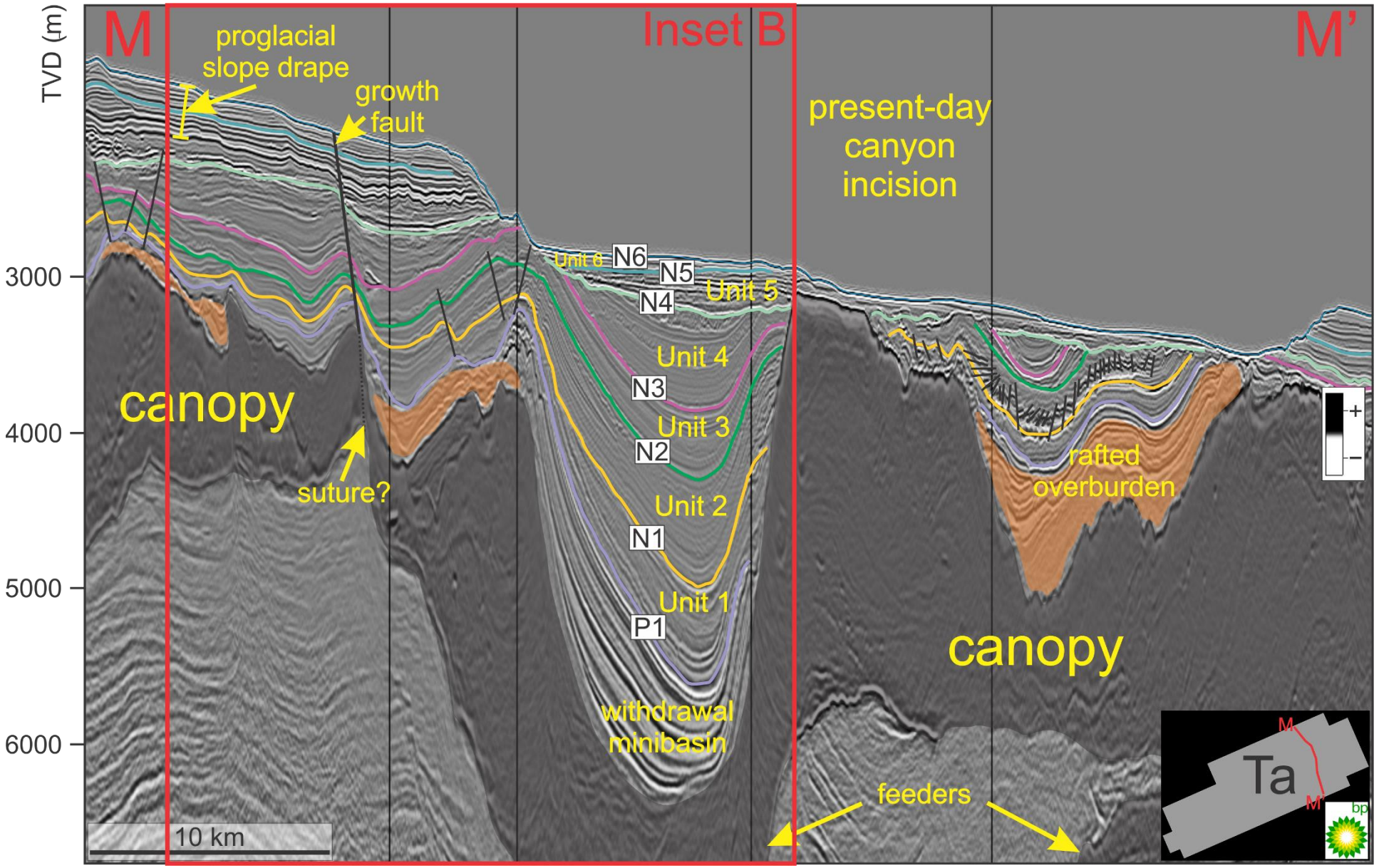

Figure 3.*32*. Representative strike-oriented seismic profile (M to M'; see Appendix VI for uninterpreted version) showing a large body of salt canopy (part of the Sable Canopy Complex) with low overburden thickness because of a present-day canyon. Data courtesy of BP Canada Exploration Ltd. via NSDNRR.

3.4. Interpretations and Discussion

3.4.2. Sedimentary processes and depositional environments

The entire evolution of the Cenozoic has been heavily influenced by primarily paleoclimatic conditions that favoured significant eustatic sea-level changes and related oceanographic circulation that affected slope sedimentation due to the presence of: three sediment drift packages, four paleocanyons, three major slope draping packages, and two major MTD units, explained below.

Sediment drifts

Contourites are sedimentary deposits originated from the re-distribution of sediments by ocean bottom currents, which are caused by oceanographic circulation. Contourites can be classified as fine-grained or coarse-grained. Viana et al. (2007) suggested that the coarser the sediments and the thicker the contourite deposits are, the stronger and the longer the current activity was likely to be. There are three major occurrences of sediment drift or contourite packages in the Tangier 3D area in different time periods from the Eocene (Unit 1) to Late Miocene (Units 3-4) recognized with sigmoidal reflections interpreted as sediment waves (e.g., Figs. 3.16; 3.18). This suggests that the ocean bottom currents and available sediment supply during this time were strong enough to be influential, causing localized along-slope re-distribution of sediments in the study area.

Paleocanyons

The Tangier 3D survey shows that the shallow Cenozoic stratigraphy is highly truncated by paleochannels and canyons on the slope in the Paleogene and the Neogene. There are four generations of paleocanyons in the study area from the Eocene (P1-N1; Unit 1), the Oligocene (N1-N2; Unit 2), the Miocene (N2-N3 and N3-N4; Units 3 and 4), and the Quaternary (N5-N6; Unit 6). The presence of such stratigraphic features suggests significant eustatic sea-level fall that triggered advancement of river systems from the shelf to the slope in the Paleogene coupled glaciation, possibly from the upper parts of the Miocene onwards.

Canyons mapped within Unit 1 suggest that the Cretaceous strata in this part of the study area was a mixed turbidite-contourite system as evidenced by the presence of sediment waves and lateral migration (e.g., Fig. 3.20; Rodrigues et al., 2022). However, from Late Cretaceous to Late Paleocene, the slope sedimentary process evolved to the deposition of chalk units observed as a series of high amplitude reflections, followed by mounded drifts indicated by high amplitude reflections with mounded morphology and canyons observed as a moderate amplitude reflection, that resulted in widespread canyon erosion truncating the upper Late Cretaceous (Deptuck and Kendell, 2020; Rodrigues et al., 2022), which are now manifested within these P1-aged canyons. These canyons are truncating the younger deposits above P1 are draping over the Late Cretaceous strata (Fig. 3.20B) over these wide P1 canyon floors (Deptuck and Kendell, 2020).

A canyon mapped within Units 1 and 2 is mapped by N1 horizon as moderate to high amplitude reflections in the Late Oligocene (Thomas, 2004; Deptuck and Kendell, 2020) that is interpreted to be a widespread erosive surface, that in some parts of the slope, has paleocanyons on it that eroded more deeply. Truncation of the canyon on the slope originated from the shelf, which possibly occurred due to the development of the Late Oligocene Wenonah Canyon (Thomas, 2004; Deptuck and Kendell, 2020) since N1 horizon is close to the Late Miocene Unconformity

(Fig. 3.3) with both Oligocene and Miocene infill on top, depending on the location where the wells penetrate on the slope. Unit 2 paleocanyon possibly developed due to the global sea-level fall related to the expansion of the Antarctic ice sheet resulting to a global cooling period in the Oligocene (e.g., Zachos et al., 2001; Liebrand et al., 2017).

The N3 paleocanyon is interpreted to be an erosive unconformity carved into the underlying contouritic sediments of Unit 3 (Fig. 3.22A). The N3 paleocanyon is floored by a sinuous channel as shown by the RMS amplitude horizon extraction and coherence attribute (Figs. 3.22A-3.22B) and preserved by moderate to high amplitude, wavy, coherent reflections in the infill, which are interpreted to be contouritic asymmetric channel infill. This could imply that development of N3 paleocanyon initiated from a sea-level fall (e.g., from Antarctic reglaciation in the Miocene; Liebrand et al., 2017) and possibly a slight sea-level rise caused the canyon erosion to wane, with contouritic infill subsequently burying and preserving the canyon. The canyon winds between multiple salt diapirs, implying that they probably had enough relief at the time to affect the flows directed down the canyon system (see *Neogene* in section 3.4.3).

N6 paleocanyons are interpreted to be canyons related to Quaternary glaciation (Piper et al., 2002). In the RMS amplitude map, areas with high amplitude values (e.g., within canyon thalwegs) suggest lithological changes within areas where the canyons are incising versus the adjacent inter-canyon areas (Fig. 3.12; Campbell et al., 2005). Moreover, there are multiple salt diapirs that generate topographical relief on the seafloor. This shows that such features can re-direct down-slope sedimentation patterns around salt diapir relief on the western part of the Tangier 3D area, as seen in the coherence map (Fig. 3.23). On the extracted coherence map, the effect of topographical difference between the seafloor and incising submarine canyons is enhanced, including revealing some features such as shallow failure scarps (Fig. 3.23). These

regions possibly host down-slope sediment transport based on the geometry of nearby failure escarpments on the coherence map (Fig. 3.23).

All the N6 canyons were buried afterwards by intervals of weakly to moderate chaotic, low to moderate amplitude reflectors interpreted as mass wasting in Unit 2, Unit 4, and Unit 5, wavy, coherent, moderate to high amplitude interpreted as contourite deposition in Unit 1 and Unit 3, and well-stratified, layered, moderate to high amplitude reflectors interpreted as proglacial sediments in Unit 5 and Unit 6 (Figs. 3.21A; 3.22A).

Slope drapes

There are three major slope draping units as parts of Unit 1 to Unit 2, from Unit 3 to Unit 4, and from Unit 5 to Unit 6, which is possibly of pre- or pro-glacial origin. Slope drapes are mostly composed of turbiditic and hemipelagic muds with layers of thin silts and sands that have relatively high continuity through the shelf and the slope and are commonly known for their sealing ability to trap leaking hydrocarbons (Straccia and Prather, 1999; Prather and Steele, 2000; Prather, 2003).

The implication of proglacial slope drapes to sedimentary environment suggests that high sedimentation rates were occurring at the time due to the strong influence of large-scale ice sheets (ice-margin environment) which resulted in glaciomarine sedimentation and possibly from prodeltaic deposition (Piper, 1988; Piper, 2000; Piper et al., 2002; MacDonald, 2006).

Slope failure complexes

There are three major MTD units in Unit 2, Unit 4, and Unit 5 in the study area. Slope failure is one of the most common sedimentary processes in deep-water settings with resulting occurrences of slope failure deposits (e.g., mass transport, debris flow, slumps). Failure scarps are also observed as sharp, arcuate boundaries in coherence maps, which can also be used as kinematic indicators of mass transport movement along the slope because they normally form up-slope from where the MTD passed along transport corridors or was eventually deposited (Fig. 3.26).

3.4.3. Interpretation of salt bodies and related structures

Diapir-related structures

The presence of salt wings in the Tangier 3D area suggests that salt mobility experienced a period of passive diapirism where the salt extruded onto the seafloor, expanding over the top of seafloor sediments, and deposited concurrently with the sediments, forming projecting diapir flanks (Figs. 3.22A; 3.30). They form when the upward velocity of salt movement exceeds the rate of sediment deposition (Jackson et al., 1994; Davison et al., 2000a; Hudec and Jackson, 2006; Hudec and Jackson, 2007; Jackson and Hudec, 2017; Rowan and Giles, 2021). Most of the salt wings observed in the study area are observed within the Cenomanian to Ypresian when the sedimentation rate was slow and dominated by carbonates and was outpaced by rate of salt motion (Fig. 3.30).

In contrast, active diapirism is the rise of a buried salt diapir in response to its overburden due to either pressure exerted on the salt in adjacent minibasins or from regional lateral compression (Hudec and Jackson, 2007; 2011). Christians (2015) concluded that compressional active diapirism occurred in several diapirs on the central Scotian Slope. Just up-slope and overlapping

with the Tangier 3D area (e.g., Thrumcap and Weymouth 3D surveys; locations in Fig. 3.27), compressional active diapirism is expressed by diversion of canyons, stratal thinning of overburden, pinched salt diapirs, crestal faulting, and other features (e.g., Figs. 3.28-3.32). Crestal faulting is an indicator that salt diapirs experienced a period of compressional active diapirism (Hudec and Jackson, 2006; Hudec and Jackson, 2007; Christians, 2015; Jackson and Hudec, 2017; Rowan and Giles, 2021). The possible origins of lateral compression in the central Scotian Slope that rejuvenated salt mobility between the Bartonian and Pliocene with most activity in the Miocene, are speculated. Christians (2015) suggested that possible origins are shelf-edge deltas, thermal uplift, loading by an ice sheet, localized linked systems, and sediment loading and contourite deposition.

Therefore, it is more than likely that the several vertical salt diapirs in the Tangier 3D area also experienced episodes of both passive and active salt diapirsm that contributed to the stratal deformation history within the area.

Canopy-related structures

The canopy complex extends from the shelf into the deeper waters of the Scotian Slope and was initially developed in the Jurassic and Early Cretaceous due to differential sediment loading from the Sable Delta Complex in the north, salt withdrawal, and growth faulting, which together expelled the salt seaward (Albertz et al., 2010; Kendell, 2012). Over the canopy, a second, younger phase of salt withdrawal-related growth faulting and minibasins affected sediment accumulation and paleobathymetry in the study area. The growth faults above the canopy were mostly active from the Eocene to Miocene, based on thickness variation across them and

thickened strata in the associated minibasins, visible in the isochore maps (Figs. 3.35-3.37). Withdrawal basins are regions where salt has been displaced over time due to overburden pressure resulting to the creation of paleobathymetric lows (Figs. 3.28-3.29; 3.32). These paleobathymetric lows trap sediments and create areas with thick sediments in isochore maps. In contrast, salt highs are located adjacent to the withdrawal basins from which salt was expelled. Regions of salt highs form positive relief where younger stratigraphic intervals thin as the result of ongoing salt mobility (Figs. 3.29-3.32).

3.4.4. Stratal deformation history

To describe and characterize the Paleogene to the Neogene salt-related stratal deformation history in the study area, stratigraphic thickness maps were generated from the seismic units defined previously (Units 1 to 6). Cenozoic salt-related deformation is only observed locally in the study area. Linking these results to a more regional setting would require additional investigation of the adjacent surveys (e.g., Deptuck and Kendell, 2020). The interpretation of the timing of salt movement is based on the interpreted thickness variations and subsurface seismic stratigraphic and structural architecture.

Paleogene

The assessment of localized salt mobility in the Paleogene is based on the stratigraphic thinning of Unit 1. During the Early Eocene to the Late Oligocene (P1 to N1), in the Slope Diapiric Province, the salt diapirs were more likely to be already emplaced within the associated Mesozoic strata. The evidence of stratal thinning within Unit 1 suggests that the salt diapirs were

present on the paleo-slope and generating relief due to their motion. The eastern part of the survey (Figs. 3.33 (Inset B); 3.36) has more variations in sediment thickness due to salt canopy being expelled laterally which caused lateral deformation of the Cenozoic strata, which resulted in the formation of bathymetric lows such as withdrawal minibasins.

In the western Tangier area, the sediment thicknesses are much more uniform with occasional bull's-eye-like thins, where the sediment thickness are relatively equal on both sides of the salt diapir with stratal thinning of Unit 1 occurs as the salt diapirs moves vertically (Figs. 3.33 (Inset A); 3.36). In some instances, P1 horizon appears absent at the center of the vertical salt diapirs in map view (Fig. 3.36) due to salt mobility. This could have resulted as both P1 and N1 horizons merge at the crests of the diapirs to give zero thicknesses rather than either one being absent. It is also possible that one or the other horizons is non-existent as shown as black regions. As seen in Fig. 3.33 (Inset A), P1 horizon mostly onlaps with salt diapirs.

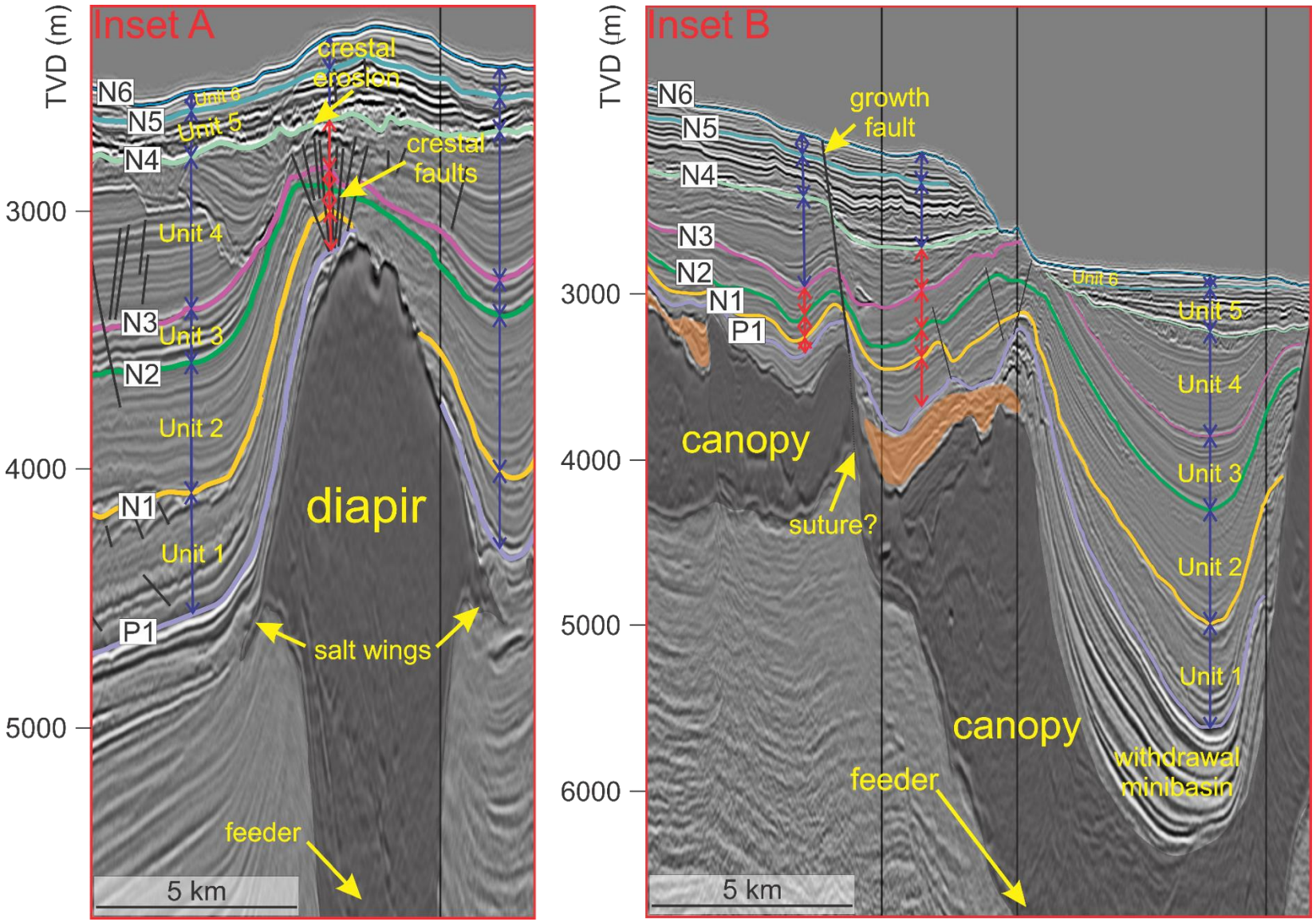

Figure 3.33. Close-up views from Figures 3.30 and 3.32 represented by Inset A and Inset B. Inset A illustrates the common stratal deformation regime of Cenozoic sediments above a salt diapir on the western diapir-dominated part of the Tangier 3D area. Inset B illustrates stratal deformation and salt-related features associated with the expulsion of salt canopy bodies on the eastern canopy complex part of the Tangier 3D area. Blue arrows demonstrate seismic units with maximum thickness and minimal thinning, whereas red arrows show obvious stratal thinning related to salt mobility by two different salt morphologies. Data courtesy of BP Canada Exploration Ltd via NSDNRR.

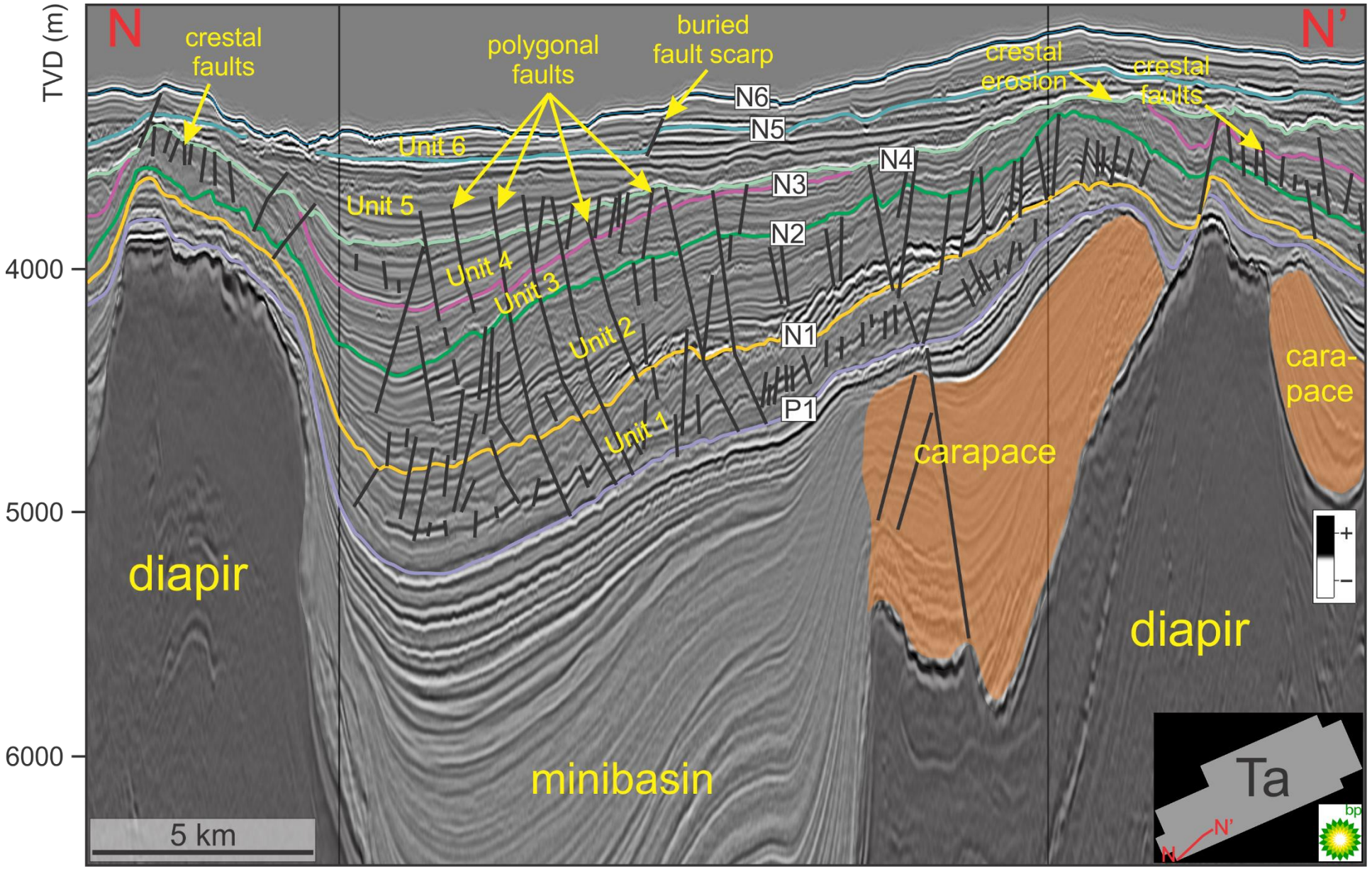

Figure 3.34. Representative composite seismic line (N to N'; see Appendix VI for uninterpreted version) showing polygonal and radial faulting of the Cenozoic strata around salt diapirs that are common features associated with salt mobility. Data courtesy of BP Canada Exploration Ltd via NSDNRR.

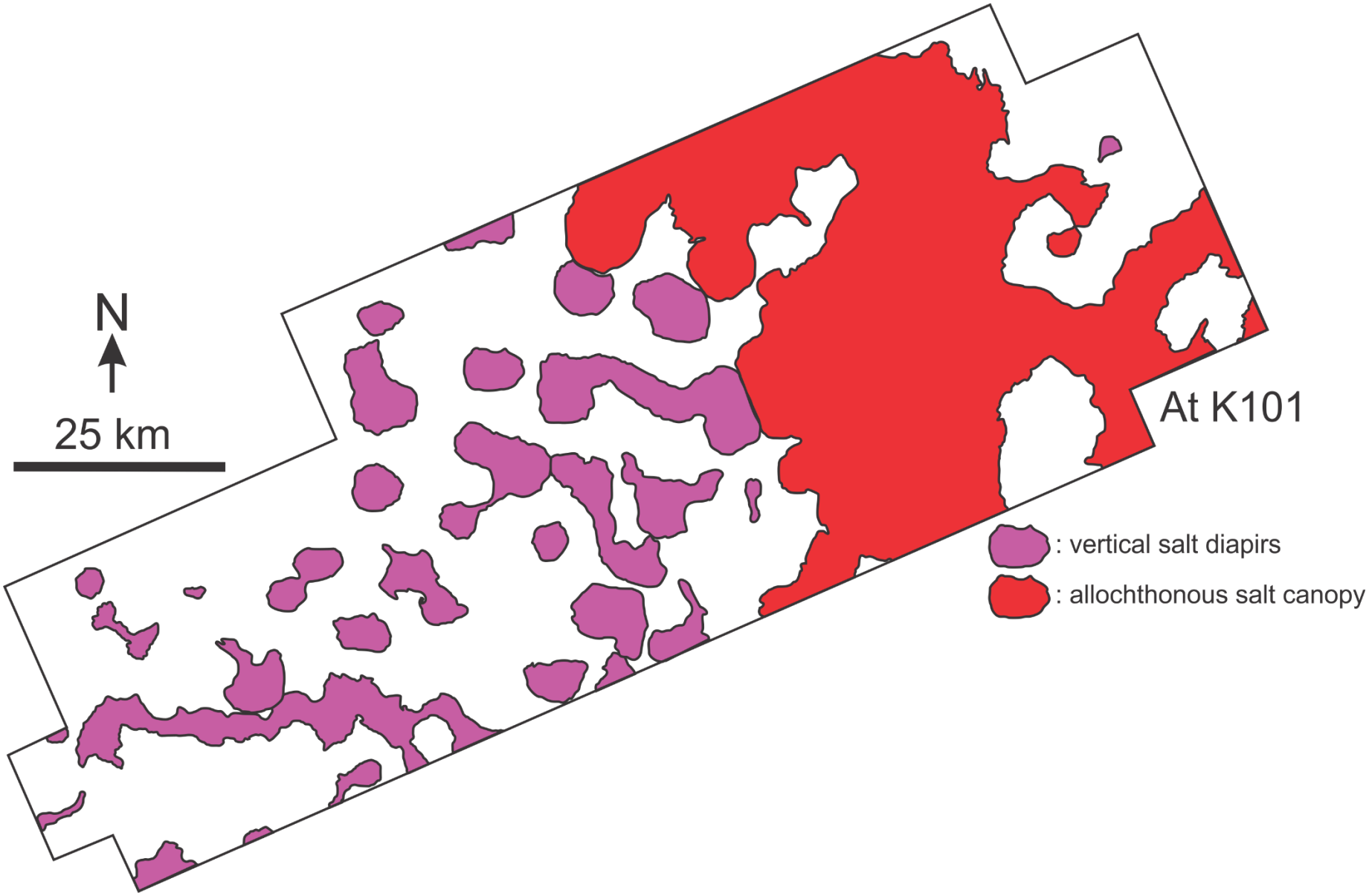

Figure 3.35. Relative extent of vertical salt diapirs and allochthonous salt canopy within the Tangier 3D area at K101 (Late Albian Unconformity; salt outline derived; Deptuck and Kendell, 2020). Non-occupied regions by salt bodies are in white.

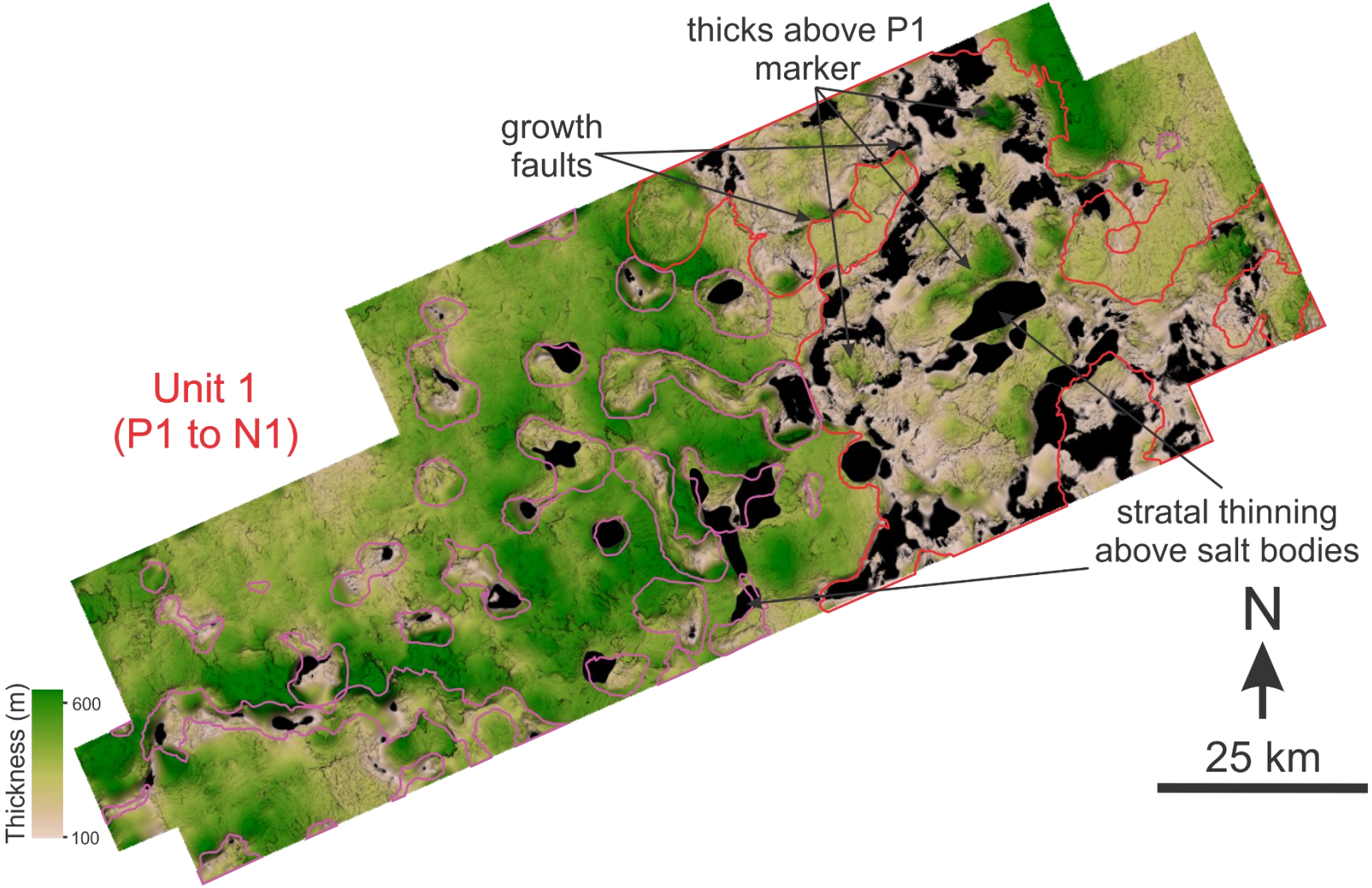

Figure 3.36. Isochore maps showing stratigraphic thickness of Unit 1 (P1 to N1; see Appendix V for uninterpreted version). P1 to N1 represents the Early Eocene to Late Oligocene. Stratal thinning above salt diapirs and in the canopy withdrawal region are highlighted in black boxes. Purple and red polygons are overlain to represent vertical salt diapirs and the allochthonous salt canopy at K101 in Fig. 3.35, respectively. Black regions represent areas where one or other of the horizon is non-existent.

Neogene

From possibly as early as the Late Oligocene, and by Late Miocene (N1 to N2), the stratigraphic thinning of Unit 2 suggests that the local salt bodies were still in motion and heavily influencing Cenozoic sediments as shown in the Unit 2 (Fig. 3.37A), creating bathymetric salt highs. Unit 2 shows much more pronounced crestal faults, which are observed as crestal faulting around salt diapirs, and polygonal fault network are present on the flanking strata around the diapir compared to Unit 1 (e.g., Fig. 3.37A).

Crestal faults are also present during the Neogene (Figs. 3.37A-3.37B; 3.38A-3.38B) but are not as pronounced towards the end of Neogene (Figs. 3.39A-3.39B; 3.40).

In the western Tangier area, bull's-eye-like thins in Unit 2 imply that salt bodies formed positive relief paleobathymetric features at the time of deposition. In the eastern Tangier, increased sediment accumulation on the slope in withdrawal minibasins is observed in several areas, as shown in Fig. 3.33 (Inset B) and Fig. 3.37B (Inset C). In addition, there are pronounced growth faults in relation to renewed salt canopy expulsion (Kendell, 2012).

During the Late Miocene (N2 to N3), the stratigraphic thinning of Unit 3 (Insets A and B) in the western Tangier area suggests that the local salt diapirs were still moving, creating regions of stratal thinning and bathymetric salt-related highs. A large-scale elongated drift (Shubenacadie Drift) was emplaced based on the Unit 3 thickness map (also discussed in the sediment drift section) and it was deformed by the moving vertical salt diapirs as indicated by the presence of radial faulting around the salt diapirs, highlighted in purple polygons (Fig. 3.38A). In addition, an interpreted paleocanyon was affected by salt motion due to some indication of flow diversion around the diapirs from Fig. 3.38A and 3.38B. This can also be noticed in the RMS amplitude and coherence maps from Fig. 3.29B, where there was also evidence the canyon was diverting its

flow around the diapir. In the eastern Tangier area, regions of sediment thicknesses are observed above N1 horizon, which suggest that the preferential sedimentation accumulation above the canopy-related minibasins and continued growth faulting.

The stratigraphic thinning of Unit 4 (N3 to N4) in the western Tangier area suggests that the influence of localized salt mobility was still significant due to the stratal thinning above salt diapirs highlighted in black boxes (Fig. 3.38B), although some of this is due to significant erosion observed at N4 horizon, which has removed some strata over the crest of the diapir-related structures. The difference of stratal thinning caused by salt bodies versus post-deposition can be determined as the latter commonly shows a truncating surface (e.g., N4 horizon) overlying the strata above salt bodies.

In map view, post-deposition thinning above salt bodies can be classified if there are occurrences of slope failure escarpments showing that the thinning may be related to erosion or sediment transport down-slope. In terms of sediment thickness, there is an area of sediment thickness is observed above Unit 3 paleocanyon (Fig. 3.38B) in the central Tangier area. In the eastern Tangier area, there is minimal influence of the salt canopy bodies but there are still some increased sediment thickness above the minibasins formed below. Several expressions of modern-day canyons are also visible in Units 3 and 4, which shows how deeply modern canyon erosion cuts into the Cenozoic subsurface.

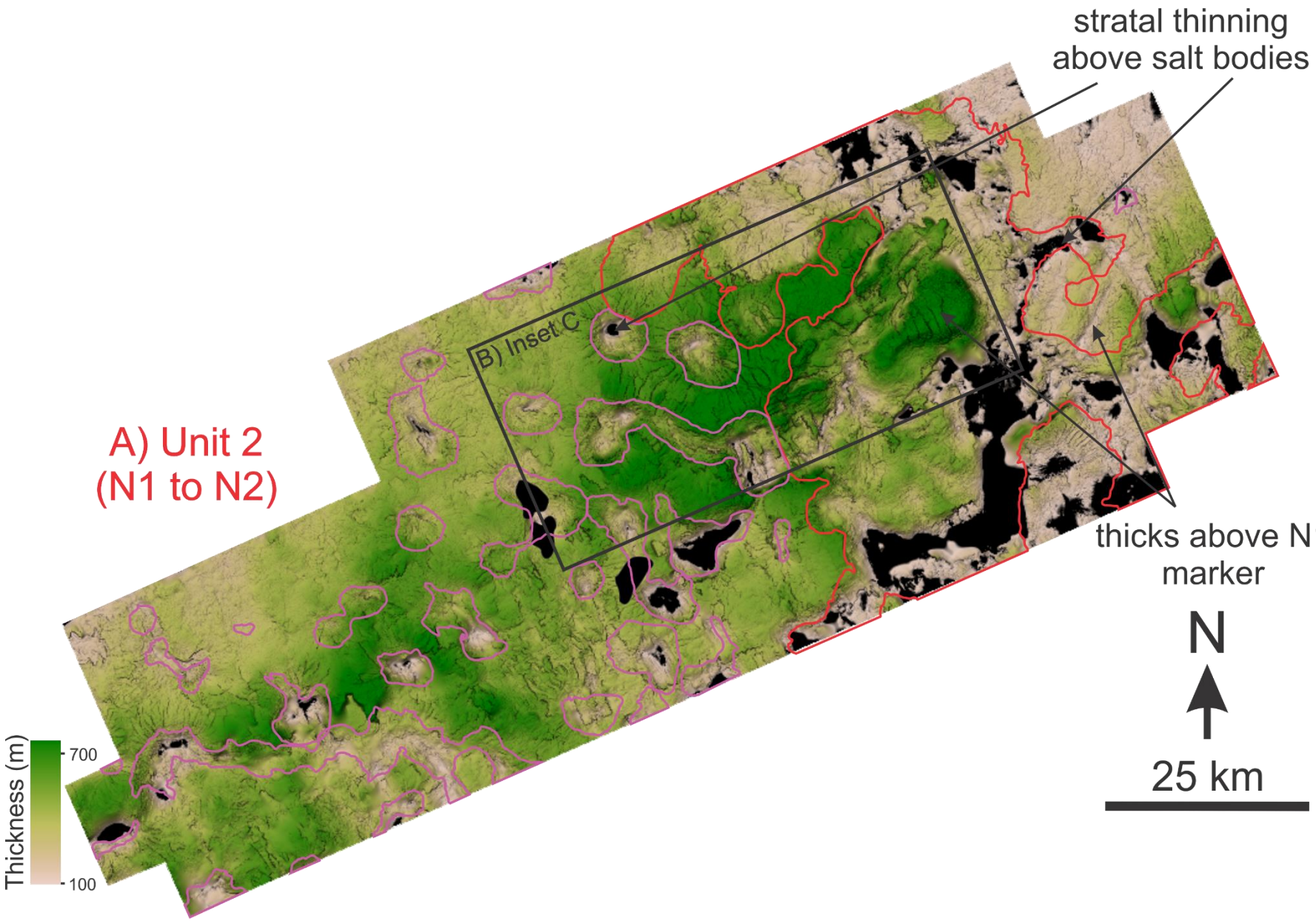
stratal thinning
above salt bodies
B) Inset C
A) Unit 2
(N1 to N2)
thicks above N1
marker
N
25 km
Thickness (m)
700
100

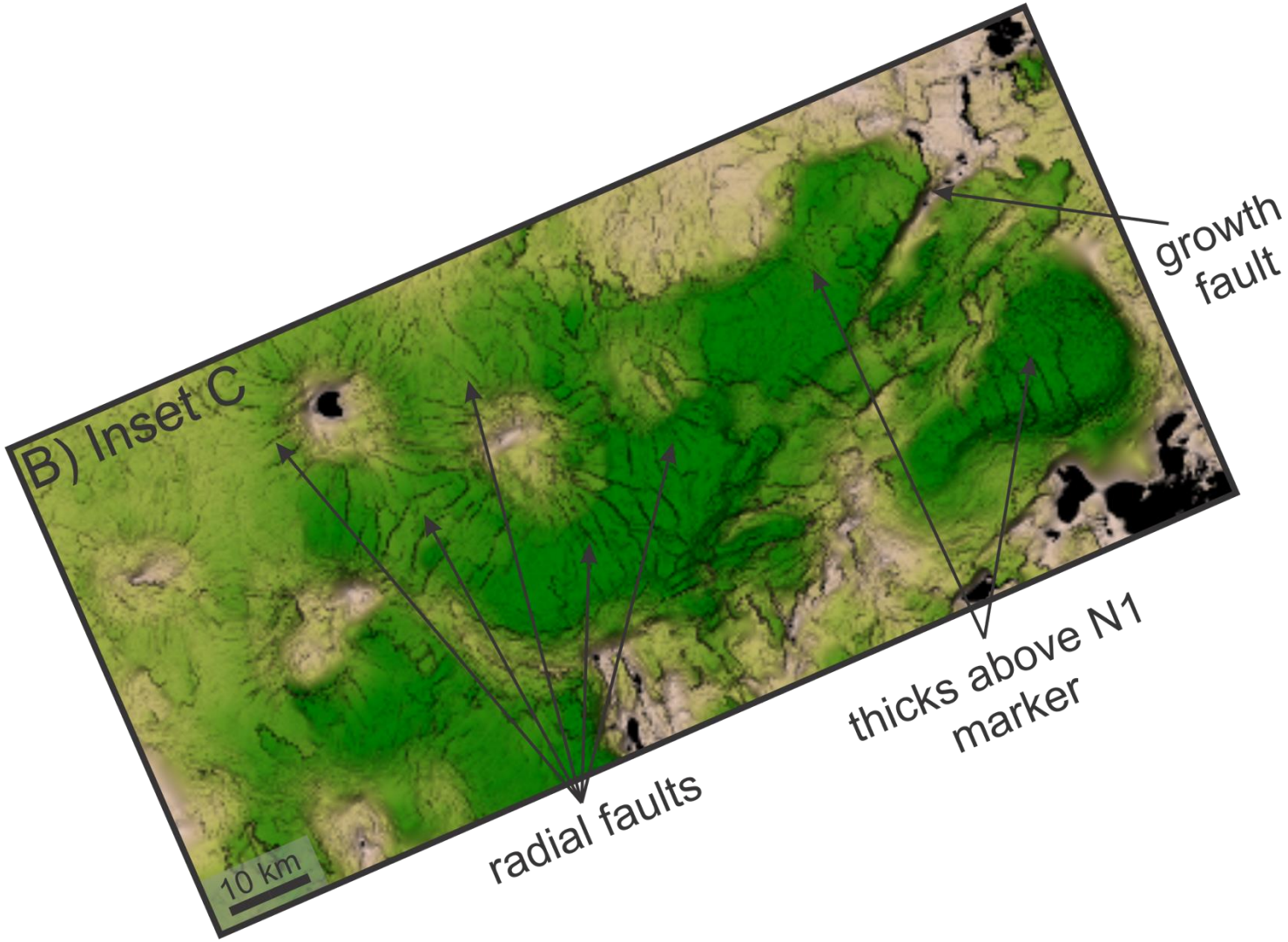

Figure 3.37A and 3.37B. Isochore maps showing stratigraphic thickness of Unit 2 (see Appendix V for uninterpreted version), which is mapped between N1 and N2 horizons. This isochore map represents the Late Oligocene to Late Miocene. Stratal thinning above salt diapirs is highlighted above purple polygons. There are some regions where stratal thinning occurs in the salt canopy region, however, there are also increased sediment thicknesses above the developing withdrawal minibasins shown in Fig. 3.36. Radially oriented crestal faults are pronounced in this interval. Purple and red polygons are overlain in A to represent vertical salt diapirs and the allochthonous salt canopy at K101 in Fig. 3.35, respectively. Black regions represent areas where one or other of the horizons (N1 or N2) is non-existent.

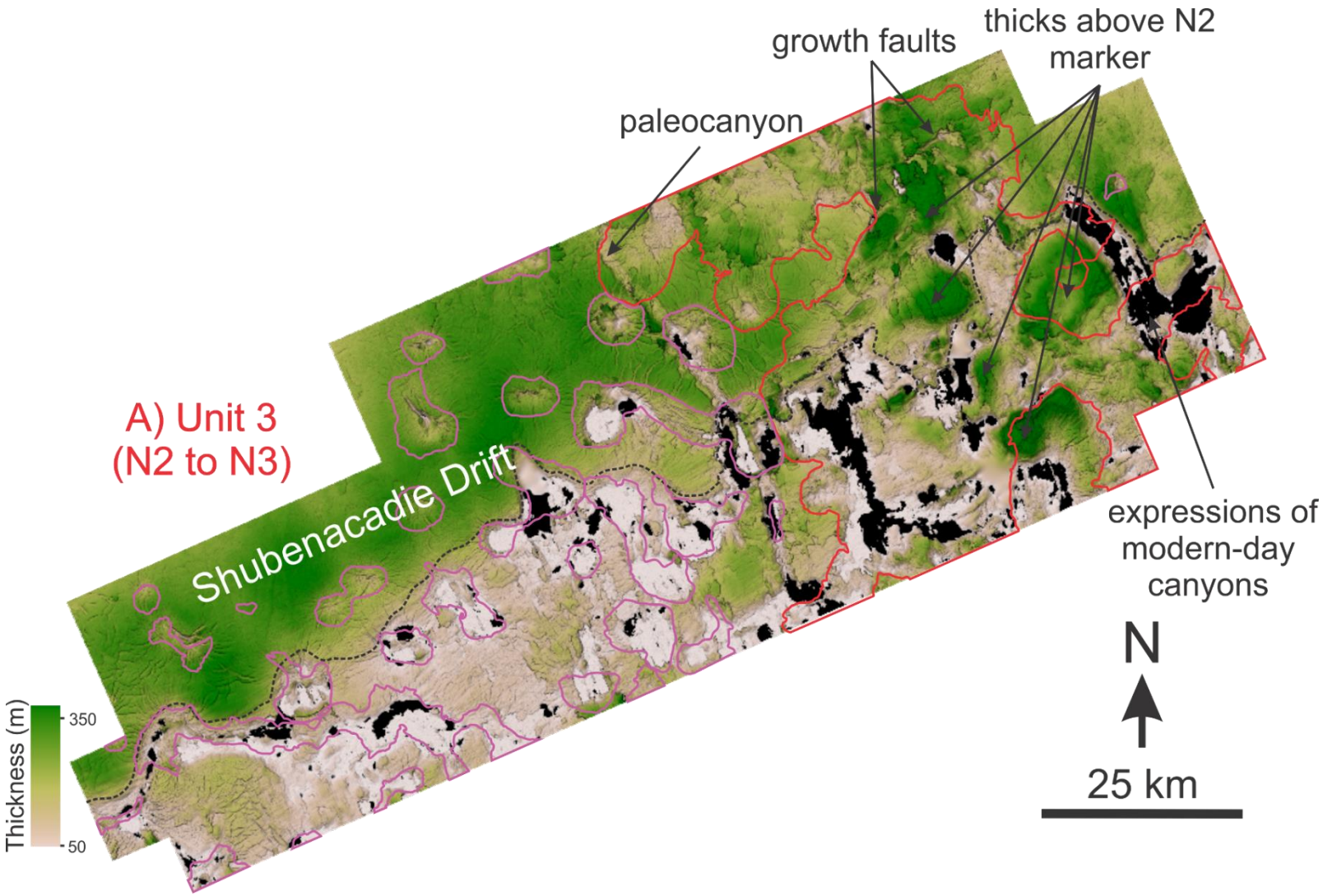
growth faults
thicks above N2 marker
paleocanyon
A) Unit 3
(N2 to N3)
Shubenacadie Drift
expressions of modern-day canyons
N
25 km
Thickness (m)
350
50

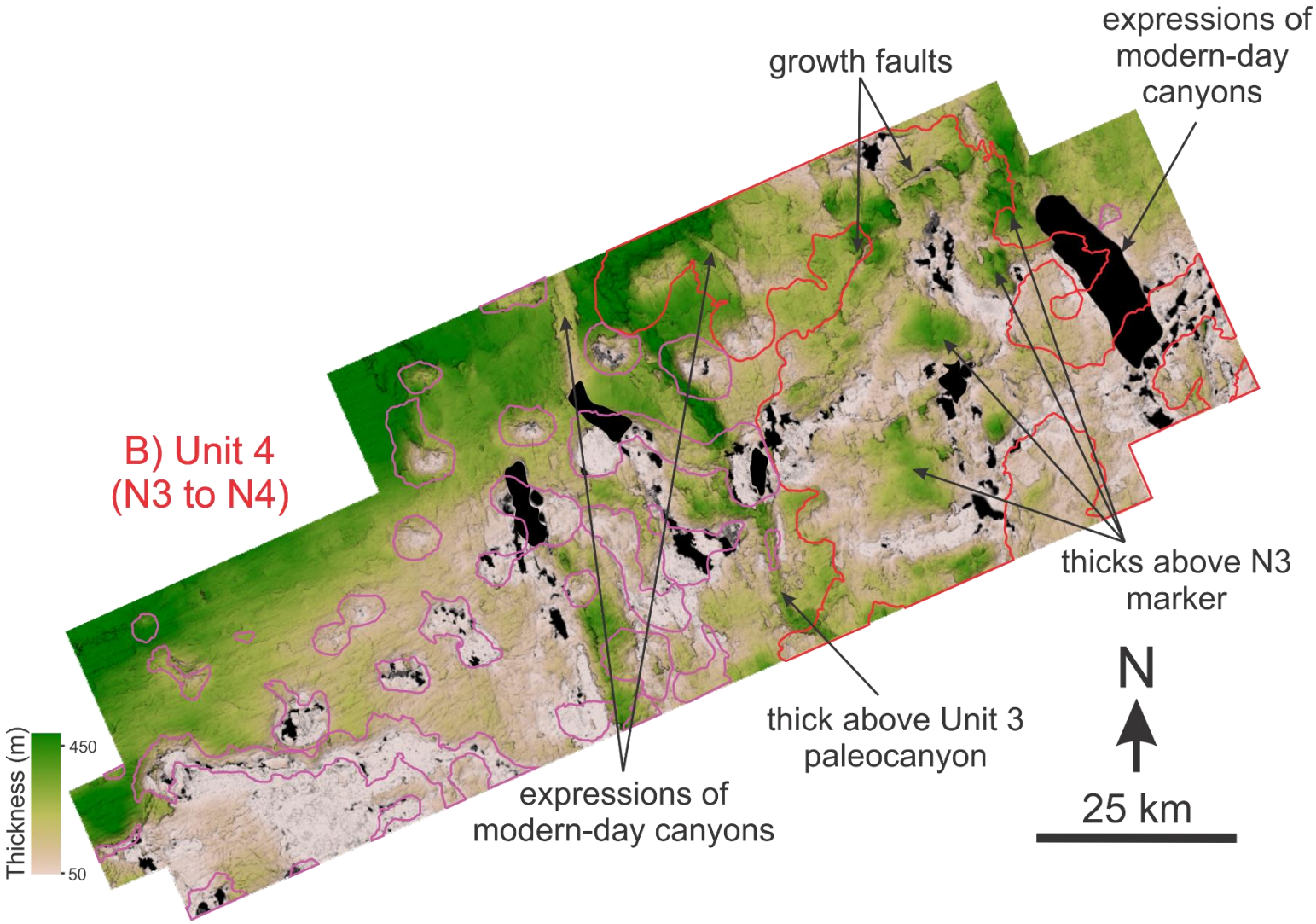

Figure 3.38A and 3.38B. Isochore maps showing stratigraphic thicknesses of Units 3 (A) and 4 (B) (see Appendix V for uninterpreted version), which are mapped between N2 and N3, and N3 and N4 horizons, respectively. N2 to N4 horizon represents the Late Miocene. Stratal thinning above salt diapirs is still present in these maps highlighted by black boxes with an evolving canopy withdrawal region featuring continued minibasin sediment accumulation. A paleocanyon is observed in Unit 3 (thinned areas) and its infill in Unit 4. Subsurface expressions of modern-day canyons are also shown in these maps due to their downcutting into older horizons in some areas. Purple and red polygons are overlain to represent vertical salt diapirs and the allochthonous salt canopy at K101 in Fig. 3.35, respectively. The extent of the Shubenacadie Drift is highlighted in A via dashed lines (derived from Deptuck and Kendell, 2020). Black regions represent areas where one or the other horizons is non-existent.

Compared to earlier units, the stratigraphic thinning for Units 5 (N4 to N5) and 6 (N5 to N6) suggest that the localized salt mobility had minimal effect on the development of the shallow Cenozoic strata at the end of Neogene up to the near modern-day times (e.g., Fig. 3.40). This is supported by the appearance of only limited thinning of Unit 5 and Unit 6 above salt diapirs in the western Tangier area compared to earlier units. Crestal erosion is also common during these periods, particularly starting at N4 horizon (Fig. 3.34). Some small-scale buried paleocanyons (Fig. 3.32A) are present that are also observed in N4 coherence map (Fig. 3.33).

During this period, it is also evident that the slope was dominated by slope failure processes as shown by the buried failure scarps across the Tangier 3D area that by their arcuate shapes, indicate the down-slope transport direction. Remnants of slope failure processes are highlighted in red arrows, suggesting flow direction by observing the slope failure scarp features (Fig. 3.39A and 3.39B). In addition, this is also the period where modern-day canyons were initially developing across the slope (Fig. 3.39A and 3.39B). In the western Tangier area, growth faults continued to develop as the salt canopy was loaded (Fig. 3.33; Inset B).

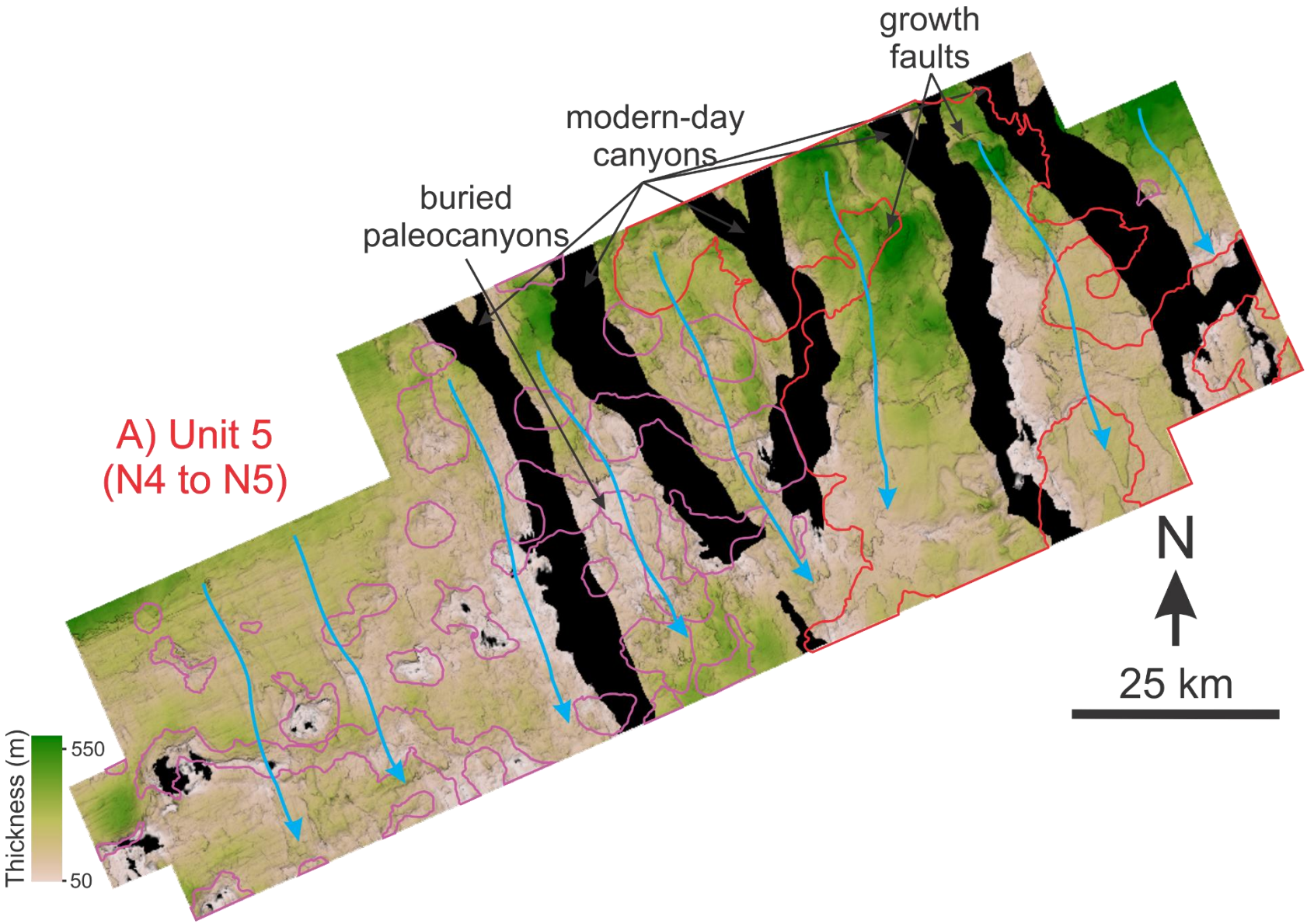
growth
faults
modern-day
canyons
buried
paleocanyons
A) Unit 5
(N4 to N5)
N
25 km
Thickness (m)
550
50

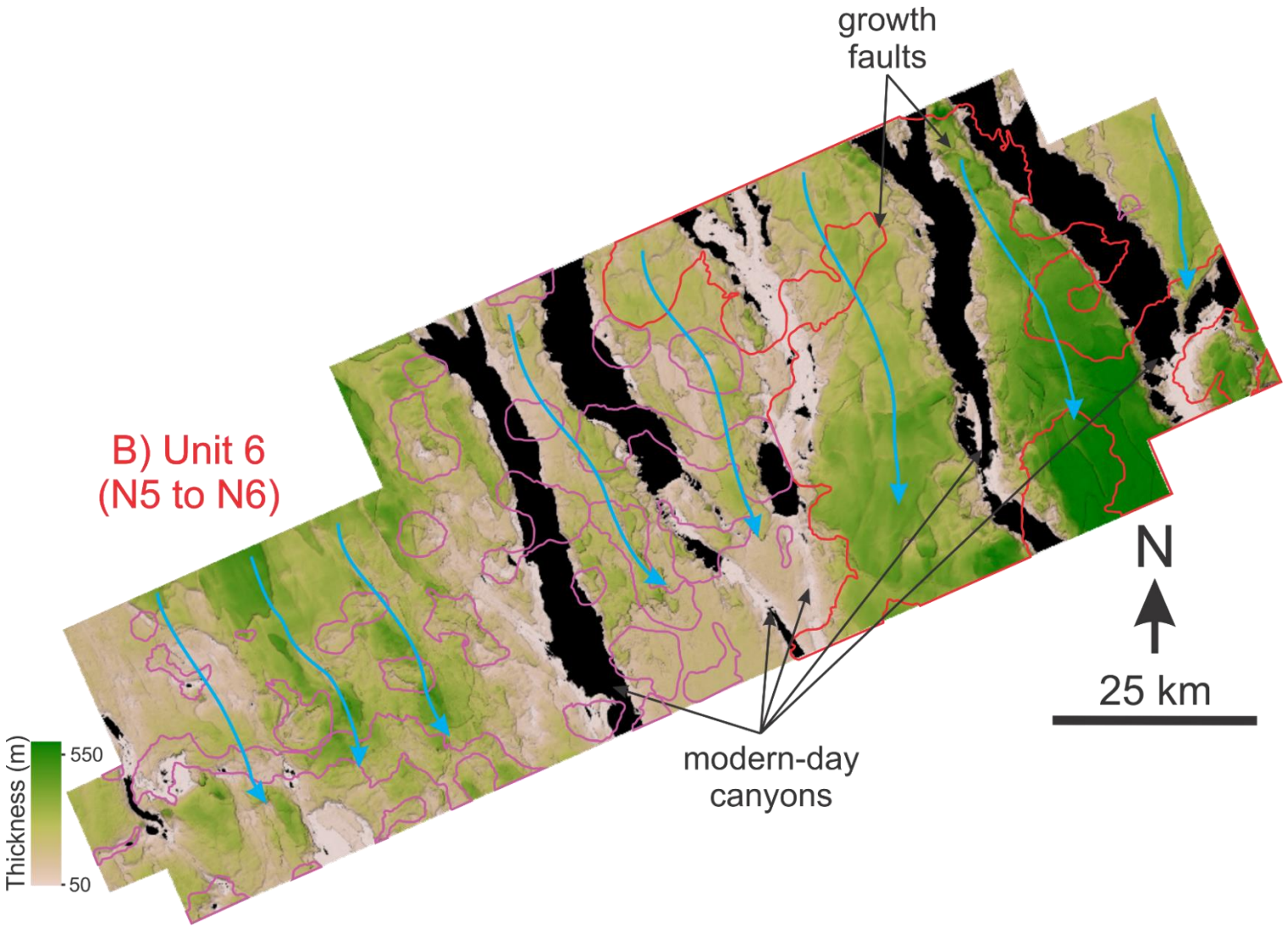

Figure 3.39A and 3.39B. Isochore maps showing stratigraphic thicknesses of Units 5 (A) and 6 (B) (see Appendix V for uninterpreted version), which are mapped between N4 and N5, and N5 and N6 horizons, respectively. These horizons represent the age towards the end of the Neogene. Stratal thinning above salt diapirs is still present but drastically diminished compared to earlier units (black boxes). There is also less influence of the canopy withdrawal region, but some of the growth faults that developed in P1 horizon persist through to near the seafloor. During the deposition of these units, the erosion of modern-day canyons dominates the slope along with slope failure processes, with their flow direction highlighted in light blue. Purple and red polygons are overlain to represent vertical salt diapirs and the allochthonous salt canopy at K101 in Fig. 3.35, respectively. Black regions represent areas where one or the other horizons is non-existent.

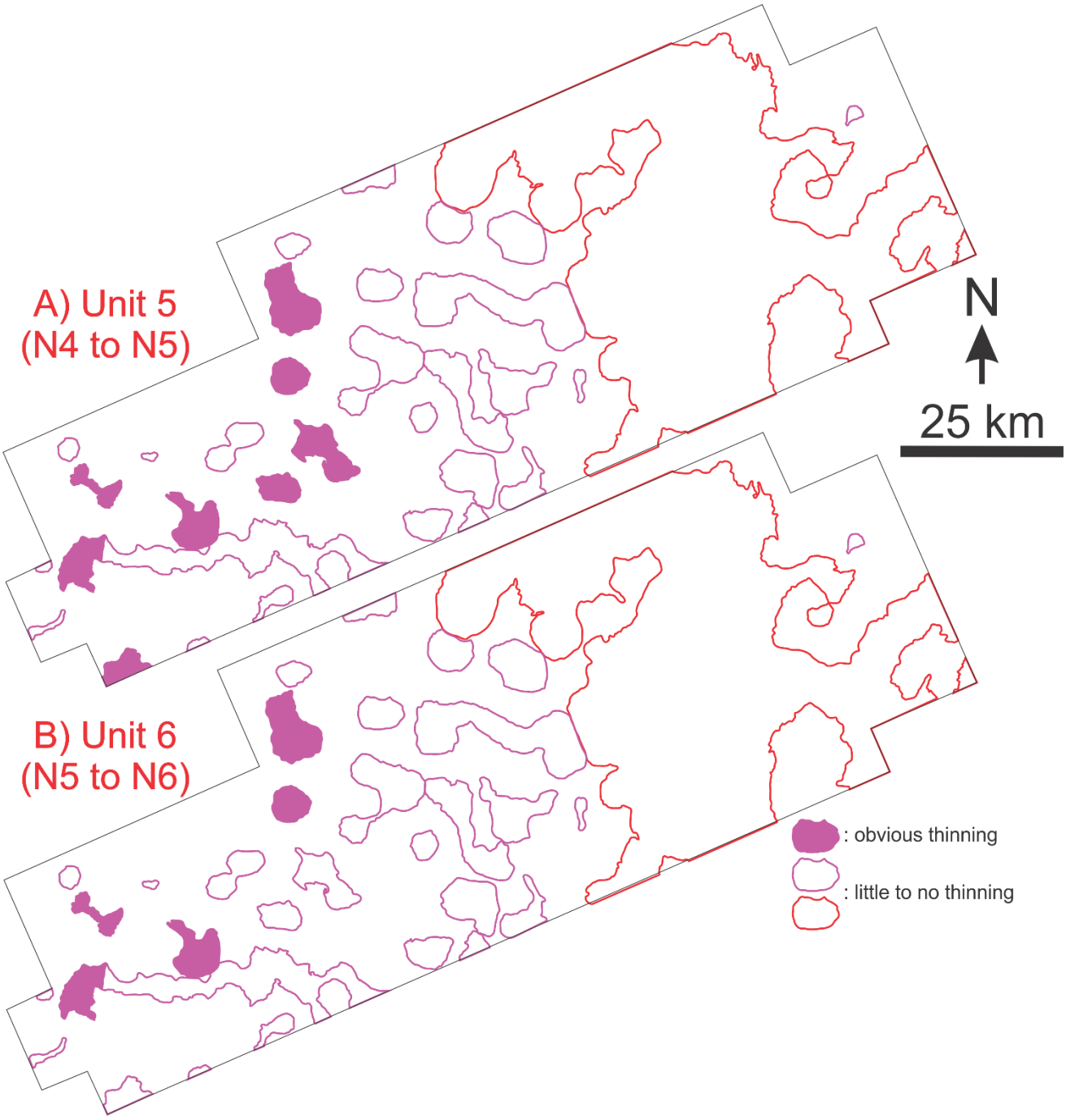

Figure 3.40. Classification of the effect of salt mobility in the Tangier 3D area (e.g., vertical salt diapirs and allochthonous salt canopy) from isochore maps of Unit 5 and 6 from Figs. 3.39A and 3.39B highlighting salt bodies with obvious thinning versus salt bodies with little to no thinning towards the end of the Neogene (N4 to N6 horizons).

3.5. Conclusion

The Tangier 3D Seismic Survey is one of the most geologically complex regions of the Scotian Slope. This chapter characterizes the Cenozoic subsurface geology of the Tangier 3D Seismic Survey on the central Scotian Slope. In addition, this chapter also characterizes local salt bodies in the Tangier 3D area and its influence on the deformation regime on the Paleogene to Neogene sediments on this part of the Scotian Slope.

The seismic survey hosts a complex subsurface geology that comprises well-stratified sediments from hemipelagic deposition incised by paleochannels. Multiple generations of paleochannels truncate the Cenozoic slope as mapped by P1, N1, N3, and N6 horizons in the study area. Sediment drift deposits are also common in the study area, observed as possibly mainly Eocene-aged drift in Unit 1, the large-scale Shubenacadie Drift in Unit 3, and a smaller-scale Late Miocene Drift in Unit 4. The presence of sediment drift deposits suggests different periods of significant influence of bottom current circulation. In addition, the Tangier 3D area is dominated by mass transport deposits, in different periods, which are mapped in upper Unit 2 (N1 to N2) and upper Unit 4 (N3 to N4). These sedimentary slope processes appear to be alternating throughout the Cenozoic suggesting mainly influence of paleoclimatic conditions favouring eustatic sea-level changes and oceanographic circulation. However, further study is needed to determine what factors dictate the cyclicity of these slope sedimentary processes.

The Tangier 3D Seismic Survey is uniquely positioned across the boundary of the Slope Diapiric Province (western Tangier) and the Slope Canopy Complex (eastern Tangier). The investigation of the Cenozoic strata revealed contrasting stratal deformation history between the western and the eastern Tangier areas in relation to the underlying salt structures.

In the western diapiric-dominated part of the Tangier, vertical salt diapir mobility was influential during the Paleogene, which led to radial faulting and stratal thinning above the diapirs that persisted to the start of the Neogene, as shown in isochore maps for Unit 1 and Unit 2. Such salt mobility and its stratal deformation persisted through the Neogene with continued stratal thinning above salt diapirs, as shown in Unit 3 and Unit 4 isochore maps. Towards the end of the Neogene, crestal faulting followed by crestal erosion is common above these vertical diapirs up to the N4 horizon. The N4 horizon marks the time when the movement of vertical salt diapirs significantly slowed because less stratal thinning features were observed in Unit 5 and Unit 6 isochore maps.

In the eastern part of Tangier during the Paleogene, the movement of the canopy complex was critical to the development of growth faults and withdrawal minibasins. Increased sediment accumulation occurred above minibasins starting at the P1 horizon and was observed as regions of sediment thicks from that point onward. During the Neogene, growth faulting was still persistent with more sediment accumulation above the withdrawal minibasins. Stratal thinning above the salt canopy is also observed during this period. Near the end of the Neogene (i.e., after N4), the growth faulting was still present, however, there is relatively weak influence of salt canopy mobility in this period due to less indication of stratal thinning.

3.6. Works cited

Adam, J., and Krezsek, C. (2012). Basin-scale salt tectonic processes of the Laurentian Basin, Eastern Canada: insights from integrated regional 2D seismic interpretation and 4D physical experiments. *The Geological Society of London, 363*, 331–360.

Albertz, M., Beaumont, C., Shimeld, J. W., Ings, S. J., and Gradmann, S. (2010). An investigation of salt tectonic structural styles in the Scotian Basin, offshore Atlantic Canada: 1. Comparison of observations with geometrically simple numerical models. *Tectonics, 29*, 1–29.

Bondurant, C. (2016). Tangier 3D Interpretation Report, Offshore Nova Scotia. BP Canada Exploration Ltd.

BP Canada Exploration Ltd. (2019). *Subsurface Well History Report for CNSOPB* (Report CN001-SS-REP-600-00004).

Brown, D. E. (2008). *Regional geology of the Scotian Basin*. Canada-Nova Scotia Offshore Petroleum Board Report, Halifax, Nova Scotia, 1–13.

Bull, S., Cartwright, J., and Huuse, M. (2009). A review of kinematic indicators from mass-transport complexes using 3D seismic data. *Marine and Petroleum Geology, 26*, 1132–1151.

Campbell, D. C. (2005). Major Quaternary mass-transport deposits in southern Orphan Basin, offshore Newfoundland and Labrador. Geological Survey of Canada, Current Research 2005-D3, 1–12.

Campbell, D. C. (2011). *The Late Cretaceous and Cenozoic Geological History of the Outer Continental Margin off Nova Scotia, Canada: Insights intp Margin Evolution from a Mature Passive Margin* (PhD thesis). Dalhousie University, Halifax, NS.

Campbell, D. C. and Deptuck, M. E. (2012). Alternating bottom-current-dominated and gravity-flow-dominated deposition in a lower slope and rise setting – Insights from the seismic geomorphology of the western Scotian Margin, Eastern Canada. *Applications of the Principles of Seismic Geomorphology to Continental-Slope and Base-of-Slope Systems: Case Studies from Seafloor and Near-Seafloor Analogues.* SEPM, Special Publication No. 99, 329–346.

Campbell, D. C. and Mosher, D. C. (2016). Geophysical evidence for widespread Cenozoic bottom current activity from the continental margin of Nova Scotia, Canada. *Marine Geology*, 237–260.

Campbell, D. C., Piper, D. J. W., Mosher, D. C., and Jenner, K. A. (2005). Surficial geology and sun-illuminated seafloor topography, Logan Canyon, Scotian Slope, Offshore Nova Scotia. Geological Survey of Canada, Natural Resources Canada.

Campbell, D. C., Shimeld, J., Deptuck, M. E., and Mosher, D. C. (2015). Seismic stratigraphic framework and depositional history of a large Upper Cretaceous and Cenozoic depocenter off southwest Nova Scotia, Canada. *Marine and Petroleum Geology, 65*, 22-42.

Canada-Nova Scotia Offshore Petroleum Board. (2016). *Call for Bids NS16-1*. Retrieved from https://callforbids.cnsopb.ns.ca/2016/01/ns16-1-parcels/exploration-history.

Carruthers, D., Cartwright, J., Jackson, M. P. A., and Schutjens, P. (2013). Origin and timing of layer-bound radial faulting around North Sea salt stocks: New insights into the evolving stress state around rising diapirs. *Marine and Petroleum Geology, 48*, 130–148.

Cartwright, J. A. and Lonergan, L. (1996). Volumetric contraction during the compaction of mudrocks: a mechanism for the development of regional-scale polygonal fault systems. *Basin Research, 8*, 183–193.

Christians, A. (2015). *Late Cretaceous to Cenozoic Reactivation of Central Scotian Slope Salt Bodies and the Impact on Slope Depositional Systems* (MSc thesis). Dalhousie University. Halifax, NS.

Coleman, A. J., Jackson, C. A.-L., Duffy, O. B., and Nikolinakou, M. A. (2018). How, where, and when do radial faults grow near salt diapirs? *Geology, 46 (7)*, 655–658.

Davison, I., Alsop, G. I., Evans, N. G., and Safaricz, M. (2000a). Overburden deformation pattens and mechanisms of salt diapir penetration in the Central Graben, North Sea. *Marine and Petroleum Geology, 17 (5)*, 601–618.

Deptuck, M. E. (2010). The "slope detachment zone" on the western Scotian Slope, offshore Nova Scotia: Structural style, timing, and implications for margin evolution. *Central and North Atlantic Conjugate Margins, IV*, 87–95.

Deptuck, M.E. and Campbell, D.C. (2012). Widespread erosion and mass failure from the ~51 ma Montagnais marine bolide impact off southwestern Nova Scotia, Canada. *Canadian Journal of Earth Sciences, 49*, 1567–1594.

Deptuck, M. E. and Kendell, K. L. (2017). A Review of Mesozoic-Cenozoic Salt Tectonics Along the Scotian Margin, Eastern Canada. In J. Soto, J. F. Flinch, and G. Tari (Eds.), *Permo-Triassic Salt Provinces of Europe, North Africa, and the Atlantic Margins* (Ch. 13, pp. 287-312). Amsterdam, Netherlands: Elsevier.

Deptuck, M. E. and Kendell, K. L. (2020). *Atlas of 3D seismic surfaces and thickness maps, central and southwestern Scotian Slope*. Canada-Nova Scotia Offshore Petroleum Board, Geoscience Open File Report 2020-002MF – 2020-006MF, 1–51.

Faugères, J-C, and Stow, D. A. V. (1993). Bottom current-controlled sedimentation: a synthesis of the contourite problem. *Sedimentary Geology, 82 (1-4)*, 287–297.

Faugères, J-C, Stow, D. A. V., Imbert, P., and Viana, A. (1999). Seismic features diagnostic of contourite drifts: *Marine Geology, 162*, 1–38.

Faugères, J.C. and Stow, A.V. (2008). Contourite drifts: nature, evolution and controls.In M. Rebesco, A. Camerlenghi, (Eds.), *Contourites. Developments in Sedimentology*, (v. 60, pp. 259–288). Elsevier.

Fenton, J. P. G. and Pardon, A. (2003). *Imperial Oil Resources Ventures Limited Balvenie B-79 well, offshore Nova Scotia, biostratigraphy of the interval 2780 m-4750 m TD*. Roberston Research International Ltd. Report No. 6558/Ib, Project No. Ib/GF441, December 2003.

Fensome, R. A., Crux, J. A., Gard, I. G., MacRae, R. A., Williams, G. L., Thomas, F. C., Fiorini, F., and Wach, G. (2008). The last 100 million years on the Scotian Margin, offshore eastern Canada: an event-stratigraphic scheme emphasizing biostratigraphic data. *Atlantic Geology, 44*, 93–126.

Given, M. M. (1977). Mesozoic and Early Cenozoic Geology of Offshore Nova Scotia. *Bulletin of Canadian Petroleum Geology, 25 (1)*, 63–91.

Hudec, M. R., and Jackson, M. P. A. (2006). Growth of allochthonous salt sheets in passive margins and orogens. *AAPG Bulletin, 90*, 1535–1564.

Hudec, M. R. and Jackson, M. P. A. (2007). Terra infirma: Understanding salt tectonics. *Earth-Science Reviews, 82*, 1–28.

Hudec, M. R. and Jackson, M. P. A. (2011). The Salt Mine: a Digital Atlas of Salt Tectonics. *AAPG Memoir, 99*, 305.

Ings, S. J. and Shimeld, J. W. (2006). A new conceptual model for the structural evolution of a regional salt detachment on the northeast Scotian margin, offshore eastern Canada. *The American Association of Petroleum Geologists Bulletin, 90 (9)*, 1407–1423.

Jackson, M. P. A., and Hudec, M. R. (2017). Salt Tectonics: Principles and Practice (Part II), 1-498. Cambridge, UK: Cambridge University Press.

Jackson, M. P. A., Vendeville, B. C., and Schultz-Ela, D. D. (1994). Structural dynamics of salt systems. *Annual Review of Earth Planet Science, 22*, 9–117.

Kendell, K. L. (2012). Variations in salt expulsion style within the Sable Canopy Complex, central Scotian margin. *Canadian Journal of Earth Sciences, 49*, 1504–1522.

Kidston, A. G., Brown, D. E., Altheim, B., and Smith, B. M. (2002). Hydrocarbon potential of the deep-water Scotian slope. *Canada-Nova Scotia Offshore Petroleum Board Open Report*, 1–111.

Kidston, A. G., Smith, B. M., Brown, D. E., Makrides, C., and Altheim, B. (2007). Nova Scotia deepwater post-drill analysis 1982-2004. *Canada-Nova Scotia Offshore Petroleum Board Open Report*, 1–182.

Leon, L. and Guirguis, S. (2016). *Data Processing Report for BP Exploration Canada Limited*. Houston, TX: Schlumberger.

Li, J., Mitra, S., and Qi, J. (2020). Seismic analysis of polygonal fault systems in the Great South Basin, New Zealand. *Marine and Petroleum Geology, 111*, 638–649.

Liebrand, D., de Bakker, A. T. M., Beddow, H. M., Wilson, P. A., Bohaty, S. M., Ruessink, G., Pälike, H., Batenburg, S. J., Hilgen, F. J., Hodell, D. A., Huck, C. E., Kroon, D., Raffi, I., Saes, M. J. M., van Dijk, A. E., and Lourens, L. J. (2017). Evolution of the early Antarctic ice ages. *Proceedings of the National Academy of Sciences, 114 (15)*, 3867-3872.

MacDonald, A. W. (2006). *Cenozoic seismic stratigraphy of the Central Nova Scotian Continental Margin: The interplay of erosion, deposition, and salt tectonics* (MSc thesis). Saint Mary's University, Halifax, NS.

McIver, N. L. (1971). Cenozoic and Mesozoic Stratigraphy of the Nova Scotia Shelf. *Canadian Journal of Earth Science, 9*, 54–70.

Mosher, D. C., Piper, D. J. W., Campbell, D. C., and Jenner, K. A. (2004). Near-surface geology and sediment-failure geohazards of the central Scotian Slope. *AAPG Bulletin, 88 (6)*, 703-723.

Offshore Energy Research Association. (2011). *Play Fairway Analysis Atlas*. Retrieved from https://oera.ca/research/play-fairway-analysis-atlas.

Piper, D. J. W. (1988). Glaciomarine sedimentation on the Continental Slope off Eastern Canada. *Geoscience Canada, 15*, 23–28.

Piper, D. J. W. (2000). Pleistocene ice outlets on the central Scotian Slope, offshore Nova Scotia. Geological Survey of Canada, Current Research 2000-D7, 1–8.

Piper, D. J. W., Mosher, D. C., and Newton, S. (2002). Ice-margin seismic stratigraphy of the central Scotian Slope, eastern Canada. Geological Survey of Canada, Current Research 2002-E16, 1–16.

Piqué, A. and Laville, E. (1996). The Central Atlantic Rifting: Reactivation of Palaeozoic Structures? *Journal of Geodynamics, 21 (3)*, 235–255.

Posamentier, H. W., Davies, R. J., Cartwright, J. A., and Wood, L. (2007). Seismic geomorphology – an overview. In R. J. Davies, H. W. Posamentier, L. J. Wood, and J. A. Cartwright (Eds.), *Seismic Geomorphology* (vol. 277, pp. 1–14). Geological Society of London Special Publication.

Posamentier, H. W. and Kolla, V. (2003). Seismic geomorphology and stratigraphy of depositional elements in deep-water settings. *Journal of Sedimentary Research, 73 (3)*, 367–388.

Prather, B. E. (2003). Controls on reservoir distribution, architecture, and stratigraphic trapping in slope settings. *Marine and Petroleum Geology, 20*, 529–545.

Prather, B. E. and Steele, D. R. (2000). Methodologies for uncertainty assessment of deepwater facies and basins. International Geological Congress Turbidite Workshop at Rio de Janeiro.

Rebesco, M. and Stow, D. (2001). Seismic expression of contourites and related deposits: a preface. *Marine Geophysical Research, 22*, 303–308.

Rodrigues, S., Deptuck, M. E., Kendell, K. L., Campbell, C., and Hernández-Molina, F. J. (2022). Cretaceous to Eocene mixed turbidite-contourite systems offshore Nova Scotia (Canada): Spatial and temporal variability of down- and along-slope processes. *Marine and Petroleum Geology, 138*, 1–26.

Rowan, M. G. and Giles, K. A. (2021). Passive versus active salt diapirism. *AAPG Bulletin, 105 (1)*, 53–63.

Shimeld, J. (2004). A Comparison of Salt Tectonic Subprovinces Beneath the Scotian Slope and Laurentian Fan. In P. J. Post, D. L. Olson, K. T. Lyons, S. L. Palmes, P. F. Harrison, and N. C. Rosen (Eds.), *Salt Sediment Interactions and Hydrocarbon Prospectivity Concepts, Applications and Case Studies for the 21st Century*. SEPM Society for Sedimentary Geology.

Stow, D. A. V., and Faugères, J-C. (1998). Contourites, Turbidites and Processes Interaction. *Sedimentary Geology Special Issue*, 115 (1–4).

Stow, D. A. V., Pudsey, C. J., Howe, J. A., Faugères, J-C., and Viana, A. R. (2002). Deep-Water Contourites: Modern Drifts and Ancient Series, Seismic and Sedimentary Characteristics. *Geological Society of London Memoirs*, 22.

Straccia, J. R. and Prather, B. E. (1999). Stratigraphic Traps in Deep-Water Turbidite Reservoirs at the Base of Depositional Slope. *Society of Petroleum Engineers, Offshore Europe Conference*.

Thomas, F. C. (2004). Oligocene benthic foraminifera from the Paleogene Wenonah Canyon, Scotian Shelf – normal versus canyon assemblages. *Atlantic Geology*, *46*, 1–16.

van Helden, B. G. T. (2004). Encana et al. Weymouth A-45 well, Scotian Shelf. *Palynological analysis of the section between 4395 m and 6526 m (TD)*. Biostratigraphic Services Report.

Varnes, D. J. (1978). Slope movement types and processes. In R. L. Schuster, R. J. Krizek (Eds.), *Landslides, Analysis and Control* (Special Report 176, pp. 11–33). National Academy of Sciences, Washington.

Viana, A. R., Almeida Jr., W., Nunes, M. C. V., and Bulhoes, E. M. (2007). The economic importance of contourites. In A. R. Viana and M. Rebesco (Eds.), *Economic and Paleooceanographic Significance of Contourite Deposits* (Special Publications, 276, pp. 1–23). Geological Society of London.

Wade, J. A., and MacLean, B. C. (1990). The geology of the southeastern margin of Canada. In M. J. Keen and G. L. Williams (Eds.), *Geology of the continental margin of eastern Canada* (Ch. 5, pp. 167–238). Canada: Geological Survey of Canada.

Weston, J. F., MacRae, R. A., Ascoli, P., Cooper, M. K. E., Fensome, R. A., Shaw, D., and Williams, G. L. (2012). A revised biostratigraphic and well-log sequence-stratigraphic framework for the Scotian Margin, offshore eastern Canada. *Canadian Journal of Earth Science, 49,* 1417–1462.

Withjack, M. O., Schlische, R. W., and Olsen, P. E. (2012). Development of the passive margin of Eastern North America: Mesozoic rifting, igneous activity, and breakup. In D. G. Roberts and A. W. Bally (Eds.), *Phanerozoic Rift Systems and Sedimentary Basins* (Ch. 13, pp. 301–335). Amsterdam, Netherlands: Elsevier.

Zachos, J., Pagani, M., Sloan, L., Thomas, E., and Billups, K. Trends, Rhythms, and Aberrations in Global Climate 65 Ma to Present. (2001). *Science, 292 (5517),* 686-693.

Chapter 4. Investigation of Subsurface Architecture and Potential Migration Pathways from Possible Source/Reservoir Rock Interval to Selected Direct Hydrocarbon Indicators within the Tangier 3D Seismic Survey, Central Scotian Slope

4.1. Introduction

The Play Fairway Analysis (OERA, 2011) presented an estimated 120 Tcf of gas and 8 Bbbl of oil in offshore Nova Scotia. In shallow waters, the potential for both oil and gas could reside within small-scale traps. In deep-water settings, such as the slope, large-scale gas/condensate opportunities were predicted to exist along the northeastern part of the Scotian Margin. On the southwestern margin, the prediction was primarily an oil-charged play.

Hydrocarbon production on the Scotian Margin has been limited to the Sable Subbasin where the Sable Offshore Energy Project and Deep Panuke, produced gas, and the Cohasset-Panuke project produced light oil (CNSOPB, 2000). However, there are a few discoveries and wells with hydrocarbon shows outside the Sable Subbasin. Previous analysis suggested that the only proven source of hydrocarbons are the Upper Jurassic (Tithonian) source rocks along the margin, though there are signs of other possible sources (OETR, 2011). For example, additional studies suggest that other sources are associated with early Cretaceous deltaic sequences (CNSOPB, 2000; Kidston et al., 2002; Mukhopadhyay, 2006; Kidston et al., 2007; OERA, 2011; Fowler et al., 2016). The findings of the PFA also predicted a more regional Lower Jurassic source rock that potentially extends beyond the Sable Subbasin and across the Scotian Margin. Geochemical analyses suggest that different mature source rocks are present in different regions. The western half of the margin was predicted to host oil-prone source rocks, whereas the eastern part of the

margin hosts more gas-prone source rocks (CNSOPB, 2000; Kidston et al., 2002; Mukhopadhyay, 2006; Kidston et al., 2007; OERA, 2011; Fowler et al., 2016).

The PFA also predicted the presence of reservoir rocks beyond the hydrocarbon production within the Sable Subbasin. The PFA developed predictive models using detailed seismic stratigraphy to distinguish four reservoir intervals that serve as the main play fairways of the Scotian Margin: (1) Mic Mac Upper Jurassic delta sequence (reservoir for the northeastern part of the margin), (2) Abenaki Carbonate Bank (reservoir for the Deep Panuke field), (3) and (4) Two Lower Cretaceous delta sequences (reservoirs in the Sable Subbasin and eastern Scotian Shelf such as Abenaki, Huron, and Laurentian Subbasins). In addition, OETR (2011) also discovered untested reservoirs located in the western part of the margin and in the most likely area with oil-prone source rocks. These untested reservoir rocks include Middle Jurassic Mohican Delta siliciclastics and carbonate oolites, which occurs in the Shelburne Subbasin region, and Upper Jurassic and Lower Cretaceous delta sequences found in the Georges Bank area (southwest part of the margin).

Although mature source and reservoir rocks are predicted within the Scotian Margin, the origin of the hydrocarbon sources would still be difficult to accurately pinpoint due to increased exploration uncertainty in areas with limited drilling, especially in deep-water settings. Therefore, in 2015, the Piston Coring Geochemistry Program along with the Genomic Application Partnership Program (GAPP) was started with the attempt to de-risk exploration in these environments by looking at near-surface evidence of hydrocarbon seepage from deeper levels.

Hydrocarbon seep sites have been investigated since 2015 by the Piston Coring Geochemistry Program (Fowler et al., 2016; 2017; 2017; 2019) conducted by the Offshore Energy Research

Association (OERA), Nova Scotia Department of Natural Resources and Renewables, and Geological Survey of Canada. This seep characterization program involved different sampling cruises conducted using Canadian Coast Guard Ships (CCGS) spanning from 2015, 2016, 2018 (CCGS Hudson), 2017 (CCGS Coriolis II), 2020 (Pacific Constructor – no sampling; only AUV Multibeam), and 2021 (Atlantic Condor). Some of these cruises (2018, 2020, 2021) also involved the surveying of seep sites using an Autonomous Underwater Vehicle (AUV) and a Remotely Operated Vehicle (ROV) to help position piston core samples.

The Genomic Application Partnership Program (GAPP) is a collaboration between several academic and governmental institutions across Canada. The program's goal is to confirm the presence of an active working petroleum system in deeper waters that involves integrated application of microbiological, geochemical, and geoscience investigative techniques. This thesis will mainly focus on the geophysical aspect of the program, that focuses on hunting amplitude anomalies, such as bright spots, dim spots, flat spots, and gas chimneys.

Bright spots are classified as having strong amplitude anomalies with negative reflection coefficient. Commonly, these seismic features are strongly linked to gas-charged reservoirs, probably sandy/sandstone or silty/siltstone reservoirs, trapped by shale/clay, giving drastic difference in acoustic impedance, and thus creating a bright spot (Brown, 1999; Schroot and Schüttenhelm, 2003; Nanda, 2016). In complex geologic setting, interpretation of bright spots can be misleading as several geologic features such as volcanic sills (Infante-Paez and Marfurt, 2018; Kumar et al., 2019), calcareous sands (Zeng et al., 2011), coal beds, diagenetic cementation, over-pressured sands and shales (Hanafy et al., 2018), and tuning effects of thinning beds (Guo et al., 2015; Cichostepski et al., 2019;), can all potentially create bright spots in seismic profiles (Nanda, 2016).

The opposite, dim spots are classified to be a weak, low amplitude anomaly with a positive reflection coefficient. It is known to be strongly linked to gas-charged carbonate and sandstone reservoirs (Brown, 1999; Nanda, 2016;). In some cases, dim spots provide lower amplitude even if hydrocarbons are present due to the response of decreasing porosity and increasing velocity within the reservoir (Brown, 2010; 2012). In addition, a higher degree of compaction and quartz cementation are also causes of dim spots in deeper stratigraphic levels implying low fluid signal (Wojcik et al., 2016).

Flat spots are distinguished from bright and dim spots by being characterized as moderate to high amplitude, concordant reflectors with positive polarity that commonly show horizontal contact between fluids (oil-gas, oil-water, gas-water contacts; Brown, 1999; Nanda, 2016;) due to difference in fluid density. These hydrocarbon-water contacts are identified by their discordant flatness. In some cases, flat spots are known to be strongly linked to low saturation of gas in reservoirs (Brown, 1999; Nanda, 2016). Some features such as lithologic variations, edge or base of a channel, low-angle faults, processing artifacts, diagenetic fronts, or tuning effects can be misidentified as flat spots (Guo et al., 2015).

Gas chimneys are characterized as vertically oriented low amplitude anomalies with low coherency that are associated with upward migration of fluid. Gas chimneys occur when a hydrocarbon build-up leaks from a seal, usually along a fault plane. This produces sag effects (velocity pull-down) within the overlying reflectors due to the reduced velocity in gas-bearing zones compared to adjacent areas. Gas chimney can be interpreted as a migration pathway from the reservoir to the amplitude anomaly that makes such a DHI, or they can be used to look for potential seepage site to the seafloor (Heggland, 1997; Heggland et al., 2000; Meldahl et al., 2001; Heggland, 2004; Nanda, 2016; Dixit and Mandal, 2020; Ma et al., 2021).

The main objectives of this chapter are to locate amplitude anomalies that could be fluid related (potential direct hydrocarbon indicators) and evaluate their quality to link prospective direct hydrocarbon indicators (DHIs) to possible working petroleum systems, and to incorporate available autonomous underwater vehicle (AUV) data (multibeam bathymetry) for selected amplitude anomalies to investigate seafloor morphology, attempting to answer the following questions:

a) What is the distribution of amplitude anomalies in the Tangier 3D Seismic Survey? Can any of these be reasonably interpreted as fluid-related (e.g., hydrocarbons) anomalies (DHIs)? Can these DHIs be structurally and stratigraphically linked to a potential reservoir or source rock deeper down, migrating to the DHIs? Is there evidence that these DHIs are associated with potential seepage sites?
b) How does the abundance and distribution of DHIs in the Tangier 3D Seismic Survey compare to the adjacent Shelburne 3D survey (e.g., Owino, 2022) on the Scotian Slope? What are the main reasons for any difference in the abundance and distribution of possible fluid-related amplitude anomalies between the two seismic surveys?

4.2. Methodology

The methods used in this chapter are seismic facies analysis of shallow and deep seismic sections (up to 10 km in TVD; up to 6 s in TWT) for tracking prospective DHIs and generation of attribute-based maps with the focus on the investigation of shallow amplitude anomalies and tracking possible migration pathways (see Chapter 2 for more details).

Using RMS amplitude map at the N3 horizon (e.g., Figs. 4.6; 4.12), three shallow amplitude anomalies were selected for further analysis.

4.2.1. Evaluation of amplitude anomalies

Amplitude anomalies are mainly changes in amplitude laterally or vertically compared to adjacent areas. The presence of fluids (e.g., hydrocarbons) changes the elastic properties of rocks and sediments (e.g., Young's modulus, shear modulus, etc.), which typically create amplitude anomalies in seismic data as DHIs. DHIs are mainly common in relatively young, unconsolidated siliciclastic sediments that have large impedance contrast across lithologic boundaries (Brown, 1999; Nanda, 2016).

In this thesis, the selection of DHIs is based on the type of amplitude anomaly. Types of amplitude anomaly that are considered are bright spots (local increase in amplitude), dim spots (local reduction in amplitude), flat spots (discordant flat reflector), phase change (local decrease in velocity) and gas chimneys (velocity pull-ups or push-downs).

After characterizing amplitude anomalies that were found in the Tangier 3D area, this was further assessed by linking these potential DHIs to the elements of an active petroleum system by reflecting on the following questions:

- What are the potential source and reservoir rocks in this part of the Scotian Slope that could lead to the generation of fluids for these potential DHIs?
- What geological processes could potentially facilitate hydrocarbon migration in this part of the Scotian Slope?
- What type of traps (e.g., structural or stratigraphic) are occurring in this part of the Scotian Slope that are hosting these DHIs?
- What lithologies are present at the shallowest depth in this part of the Scotian Slope that could potentially act as seal for these DHIs?

4.3. Results

4.3.1. Diapir-related shallow amplitude anomalies

There are three observed shallow amplitude anomalies (labelled AA1 to AA3) located within the boundaries of the Tangier 3D area (Fig. 4.1). They are dominated by bright spots, with effects of polarity reversal. The anomalies are located within the central and eastern parts of the Tangier 3D area (Fig. 4.1).

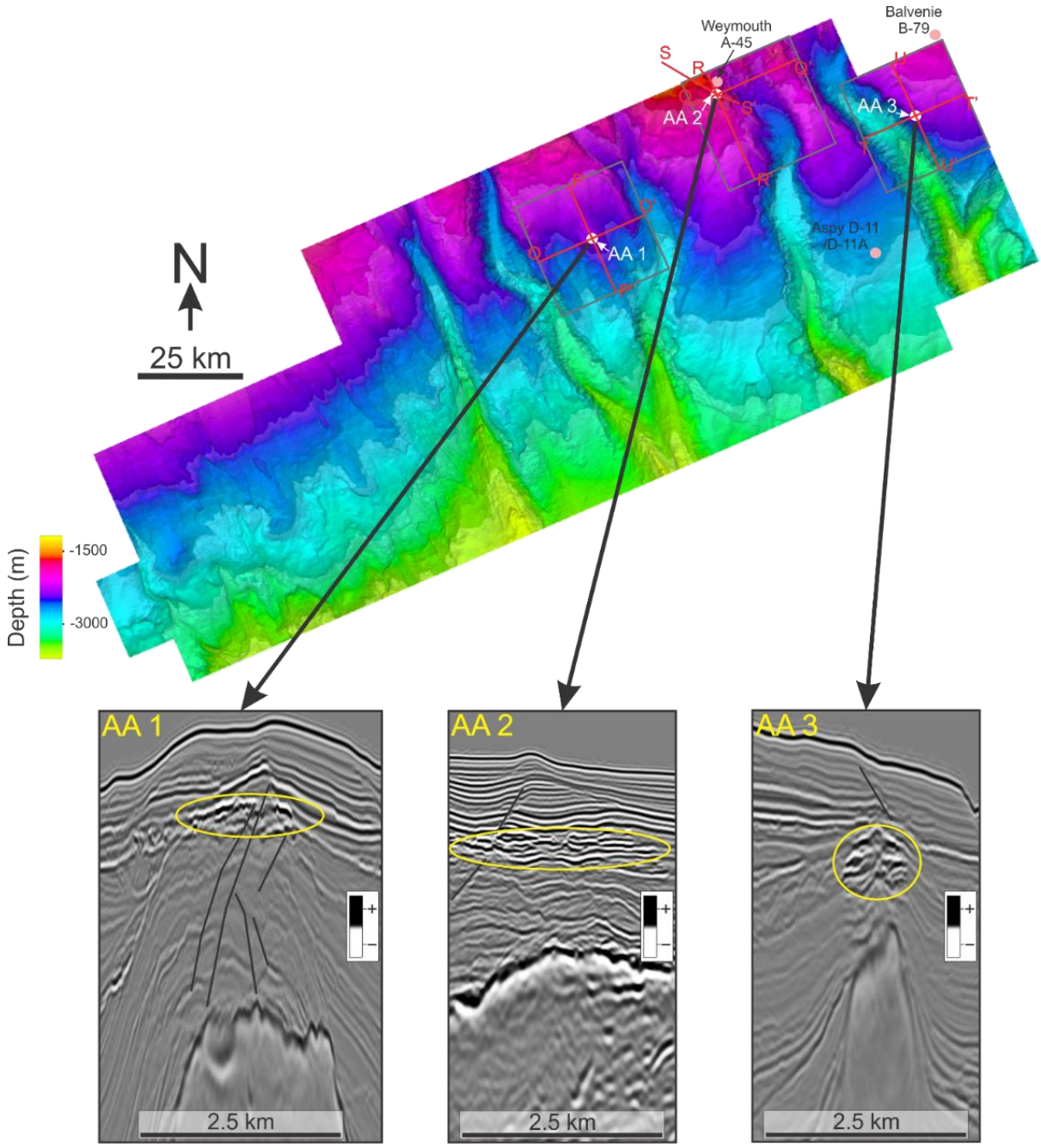

Figure 4.1. Reference seafloor map with the locations of investigated amplitude anomalies (labelled AA 1, AA 2, AA 3) and exploration wells near to or within the Tangier 3D area. Investigated amplitude anomalies are highlighted in seismic sections (O-O' is Figs. 4.2, 4.13, and 4.17; P-P' is Fig. 4.3; Q-Q' is Fig. 4.9; R-R' is Figs. 4.10, 4.15, and 4.18; S-S' is Figs. 4.11 and 4.16; T-T' is Fig. 4.4; U-U' is Figs. 4.5, 4.14, and 4.19). Data courtesy of BP Canada Exploration Ltd via NSDNRR. In the Tangier 3D area, there are two amplitude anomalies, which are situated above two salt diapirs, located on the central and eastern region of the survey (Fig. 4.1). Amplitude anomalies 1 and 3 (Figs. 4.2-4.5) are bright spots with minor interference of dim spot reflectors.

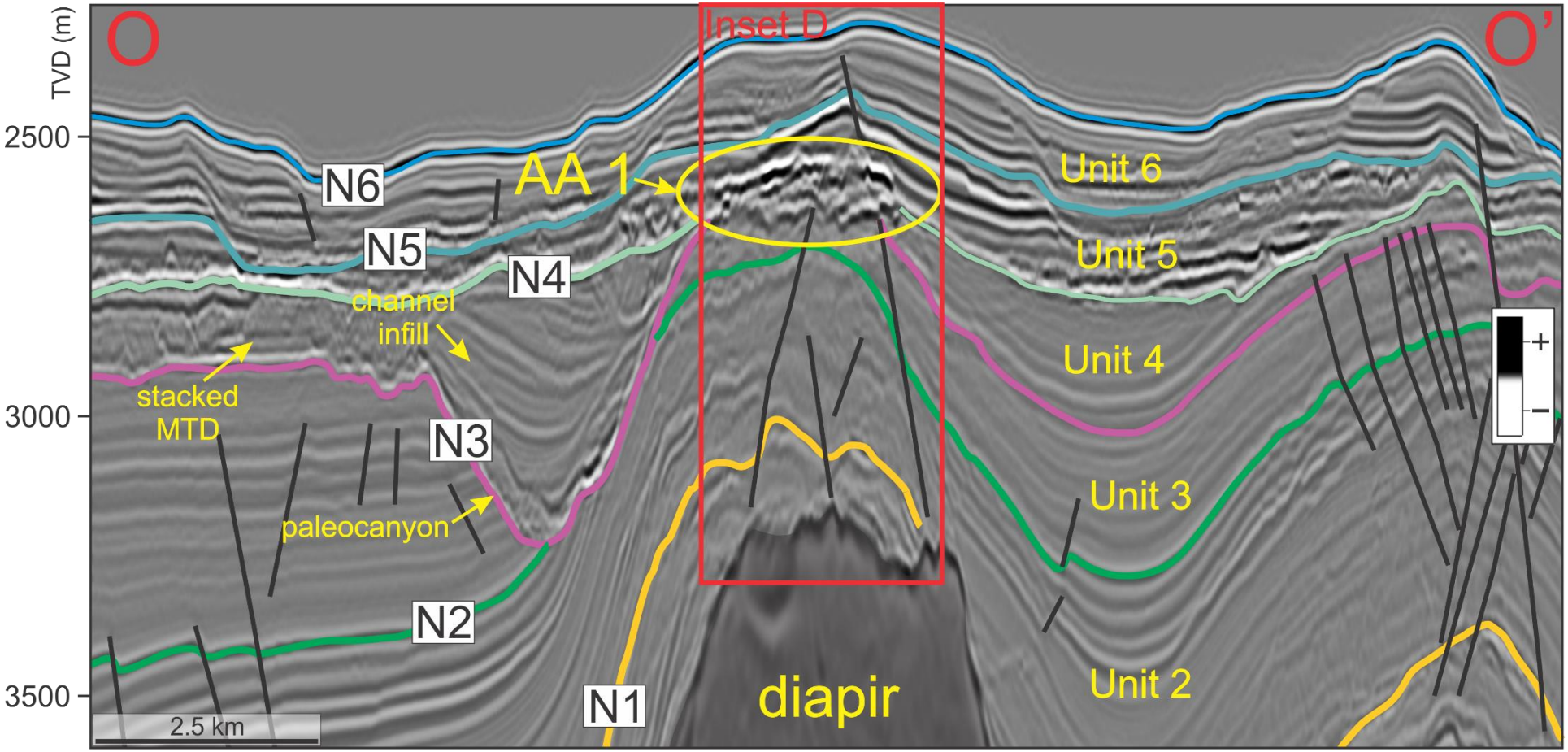

Figure 4.2. Representative strike-oriented section showing Amplitude Anomaly 1 (AA 1; see Appendix VI for uninterpreted version) situated above a salt diapir located at central Tangier (Fig. 4.1). Some notable features include the N3-level paleocanyon and its contouritic and mass transport infill (left), crestal faulting above the diapir at AA 1, and a fault from AA 1 to near surface, which could be a seepage pathway. Data courtesy of BP Canada Exploration Ltd via NSDNRR.

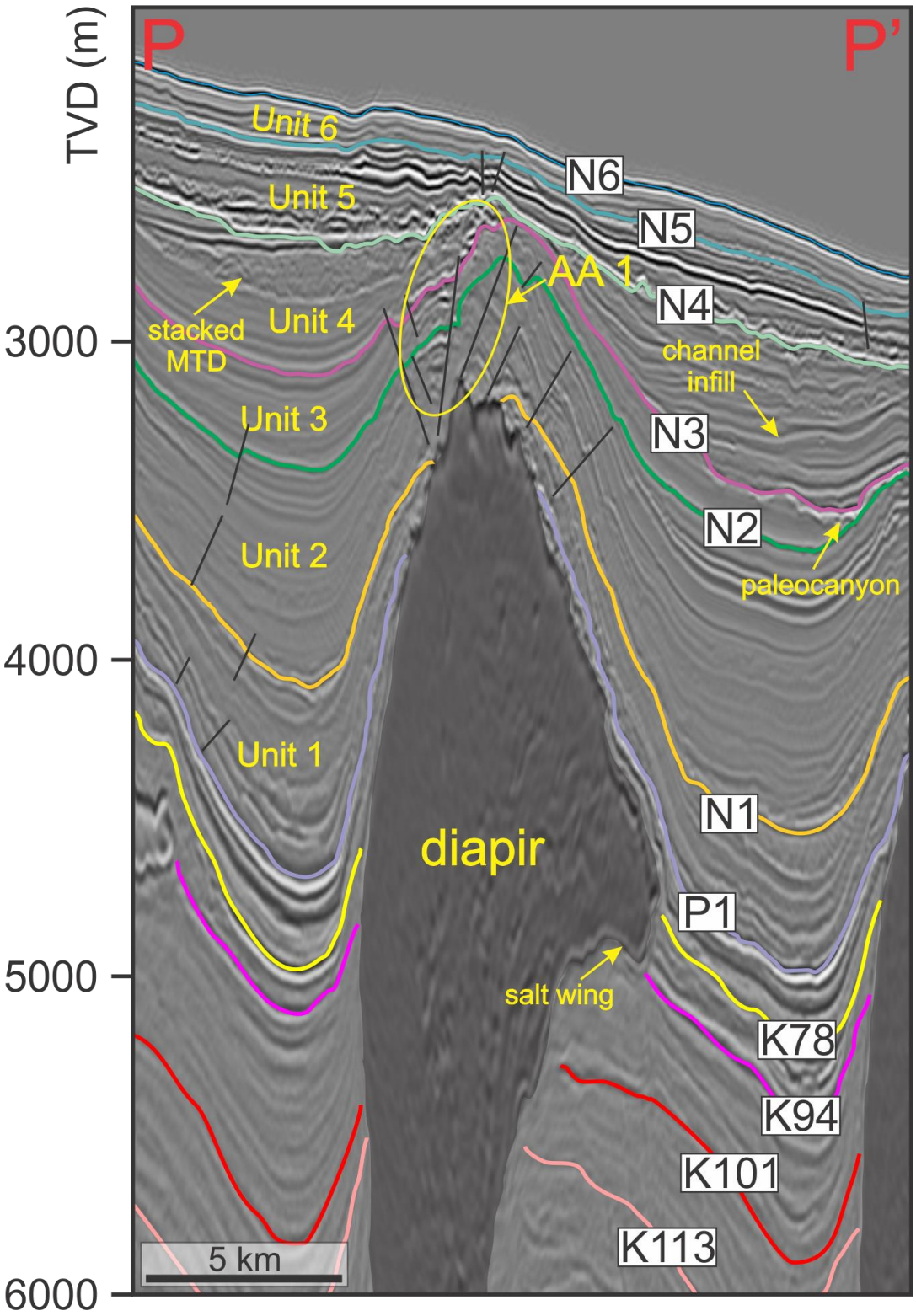

Figure 4.3. Dip-oriented section showing AA 1 (P-P', location in Fig. 4.1; see Appendix VI for uninterpreted version) in a different orientation with associated structures from Fig. 4.2. Data courtesy of BP Canada Exploration Ltd via NSDNRR.

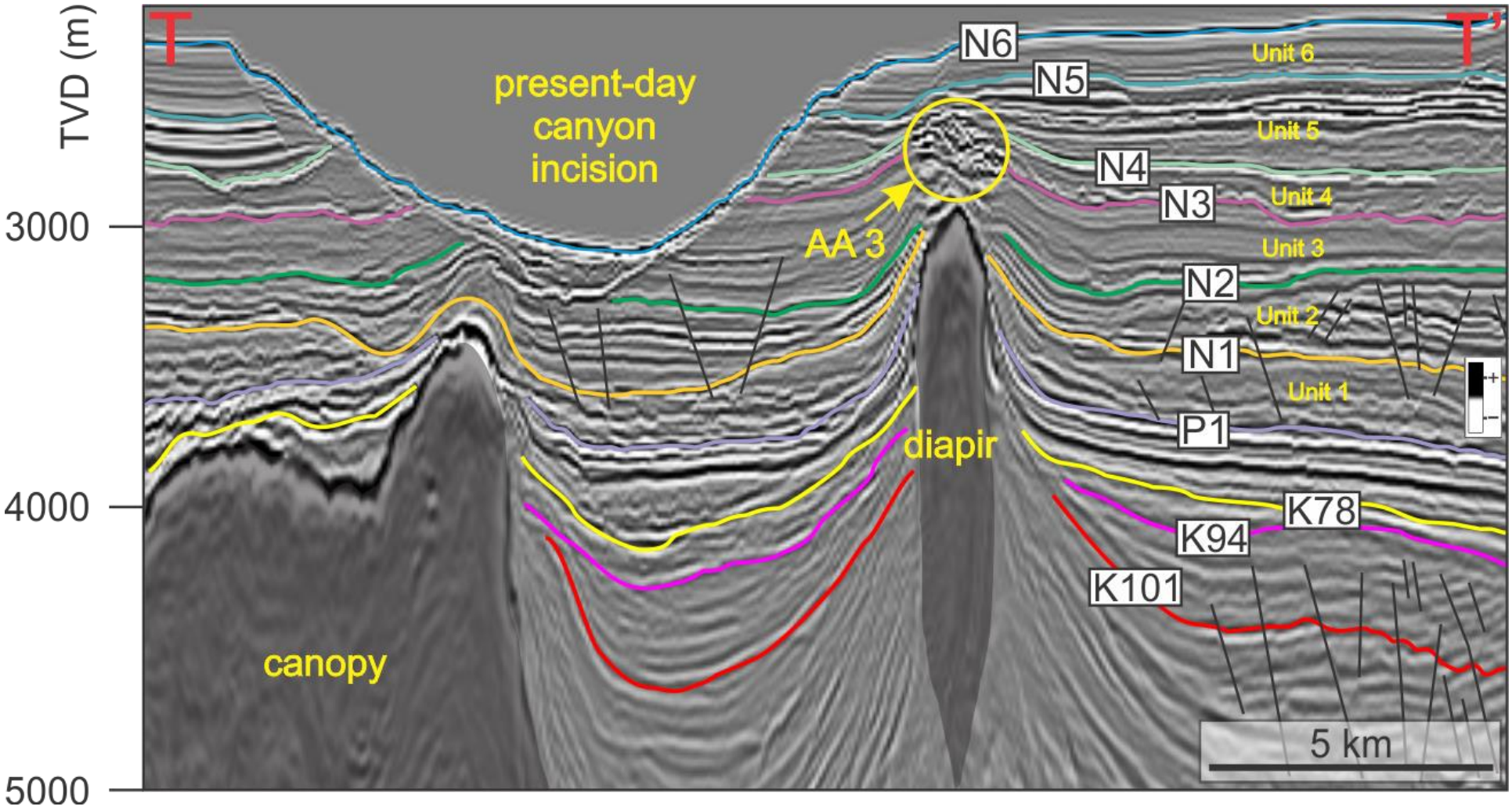

Figure 4.4. Representative strike-oriented seismic section (T-T', location in Fig. 4.1; see Appendix VI for uninterpreted version) showing amplitude anomaly 3 (AA 3) with its associated architecture. AA 3 is located at the crest of a salt diapir located at the eastern Tangier (Fig. 4.1). Data courtesy of BP Canada Exploration Ltd via NSDNRR.

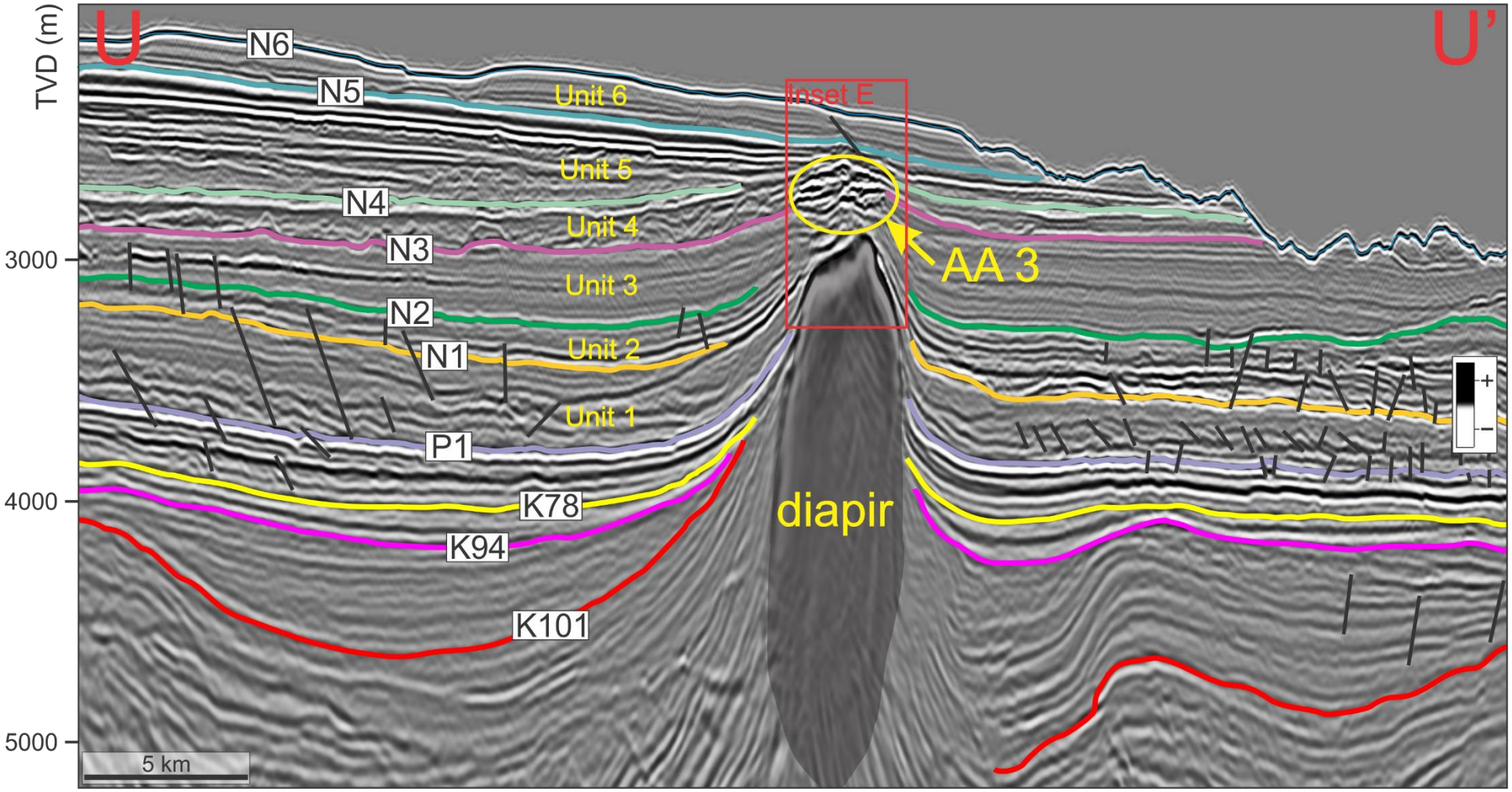

Figure 4.5. Representative dip-oriented seismic section (U-U'; location in Fig. 4.1; see Appendix VI for uninterpreted version) showing a different orientation of AA 3 that is located at the crest of a salt diapir in Fig. 4.4. AA 3 is situated within the post-N3 mass transport deposit, above the crest of the salt diapir. Data courtesy of BP Canada Exploration Ltd via NSDNRR.

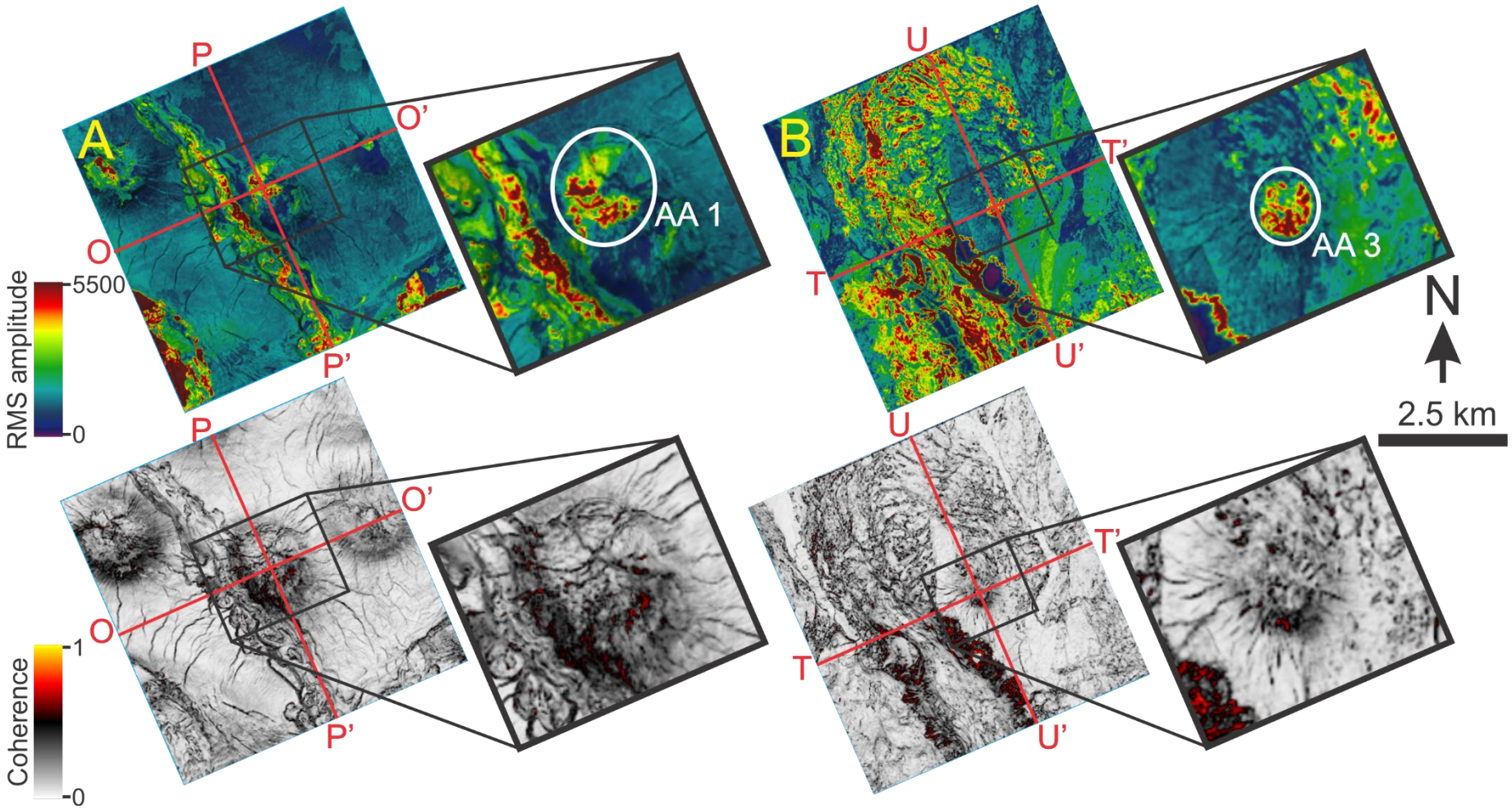

Figure 4.6A and 4.6B. Extracted RMS amplitude and coherence maps from N3 horizon for both AA 1 (left) and AA 3 (right) (see Appendix III and IV for uninterpreted versions). RMS amplitude maps depict the location of both amplitude anomalies. Coherence maps illustrate the structural complexity associated with the amplitude anomalies, such as radially oriented crestal faults just below the amplitude anomalies, faults interpreted to have influence on fluid migration. Geographical locations of seismic sections above (O-O', P-P', T-T', U-U') are included.

AA 1 is observed within Unit 3, Unit 4, and Unit 5, bounded by N2-N3, N3-N4, and N4-N5 horizons, respectively (see Chapter 3). The anomaly is located above the crest of a diapir (Figs. 4.2 and 4.3). AA 1 is situated within the weak, chaotic reflectors of Unit 3 to Unit 5 and close to the adjacent N3 paleocanyon (Figs. 4.2 and 4.3). Stratal termination or offset is observed in Figure 4.7A (e.g., a fault above AA 1), but lacks of velocity pull-ups or push-downs.

AA 3 is also located within Unit 3, Unit 4, and Unit 5 (Figs. 4.4 and 4.5). This anomaly is partially situated within the post-N3 mass transport deposit in Unit 4 (Figs. 4.4 and 4.5). The AA 1 and AA 3 amplitude anomalies are found within 100 m to 300 m below seafloor. Figure 4.7B shows stratal offset above AA 3 with velocity pull-ups or push-downs. Figure 4.8 exhibits a bathymetric seafloor image of AA 3 and its vicinity. Some morphological features can be observed such as pockmarks and fault scarps (Fig. 4.8).

Both AA 1 and AA 3 amplitude anomalies are also observed in map view within RMS amplitude and coherence attribute maps (Figs. 4.6A; 4.6B). Both amplitude anomalies look similar in RMS amplitude at the N3 horizon, at which they appear to be an isolated, cluster of amplitude anomalies that have elliptical geometry, and are 1 to 1.5 km wide, concentrated at the crest of the diapirs. The vertical zone of sediments where AA 1 and AA 3 reside is about 200 to 300 m thick. In coherence, both maps show radially oriented crestal faults present within the proximity of the amplitude anomalies at N3 horizon.

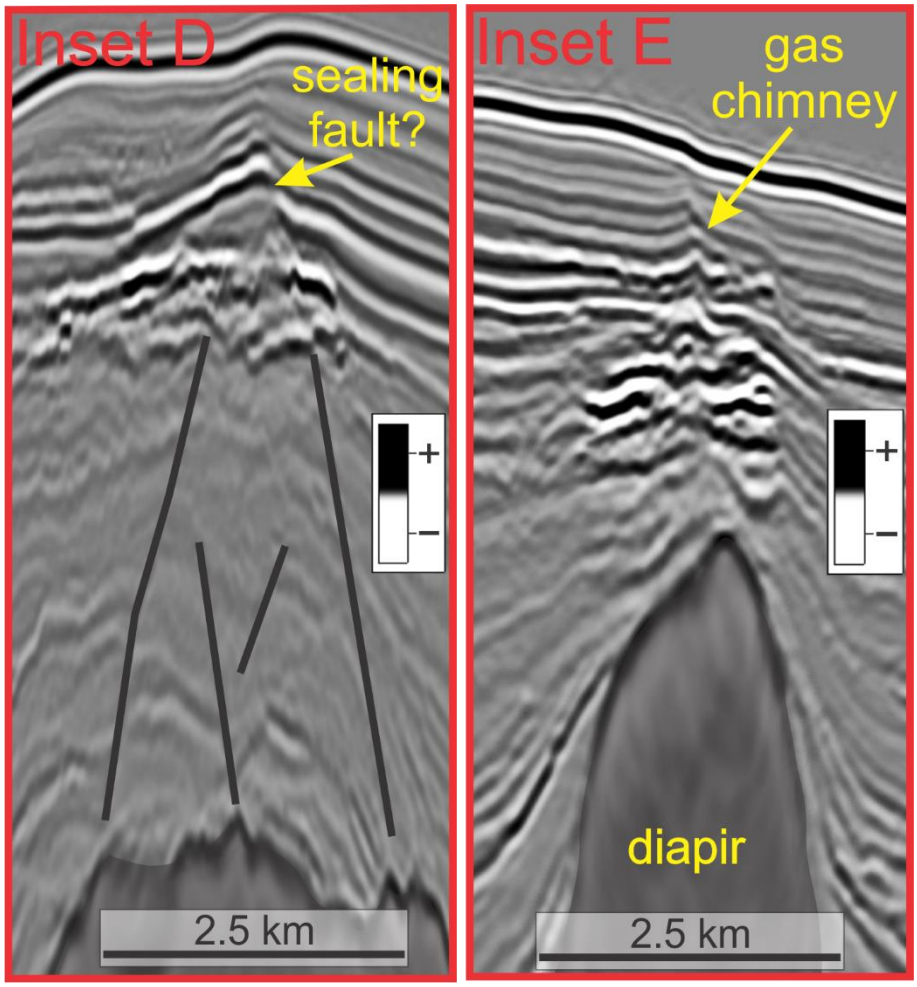

Figure 4.7A (Inset D in Fig. 4.2) and 4.7B (Inset E in Fig. 4.5). Inset D in strike orientation shows a fault that could be sealing AA 1 due to lack of velocity pull-ups that would suggest presence of a gas chimney. Inset E in dip orientation depicts velocity pull-ups above AA 3 in a possible gas chimney, which suggests that fluids are leaking to near surface (i.e., a seepage site). Data courtesy of BP Canada Exploration Ltd via NSDNRR.

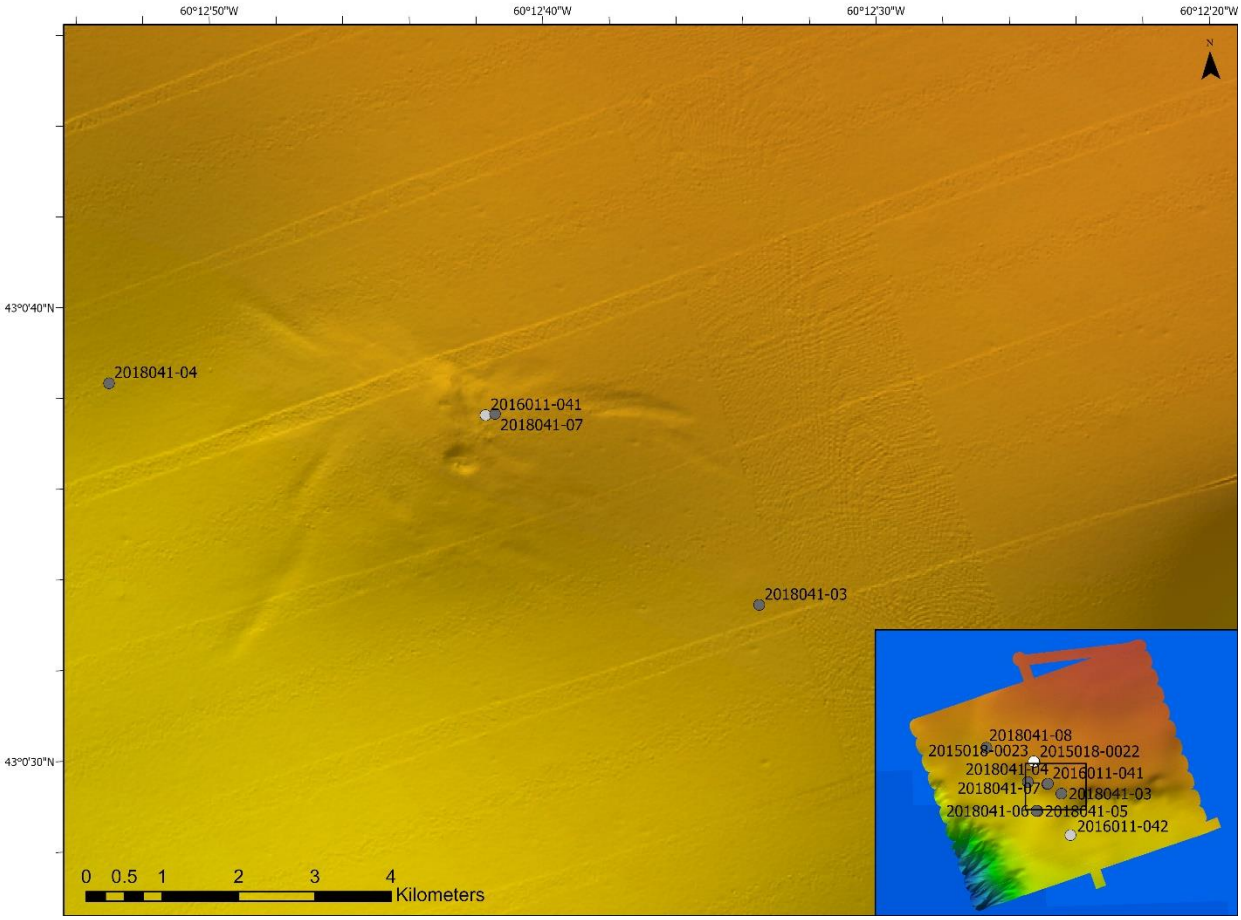

Figure 4.8. Bathymetric seafloor images extracted from the 2020 AUV Survey of the AA 3 seep site (Bennett and Desiage, 2022). These images depict structural features related to the seep site such as pockmarks and surface fault scarps. Sampling locations are also illustrated here from different sampling cruises conducted by the GAPP.

4.3.2. Canopy-related shallow amplitude anomaly

Amplitude Anomaly 2 (AA 2) is dominated by bright spots with notable flat spots (Inset G; Fig. 4.11) with effects of polarity reversal. It is located 300 to 500 m below seafloor, within a mass transport deposit above the N4 horizon in the eastern part of the Tangier survey (Figs. 4.9 and 4.10).

AA 2 can also be observed at depth in map view as it is intersected by the N4 horizon (Fig. 4.12). The RMS amplitude map at this level shows an isolated cluster of amplitude anomalies, that have elliptical geometry, over an area 1.5 to 2 km wide, concentrated near a broad structural high in the underlying canopy. The vertical interval of sediments where AA 2 resides is about 200 to 300 m thick. The coherence map (Fig. 4.12) resolves crestal faults, which are illustrated in the P-P' and Q-Q' seismic profiles.

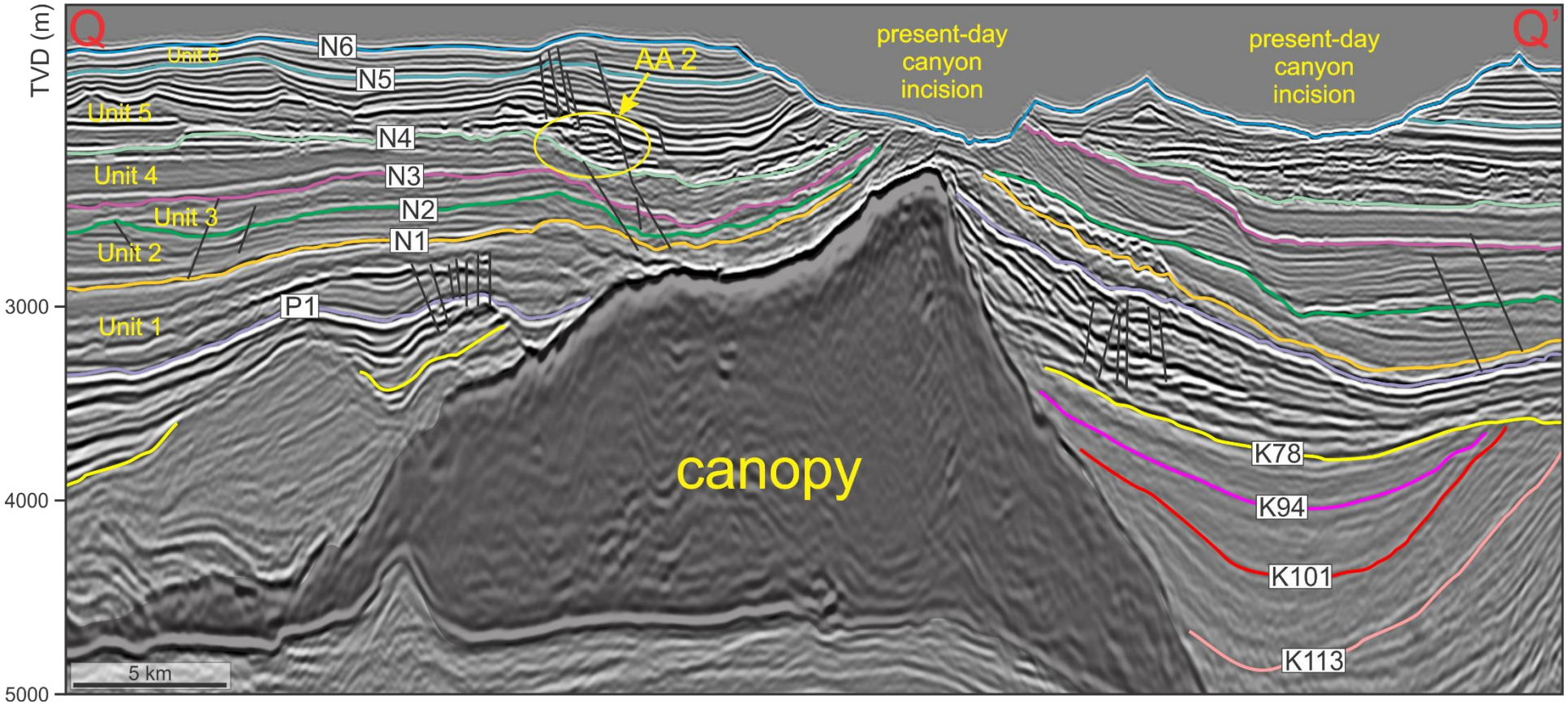

Figure 4.9. Representative strike-oriented seismic profile (Q-Q', location in Fig. 4.1; see Appendix VI for uninterpreted version) showing amplitude anomaly 2 (AA 2) and its associated architecture. Data courtesy of BP Canada Exploration Ltd via NSDNRR.

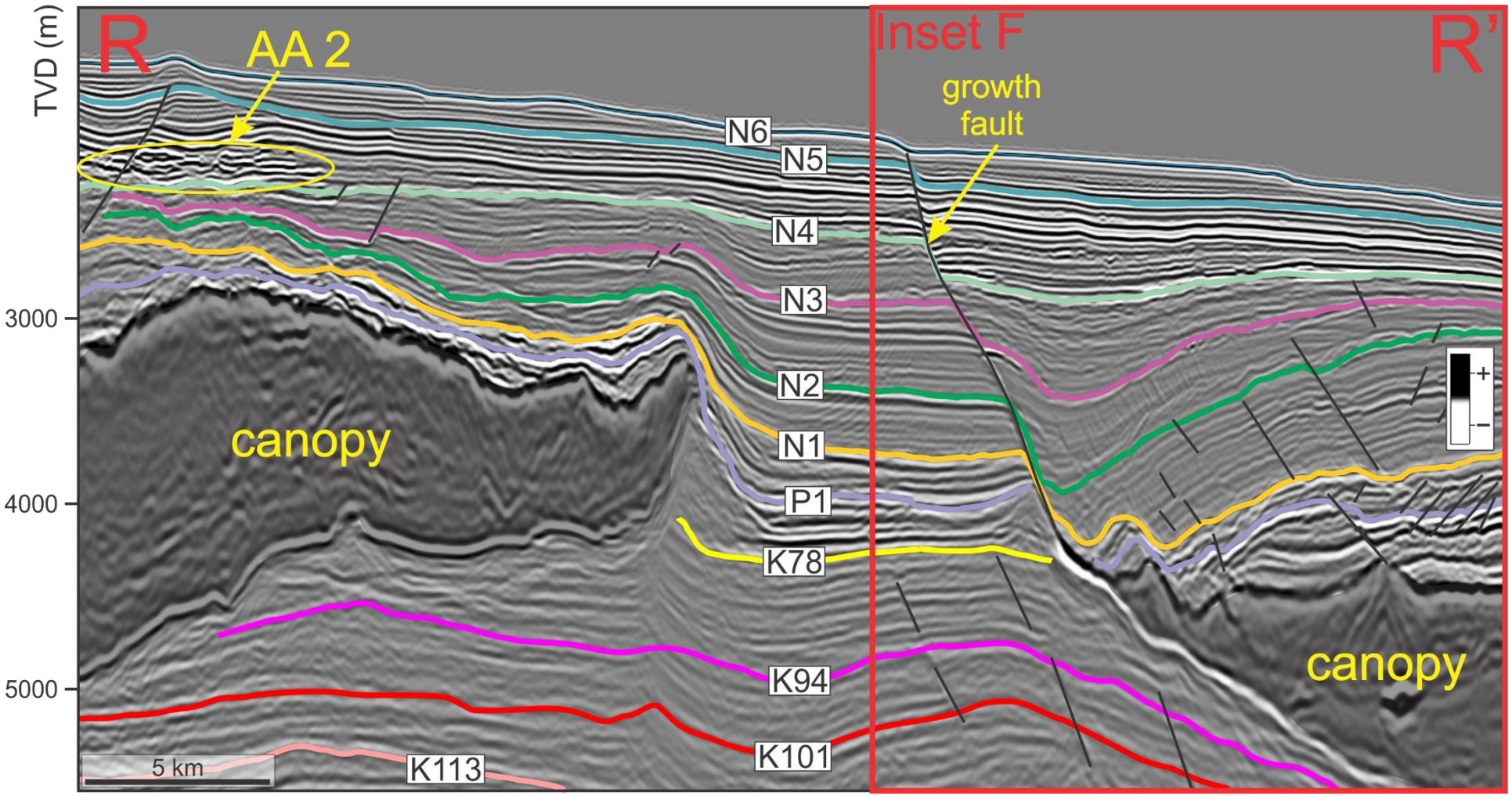

Figure 4.10. Representative dip-oriented seismic profile (R-R', location in Fig. 4.1; see Appendix VI for uninterpreted version) showing a different orientation of AA 2 and its proximity to the salt canopy body situated on the eastern Tangier. A dominant canopy-related feature near to AA 2 is a growth fault above the second canopy body. The Mesozoic stratigraphy is also shown, which is buried underneath and covered by the salt canopy bodies. Data courtesy of BP Canada Exploration Ltd via NSDNRR.

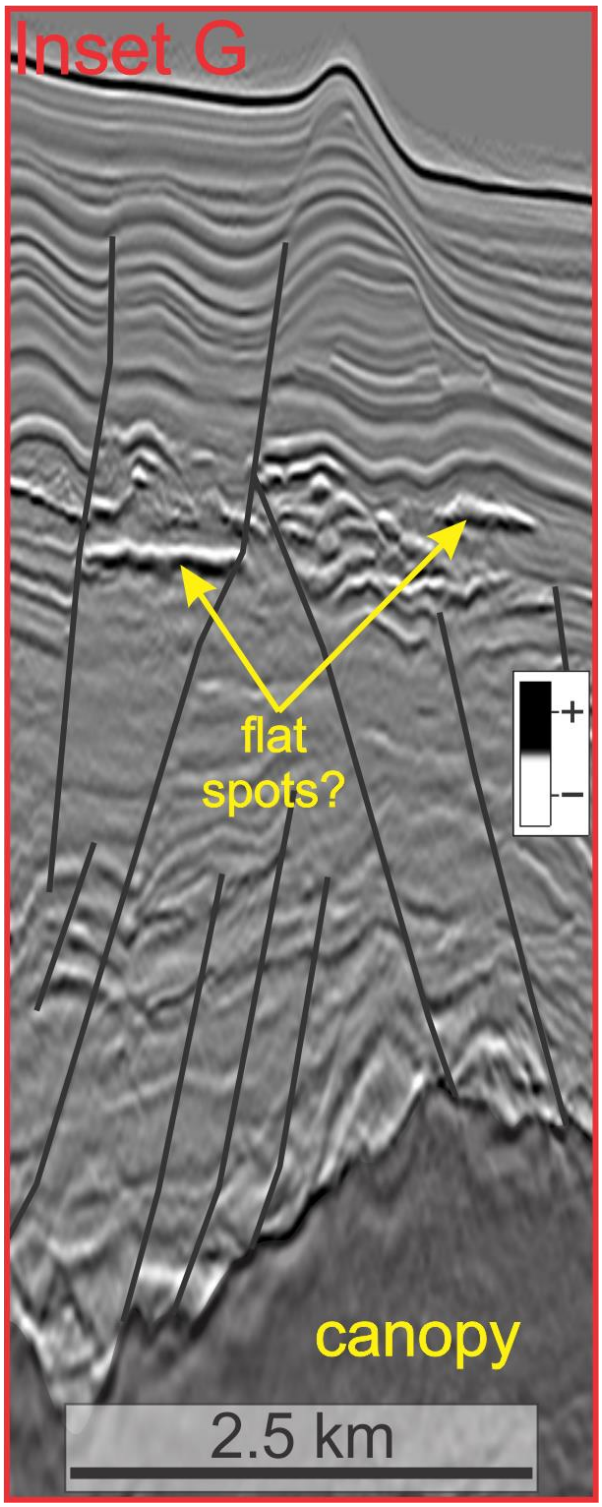

Figure 4.11 (Inset G in Fig. 4.16). Time-domain detail of part of the Weymouth 3D (refer to Fig. 4.16) illustrating a closer view of AA 2 showing potential flat spots possibly indicating a horizontal contact between fluids in the subsurface. This inset also shows the proximity of the amplitude anomaly with possible migration pathways via faults above the crest of the canopy body. Data courtesy of Ovintiv (former EnCana) via NSDNRR.

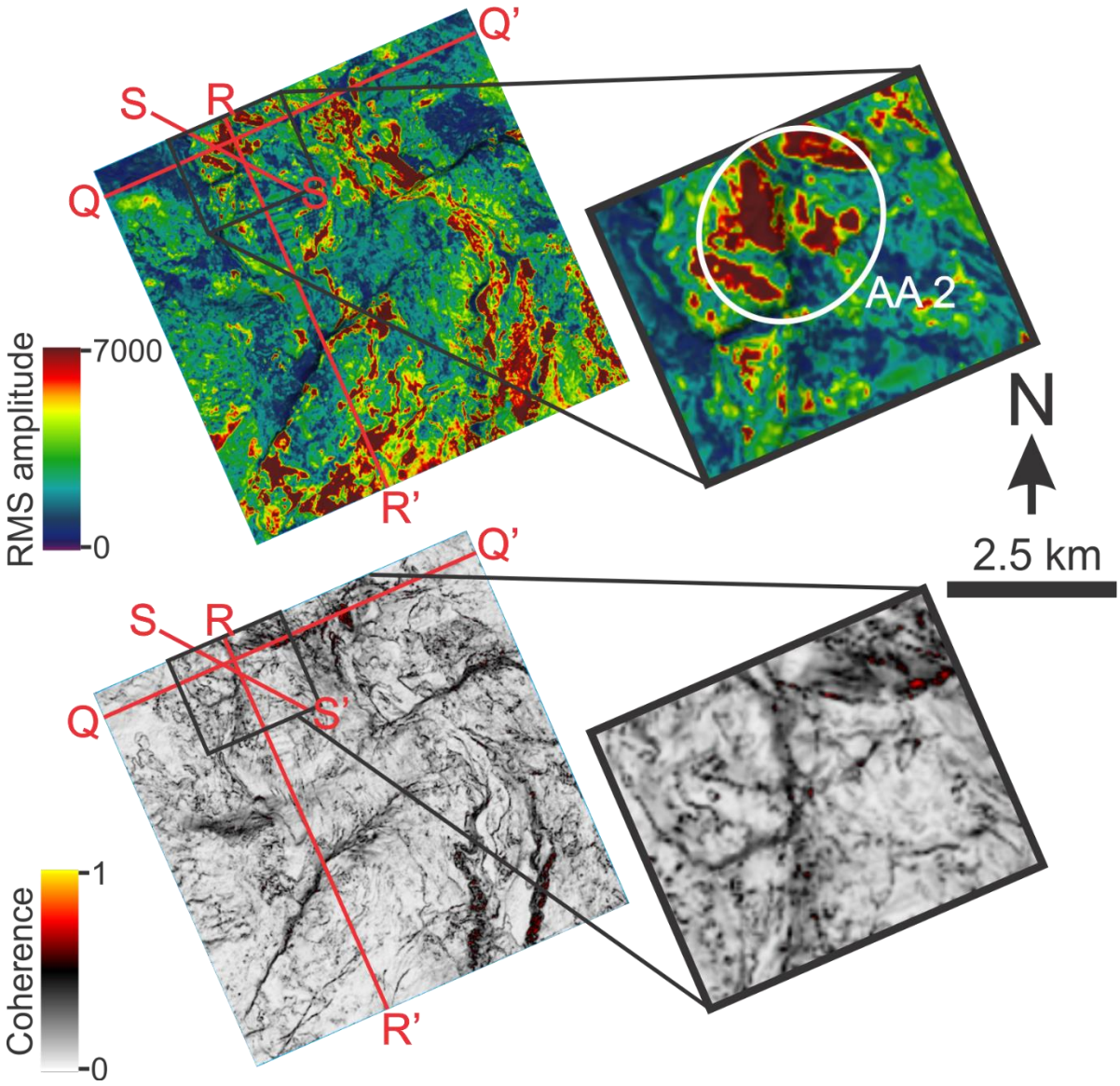

Figure 4.12. RMS amplitude and coherence maps extracted from N4 horizon (Fig. 4.10) depicting the AA 2 shown by the insets on the right. The RMS amplitude map shows moderate to high amplitude reflectors that indicate how AA 2 looks in map view. The coherence map shows more of the topographical structure of AA 2. Geographical locations of seismic profiles for AA 2 (Q-Q', R-R', S-S') are included.

Inset G (Fig. 4.11), which is in the time domain, shows AA 2 with a trough-peak pair, sub-horizontal anomaly also known as flat spots and surrounded with bright spots. Recognition of these potential flat spots should be done with caution because the survey is in the time domain.

What appears “flat” and horizontal in the time domain may not be its character in the real world in depth due to velocity effects.

4.3.3. Deeper seismic horizons

Investigation of the deeper stratigraphy is limited to the vicinity of the fluid-related amplitude anomalies (AA 1, AA 2, AA 3). At least nine seismic horizons were mapped in the Mesozoic below P1 horizon derived from existing horizons (“K” for Cretaceous; “J” for Jurassic) of the Play Fairway Analysis (OETR, 2011) and Deptuck and Kendell (2020) including Cretaceous markers such as K78, K94, K101, K113, K130, K147, and Jurassic markers such as J144 and J150. These markers are peak reflectors and laterally extensive throughout the Scotian Margin.

4.4. Interpretation and Discussion

4.4.1. Insights on lithostratigraphy for potential source and reservoir rocks based on deeper seismic horizons

This is an attempt to provide interpretative insight to the lithology below the amplitude anomalies, particularly because AA 3 is proven from geochemical data to be gas hydrates with thermogenic origin that likely have a deeper source (Fowler et al., 2017; 2017).

- K78 represents a strong impedance contrast caused by a relatively thin interval of Campanian chalks overlain by thicker interval of Campanian to Maastrichtian chalks, marls, and calcareous mudstones (Weston et al., 2012; Deptuck and Kendell, 2020). On the shelf, K78 defines the top of the Campanian Wyandot Formation in many areas. On the slope, K78 is both underlain and overlain by chalks that could all be considered as the

Wyandot Formation. This horizon is present below all amplitude anomalies mapped as DHIs in this study (Fig. 4.13-4.15).

- K94 is mapped within the Petrel Member of the Dawson Canyon Formation and closely correlates with the Turonian-Cenomanian Unconformity or its lateral equivalent (Weston et al., 2012; Deptuck and Kendell, 2020). At Shubenacadie H-100 well (location in Figs. 2.1; 3.20), K94 represents a lithological change from shale below to shale, siltstone, and marls above (Deptuck and Kendell, 2020). This horizon is present below all amplitude anomalies mapped as DHIs in this study (Fig. 4.13-4.15).
- K101 closely represents the Late Albian Unconformity or its lateral equivalent and located near the top of the Logan Canyon clastic sequences entering the slope depositional processes. This horizon is present below all amplitude anomalies mapped as DHIs in this study (Fig. 4.13-4.15).
- K113 is within the Logan Canyon Formation close to the Aptian-Albian boundary, corresponding approximately to the base of the Cree Member (or its lateral equivalents on the slope). K113 lies within a succession of gray marine claystone, near the top of the Aptian (Deptuck and Kendell, 2020). This horizon is present below all amplitude anomalies mapped as DHIs in this study (Fig. 4.13-4.15).
- K130 is close to the Hauterivian-Valanginian boundary (Intra-Hauterivian MFS) and the O-Marker limestone event on the shelf. Below this is the Middle and Lower Missisauga Formation, the clastic succession that was a primary target interval of the Weymouth A-45 well. K130 is calibrated at Newburn H-23, Weymouth A-45, Cheshire L-97, and Monterey Jack E-43 wells (locations in Figs. 2.1; 3.20), where it lies within a marine

clastic succession (Deptuck and Kendell, 2020). This horizon is present below all amplitude anomalies mapped as DHIs in this study (Fig. 4.13-4.15).

- K137 is within the Lower Missisauga Formation close to the Berriasian-Valanginian boundary (Near Base Cretaceous unconformity of Weston et al., 2012). This horizon is present below all amplitude anomalies mapped as DHIs in this study (Fig. 4.13-4.15).
- J144 is close to the start of Mic Mac Formation deposition that is close to the boundary between Tithonian-Berriasian. This horizon is strongly evident below AA 2 (Fig. 4.15) and AA 3 (Fig. 4.14) but not resolvable below AA 1 (Fig. 4.13).
- J150 is within the Mic Mac Formation. This horizon is close to the Kimmeridgian-Tithonian boundary. This is the predicted primary source rock of fluids on the Scotian Margin (Upper Jurassic Tithonian source rock interval mapped by J144 and J150). In the shelf, the Mic Mac Formation is characterized by sandy fluvial channels and sandy delta sequences. In the slope, J150 is calibrated to Cheshire L-97/L-97A and Monterey Jack E-43/E-43A wells, where Tithonian clay-rich carbonates are present in both. This horizon is strongly evident below AA 2 (Fig. 4.15) and AA 3 (Fig. 4.14) but not resolvable below AA 1 (Fig. 4.13).

4.4.2. Potential pathways for fluid migration and associated trapping and sealing mechanisms of shallow amplitude anomalies

Migration from deeper depths

Movement of Triassic-Early Jurassic-aged salt has played a major role in the development of structural deformation in the deeper Mesozoic up to the shallow Cenozoic strata. This likely generated several potential migration pathways: (i) faults developed by salt mobility at depth,

and (ii) other faults above the salt bodies (e.g., crestal faults; Wood and Giles, 1982; Mattos et al., 2016; Roelofse et al., 2020) as potential pathways from the source to the shallow, permeable strata where the interpreted DHIs occur (Fig. 4.17-4.19).

The other factor that drives fluid flow at depth is geologic overpressure. Geologic overpressure is the inability of connate pore fluids to escape as the surrounding matrix compacts under the lithostatic pressure caused by the overburden (Chi and Xue, 2011). Geologic overpressure can be generated by multiple processes, such as when fluid escape is impeded by the surrounding impermeable layers (e.g., evaporites, shales and mudstones, and cemented sandstones) resulting in increased rate of change in pore space and fluid volume (Chi and Xue, 2011). Other common examples of geological processes that produce fluid overpressure are by thermal expansion of fluid, hydrocarbon generation, mineral dewatering, overpressure generated by allochthonous salt bodies such as canopy complexes as such salt bodies add to the weight of the overburden, and presence of low permeability seals (Neglia, 1979; Chapman, 1980; Bethke, 1985; Zhao et al., 1998a; Swarbrick et al., 2002; Davison, 2009; Chi and Xue, 2011; Nelskamp et al., 2012).

In terms of salt bodies inducing fluid overpressure, according to Jackson and Hudec (2009; 2017), the geomorphologic style of canopy-margin thrusts may be used as a tool to predict fluid overpressure beneath salt canopies because the canopy moves over and adds to the load on top of the sediments beneath, while also acting as a relatively effective low permeability seal to the migration of fluids from deeper source. It is also suggested that the pressure prediction has been of great interest in offshore hydrocarbon exploration as subsalt overpressure is considered as a drilling hazard in the sedimentary basin such as in the Gulf of Mexico (O'Brien and Lerche, 1994; Malloy et al., 1996) and in some parts of the Scotian Margin, where several exploration wells have penetrated the allochthonous salt canopy (see Figs. 4.21-4.22) such as where Aspy D-

11/D-11A encountered highly overpressured and gas-charged siltstones immediately beneath the salt. At shallow depths, Ma et al. (2021) suggested that the driving force for fluids to seep through the seafloor is predicted to be localized overpressure, where it is induced by the continuous accumulation of fluids in a subsurface reservoir.

In the Tangier 3D area, anomalies AA 1 and AA 3 are located above salt diapirs. Given the association with these structures, the salt diapirs are the most plausible controlling geological body responsible for providing pathways for upward fluid migration, both due to the slope of strata on the flanks of the structures, facilitating along-bed flow, and the occurrence of faults in relation to the salt deformation. The motion of the salt from its origin in the autochthonous salt layer to shallower depths produces the breaches in the surrounding stratigraphy that can serve as a potential conduit for fluid migration, even if the salt itself is no longer present, such as along a salt weld.

Figure 4.14 illustrates the possibility of migration pathways for AA 3 as it shows where the feeder of the diapir is located at least around 10 km in depth. AA 3 is the only amplitude anomaly in the Tangier 3D area that has been proven to be gas hydrates to have a signature of thermogenic origin, based on isotopic analyses (Fowler et al., 2017; 2017). This seismic profile shows that this diapir could have provided a migration pathway for the generated fluids from the predicted Upper Jurassic source rocks mapped by J144 and J150 horizons (from OETR, 2011), including targeted siliciclastic sequences of the lower Cretaceous (e.g., K130 horizon) predicted as reservoir rock (OETR, 2011) that could have possible been breached by salt diapirism. In other parts of the world, it has been documented that salt diapirs are susceptible to hydrocarbon leakage from deeper reservoirs and may strongly contribute to long term seafloor seepage (Taylor et al., 2000; Gay et al., 2007; Chand et al., 2008; Geletti et al., 2008; Serié et al., 2012;

Wenau et al., 2015; de Mahiques et al., 2017; Jatiault et al., 2019; Roelofse et al., 2020; Ma et al., 2021; Römer et al., 2021).

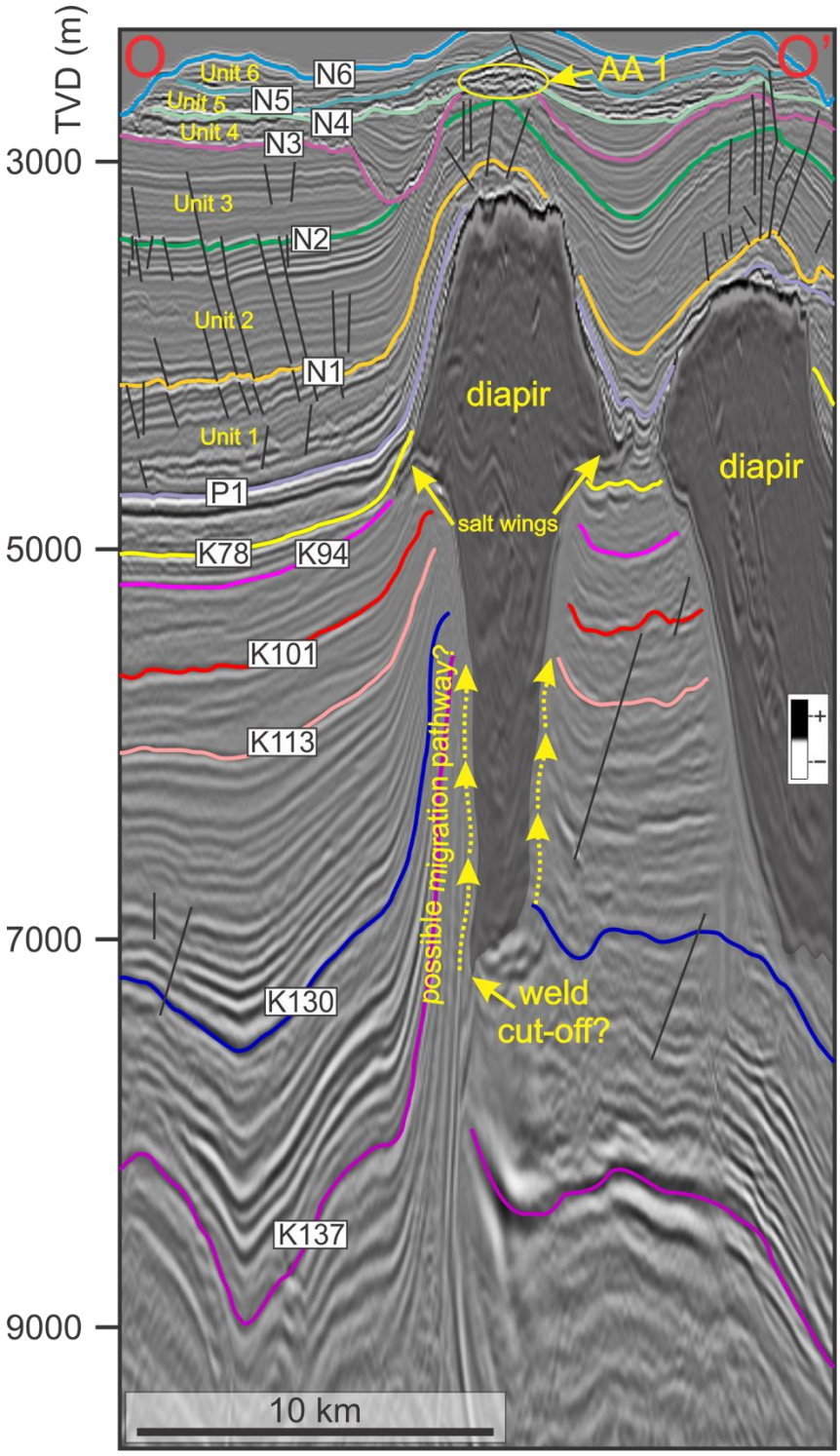

Figure 4.13. Representative deeper seismic section profile, O-O' (Fig. 4.2), depicting potential upward fluid migration pathways from the source or reservoir rock to AA 1, initiated by the deeper welding of the salt diapir and up-dip migration along carrier beds. This deeper seismic profile also illustrates deeper seismic horizons that corresponds to lithostratigraphy below AA 1 extrapolated from Balvenie B-79 and Weymouth A-45 (OERA, 2011). Data courtesy of BP Canada Exploration Ltd via NSDNRR.

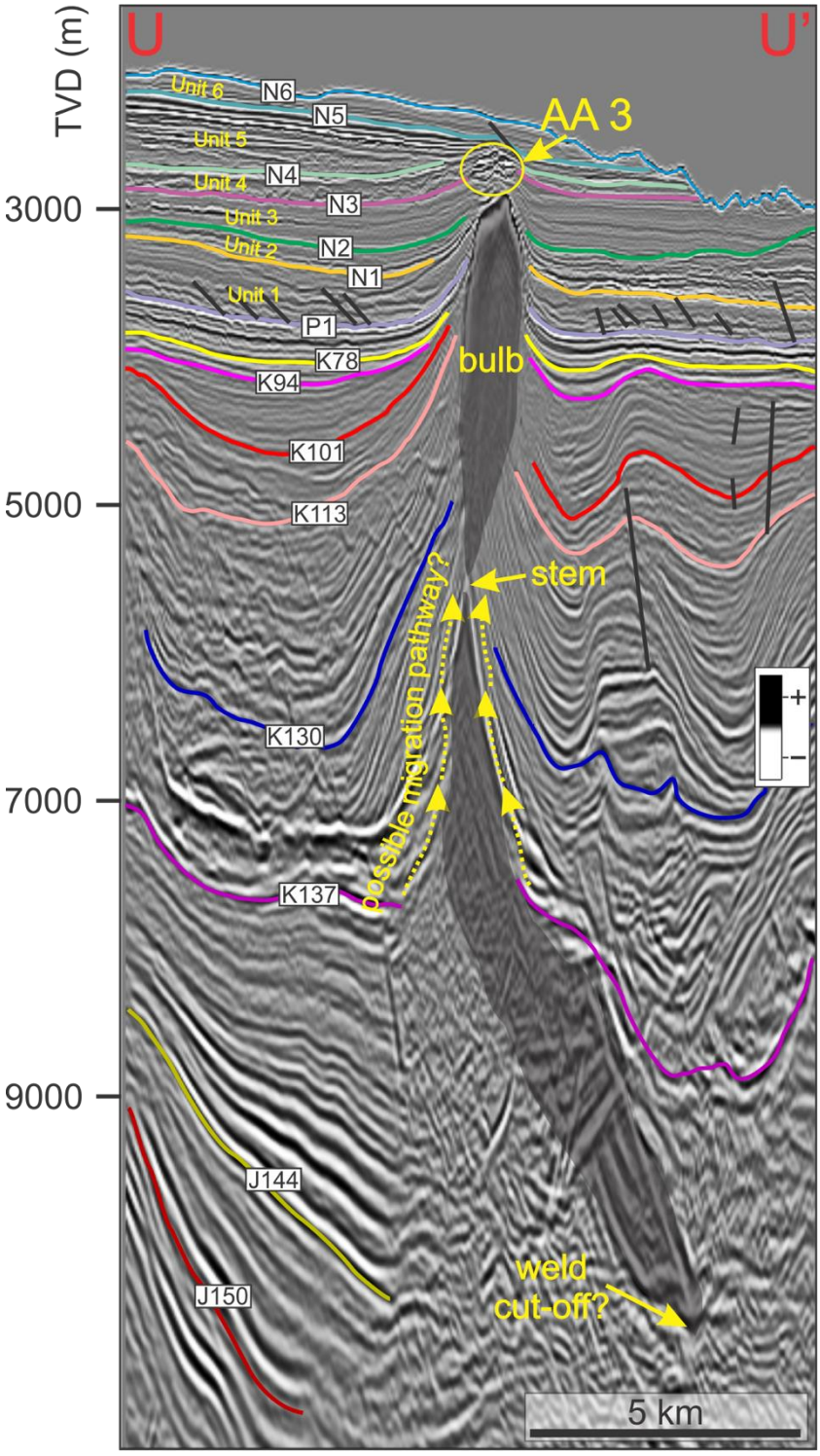

Figure 4.14. Representative deeper interval of seismic profile, U-U' (Fig. 4.5), illustrating potential migration pathways provided by steep flanking beds and salt welding of the diapir from the source rock to AA 3. This profile also illustrates mapped deeper seismic horizons that correspond to lithostratigraphy tied to Balvenie B-79 and extrapolated from Weymouth A-45 (OERA, 2011). Data courtesy of BP Canada Exploration Ltd via NSDNRR.

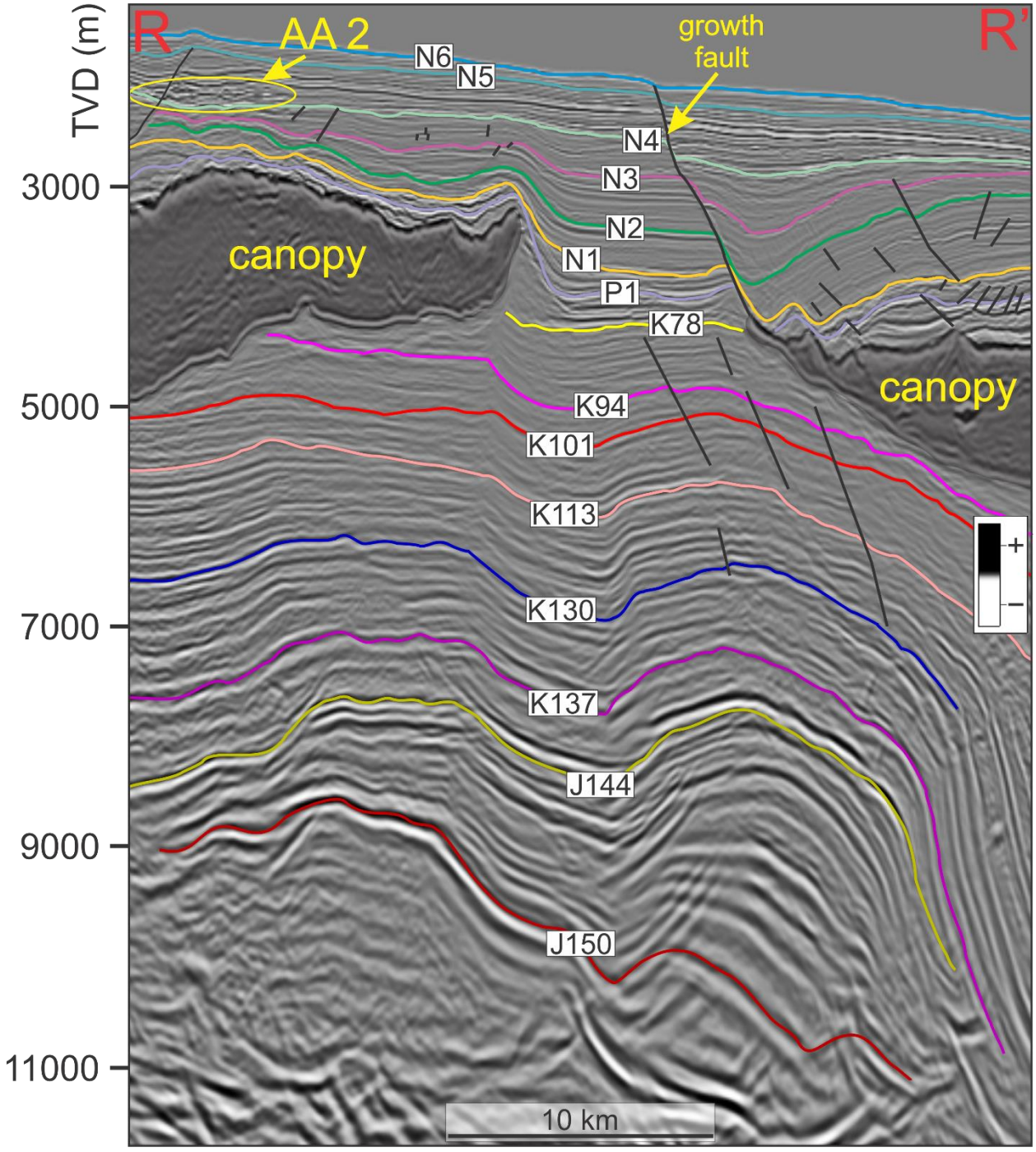

Figure 4.15. Deeper seismic interval of P-P' from Fig. 4.10 that depicts mapped deeper seismic horizons to investigate lithostratigraphy below AA 2 and the possible migration pathway provided by salt canopy expulsion. This profile also illustrates deeper seismic horizons that correspond to lithostratigraphy tied to Weymouth A-45 and extrapolated from Balvenie B-79 (OERA, 2011). Data courtesy of BP Canada Exploration Ltd via NSDNRR.

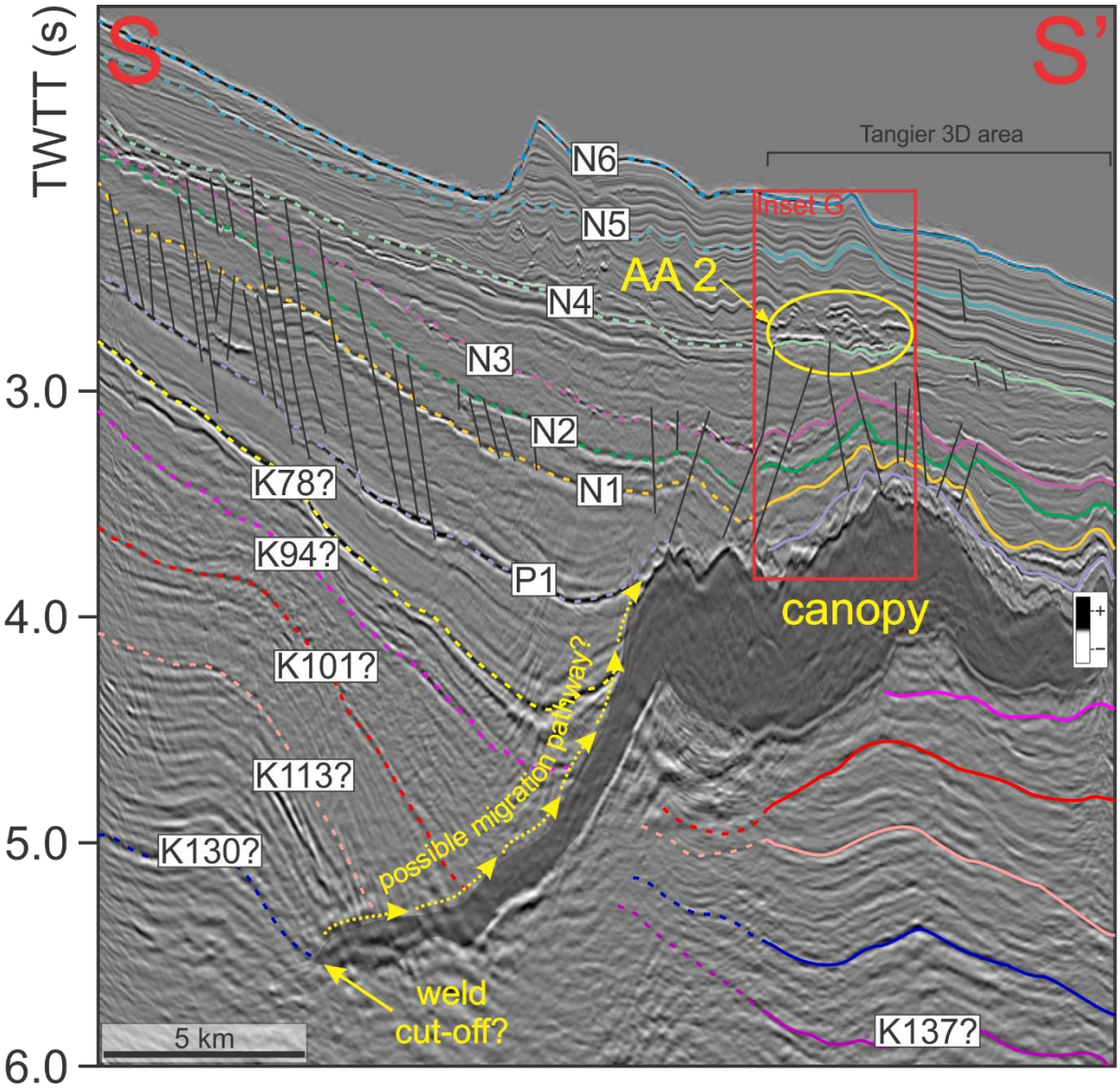

Figure 4.16. Representative dip-oriented section in the time domain (S-S', location in Figs. 4.1 and 4.11; see Appendix VI for uninterpreted version) from Weymouth 3D area (see location of Weymouth 3D in Figs. 2.1 and 3.20) showing the starting position of salt canopy expulsion from the feeder. This seismic profile also shows the possible migration pathway that the canopy created during its expulsion from the source or reservoir rock level. At the crest of the canopy, several crestal faults are observed that potentially caused the fluids to migrate to the shallow, unconsolidated Cenozoic strata as indicated by the presence of the amplitude anomaly there. Data courtesy of Ovintiv (former EnCana) via NSDNRR.

For AA 2, a salt canopy is possibly providing a migration pathway for fluids (including hydrocarbons) from deeper depths where source and/or reservoir rocks might be residing.

Figures 4.15 and 4.16 depict the possible migration pathway for AA 2, a pathway that starts from at least the salt weld cut-off. Due to the cut-off of the salt weld and the effect of seismic artefacts in the Weymouth 3D Seismic Survey (Fig. 4.16; see location in Fig. 2.1 and 3.19), the allochthonous salt canopy body is not resolvable at deeper depths, which hindered identification of the implied autochthonous source.

The expulsion and movement of the salt canopy to shallower depths beneath AA 2 created a candidate migration pathway for the fluids that likely breached the predicted source (e.g., Upper Jurassic) or reservoir intervals (e.g., Lower Cretaceous). The salt expulsion of the slope canopy complex evolved due to significant sediment loading that occurred from the Late Jurassic through Early Cretaceous due to the development of prograding Sable Delta that covered a large portion of the central Scotian Slope (Ge et al., 1997; Ings and Shimeld, 2006; Albertz et al., 2010; Kendell, 2012). Expulsion of the canopy and associated deformation continued into the Cenozoic, though in general, it was less extensive than earlier periods and eventually sedimentation thickly covered the canopy, driving the supra-salt growth fault systems.

Migration to shallow depths

Crestal faults are known to have influence in controlling migration of deep fluids in other areas (e.g., Davison et al., 2000a; 2000b; Mattos et al., 2016) and may be used to characterize paleostress conditions caused by salt mobility (e.g., Quintà et al., 2012; Carruthers et al., 2013; Ho et al., 2013; Nikolinakou et al., 2014; Roberts et al., 2015).

In 3D projected coherence maps with associated seismic profiles (Figs. 4.17-4.19), all interpreted DHIs are situated above the apex of salt bodies with pronounced crestal faults, as seen at the

level of the N2 horizon. Existing polygonal fault networks are also present within the proximity of salt bodies. These polygonal faults are a network of normal faults that are layer-bounded, formed by compaction and dewatering that is common in fine-grained sediments, independent of salt tectonism (Cartwright and Lonergan, 1996; Carruthers et al., 2013; Li et al., 2020). Based on the observed changes in fault geometry, the stress caused by salt diapirism, primarily squeezing (e.g., Carruthers et al., 2013), caused structural and geometrical changes in the polygonal fault networks and transformed such faults to radially-oriented crestal faults and likely provided pathways for fluids from the subsurface (Chand et al., 2008; Carruthers et al., 2013; Ho et al., 2013; Roberts et al., 2015).

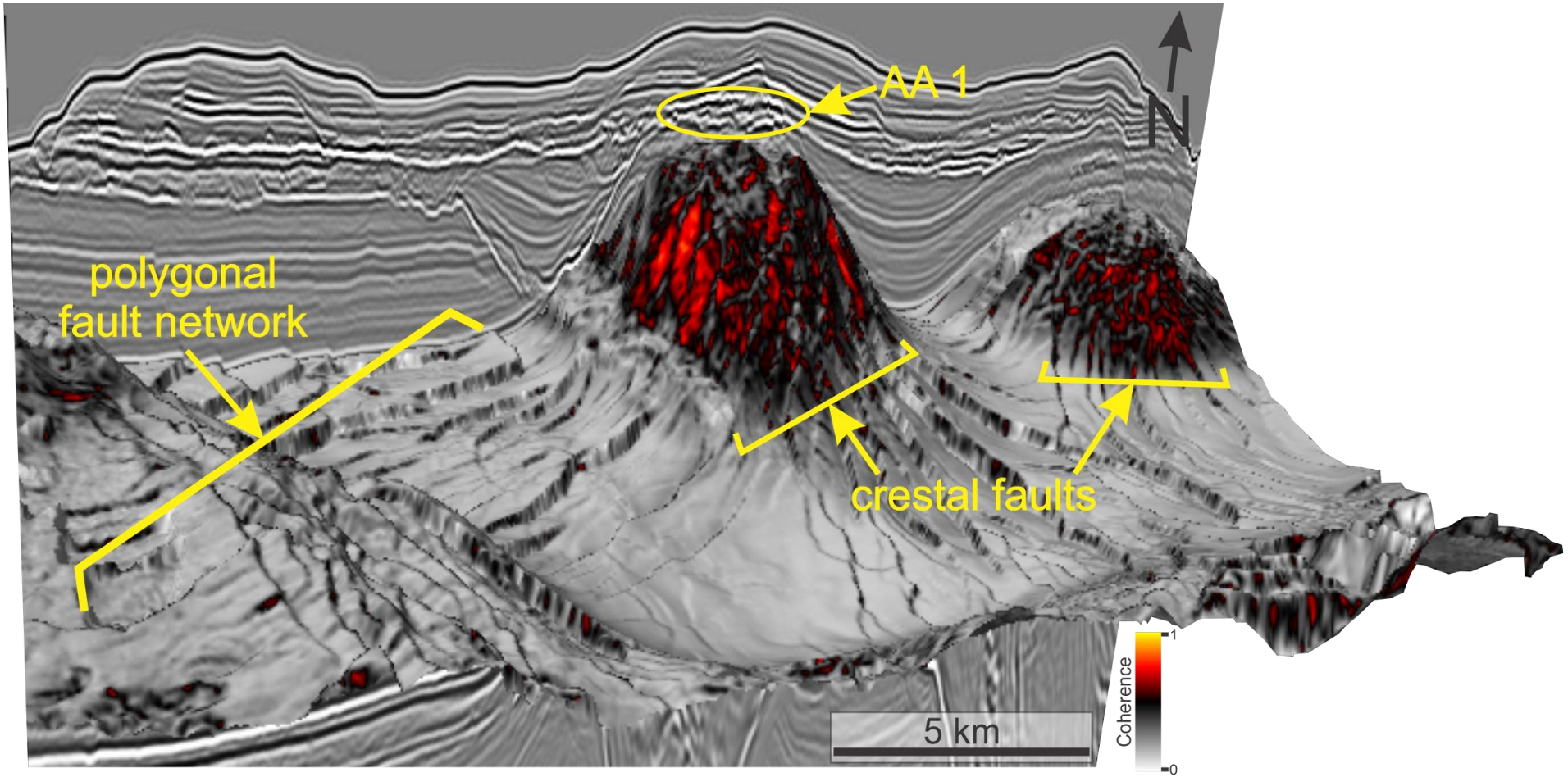

Figure 4.17. Representative strike-oriented seismic profile O-O' (from Fig. 4.2) with N2 coherence map in 3D rotated view. The coherence map shows notable polygonal fault network at the salt diapir flanks. At the crest, radial and crestal faults are present, which could be the main pathway for fluids feeding into AA 1.

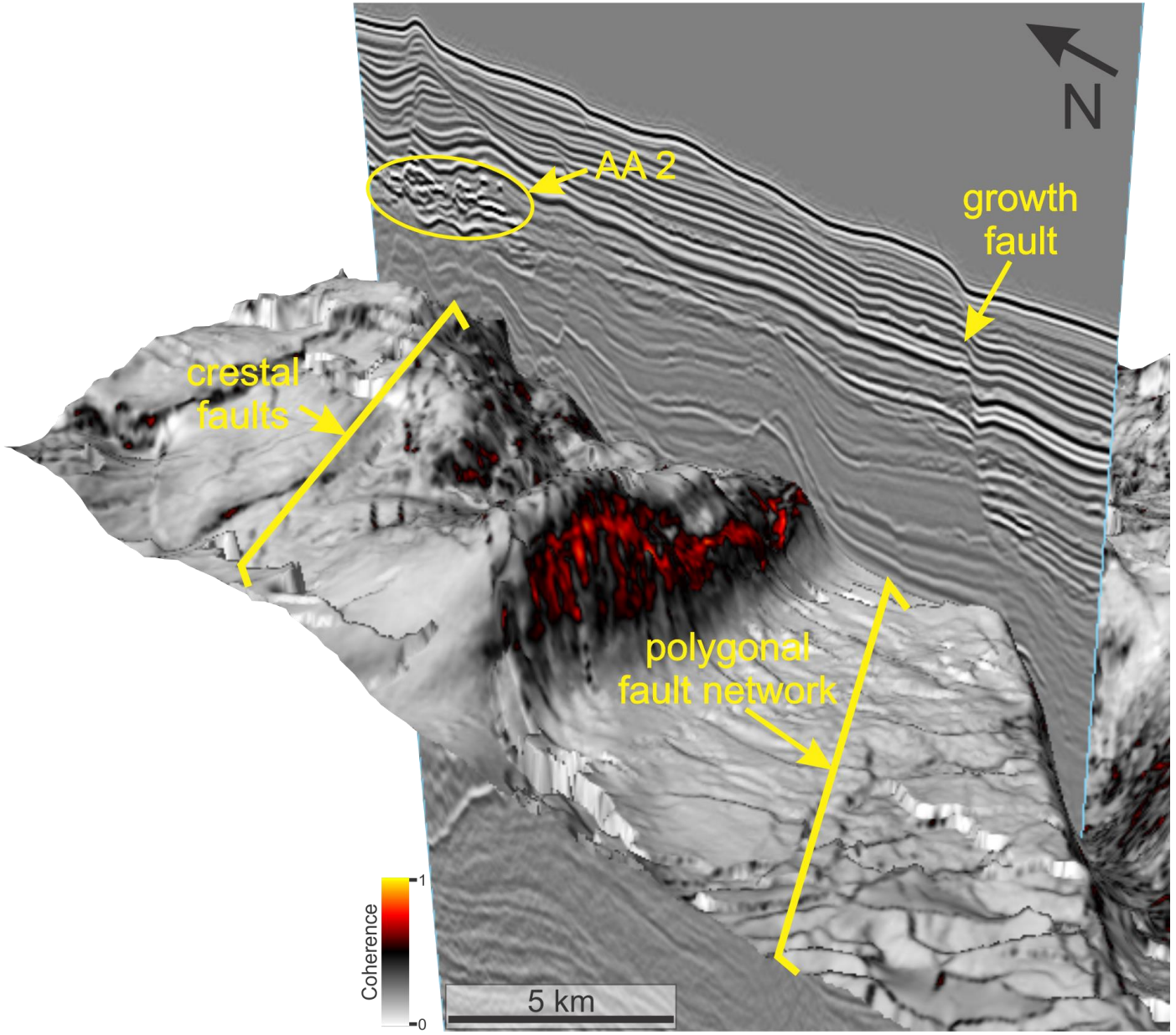

Figure 4.18. Representative dip-oriented seismic profile R-R' (from Fig. 4.10) with N2 coherence map in 3D rotated view. The coherence map depicts polygonal faults with radial and crestal faults above the salt canopy, suggesting that such faults could be the main pathway of fluid flow from the subsurface to AA 2.

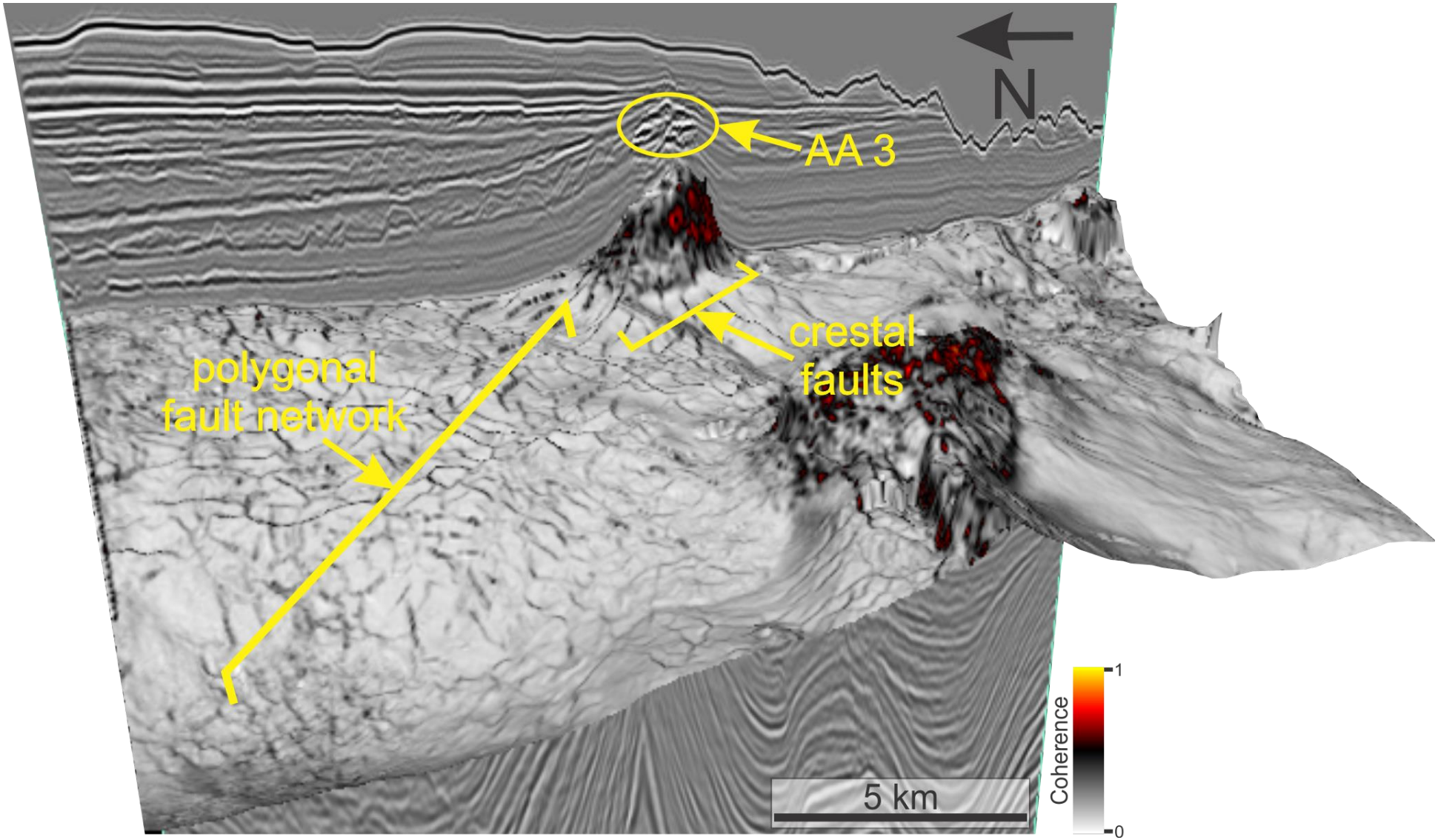

Figure 4.19. Representative dip-oriented seismic profile U-U' (from Fig. 4.5) with N2 horizon coherence map in 3D rotated view. The coherence map illustrates radially-oriented crestal faults above the diapir, indicating the likely migration pathway for fluids feeding into AA 3.

In terms of determining potential seepage sites, there is no indication of a gas chimney anomaly above AA 1 and AA 2 to near surface, however, there are faults present from the level of AA 1 and AA 2 to near surface (Fig. 4.7A; Inset D). For AA 1 (Inset D in Fig. 4.7A) and AA 2 (Fig. 4.11; Inset G in Fig. 4.16), the lack of sag effect in the reflectors such as velocity pushdowns or pull-ups suggests no indications of gas chimneys. These faults approach near the surface (<500 m) above both DHIs but could be acting as sealing faults preventing fluid flow to the surface (Aydin, 2000).

In AA 3, potential gas chimney is present to near surface as several reflectors within the fault above AA 3 (Fig. 4.7B; Inset E) shows velocity pull-ups, which is a common feature of gas chimneys. This agrees with the previous assessment of AA 3 as a seep site under the GAPP (labelled 2016011-041 in Fowler et al., 2017; labelled 2018041-007 in Fowler et al., 2019; Site 1-1 in Bennett and Desiage, 2022). AA 3 has been sampled numerous times in different sampling cruises and a bathymetric seafloor image within the proximity of AA 3 has been generated from AUV survey. This revealed existence of pockmarks in the region near AA 3 along with some possible surface fault scarp expression (Fig. 4.8). This site is also proven to be a site of thermogenic hydrocarbons (discussed in Chapter 1, section 1.9) from geochemical analyses (Fowler et al., 2017; 2017).

In terms of trap and sealing mechanisms, these DHIs are at the top of salt diapirs and canopy body (AA 1, AA 2, AA 3) that are hosted in anticlinal trap structures caused by such salt bodies and sealed by overlying proglacial muds. Stratal thinning over the crest of salt structures is quite significant during the earlier movement of the salt diapirs in the Cenozoic. However, towards the end of the Neogene (N4 to N6 horizon), the relatively continuous thickness of Neogene sediments above the diapir crests from N4 to N6 horizons implies that salt mobility was minimal

at this time (i.e., it probably did not form a bathymetric high). The decrease in salt mobility could create a trapping mechanism by having better stratigraphic continuity over the salt structures during these younger times versus earlier when the stratigraphy was regularly breached by an array of multiple active faults. Limited motion may make it more likely any faults that are present, are sealing.

These observations provoke a question as to why only two salt diapirs in the entire Tangier 3D area have DHIs at their crest and why there are no other DHI located in any of the wide region that the allochthonous canopy is covering. It is possible that while there are potential migration pathways provided by the diapirs and assuming that fluid migration occurs in these conduits, the trap and sealing mechanisms above diapirs without DHIs do not exhibit high integrity because of the presence of crestal faults, which of some are reaching the seafloor, that potentially leak fluid to the seafloor.

This is most likely happening to the diapirs with the shortest distance to the seafloor and with their crests riddled by faults. It is also possible that the salt diapirs themselves are acting as traps and seals for fluids at greater depth. In the canopy area, it is likely that the canopy itself is impeding vertical fluid migration. The canopy area also is dominated by salt-related growth faults that reach the seafloor, so it is possible that these faults are pathways for direct leakage to the seafloor leaving no hydrocarbon-related geophysical signature to form.

4.4.3. Abundance and distribution of shallow amplitude anomalies on the broader Scotian Slope

On the Scotian Slope, there are a significant number of shallow amplitude anomalies that are interpreted to be DHIs, which could very well be within the gas hydrate stability zone (LeBlanc

et al., 2007; Mosher, 2008). In this section, two seismic surveys on the slope (Fig. 3.15) are compared, mainly the Shelburne 3D (Owino, 2022) and the Tangier 3D (this thesis), based on the abundance and distribution of investigated shallow amplitude anomalies in each survey. In the Tangier area, only three shallow DHIs are observed (Fig. 4.1), of which two are situated above diapirs and one above an allochthonous salt canopy. In the adjacent Shelburne area, Owino (2022) found thirty-six shallow DHIs situated above salt diapirs. All the DHIs observed in both surveys are shallow (within 100 to 300 m below seafloor), located in the uppermost Neogene, and mostly above salt diapirs, especially throughout the Shelburne area. This prompts the question of what the controlling factors are that makes the Shelburne 3D area richer in the abundance of shallow amplitude anomalies compared to the DHI-sparse Tangier 3D area (Fig. 4.20). In this section, multiple plausible scenarios are provided, which will attempt to answer the question, though not with a definite conclusion.

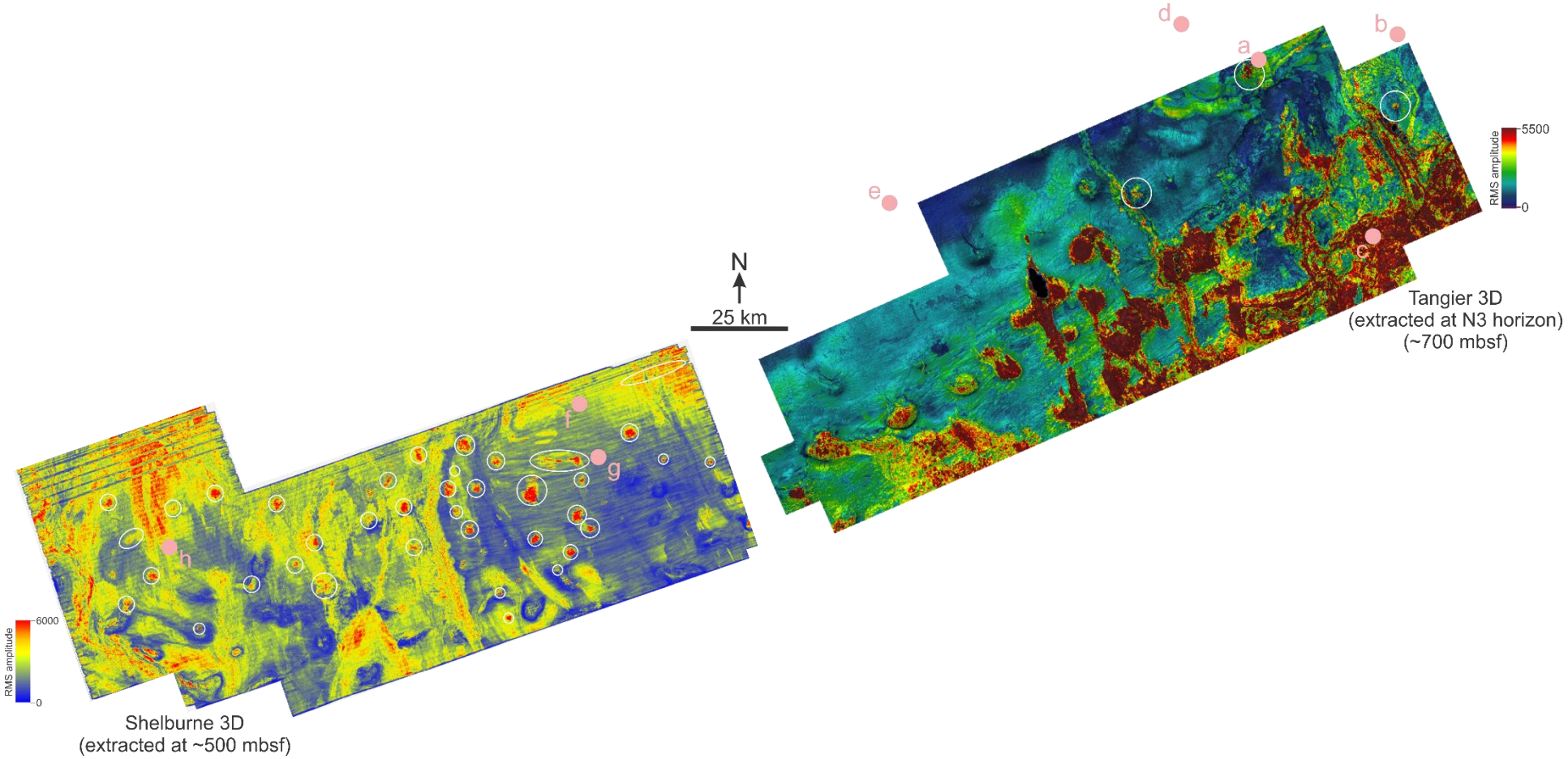

Figure 4.20. Locations of interpreted amplitude anomalies that are possibly fluid related across the Shelburne (Owino, 2022) and Tangier 3D (this thesis) areas highlighted in white circles in the extracted RMS amplitude maps (note: colour scales and amplitude ranges differ for the two surveys). The interpreted DHIs in the Shelburne 3D area are significantly more abundant (36) than the DHIs in the Tangier 3D area (3). Slope exploration wells: (a) Weymouth A-45; (b) Balvenie B-79; (c) Aspy D-11/D-11A; (d) Newburn H-23; (e) Shubenacadie H-100; (f) Torbrook C-15; (g) Cheshire L-97/L-97A; (h) Monterey Jack E-43/E-43A.

Scenario 1: Mesozoic reservoir potential

The sedimentation history between the Shelburne 3D and Tangier 3D areas at the start of the Mesozoic is drastically different. On the central Scotian Margin, the beginning of salt tectonics in the Sable Subbasin started at the end of the deposition of salt in the Jurassic. As the delta systems prograded seaward through the Late Jurassic and Early Cretaceous, these delta systems eventually reached the modern-day shelf edge and triggered the salt expulsion of the Slope Canopy Complex as part of the Sable Canopy (Albertz et al., 2010; Kendell, 2012). On the southwestern Scotian Margin, the sediment loading differed in the Shelburne Subbasin since the Sable Delta was not present at the same time it was depositing significant amount of sediments in the Sable Subbasin. The sedimentation style was mostly carbonate deposition in this part of the margin through the Jurassic and Early Cretaceous. Overall, the sediment load was relatively much less. Differential sediment loading that occurred in both subbasins resulted to the difference in salt structural styles across the Scotian Margin. The Sable Subbasin is within SPs II and III, whereas the Shelburne Subbasin is classified within SP II (see Chapter 1, section 1.6.1).

In the Tangier 3D area, the sediment thicknesses from J145 (Berriasian) to K125 (Barremian), from K125 (Barremian) to K112 (Aptian), from K112 (Aptian) to K101 (Albian), and from K101 (L. Albian) to K94 (Cenomanian) range from approximately 400 m to 9500 m. In the Shelburne 3D area, the total sediment thicknesses in the Early Cretaceous strata from the same seismic horizons listed above are ranging from estimated 400 m with some areas reaching up to 2500 m in thickness (estimated total sediment thicknesses from isopach maps in Deptuck and Kendell, 2020). While the Tangier 3D area received significant amount of sediment from the prograding Sable Delta, despite its distal location on the present-day slope, the Shelburne 3D area was comparatively sediment-starved at the time. This could possibly explain why the Tangier 3D area

has less fluid-related shallow amplitude anomalies, especially on its western part, because the entire region has higher Mesozoic reservoir potential than in the Shelburne 3D area (OERA, 2011), where fluids could reside and be trapped at depth, instead of residing at much shallower, unconsolidated strata (e.g., Cenozoic). This could also suggest that salt diapirs on the western part of the Tangier 3D area possibly act as a trap for the fluids, resulting in no appearance of shallow DHIs above these diapirs.

Scenario 2: Allochthonous salt canopy complex acts as barrier to vertical hydrocarbon migration

The progradation of the Sable Delta in the Jurassic and Early Cretaceous lead to the development of the allochthonous canopy complex on the Scotian Slope (Ge et al., 1997; Ings and Shimeld, 2006; Albertz et al., 2010; Kendell, 2012), which is theorized to act as a barrier to vertical hydrocarbon migration. The low permeability of the salt prevents vertical hydrocarbon migration in sedimentary basins with large-scale allochthonous salt canopy, and causes the migration pathways to be laterally deflected, following the dip of the salt (Pepper and Yu, 1995; McBride et al., 1999).

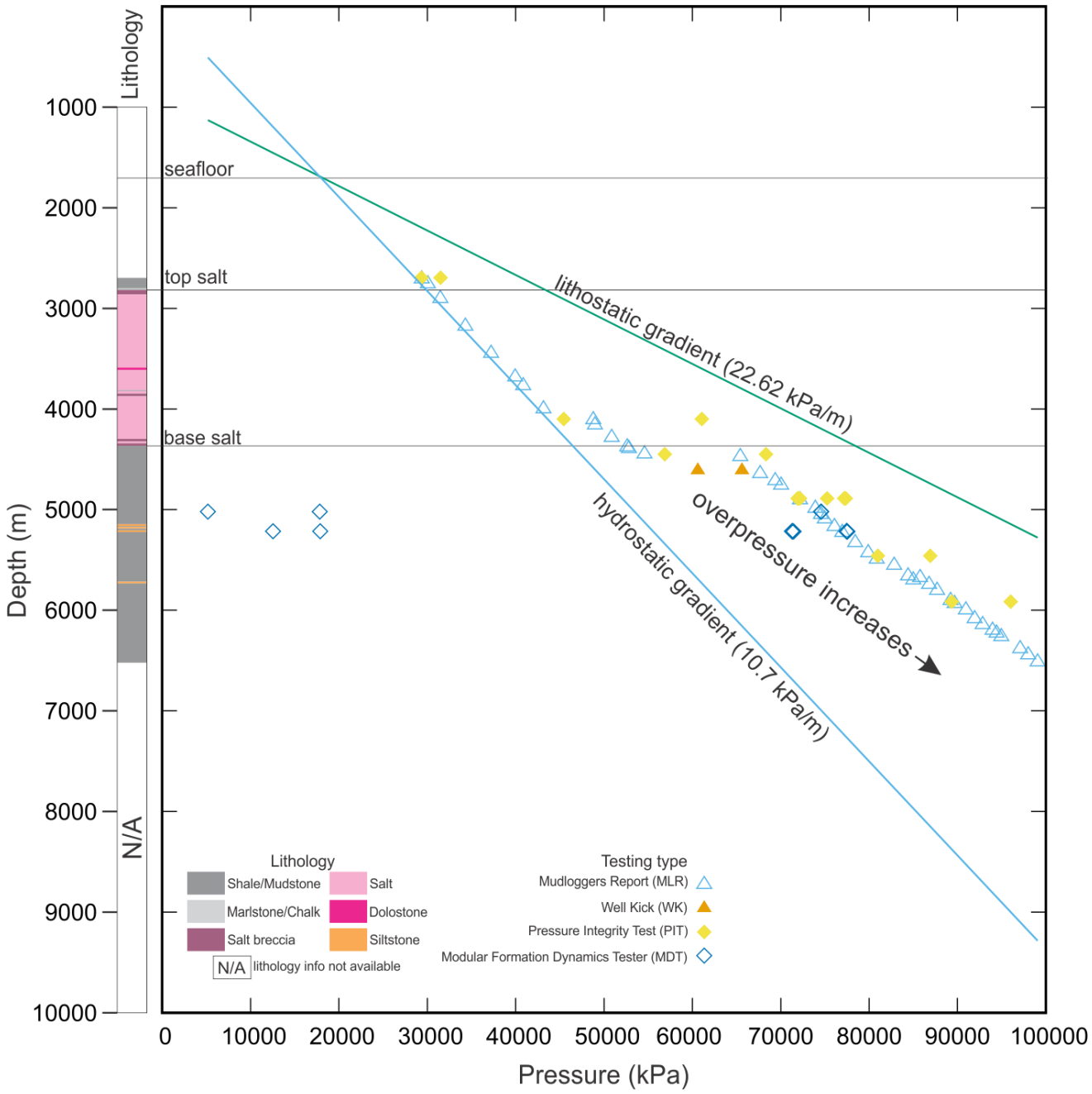

Figure 4.21. Cross-plot of depth (m) vs pressure (kPa) from Weymouth A-45 well with corresponding lithology. The plot shows lithostatic and hydrostatic gradients with overpressure trend increasing underneath the allochthonous salt canopy in this area. Cross-plot is generated from the BASIN Database. Data courtesy of Ovintiv (formerly EnCana) (2004) via the BASIN Database.

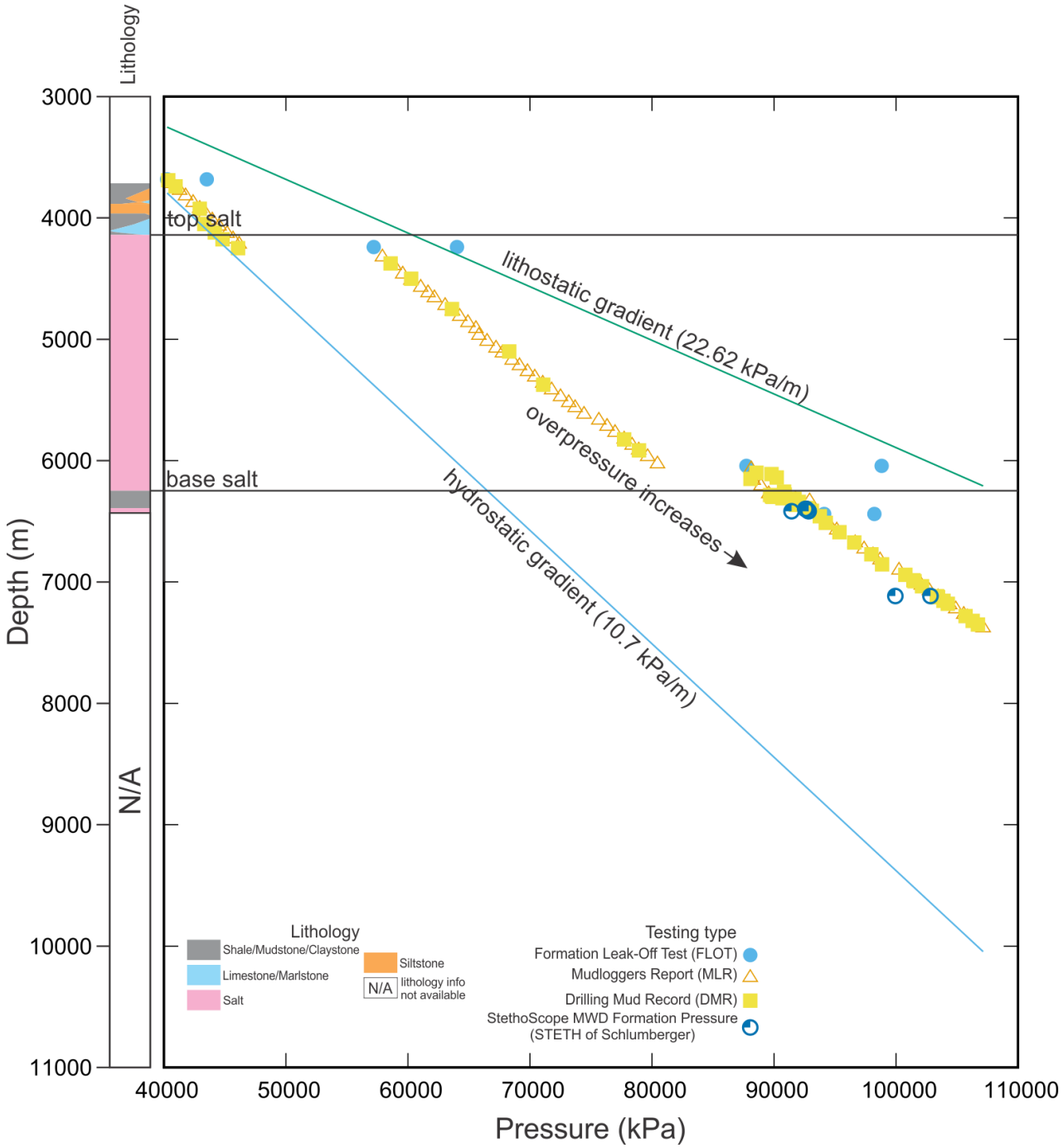

Figure 4.22. Cross-plot of depth (m) vs pressure (kPa) from Aspy D-11/D-11A well with corresponding lithology. The plot shows lithostatic and hydrostatic gradients with overpressure trend increasing underneath the allochthonous salt canopy in this area. Cross-plot is generated from the BASIN Database. Data courtesy of BP Canada Exploration Ltd (2018) via NSDNRR and the BASIN Database.

In the Tangier 3D area, its eastern part is dominated by the allochthonous salt canopy, whereas, on the Shelburne 3D area, there is little presence of salt canopy bodies in the entire area (e.g., salt tongues developed in the Middle Jurassic in some areas). This could suggest that if hydrocarbons have been generated at depth in the Tangier 3D area, there is substantial vertical fluid migration only where not blocked by the large-scale allochthonous salt canopy. This will result in deflection of vertical fluid migration (Figs. 4.15-4.16) and relatively less abundance of shallow amplitude anomalies that could be interpreted as thermogenic-related fluids compared to Shelburne 3D area. In contrast, the Shelburne 3D area is dominated by vertical salt diapirs, that provide potential direct conduits from the source or reservoir rocks at depth.

In addition, contrary to Scenario 1, even though the northeastern region is more reservoir prone, it was easier for hydrocarbons to escape during earlier times, leaving scarce amounts of hydrocarbons in the Cenozoic to form shallow DHIs now. However, based on the wells within the Tangier 3D area, there is still evidence of overpressure present beneath the allochthonous salt canopy at places where Weymouth A-45 and Aspy D-11/D-11A wells penetrate (Figs. 4.21-4.22; see locations in Figs. 2.1; 3.20; 4.1). These two wells found that there is very little reservoir penetrated in the slope area, which are composed of mostly shale/mudstone, except for Newburn H-23, which starts to have decent intervals of sandstone units in the Early Cretaceous even though mudstone is still the dominant lithology. In addition, there were evidence of gas-charged siltstones beneath the salt at Aspy D-11/D-11A, in Newburn H-23, in Balvenie B-79, in Tantallon M-41, and Annapolis B-24/G-24, although some of these wells are outside the study area on the slope.

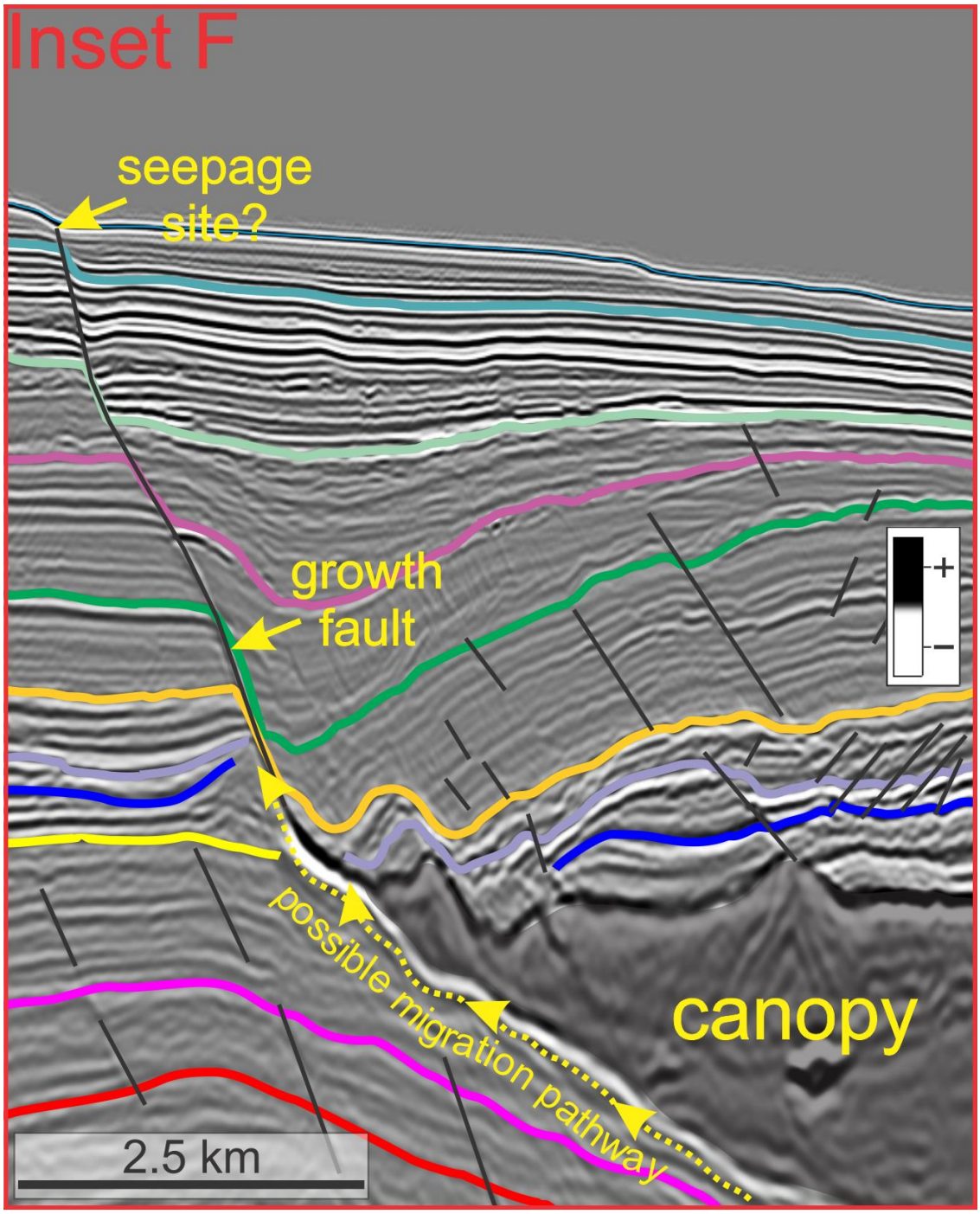

Figure 4.23 (Inset F in Fig. 4.10). Possible migration pathway due to the deflection of vertical fluid migration caused by allochthonous salt canopy on the Scotian Slope and possibly migrating through the existing growth fault and leaking directly to the seafloor.

Scenario 3: Growth faults potentially provide pathways directly to the seafloor

The presence of faults in a sedimentary basin can modify subsurface fluid migration, either faults can be pathways for fluid migration or act as traps. Direct and indirect evidence of large-scale fluid flow along high-angle growth faults suggest that such faults play a major role in hydrocarbon migration rooted from deeper petroleum kitchens to shallow reservoirs (Weber, 1987; Losh, 1998; Losh et al., 1999; Zhang et al., 2006).

In the Tangier 3D area, the eastern part is dominated by growth faults (e.g., N4 coherence map in Fig. 3.19) related to the stratal deformation initiated by the movement of allochthonous salt canopy. Inset F (Fig. 4.23) illustrates a possible migration pathway from the deflection of vertical fluid migration by the salt canopy on this part of the slope (by analogy to Pepper and Yu, 1995; McBride et al., 1999) which also developed a large-scale growth fault at the edge of the canopy. This could result to a possible pathway for fluids to directly leak to the seafloor from deeper reservoirs. If fluids are directly leaking to the seafloor, this would result in less shallow amplitude anomalies in the Tangier 3D area. On the contrary, the Shelburne 3D area lacks allochthonous salt canopy bodies that would provide the same conditions as in the eastern Tangier 3D area.

Scenario 4: Source rock maturity

It is possible that because of greater sediment loading and subsidence related to the Sable Delta deposition most of the deeper source rocks in the Tangier 3D area are overmature and have mostly already generated in the past except for selected areas, whereas in the Shelburne 3D area, the source rocks are possibly still actively generating hydrocarbons (e.g., Early to Late Jurassic). This is supported in Fig. 4.24, where the Tithonian source rock maturity shows a trend of

increasing maturity from the southwest to the northeast of the Scotian Margin. This trend has also been observed in the transformation ratio maps of Pliensbachian, Callovian, Valanginian, and Aptian source rock intervals (see Chapter 7 of OETR, 2011). Alternatively, it is possible that some shallower source rocks than would be expected might be mature in some of the areas where there has been a great deal of subsidence due to subsidence adjacent to or from salt withdrawal over the canopies. It is possible that very localized thermogenic generation is occurring from the Late Cretaceous to Paleogene.

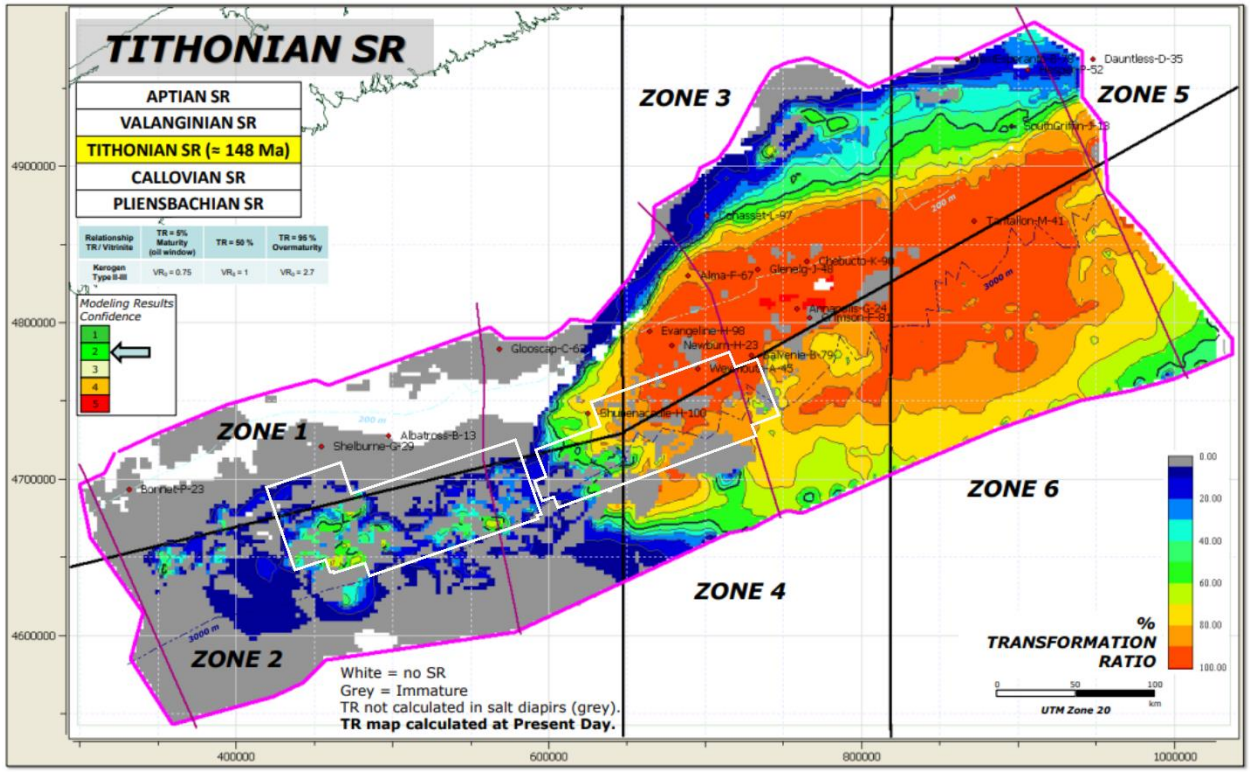

Figure 4.24. A map showing source rock maturity at the Upper Jurassic Tithonian source rock based on the calculated transformation ratio (TR) from the 2011 Play Fairway Analysis (derived from OERA, 2011) with the survey boundaries in white of the Shelburne 3D and Tangier 3D areas. The maturity trend of the Tithonian source rock increases to the northeast Scotian Margin.

Scenario 5: Most shallow DHIs are biogenic

It is proven from geochemical analyses (e.g., Fowler et al., 2017; 2017; 2019) that most DHIs in the Shelburne 3D area are hosting biogenic hydrocarbons (Fig. 4.25). It is possible that the conditions necessary for effective biogenic hydrocarbon production are not suitable in most regions of the Tangier 3D area for some reason such as the structural complexity of the allochthonous salt canopy might have disrupted focused, convective fluid flow that would supply nutrients to the relevant microbes for biogenic HC production versus a less structurally complex environment provided by vertical salt diapirs. It is also possible that there are differences in sediment thicknesses and permeability in the Cenozoic in the Shelburne and Tangier 3D areas.

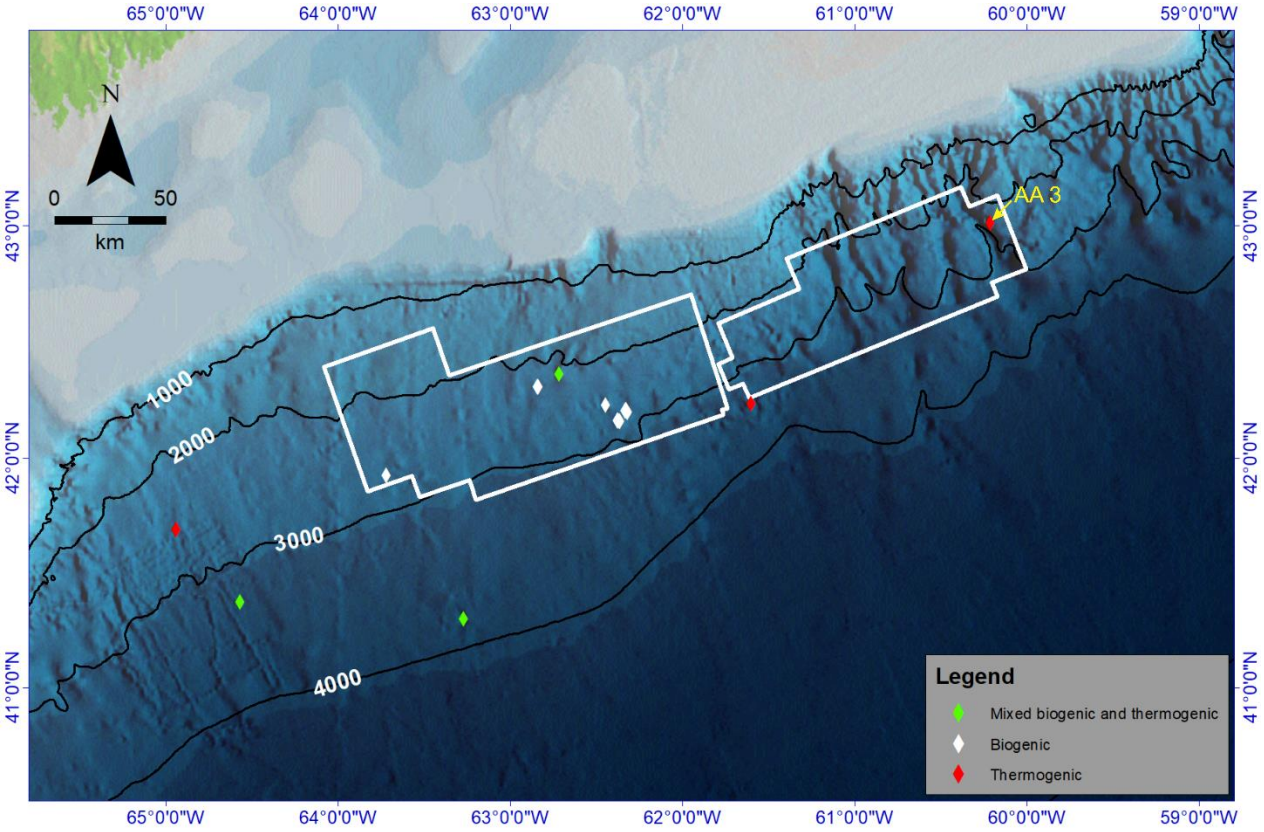

Figure 4.25. Locations of sampled seep sites with assigned geochemical signatures from geochemical analyses (derived from Fowler et al., 2017; 2017; 2019).

Scenario 6: Cenozoic reservoir and trapping mechanisms

It is also possible that there are hydrocarbons being supplied from deeper sources in both areas, but most of the potential structures in the Tangier 3D area do not have suitable permeable reservoirs to contain significant hydrocarbons (e.g., too clay-rich) or, alternatively, the sediments are too permeable to form seals (e.g., too sand-rich), in both cases for depositional reasons. The latter is not very likely given the generally clay-rich composition of most of the Cenozoic, however, these possibilities need more information because of the very limited information on lithology from exploration wells at these intermediate-shallow depths. In general, there is ample information from the top few tens of metres from scientific piston core programs, and some from deeper in the Cenozoic (km+ and below) from exploration wells, but most wells do not sample the intervening stratigraphy from ~100 m depth to a km or more.

Shallow, recently active faults may form pathways for the escape of hydrocarbon fluids to the seafloor, preventing formation of significant DHIs because of efficient leakage of potential shallow traps (i.e., trap failure). The presence of faults that reach seafloor in the canopy area (e.g., Fig. 4.23) may explain the rarity of DHIs in this region of the Tangier 3D area, and the distribution of mobile salt structures affecting the stratigraphy well into the latest Neogene in some of the Tangier 3D area (e.g., Fig. 3.31) may exclude those diapirs from being suitable for effective trap and DHI formation even if hydrocarbons are being supplied, regardless of thermogenic or biogenic sources.

4.5. Conclusion

There are three well resolved amplitude anomalies, interpreted as DHIs in the Tangier 3D area. The amplitude anomalies (AA 1 to AA 3) are generally described as bright spots with minor dim

spots. Exceptionally, AA 2 depicts some hints of flat spots, which are fluid-contact anomalies. These DHIs are situated above two diapirs (AA 1 and AA 3) and an allochthonous salt canopy (AA 2). AA 1 and AA 3 are found within the range of 100 m to 300 m below seafloor. AA 2 is observed within the ranged of 300 m to 500 m below seafloor. These observed amplitude anomalies could very well be within the gas hydrate stability zone (LeBlanc et al., 2007; Mosher, 2008).

The interpretation of salt bodies in the Tangier 3D area suggests that salt mobility on this part of the central Scotian Slope played a key role in stratal deformation history of shallow sediments, especially creating potential migration pathways for fluids from the deep subsurface to the shallow, unconsolidated sediments of the Cenozoic. The geometric interpretation of the horizons near the amplitude anomalies suggests stratal thinning was quite influential during the movement of the allochthonous salt bodies in the Paleogene (P1) and Neogene (N1-N4). Towards the end of the Neogene, the salt movement appears to have slowed down, as evidenced by minimal disruption of upper Neogene horizon thickness (e.g., N4 to N6) and fewer faults that penetrate to shallower depths or to seafloor. These less disrupted upper Neogene horizons may act as sealing sediments for possible fluid migration to near surface. In terms of a seepage site, only one amplitude anomaly (AA 3) is interpreted to have a gas chimney from the anomaly to near surface, suggesting possible fluid escape mechanisms here. A detailed seafloor map from the vicinity of AA 3 also depicts several fluid escape morphologies, such as pockmarks with occasional fault scarps surrounding the area. AA 3 is the only site with thermogenic fluid proven by geochemical analyses of shallow sediment gas hydrates.

Deep seismic horizons suggest that the lithostratigraphy below the DHIs include Upper Jurassic to Cretaceous, units that are predicted to be source rocks (e.g., J144 and J150 horizons of OERA,

2011) and potential reservoir rocks (e.g., K130), which previous studies were primary industry target intervals on the Scotian Margin.

Primary migration pathways observed below all shallow amplitude anomalies are likely affected by salt mobility along with the main driver of fluid migration, which is probably geologic overpressure at depth. For AA 1 to AA 3, the main thermogenic hydrocarbon migration pathway is speculated to be via salt welds of the diapirs and canopy on the slope. The paths these salt bodies took potentially provided direct conduits from predicted Upper Jurassic source or predicted Lower Cretaceous reservoir rocks to the shallow, unconsolidated Cenozoic sediments.

The Tangier 3D and the Shelburne 3D Seismic Surveys are compared on DHI distribution and occurrence. The Tangier 3D has significantly fewer shallow DHIs than in Shelburne 3D (Owino, 2022). Six hypothetical scenarios are provided to explain the controls on shallow DHI occurrences. These are Mesozoic reservoir potential, an allochthonous salt canopy as a barrier to vertical hydrocarbon migration, salt-related growth faults providing potential migration pathways to the seafloor, source rock maturity, biogenic gas production, and Cenozoic reservoir and trapping mechanisms. These scenarios are based on previous studies on seismic interpretation for this thesis, source rock distributions on the Scotian Margin from OERA (2011), and results from geochemical analyses of sampled seep sites as part of GAPP. Several hypotheses are not mutually exclusive. Further study is needed to resolve their mechanisms of formation and fluid dynamics through time.

4.6. Works cited

Albertz, M., Beaumont, C., Shimeld, J. W., Ings, S. J., and Gradmann, S. (2010). An investigation of salt tectonic structural styles in the Scotian Basin, offshore Atlantic Canada: 1. Comparison of observations with geometrically simple numerical models. *Tectonics, 29*, 1–29.

Bethke, C. M. (1985). A numerical model of compaction-driven groundwater flow and heat transfer and its application to paleohydrology of intracratonic sedimentary basins. *Journal of Geophysical Research, 90*, 6817–6828.

Bennett, R. and Desiage, P.-A. (2022). Expedition report 21CONDOR: Scotian Slope, August 14–29, 2021. Geological Survey of Canada, Open File 8889, 53 p. https://doi.org/10.4095/329977.

Bondurant, C. (2016). Tangier 3D Interpretation Report, Offshore Nova Scotia. BP Canada Exploration Ltd.

Brown, A. R. (1999). Reservoir Identification. In A. R. Brown (Eds.), Interpretation of Three-Dimensional Seismic Data (Ch. 5, pp. 147–187). AAPG Memoir, 42; SEG Investigations in Geophysics, 9.

Brown, A. R. (2010). Dim Spots in Seismic Images as Hydrocarbon Indicators. *Search and Discovery, 40514*, 1–3.

Brown, A. R. (2012). Dim spots: Opportunity for future hydrocarbon discoveries? *The Leading Edge, 31 (6)*, 682–683.

Canada-Nova Scotia Offshore Petroleum Board. (2000). *Technical Summaries of Scotian Shelf* (Significant and Commercial Discoveries status offshore Nova Scotia Resource Assessment Report), 1–212.

Carruthers, D., Cartwright, J., Jackson, M. P. A., and Schutjens, P. (2013). Origin and timing of layer-bound radial faulting around North Sea salt stocks: New insights into the evolving stress state around rising diapirs. *Marine and Petroleum Geology, 48*, 130–148.

Cartwright, J. A., and Lonergan, L. (1996). Volumetric contraction during the compaction of mudrocks: a mechanism for the development of regional-scale polygonal fault systems. *Basin Research, 8*, 183–193.

Chand, S., Mienert, J., Andreassen, K., Knies, J., Plassen, L., and Fotland, B. (2008). Gas hydrate stability zone modelling in areas of salt tectonics and pockmarks of the Barents Sea suggests an active hydrocarbon venting system. *Marine and Petroleum Geology, 25*, 625–636.

Chapman, R. E. (1980). Migration of Fluids in Sedimentary Basins: Discussion[1]. *The American Association of Petroleum Geologists Bulletin, 64 (9)*, 1538–1547.

Chi, G., and Xue, C. (2011). An overview of hydrodynamic studies of mineralization. *Geoscience Frontiers, 2 (3)*, 423–438.

Cichopstępski, K., Kwietniak, A., and Dec, J. (2019). Verification of bright spots in the presence of thin beds by AVO and spectral analysis in Miocene sediments of Carpathian Foredeep. *Acta Geophysica*, 1–15.

Coleman, A. J., Jackson, C. A.-L., Duffy, O. B., and Nikolinakou, M. A. (2018). How, where, and when do radial faults grow near salt diapirs? *Geology, 46 (7)*, 655–658.

Davison, I. (2009). Faulting and fluid flow through salt. *Journal of the Geological Society, London, 166*, 205–216.

Davison, I., Alsop, G. I., Evans, N. G., and Safaricz, M. (2000a). Overburden deformation pattens and mechanisms of salt diapir penetration in the Central Graben, North Sea. *Marine and Petroleum Geology, 17 (5)*, 601–618.

Davison, I., Alsop, I., Birch, P., Elders, C., Evans, N., Nicholson, H., Rorison, P., Wade, D., Woodward, J., and Young, M. (2000b). Geometry and late-stage structural evolution of Central Graben salt diapirs, North Sea. *Marine and Petroleum Geology, 17 (4)*, 499–522.

de Mahiques, M. M., Schattner, U., Lazar, M., Sumida, P. Y. G., and de Souza, L. A. P. (2017). An extensive pockmark field on the upper Atlantic margin of Southeast Brazil: spatial analysis and its relationship with salt diapirism. *Heliyon, e00257*, 1–21.

Deptuck, M. E. and Kendell, K. L. (2020). *Atlas of 3D seismic surfaces and thickness maps, central and southwestern Scotian Slope*. Canada-Nova Scotia Offshore Petroleum Board, Geoscience Open File Report 2020-002MF – 2020-006MF, 1–51.

Dixit, A. and Mandal, A. (2020). Detection of gas chimney and its linkage with deep-seated reservoir in poseidon, NW shelf, Australia from 3D seismic data using multi-attribute analysis and artificial neural network approach. *Journal of Natural Gas Science and Engineering, 83 (10356)*, 1–18.

Fowler, M., Webb, J., Obermajer, M., Monnier, F., Mort, A., Luheshi, M., and MacDonald, A. (2016). Petroleum Systems of the Scotian Basin. *AAPG Annual Convention and Exhibition, Oral Presentation*. Calgary, Alberta: Canada.

Fowler, M., Webb, J., Olsen, H., Ashraf, F., and Guldbrandsen, S. (2017). Geochemistry Data Report for 2016 Scotian Slope Piston Coring Program. *Applied Petroleum Technology*, 1–310. APT Canada Ltd.

Fowler, M. (2017). Piston Core Geochemistry – Final Report. *Applied Petroleum Technology*, 1–4. APT Canada Ltd.

Fowler, M., Webb, J., Gulbrandsen, S., Austnes, L-K, and Ashraf, F. (2019). Geochemistry Data Report for 2018 Scotian Slope Coring Program. *Applied Petroleum Technology*, 1–306. APT Canada Ltd.

Gay, A., Lopez, M., Berndt, C., and Séranne, M. (2007). Geological controls on focused fluid flow associated with seafloor seeps in the Lower Congo Basin. *Marine Geology, 244*, 68–92.

Ge, H., Jackson, M. P. A., and Vendeville, B. C. (1997). Kinematics and Dynamics of Salt Tectonics Driven by Progradation. *AAPG Bulletin, 81 (3)*, 398–423.

Geletti, R., Ben, A. D., Busetti, M., Ramella, R., and Volpi, V. (2008). Gas seeps linked to salt structures in the Central Adriatic Sea. *Basin Research, 20*, 473–487.

Guo, Q., Islam, N., and Pennington, W. D. (2015). Tuning of flat spots with overlying bright spots, dim spots, and polarity reversals. *Interpretation, 3 (3)*, SS37–SS48.

Hanafy, S., Farhood, K., Mahmoud, S. E., Nimmagadda, S., and Mabrouk, W. M. (2018). Geological and geophysical analyses of the different reasons for DHI failure case in the

Nile Delta Pliocene section. *Journal of Petroleum Exploration and Production Technology, 8*, 969–981.

Heggland, R. (1997). Detection of gas migration from a deep source by the use of exploration 3D seismic data. *Marine Geology, 137*, 41–47.

Heggland, R. (2004). Hydrocarbon Migration and Accumulation Above Salt Domes – Risking of Prospects by the Use of Gas Chimneys. In P. J. Post, D. L. Olson, K. T. Lyons, S. L. Palmes, P. F. Harrison, and N. C. Rosen (Eds.), Salt Sediment Interactions and Hydrocarbon Prospectivity Concepts, Applications and Case Studies for the 21st Century (pp. 404–420), Society for Sedimentary Geology.

Heggland, R., Meldahl, P., de Groot, P. & Aminzadeh, F. (2000). Chimney cube unravels subsurface. The American Oil and Gas Reporter, February 2000.

Ho, S., Carruthers, D., Imbert, P., and Cartwright, J. (2013). Spatial variations in geometries of polygonal faults due to stress pertubations and interplay with fluid venting features. 7th EAGE Conference and Exhibition. London, UK.

Hudec, M. R., and Jackson, M. P.A. (2009). Interaction between spreading salt canopies and their peripheral thrust systems. *Journal of Structural Geology, 31,* 1114–1129.

Infante-Paez, L., and Marfurt, K. J. (2018). In-context interpretation: Avoiding pitfalls in misidentification of igneous bodies in seismic data. *Interpretation, 6 (4),* SL29–SL42.

Ings, S. J., and Shimeld, J. W. (2006). A new conceptual model for the structural evolution of a regional salt detachment on the northeast Scotian margin, offshore eastern Canada. *The American Association of Petroleum Geologists Bulletin, 90 (9)*, 1407–1423.

Jatiault, R., Loncke, L., Dhont, D., Imbert, P., and Dubucq, D. (2019). Geophysical characterisation of active thermogenic oil seeps in the salt province of the lower Congo basin part I: Detailed study of one oil-seeping site. *Marine and Petroleum Geology, 103*, 753–772.

Kendell, K. L. (2012). Variations in salt expulsion style within the Sable Canopy Complex, central Scotian margin. *Canadian Journal of Earth Sciences, 49*, 1504–1522.

Kidston, A. G., Brown, D. E., Altheim, B., and Smith, B. M. (2002). Hydrocarbon potential of the deep-water Scotian slope. *Canada-Nova Scotia Offshore Petroleum Board Open Report*, 1–111.

Kidston, A. G., Smith, B. M., Brown, D. E., Makrides, C., and Altheim, B. (2007). Nova Scotia deepwater post-drill analysis 1982-2004. *Canada-Nova Scotia Offshore Petroleum Board Open Report*, 1–182.

Kumar, P. C., Omosanya, K. O., and Sain, K. (2019). Sill Cube: An automated approach for the interpretation of magmatic sill complexes on seismic reflection data. *Marine and Petroleum Geology, 100*, 60–84.

LeBlanc, C., Louden, K., and Mosher, D. (2007). Gas hydrates off Eastern Canada: Velocity models from wide-angle seismic profiles on the Scotian Slope. *Marine and Petroleum Geology, 24 (5)*, 321–335.

Li, J., Mitra, S., and Qi, J. (2020). Seismic analysis of polygonal fault systems in the Great South Basin, New Zealand. *Marine and Petroleum Geology, 111*, 638–649.

Losh, S. (1998). Oil Migration in a Major Growth Fault: Structural Analysis of the Pathfinder Core, South Eugene Island Block 330, Offshore Louisiana. *AAPG Bulleting, 82 (9)*, 1694–1710.

Losh, S., Eglinton, L., Schoell, M., and Wood, J. (1999). Vertical and Lateral Fluid Flow Related to a Large Growth Fault, South Eugene Island Block 330 Field, Offshore Louisiana. *AAPG Bulletin, 83 (2)*, 244–276.

Ma, G., Zhan, L., Lu, H., and Hou, G. (2021). Structures in Shallow Marine Sediments Associated with Gas and Fluid Migration. *Journal of Marine Science and Engineering, 9 (396)*, 1–26.

Malloy, S., Petersen, K., Lerche, I., and Lowrie, A. (1996). Uncertainty Analysis of Subsalt Overpressure Development in Offshore Louisiana, Gulf of Mexico. *Mathematical Geology, 28 (6)*, 687–699.

Mattos, N. H., Alves, T. M., and Omosanya, K. O. (2016). Crestal fault geometries reveal late halokinesis and collapse of the Samson Dome, Northern Norway: Implications for petroleum systems in the Barents Sea. *Tectonophysics, 690*, 79–96.

McBride, B. C., Weimer, P., and Rowan, M. G. (1999). The Effect of Allochthonous Salt on the Petroleum Systems of Northern Green Canyon and Ewing Bank (Offshore Louisiana), Northern Gulf of Mexico. AAPG Bulletin Search and Discovery Article #10003. Retrieved from https://www.searchanddiscovery.com/documents/98004/.

Meldahl, P., Heggland, R., Bril. B., and de Groot, P. (2001). Identifying faults and gas chimneys using multi-attributes and neural networks. *The Leading Edge, 20 (5)*, 474–482.

Mosher, D. C. (2008). Bottom Simulating Reflectors on Canada's East Coast Margin: Evidence for Gas Hydrate. *Proceedings of the 6th International Conference on Gas Hydrates*. Vancouver, BC, Canada.

Mukhopadhyay, P. K. (2006). *Evaluation of the petroleum systems by 1D and 2D numerical modeling and geochemical analysis in the area of most recent exploration wells on the deepwater Scotian Slope, offshore Nova Scotia*. (NSDoEM Final Report 60127404, 485 p.). Halifax, NS: Nova Scotia Department of Energy and Mines.

Nanda, N. C. (2016). Direct Hydrocarbon Indicators (DHI). In N. C. Nanda, Seismic Data Interpretation and Evaluation for Hydrocarbon Exploration and Production (Ch. 6, pp. 103–113). Springer, Cham. Retrieved from https://doi.org/10.1007/978-3-319-26491-2_6.

Neglia, S. (1979). Migration of Fluids in Sedimentary Basins. *The American Association of Petroleum Geologists Bulletin, 63(4)*, 573–597.

Nelskamp, S., Verweigj, J. M., and Witmans, N. (2012). The role of salt tectonics and overburden in the generation of overpressure in the Dutch North Sea area. *Netherlands Journal of Geoscience, 91(4)*, 517–534.

Nikolinakou, M. A., Flemings, P. B., and Hudec, M. R. (2014). Modeling stress evolution around a rising salt diapir. *Marine and Petroleum Geology, 51*, 230–238.

Offshore Energy Research Association. (2011). *Play Fairway Analysis Atlas*. Retrieved from https://oera.ca/research/play-fairway-analysis-atlas.

O'Brien, J. J., and Lerche, I. (1994). Understanding subsalt overpressure may reduce drilling risks. *Oil and Gas Journal, 92 (4)*, 28–34.

Owino, Y. (2022). *GIS Mapping of the Scotian Margin with Special Focus on the Direct Hydrocarbon Indicators within the Shelburne Subbasin, Scotian Slope, Nova Scotia* (MSc thesis). Saint Mary's University, Halifax, NS.

Pepper, A. S., and Yu, Z. (1995). Influence of an inclined salt sheet on petroleum emplacement in the Pompano Field Area, Offshore Gulf of Mexico Basin. GCSSEPM Foundation 16th Annual Research Conference.

Quintà, A., Tavani, S., and Roca, E. (2012). Fracture pattern analysis as a tool for constraining the interaction between regional and diapir-related stress fields: Poza de la Sal Diapir (Basque Pyrenees, Spain). In I. G. Alsop et al. (Eds.), *Salt Tectonics, Sediments and Prospectivity* (vol. 363, pp. 521–532). Geological Society of London Special Publications.

Roberts, D. T., Crook, A. J. L., Cartwright, J. A., and Profit, M. L. (2015). Investigating the Evolution of Polygonal Fault Systems Using Geomechanical Forward Modeling. 49th U.S. Rock Mechanics/Geomechanics Symposium. San Francisco, California.

Roelofse, C., Alves, T. M., and Gafeira, J. (2020). Structural controls on shallow fluid flow and associated pockmarks fields in the East Breaks area, northern Gulf of Mexico. *Marine and Petroleum Geology, 112 (104074)*, 1–20.

Römer, M., Blumenberg, M., Heeschen, K., Schloemer, S., Müller, H., Müller, S., Hilgenfeldt, C., Barckhausen, U., and Schwalenberg, K. (2021). Seafloor Methane Seepage Related to Salt Diapirism in the Northwestern Part of the German North Sea. *Frontiers in Earth Science, 9 (556329)*, 1–19.

Schroot, B. M., and Schüttenhelm, R. T. E. (2003). Expressions of shallow gas in the Netherlands North Sea. *Netherlands Journal of Geosciences, 82 (1)*, 91–105.

Serié, C., Huuse, M., and Schødt, N. H. (2012). Gas hydrate pingoes: Deep seafloor evidence of focused fluid flow on continental margins. *Geology, 40 (3)*, 207–210.

Swarbrick, R. E., Osborne, M. J., and Yardley, G. S., (2002). Comparison of overpressure magnitude resulting from the main generating mechanisms. In A. R. Huffman, G. L. Bowers (Eds.), *Pressure Regimes in Sedimentary Basins and Their Prediction* (Vol. 76, pp. 1–12). AAPG Memoir.

Taylor, M. H., Dillon, W. P., and Pecher, I. A. (2000). Trapping and migration of methane associated with the gas hydrate stability zone at the Blake Ridge Diapir: new insights from seismic data. *Marine Geology, 164*, 79–89.

Weber, K. J. (1987). Hydrocarbon distribution patterns in Nigerian growth fault structures controlled by structural style and stratigraphy. *Journal of Petroleum Science and Engineering, 1*, 91–104.

Wenau, S., Spiess, V., Pape, T., and Fekete, N. (2015). Cold seeps at the salt front in the Lower Congo Basin II: The impact of spatial and temporal evolution of salt-tectonics on hydrocarbon seepage. *Marine and Petroleum Geology, 67*, 880–893.

Wojcik, K. M., Espejo, I. S., Kalejaiye, A. M., and Umahi, O. K. (2016). Bright spots, dim spots: Geologic controls of direct hydrocarbon indicator type, magnitude, and detectability, Niger Delta Basin. *Interpretation, 4 (3)*, SN45–SN69.

Wood, D. H., and Giles, A. B. (1982). Hydrocarbon Accumulation Patterns in the East Texas Salt Dome Province. *Bureau of Economic Geology, Geological Circular 82-6*, 1–36.

Zeng, H., Wang, G., Janson, X., Loucks, R., Xia, Y., Xu, L., and Yuan, B. (2011). Characterizing seismic bright spots in deeply buried, Ordovician Paleokarst strata, Central Tabei uplift, Tarim Basin, Western China. *Geophysics, 76 (4)*, B127–B137.

Zhang, C., Xie, X., Jiang, T., and Liu, X. (2006). Hydrocarbon migration and accumulation along a long-term growth fault: Example from the BZ25-1 oilfield of Bohai basin, eastern China. *Journal of Geochemical Exploration, 89*, 460–464.

Zhao, C., Hobbs, B. E., and Mühlhaus, H. B. (1998a). Analysis of pore-fluid pressure gradient and effective vertical-stress gradient distribution in layered hydrodynamic systems. *Geophysical Journal International, 134*, 519–526.

Chapter 5. Summary, Conclusions, and Future Directions

5.1. Key conclusions

a) The Tangier 3D Seismic Survey characterizes the Cenozoic subsurface geology in this part of the slope by the recognition of subsurface seismic architectural features. The features observed include multiple generations of paleocanyons and channels from the Eocene to modern day suggesting canyon development and erosion at different time periods, large-scale sediment drifts (a mainly Eocene-aged drift and a Late Miocene Shubenacadie Drift) and small-scale sediment drifts (Late Miocene contouritic infill) suggesting influence of ocean bottom currents causing along-slope sediment reworking, slope failure complexes in the Neogene suggesting down-slope mass transport processes, and slope draping units and proglacial slope drapes that are quite common throughout the study area.

b) In the western Tangier area, the common salt structures present are related to vertical salt diapirs such as salt wings, salt feeders, crestal faulting and erosion, and carapaces. Some diapirs also exhibit salt stems and pedestals, when resolvable. In the eastern Tangier area, the common salt structure observed are related to allochthonous salt canopy. Most features are withdrawal minibasins, growth faults, feeders, and rafted overburden/carapace. Significant stratal deformation of salt bodies is notably observed during the Eocene up to the Miocene from isochore maps of Unit 1 to Unit 4 via the presence of bull's-eye-like features above salt diapirs and thickness variations above the canopy area. Towards the end of the Neogene, the effect of salt mobility on stratal deformation evidently slowed down due to minimal appearance of stratal thinning features above salt diapirs and thickness variations related to salt mobility in the canopy area, based on the observation from Unit 5 and Unit 6 isochore maps.

c) Three DHIs were found in the central and eastern Tangier area, located above two salt diapirs (AA 1 and AA 3) and a salt canopy body (AA 2). Given the association of these DHIs to salt tectonism, these salt bodies are the most plausible controlling geological body responsible for providing potential structural pathways for fluid migration. These DHIs are also linked to potential source rock intervals, mapped by J144 and J150 horizons (OERA, 2011), and possible reservoir rock intervals, mainly mapped by the K130 horizon (OERA, 2011) since one DHI is classified to have thermogenic fluids from geochemical analyses, the only DHI associated with a seepage site (Fowler et al., 2017; 2017; 2019).

d) There is a drastic difference in the number of DHIs between the Shelburne 3D (36) and Tangier 3D (3) areas. Several hypothetical scenarios attempt to answer the difference in the abundance and distribution of DHIs between the two survey areas. These scenarios are the difference in Mesozoic reservoir potential, presence of allochthonous salt canopy complex acting as barrier to vertical hydrocarbon migration, growth faults providing pathways directly to the seafloor, source rock maturity, most DHIs are biogenic, and Cenozoic reservoir and trapping mechanisms.

5.2. Future directions

5.2.1. Reservoir estimation

In this thesis, three shallow amplitude anomalies (DHIs) are suggested to have strong indication of fluid migration from the deep subsurface. Though details of the fluid and detailed lithological conditions within these DHIs is completely unknown, estimating the volume of these DHIs could eventually be useful to understand the reason for their occurrence. The Gross Rock Volume (GRV) has been calculated by generating two surfaces from two horizons outlining each DHIs

and is the only parameter that can be determined in the present study (see Appendix I). The next step in future work would be to estimate the Net Rock Volume (NRV) by multiplying calculated GRV to Net to Gross (NTG). This would also involve the calculation of Net Pore Volume (NPV) by multiplying it by Average Porosity (φ). Calculation of Hydrocarbon Pore Volume (HCPV) by multiplying NPV by Hydrocarbon Saturation (S_h). Finally, using a Formation Volume Factor (FVF) that can be done using Boyle's and Charles's Law. The full process of reservoir estimation mentioned above involves several steps (e.g., Hartmann and Beaumont, 1999), which could possibly be a new study on reservoir estimation of DHIs across the entire Scotian Slope, not limited to only the Tangier 3D Seismic Survey.

5.2.2. Significance of contourites

Some elements from the investigation of the Tangier 3D Seismic Survey such as the presence of contourites and asymmetric channel infills in paleocanyons could be used for studies such as paleo-oceanographic circulation (Fig. 5.1) and paleoclimatic evolution, the influence of bottom current activity in sediment deposition in passive margins (e.g., Scotian Margin), and its implications for petroleum exploration. In the Tangier 3D area, two large-scale and one small-scale contourite intervals are observed. The occurrences of the thick packages of contourites in the Eocene (in Unit 1; Fig. 3.13) and the Miocene Shubenacadie Drift (in Unit 3; Figs. 3.13-3.14; after Campbell et al., 2015) suggest that the contour current activity regime was long in duration to develop these deposits. It was likely affected by warm and cold currents from the South Atlantic and the Labrador Sea, respectively (Campbell et al., 2015; Rodrigues et al., 2022; Fig. 5.1). The small-scale Late Miocene contourite (in Unit 4; Figs. 3.15-3.16) observed in the upper

slope of the study area suggests that the contour current activity was relatively short in duration for this phase, but still influential in order to develop a contourite.

In terms of petroleum exploration, for contourites to be considered as potential hydrocarbon reservoirs, particular characteristics must be evident such as having coarse-grained sediments, excellent porosity, and permeability. Several studies have well documented occurrences of potential sandy contourite reservoirs that are dependent on its proximity to sand-rich areas and be re-worked by contour currents in various offshore sedimentary basins (Castro et al., 1998; Kenyon et al., 2002; Rodriguez and Anderson, 2004; Akhmetzhanov et al., 2007). Contourites are also documented to act as seals in petroleum systems, seals being commonly fine-grained in nature. This is common in slope and basin settings where the bottom current energy ranging from low- to medium-intensity currents.

The sources of fine-grained sediments for contourite deposits are introduced by river discharge, seafloor erosion, sediment gravity flow, and productivity from upwelling zones (Viana et al., 2007). Fine-grained contourites has been well documented in sedimentary basins (Faugères and Stow, 1993; Stow and Faugères, 1998; Faugères et al., 1999; Rebesco and Stow, 2001; Stow et al., 2002; Faugères and Stow, 2008) and have been proven to work as excellent seals. As examples, Souza Cruz (1998) and Moraes et al. (2007) suggested that thick packages of Paleogene to Lower Neogene oil-rich sandstones in the Campos Basin, offshore Brazil are overlain by a thick Middle to Upper Miocene bottom current origin wedge, acting as a seal. Duarte and Viana (2007) provided evidence that a thick sealing, low permeable Neogene Santos Drift is overlain for Paleogene oil-bearing sandstones in the northern Santos Basin, offshore Brazil.

5.2.3. Geohazard assessment

Exploration in deep-water regions, especially in assessed oil and gas sites with high certainty of quality reservoirs, poses various significant technical challenges for the development and installation of wells and rigs at extreme water depths. The investigation of seafloor and the shallow subsurface processes in deep-water areas are generally complex and poorly understood, therefore, deep-water seafloor geomorphology and surficial geology mapping could help to mitigate these geohazard risks (Piper and McCall, 2003; Mosher et al., 2004; Mosher, 2008; Mosher et al., 2010; Hough et al., 2010). Some examples of geohazards are seafloor sediment mobility (e.g., mass wasting), shallow gas, salt diapirism, and fault characterization, which are also common in this part of the slope and have been observed using the Tangier 3D Seismic Survey.

The use of seafloor and shallow subsurface geomorphology is not only limited to offshore oil and gas exploration. This can also be applicable to risk assessment for installation of facilities needed for offshore wind and tidal energy that industrialize the seafloor, especially when the province of Nova Scotia has been active advocating and implementing the use of renewable energy, although these types of installations are relevant to the Scotian Shelf rather than the Slope. A more likely relevance is the potential for natural processes such as slope failures to trigger tsunami or for gas hydrate melting and gas release to affect installations such as petroleum exploration activities or sub-sea communication cables. Fluid release also has potential relevance to sub-sea biological communities. Regardless of the exact process, the presence of likely hydrocarbon concentrations of some type in the shallow subsurface at specific, geographically limited locations has implications for any human-related activities on the Scotian Slope and the surrounding regions.

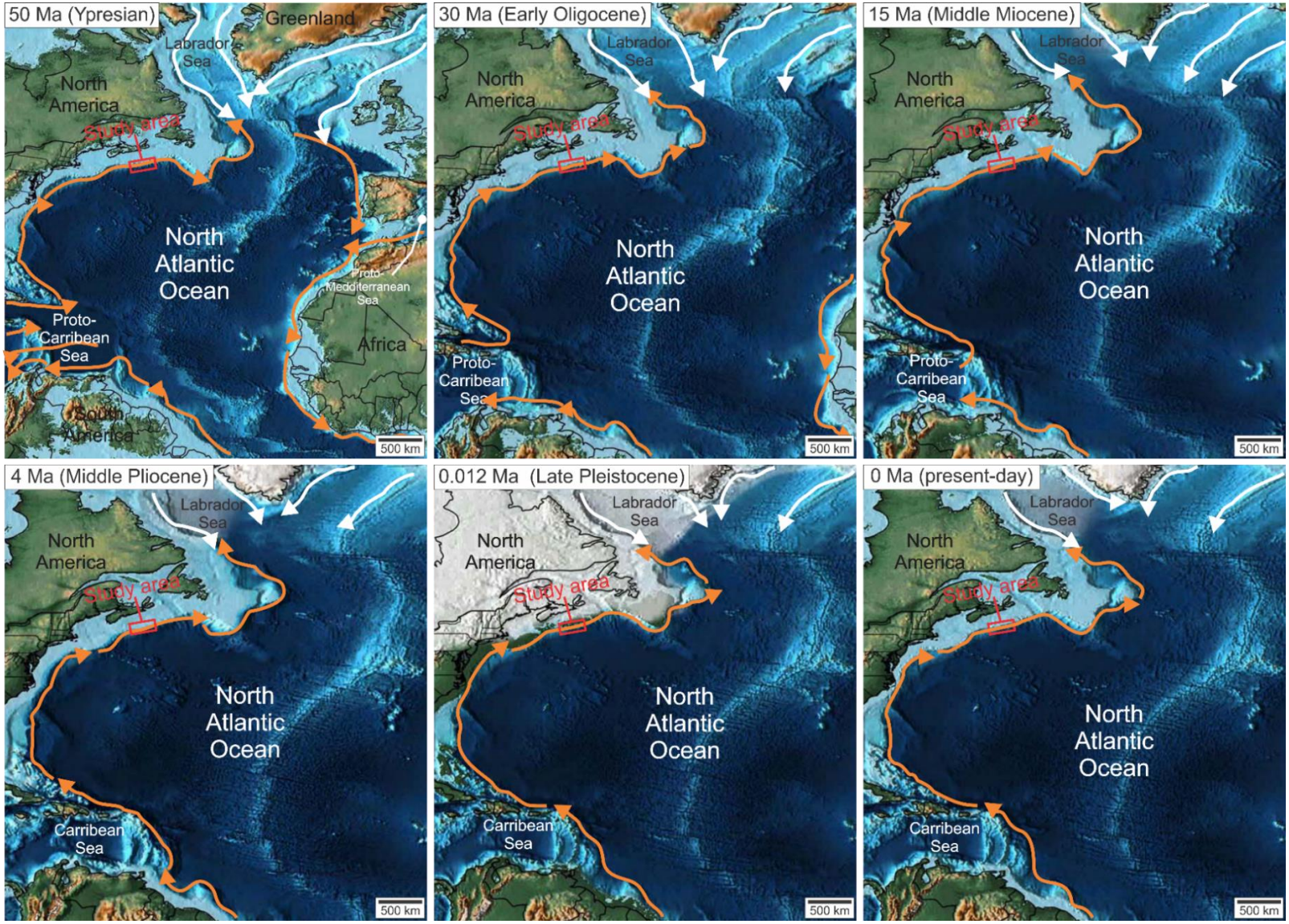

Figure 5.1. Paleogeographic reconstruction with ages (modified from Scotese and Wright, 2018) and paleooceanographic circulation (from Barron and Peterson, 1991; Straume et al., 2020) of the Cenozoic with oceanic current directions. Warm currents represented in orange arrows; Cold currents represented in white arrows. Horizons closely corresponding to geologic ages from Scotese and Wright (2018): P1 horizon = 50 Ma (Ypresian); N1 horizon = 30 Ma (Early Oligocene); N2 horizon = 15 Ma (Middle Miocene); N3 horizon = 4 Ma (Middle Pliocene); N4 horizon = 0.012 Ma (Late Pleistocene); N5 to N6 horizons = 0 Ma (present-day).

5.3. Works cited

Akhmetzhanov, A., Kenyon, N. H., Habgood, E., Van der Mollen, A. S., Nielsen, T., Ivanov, M., and Shashkin, P. (2007). North Atlantic contourite sand channels. In A. R. Viana and M. Rebesco (Eds.), *Economic and Palaeoceanographic Significance of Contourite Deposits*. Geological Society of London, Special Publications, 276, 25–47.

Barron, E. J. and Peterson, W. H. (1991). The Cenozoic ocean circulation based on ocean General Circulation Model results. *Palaeogeography, Palaeoclimatology, Palaeoecology, 81*, 1–28.

Campbell, D. C., Shimeld, J., Deptuck, M. E., and Mosher, D. C. (2015). Seismic stratigraphic framework and depositional history of a large Upper Cretaceous and Cenozoic depocenter off southwest Nova Scotia, Canada. *Marine and Petroleum Geology, 65*, 22-42.

Castro, R. O., Magalhaes, P. M., Moliterno, A. M. C., Santos, V. S. S., Blauth, M., and Caddah, L. F. G. (1998). Feeder canyon evolution model deduced from the stacking pattern of a Tertiary turbidite system in Campos Basin, Brasil. *AAPG Bulletin, 82 (10)*, 1883–1884.

Duarte, C. S. L. and Viana, A. R. (2007). Santos Drift System: stratigraphic organization and implications for late Cenozoic palaeocirculation in the Santos Basin, SW Atlantic Ocean. In: A.R. VIANA, and M. REBESCO (Eds.), *Economic and Palaeoceanographic Significance of Contourite Deposits*. Geological Society of London, Special Publications, 276, 171–198.

Faugères, J-C and Stow, D. A. V. (1993). Bottom current-controlled sedimentation: a synthesis of the contourite problem. *Sedimentary Geology, 82 (1-4)*, 287–297.

Faugères, J-C, Stow, D. A. V., Imbert, P., and Viana, A., 1999, Seismic features diagnosticof contourite drifts: *Marine Geology, 162*, 1–38.

Faugères, J.C. and Stow, A.V. (2008). Contourite drifts: nature, evolution and controls. In M. Rebesco, A. Camerlenghi, (Eds.), *Contourites. Developments in Sedimentology*, (v. 60, pp. 259–288). Elsevier.

Fowler, M., Webb, J., Olsen, H., Ashraf, F., and Guldbrandsen, S. (2017). Geochemistry Data Report for 2016 Scotian Slope Piston Coring Program. *Applied Petroleum Technology*, 1–310. APT Canada Ltd.

Fowler, M. (2017). Piston Core Geochemistry – Final Report. *Applied Petroleum Technology*, 1–4. APT Canada Ltd.

Fowler, M., Webb, J., Gulbrandsen, S., Austnes, L-K, and Ashraf, F. (2019). Geochemistry Data Report for 2018 Scotian Slope Coring Program. *Applied Petroleum Technology*, 1–306. APT Canada Ltd.

Hartmann, D. J., and Beaumont, E. A. (1999). Predicting Reservoir System Quality and Performance. In D. J. Hartmann and E. A. Beaumont, *Treatise in Petroleum Geology* (Ch. 9, pp. 1-154). The American Association of Petroleum Geologists.

Hough, G., Green, J., Fish, P., Mills, A., and Moore, R. (2010). A geomorphological mapping approach for the assessment of seabed geohazards and risk. *Marine Geophysical Research, 32*, 151–162.

Kenyon, N. H., Akhmetzhanov, A. M., and Twichell, D. C. (2002). Sand wave fields beneath the Loop Current, Gulf of Mexico: reworking of fan sands. Marine Geology, 192, 297–307.

Moraes, M. A. S., Maciel, W. B., Braga, M. S. S., and Viana, A. R. (2007). Bottom-current reworked Palaeocene-Eocene deep-water reservoirs of the Campos Basin, Brazil. In: A. R. Viana and M. REBESCO (Eds.), *Economic and Palaeoceanographic Significance of Contourite Deposits*. Geological Society of London, Special Publications, 276, 81–94.

Mosher, D. C. (2008). Submarine mass movements in Canada: Geohazards with far-reaching implications. *Proceedings of the 4th Canadian Conference on Geohazards: From Cause to Management*, 1-8. Presse de l'Universite Laval, Quebec.

Mosher, D. C., Piper, D. J. W., Campbell, D. C., and Jenner, K. A. (2004). Near-surface geology and sediment-failure geohazards of the central Scotian Slope. *AAPG Bulleting, 88 (6),* 703-723.

Mosher, D. C., Xu, Z., and Shimeld, J. (2010). The Pliocene Shelburne Mass-Movement and Consequent Tsunami, Western Scotian Slope. *Submarine Mass Movements and Their Consequences, 28*, 765-775.

Piper, D. J. W., and McCall, C. A Synthesis of the Distribution of Submarine Mass Movements on the Eastern Canadian Margin. *Submarine Mass Movements and Their Consequences, 19*, 291-298.

Rebesco, M. and Stow, D. (2001). Seismic expression of contourites and related deposits: a preface. *Marine Geophysical Research, 22*, 303–308.

Rodriguez, A. B. and Anderson, J. B. (2004). Contourite origin for shelf and upper slope sand sheet, offshore Antarctica. *Sedimentology, 51*, 699–711.

Rodrigues, S., Deptuck, M. E., Kendell, K. L., Campbell, C., and Hernández-Molina, F. J. (2022). Cretaceous to Eocene mixed turbidite-contourite systems offshore Nova Scotia (Canada): Spatial and temporal variability of down- and along-slope processes. *Marine and Petroleum Geology, 138*, 1–26.

Scotese, R. C. and Wright, N. (2018). PALEOMAP paleodigital elevation models (PaleoDEMS) for the phanerozoic, PALEOMAP project. Retrieved from https://www.earthbyte .org/paleodem-resource-scotese-and-wright-2018/.

Souza Cruz, C. E. (1998). South Atlantic paleoceanographic events recorded in the Neogene deep water section of the Campus Basin, Brazil. *AAPG Bulletin, 82 (10)*, 1883–1984.

Stow, D. A. V. and Faugères, J-C. (1998). Contourites, Turbidites and Processes Interaction. *Sedimentary Geology Special Issue*, 115 (1-4).

Stow, D. A. V., Pudsey, C. J., Howe, J. A., Faugères, J-C., and Viana, A. R. (2002). Deep-Water Contourites: Modern Drifts and Ancient Series, Seismic and Sedimentary Characteristics. *Geological Society of London Memoirs*, 22.

Straume, E. O., Gaina, C., Medvedev, S., and Nisancioglu, K. H. (2020). Global Cenozoic Paleobathymetry with a focus on the Northern Hemisphere Oceanic Gateways. *Gondwana Research, 86*, 126–143.

Viana, A. R., Almeida Jr., W., Nunes, M. C. V., and Bulhoes, E. M. (2007). The economic importance of contourites. In A. R. Viana and M. Rebesco (Eds.), *Economic and*

Paleooceanographic Significance of Contourite Deposits (Special Publications, 276, pp. 1–23). Geological Society of London.

Appendix

I. Volumetric calculation of each amplitude anomaly

A simplified, software-based volumetric calculation is used to determine the volume and area of each amplitude anomaly that is interpreted to be sourced from deeper depths (Gross Rock Volume; GRV). Two closely mapped horizons, upper and lower horizons (Fig. A1) were used to outline each amplitude anomalies to generate two bounding surfaces (Fig. A2-A4) to use a surface operation known as "volume under a surface" in Schlumberger's Petrel E&P Software Platform v2019.1.

As a result, AA 1, AA 2, and AA 3 (Fig. 2.8A to 2.8C) have calculated volume and area (Table A1). The major pitfall of this method is that the shape of the amplitude anomalies is irregular in every surrounding inline and crossline (spacing interval = 5), so horizon mapping becomes subjective from the initial sections where the amplitude anomalies are interpreted (Fig. 4.2; 4.5; 4.10) to different inlines and crosslines from the sections that are shown in Fig. 2.8. In addition, the resulting surfaces from the horizon appear to have no closure, therefore, the quality of this method and the uncertainty of calculated volume and area are increased.

Table A1. Calculated Gross Rock Volume (GRV) and area for each amplitude anomaly.

Amplitude anomaly	**Calculated GRV (m^3)**	**Calculated area (m^2)**
AA 1	3.20732×10^8	3.1611732×10^6
AA 2	7.5585×10^8	6.9103082×10^6
AA 3	1.9361×10^8	1.4726802×10^6

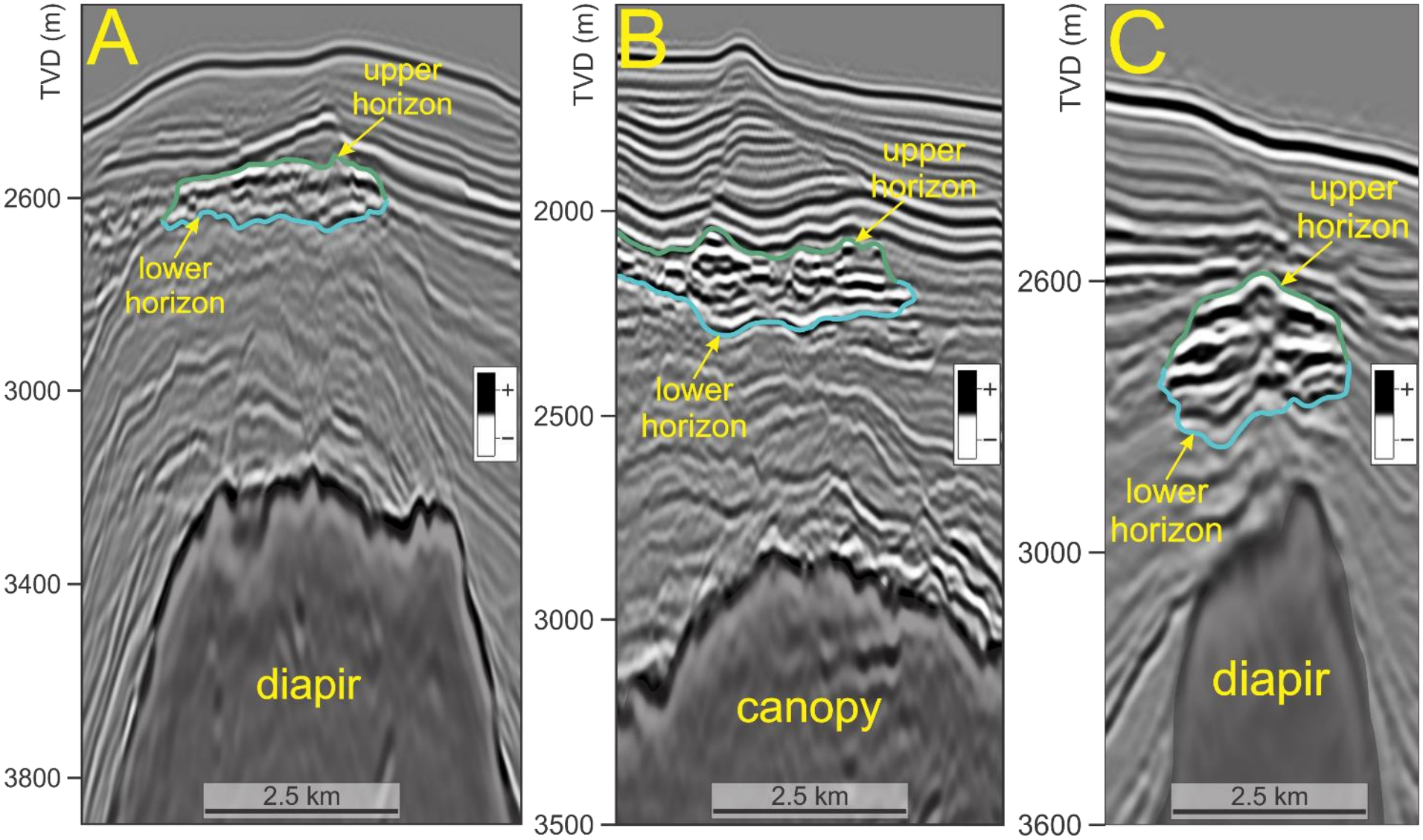

Figure A1. Representative dip-oriented section of each amplitude anomaly (cropped from Figs. 4.2 for A, 4.3 for C, and 4.7 for B). The volume calculation is based on the generated surfaces from two horizons, the upper and lower horizons (A = AA 1; B = AA 2; C = AA 3; discussed in detail in Chapter 4). Data courtesy of BP Canada Exploration Ltd via NSDNRR.

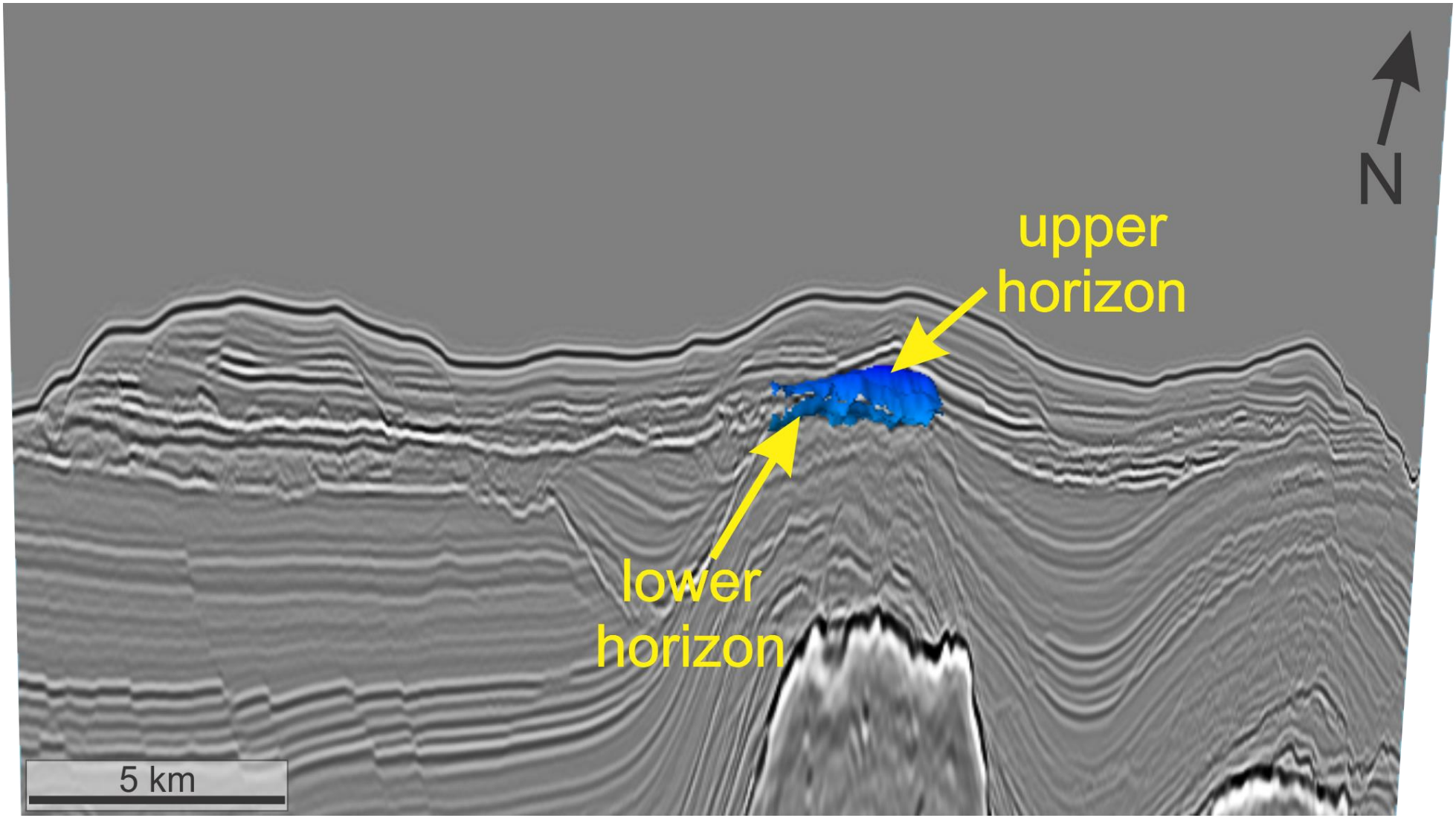

Figure A2. Resulting surfaces from mapped upper and lower horizons in Fig. A1A.

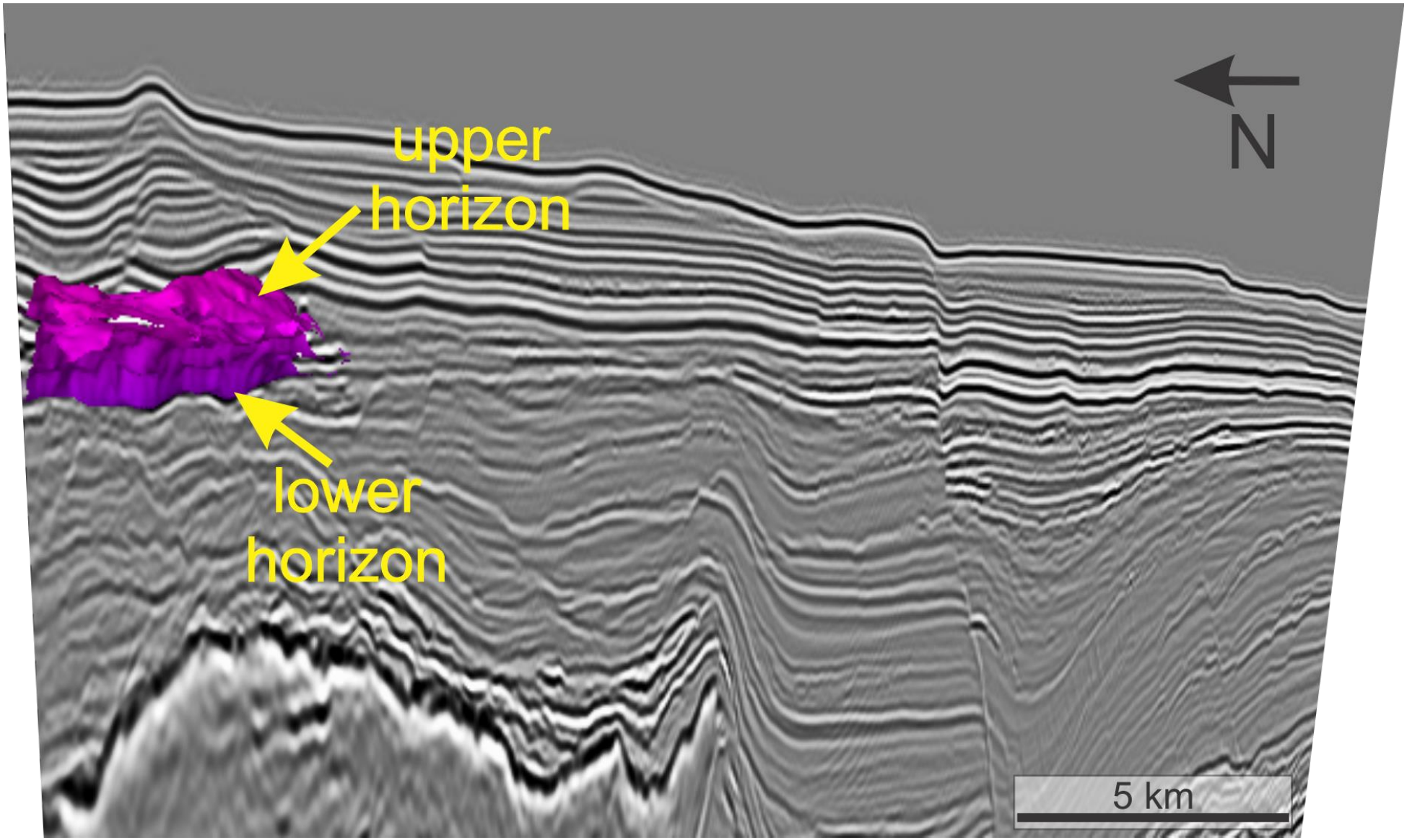

Figure A3. Resulting surfaces from mapped upper and lower horizons in Fig. A1B.

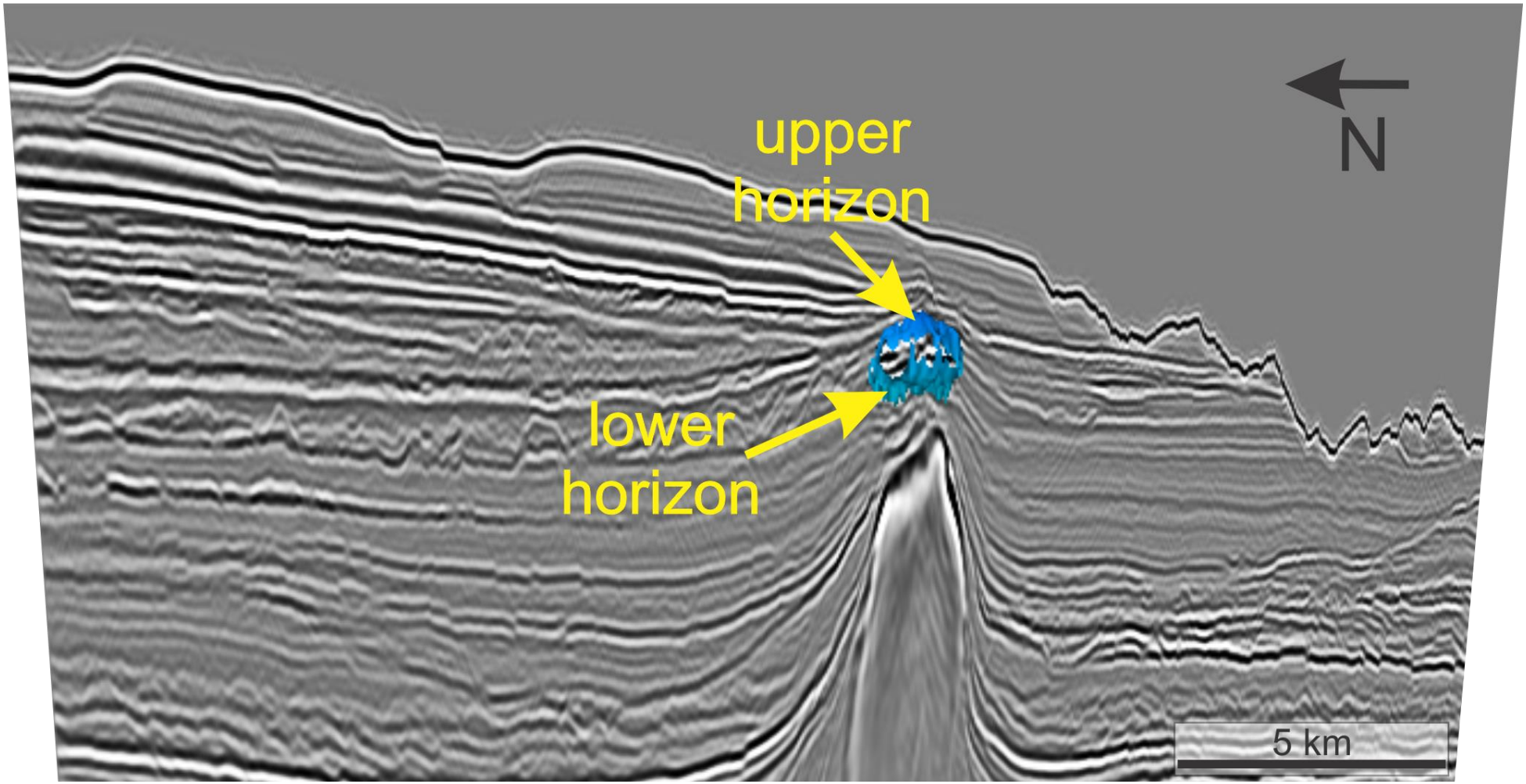

Figure A4. Resulting surfaces from mapped upper and lower horizons from Fig. A1C.

II. Raw and unannotated versions of depth-structure maps

P1 horizon

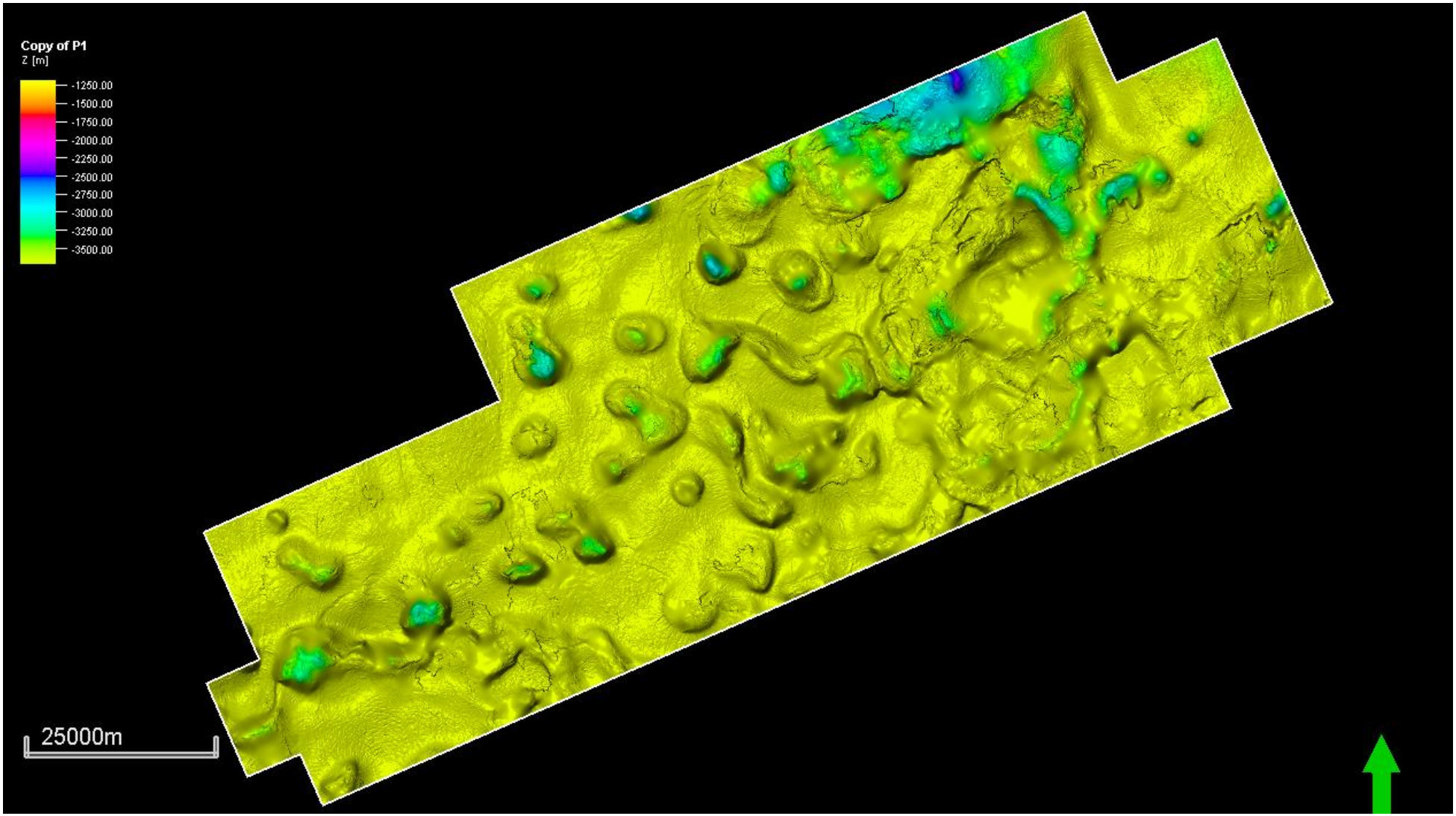

N1 horizon

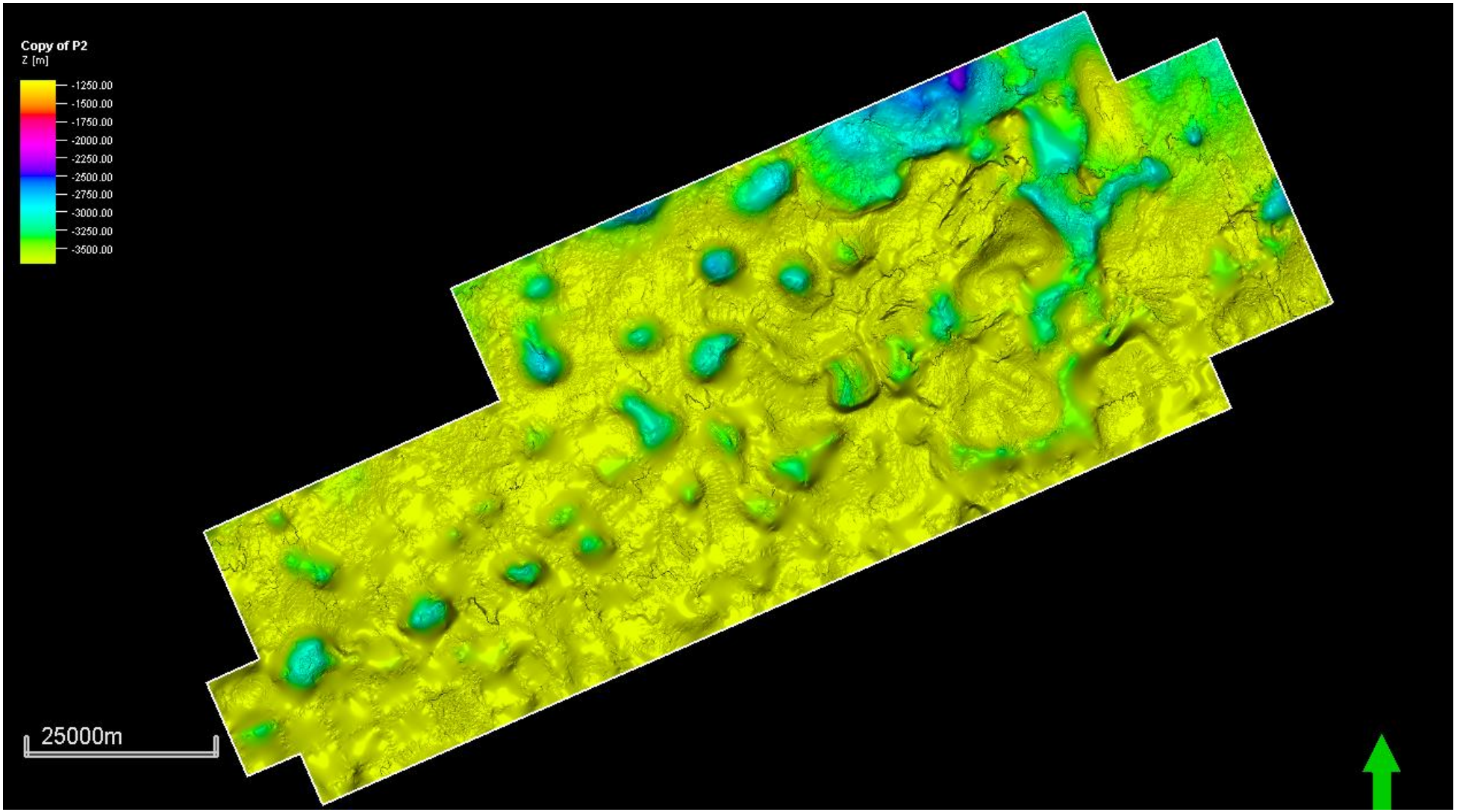
Copy of P2
Z [m]
-1250.00
-1500.00
-1750.00
-2000.00
-2250.00
-2500.00
-2750.00
-3000.00
-3250.00
-3500.00
25000m

N2 horizon

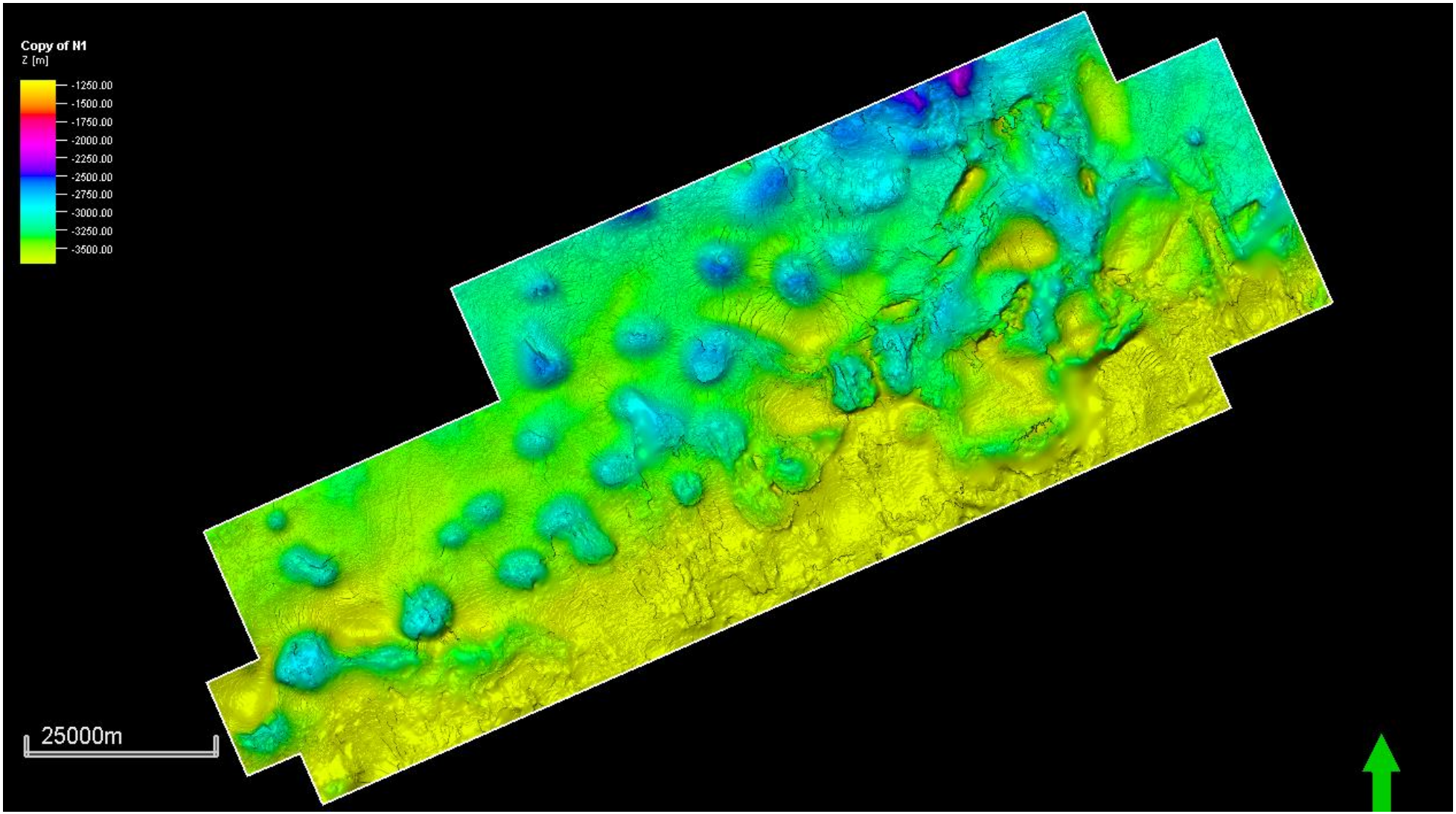
Copy of N1
Z [m]
-1250.00
-1500.00
-1750.00
-2000.00
-2250.00
-2500.00
-2750.00
-3000.00
-3250.00
-3500.00
25000m

N3 horizon

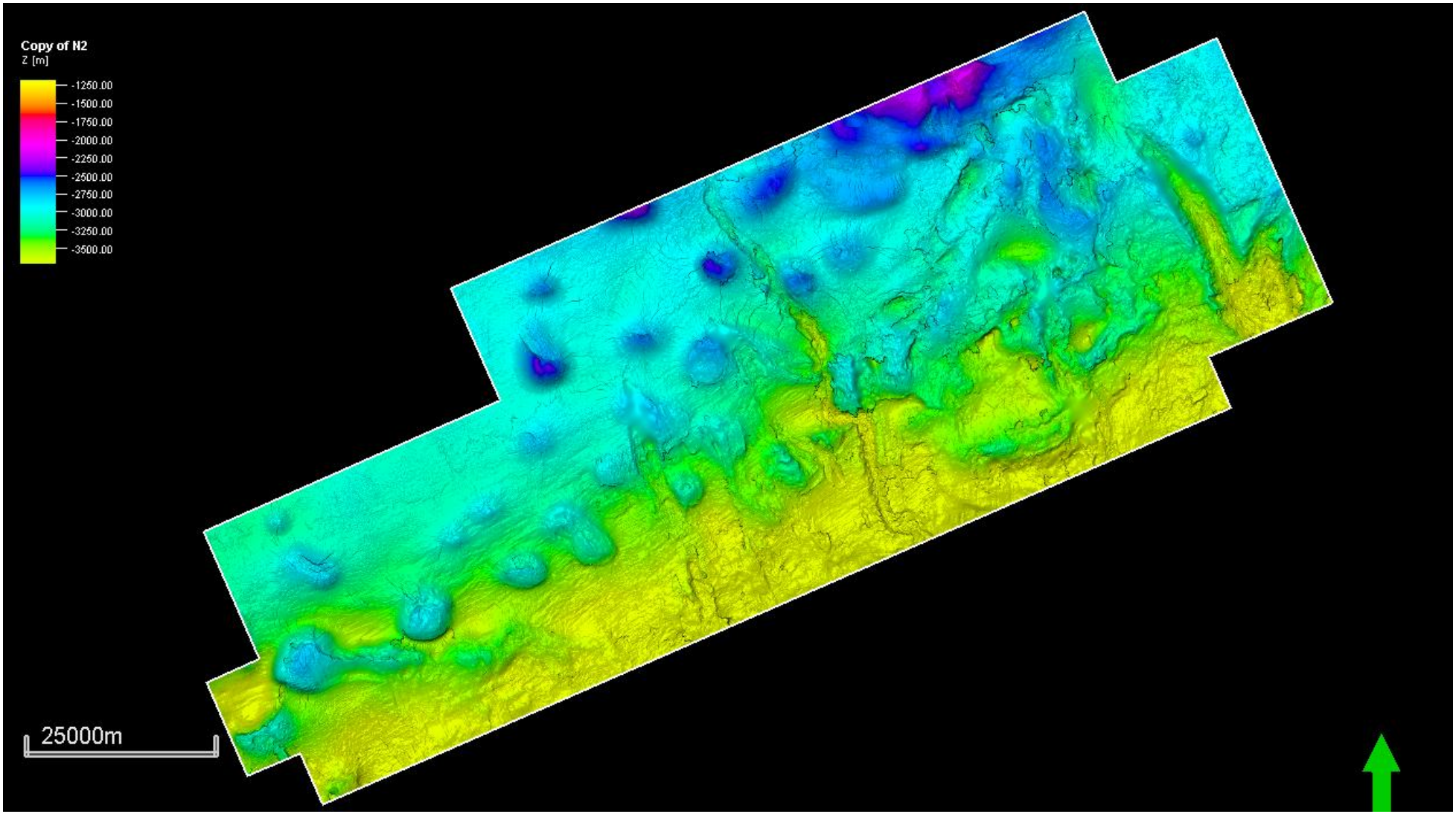
Copy of N2
Z [m]
-1250.00
-1500.00
-1750.00
-2000.00
-2250.00
-2500.00
-2750.00
-3000.00
-3250.00
-3500.00
25000m

N4 horizon

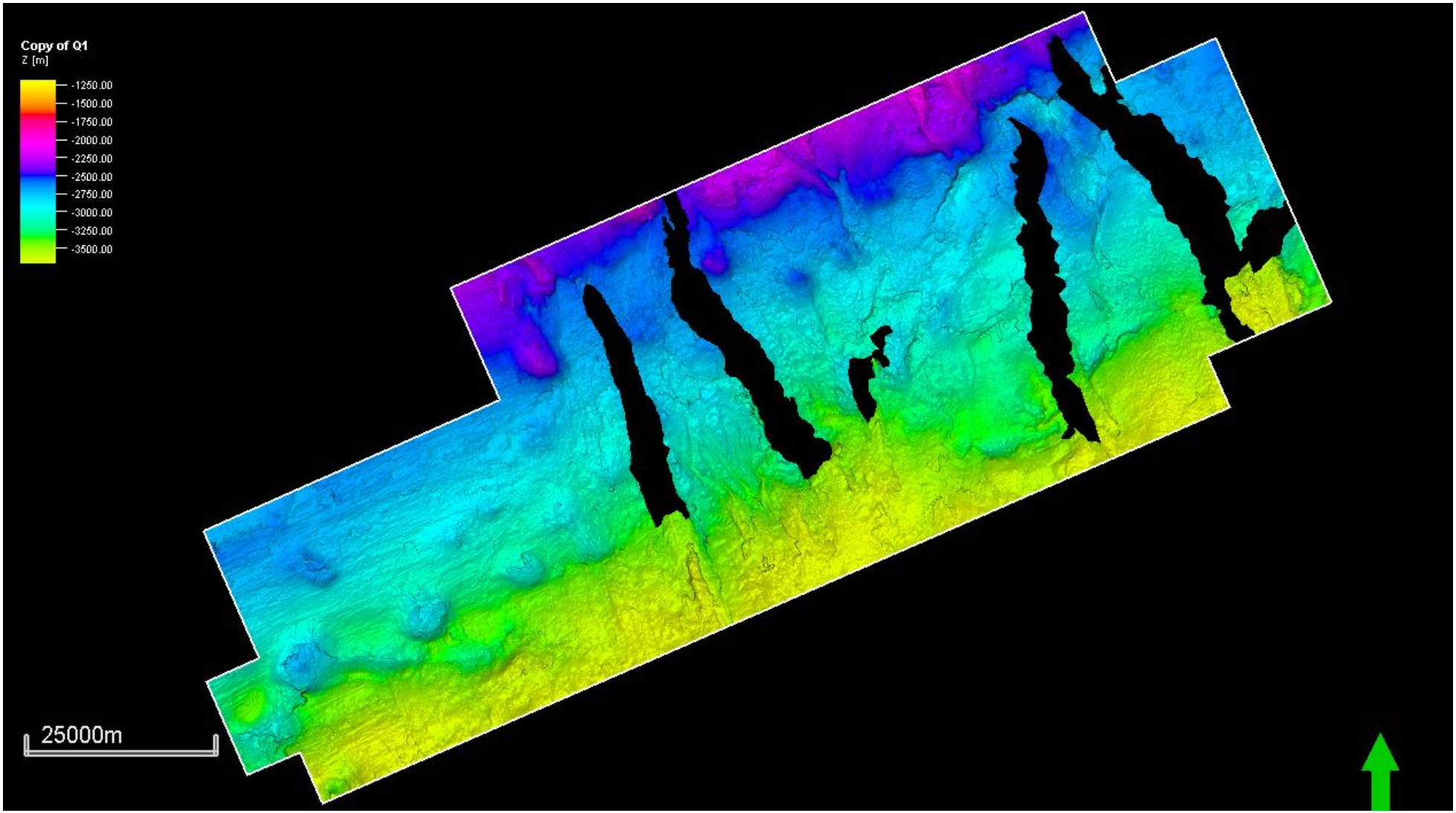
Copy of Q1
Z [m]
-1250.00
-1500.00
-1750.00
-2000.00
-2250.00
-2500.00
-2750.00
-3000.00
-3250.00
-3500.00
25000m

N5 horizon

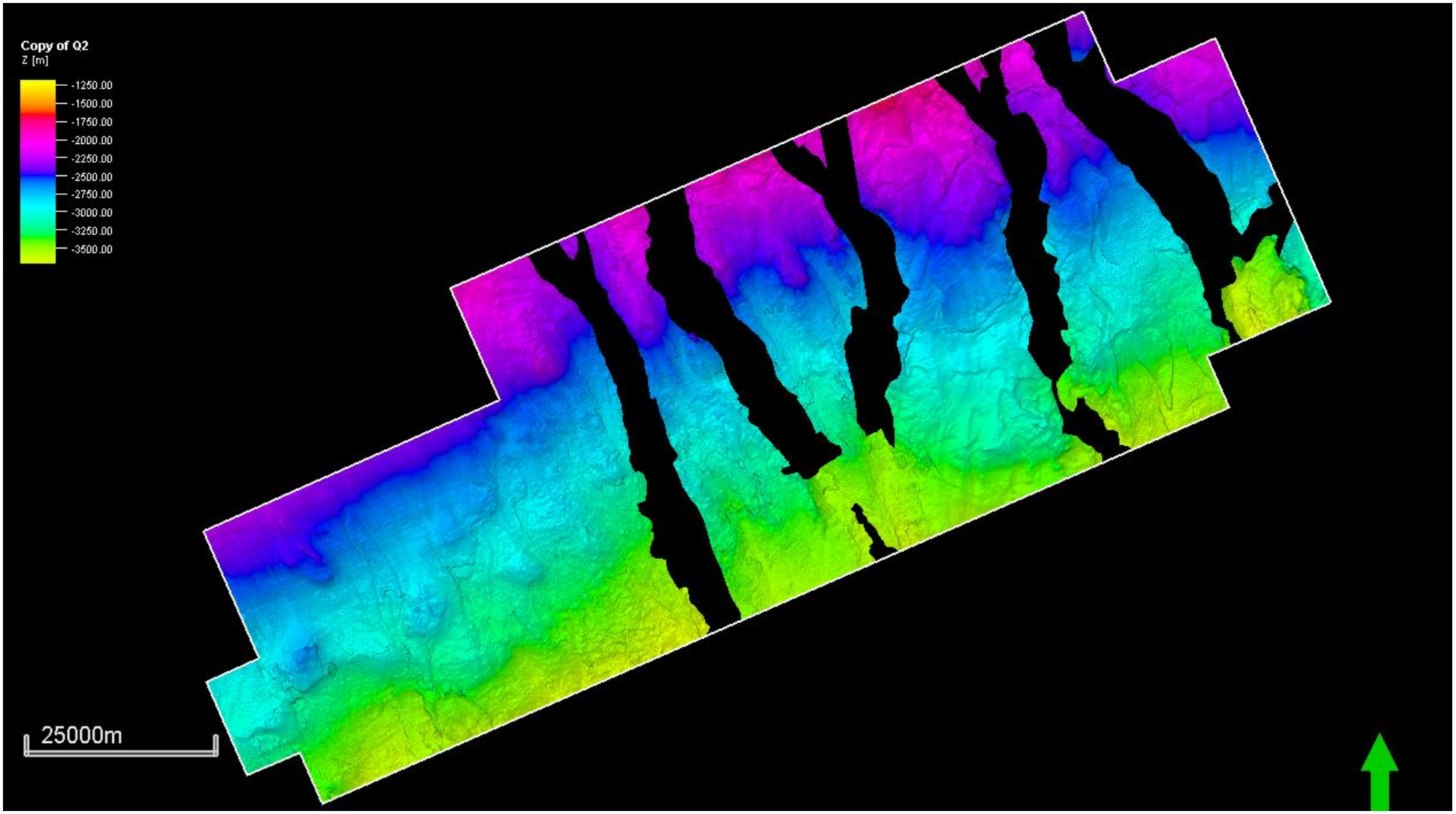
Copy of Q2
Z [m]
-1250.00
-1500.00
-1750.00
-2000.00
-2250.00
-2500.00
-2750.00
-3000.00
-3250.00
-3500.00
25000m

N6 horizon

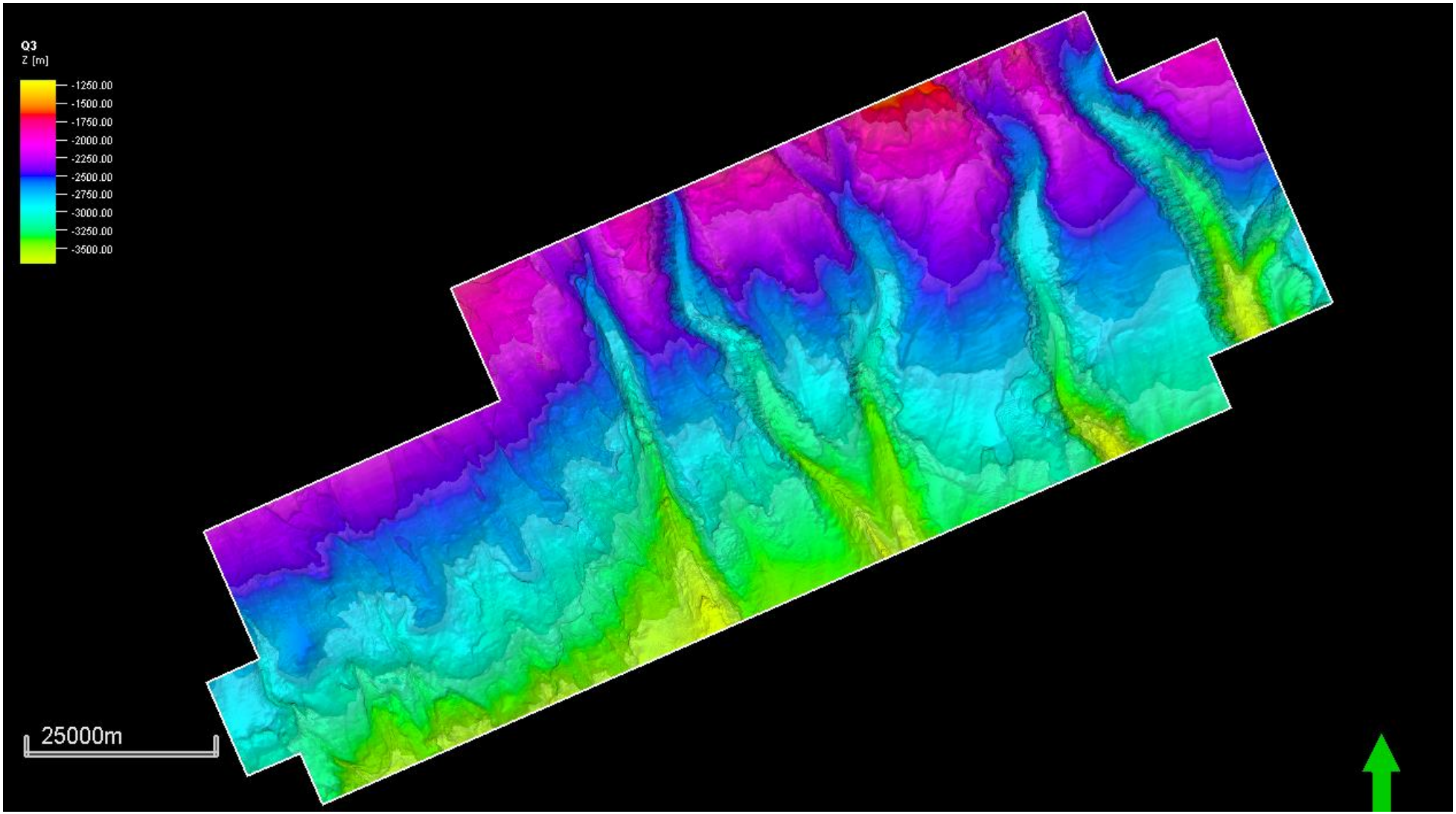
Q3
Z [m]
-1250.00
-1500.00
-1750.00
-2000.00
-2250.00
-2500.00
-2750.00
-3000.00
-3250.00
-3500.00
25000m

III. Raw and unannotated versions of RMS amplitude maps

P1 horizon

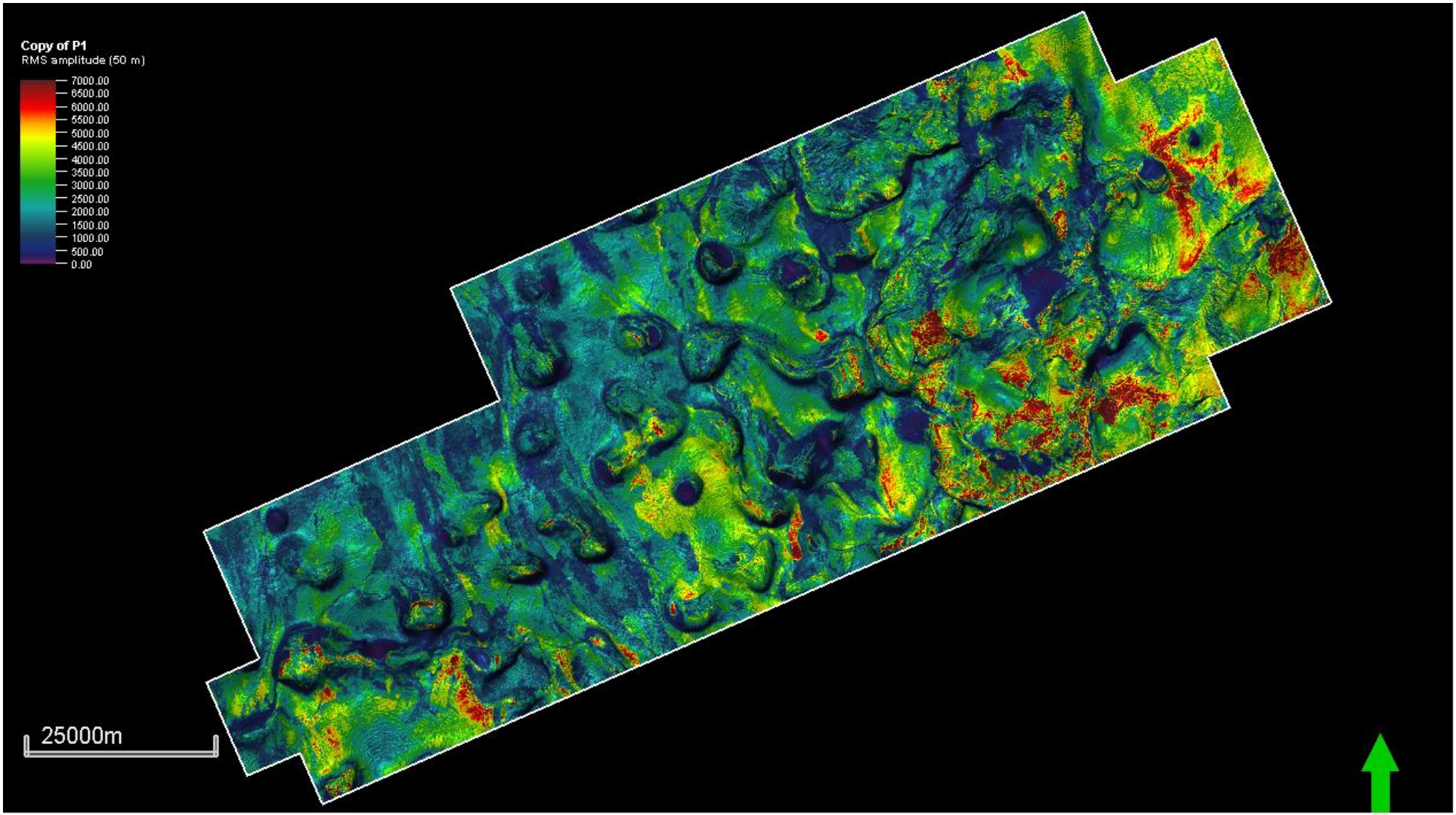

N1 horizon

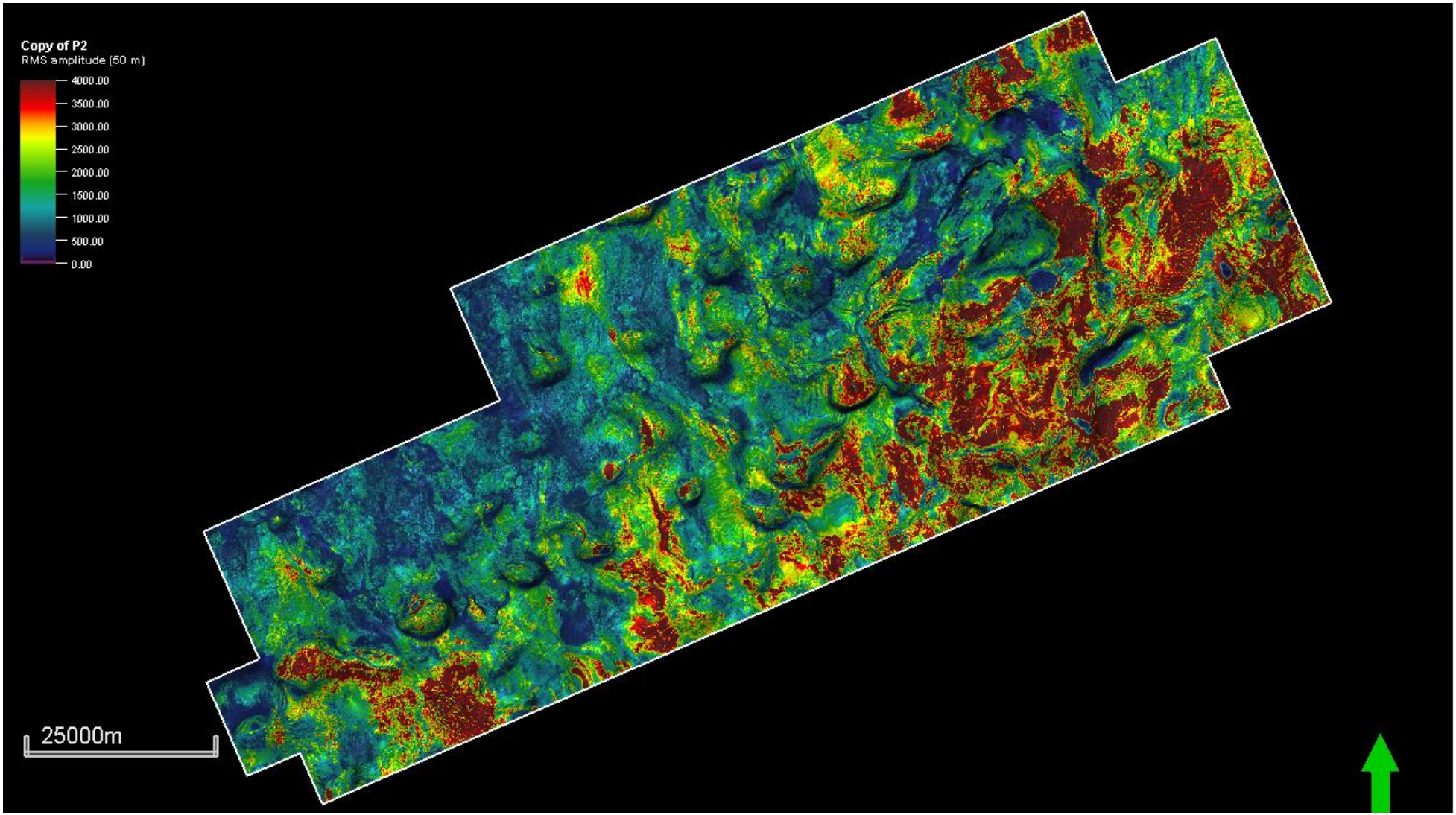
Copy of P2
RMS amplitude (50 m)
4000.00
3500.00
3000.00
2500.00
2000.00
1500.00
1000.00
500.00
0.00
25000m

N2 horizon

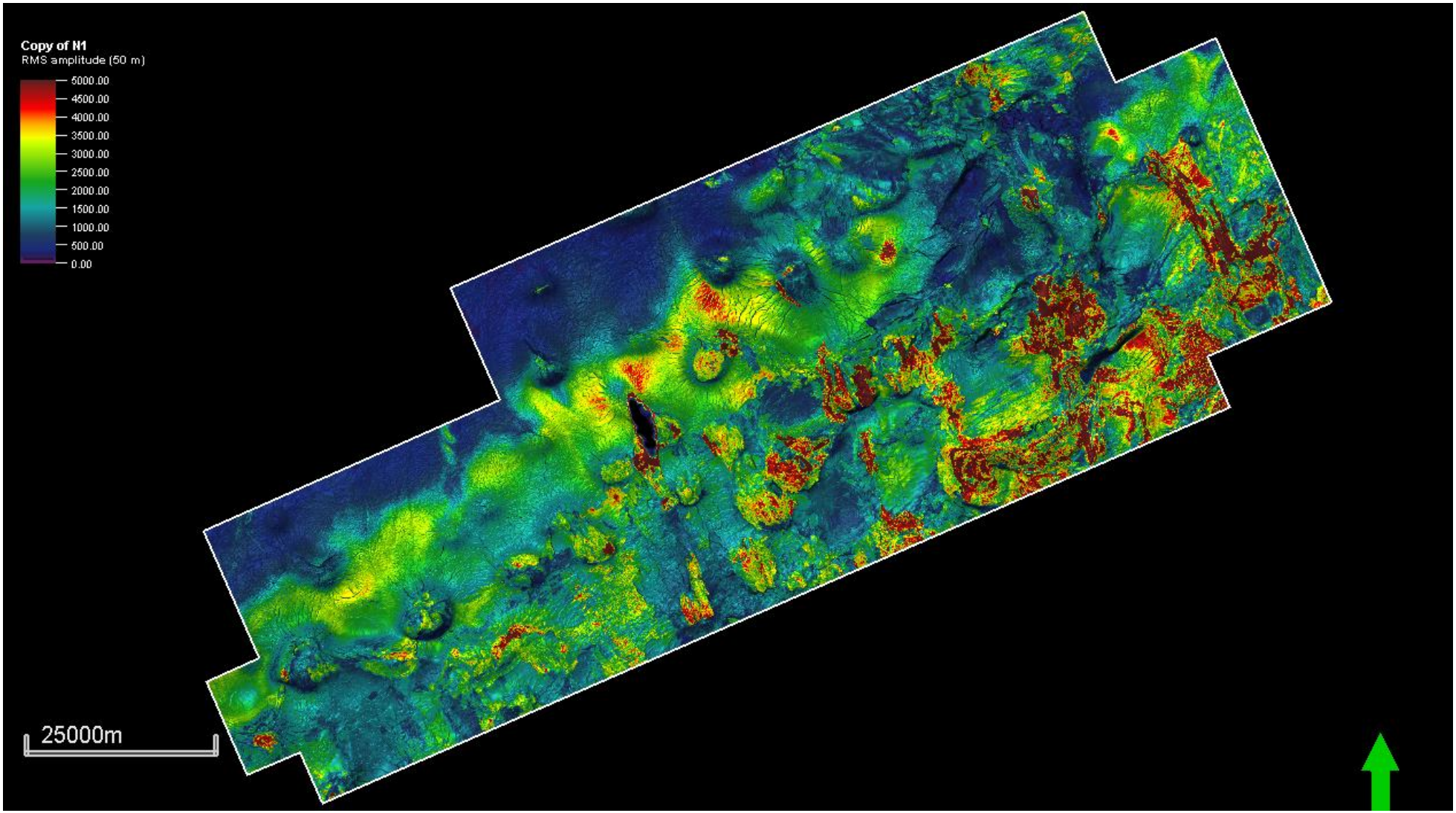
Copy of H1
RMS amplitude (50 m)
5000.00
4500.00
4000.00
3500.00
3000.00
2500.00
2000.00
1500.00
1000.00
500.00
0.00
25000m

N3 horizon

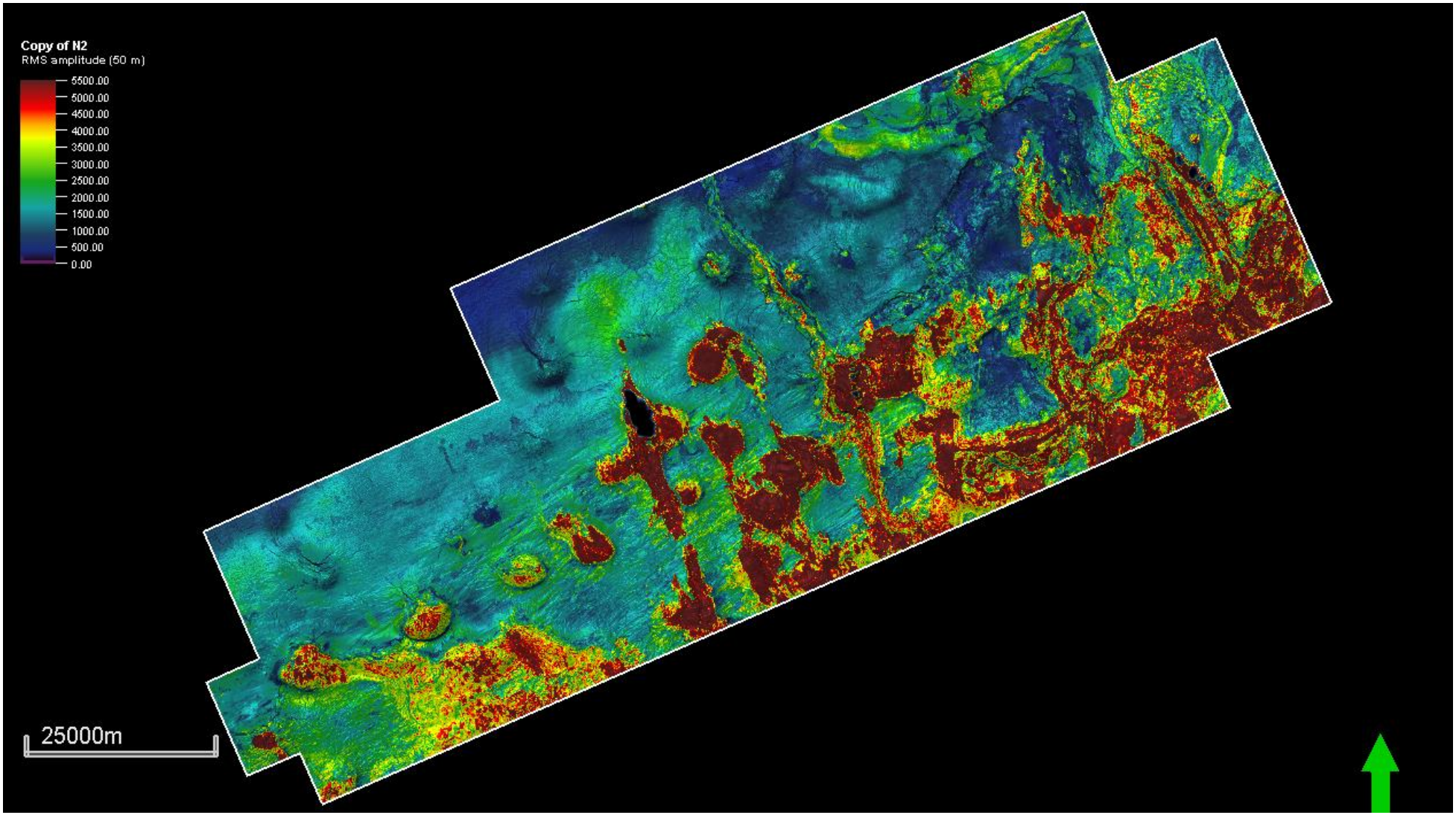
Copy of N2
RMS amplitude (50 m)
5500.00
5000.00
4500.00
4000.00
3500.00
3000.00
2500.00
2000.00
1500.00
1000.00
500.00
0.00
25000m

N4 horizon

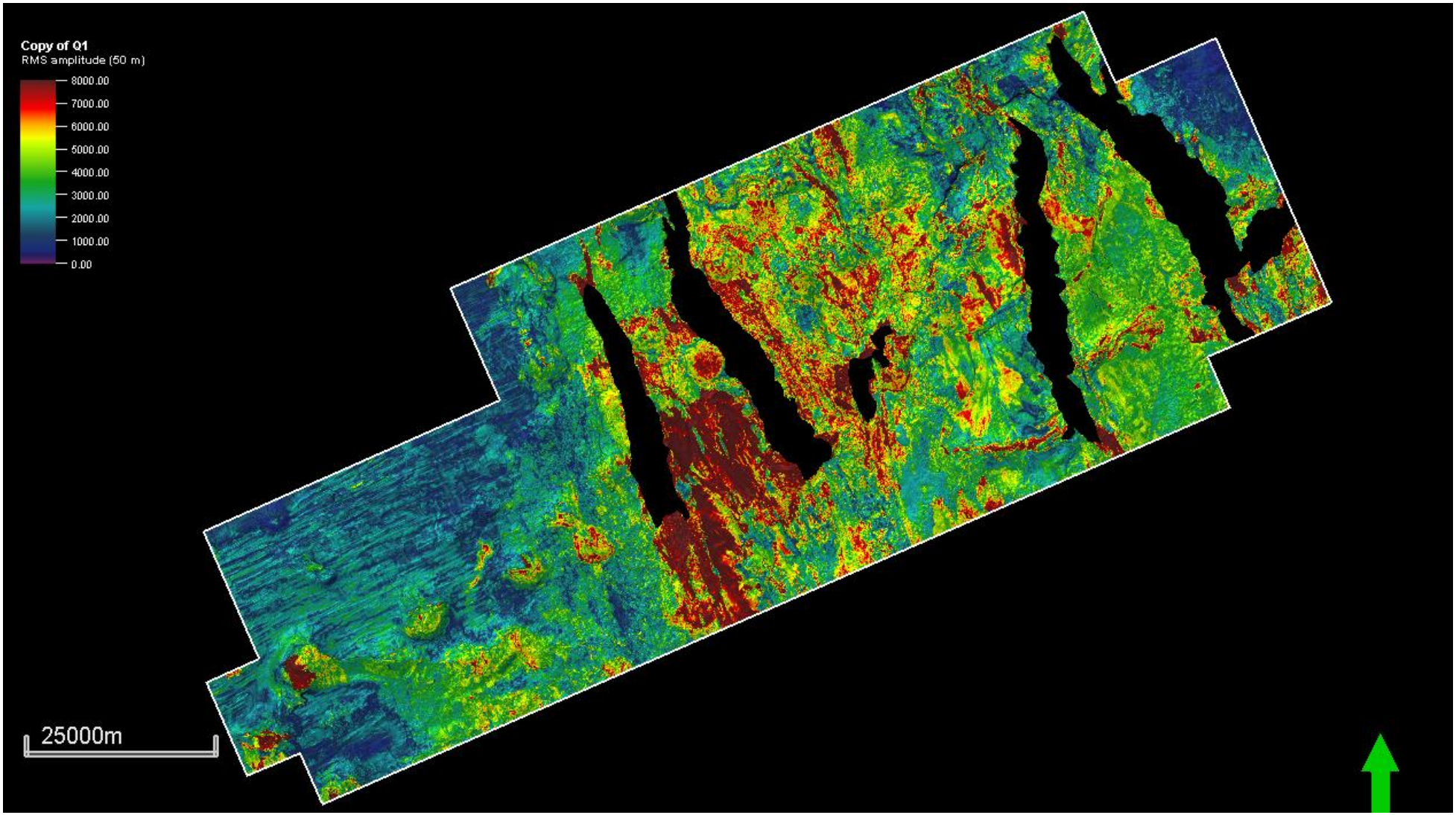
Copy of Q1
RMS amplitude (50 m)
8000.00
7000.00
6000.00
5000.00
4000.00
3000.00
2000.00
1000.00
0.00
25000m

N5 horizon

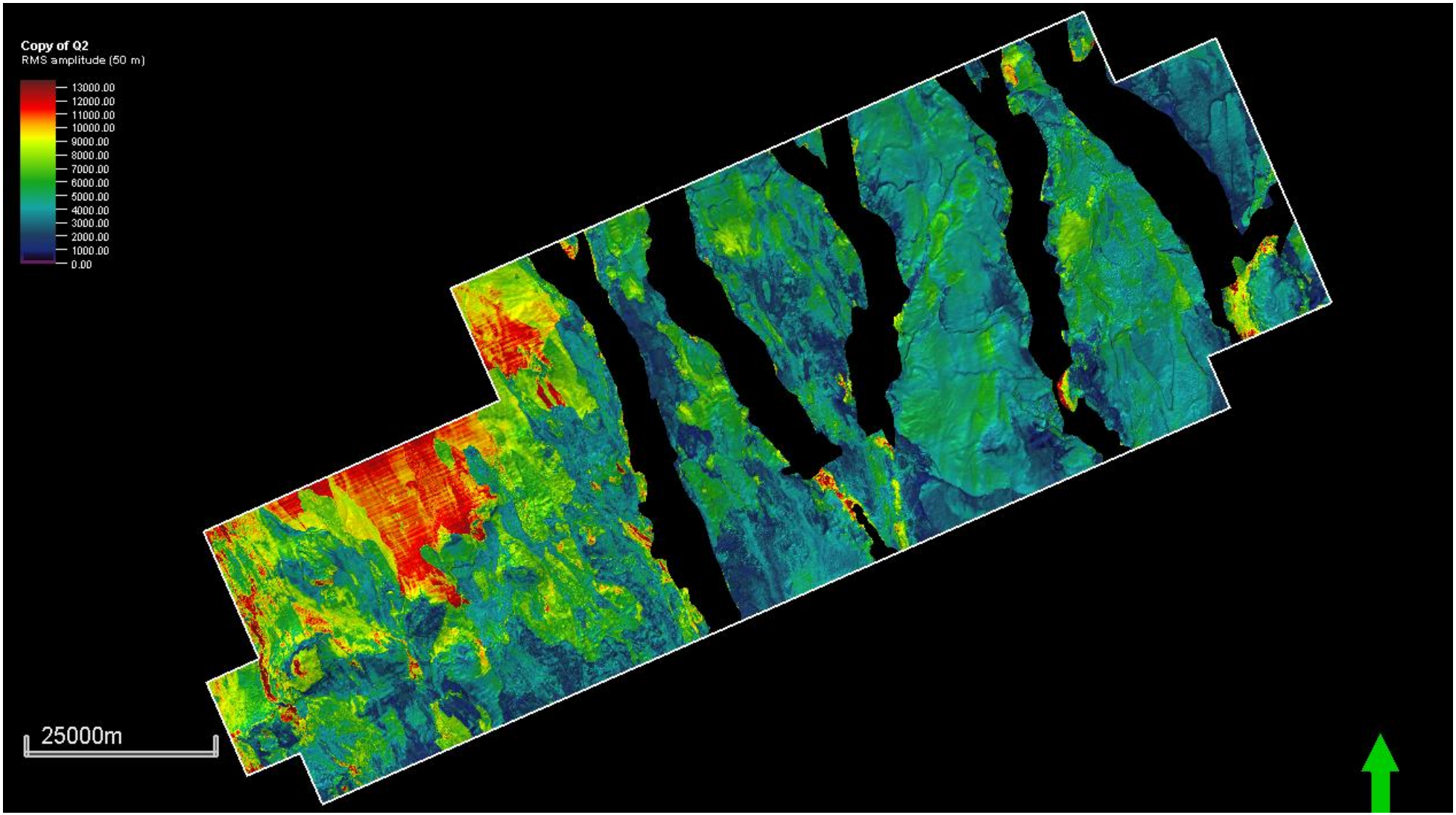
Copy of Q2
RMS amplitude (50 m)
13000.00
12000.00
11000.00
10000.00
9000.00
8000.00
7000.00
6000.00
5000.00
4000.00
3000.00
2000.00
1000.00
0.00
25000m

N6 horizon

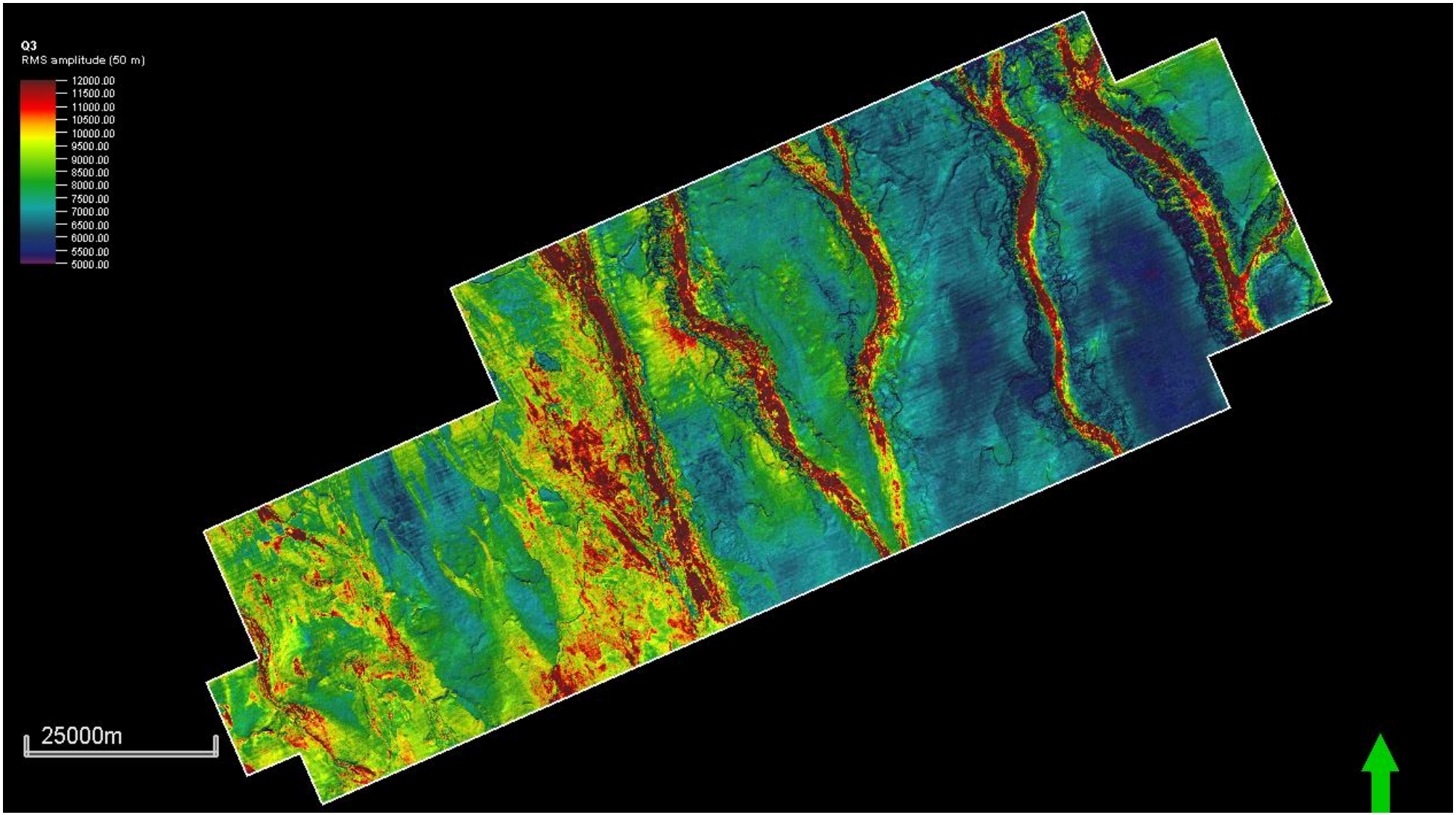
Q3
RMS amplitude (50 m)
12000.00
11500.00
11000.00
10500.00
10000.00
9500.00
9000.00
8500.00
8000.00
7500.00
7000.00
6500.00
6000.00
5500.00
5000.00
25000m

IV. Raw and unannotated versions of coherence maps

P1 horizon

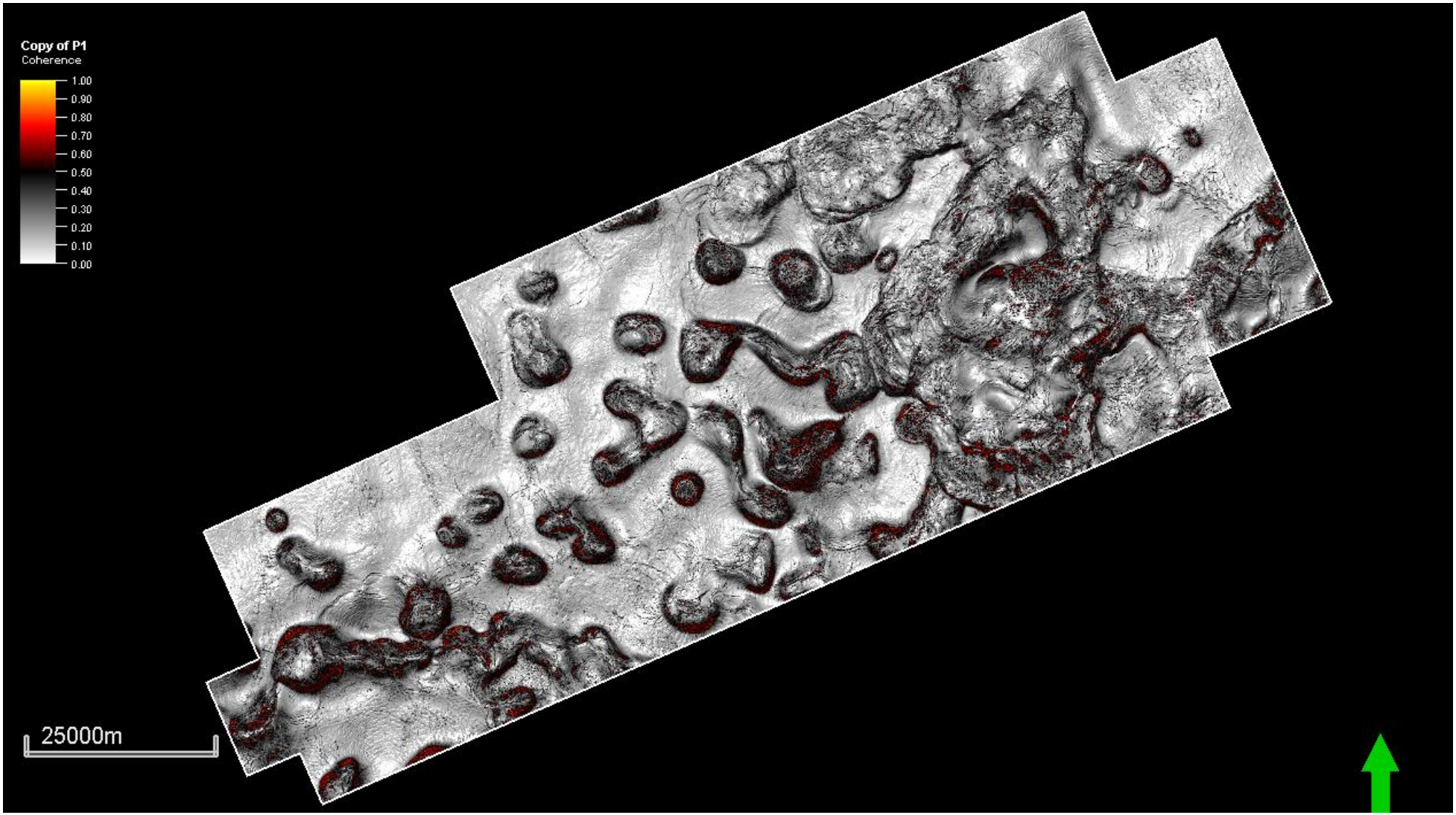

N1 horizon

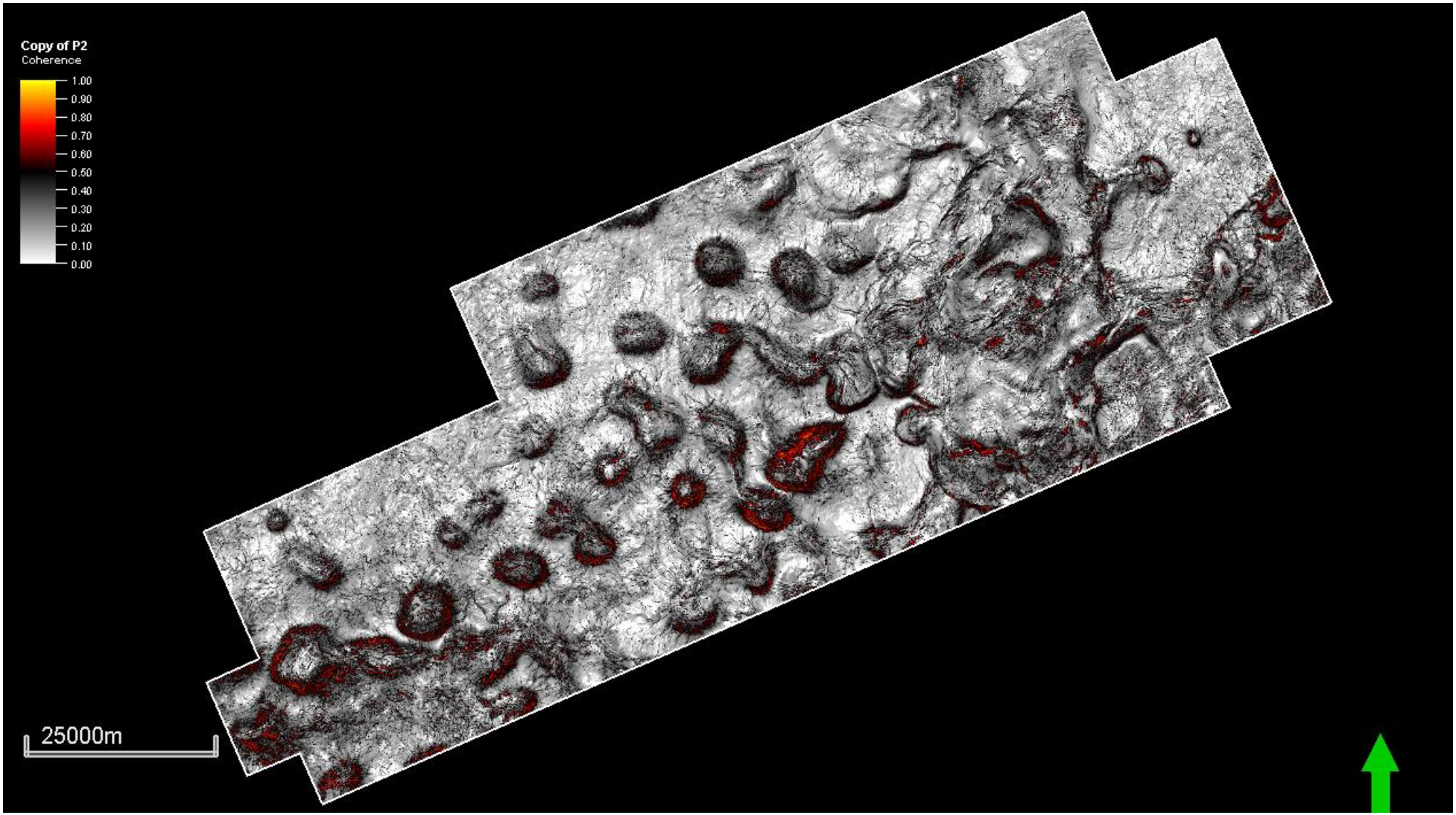
Copy of P2
Coherence
1.00
0.90
0.80
0.70
0.60
0.50
0.40
0.30
0.20
0.10
0.00
25000m

N2 horizon

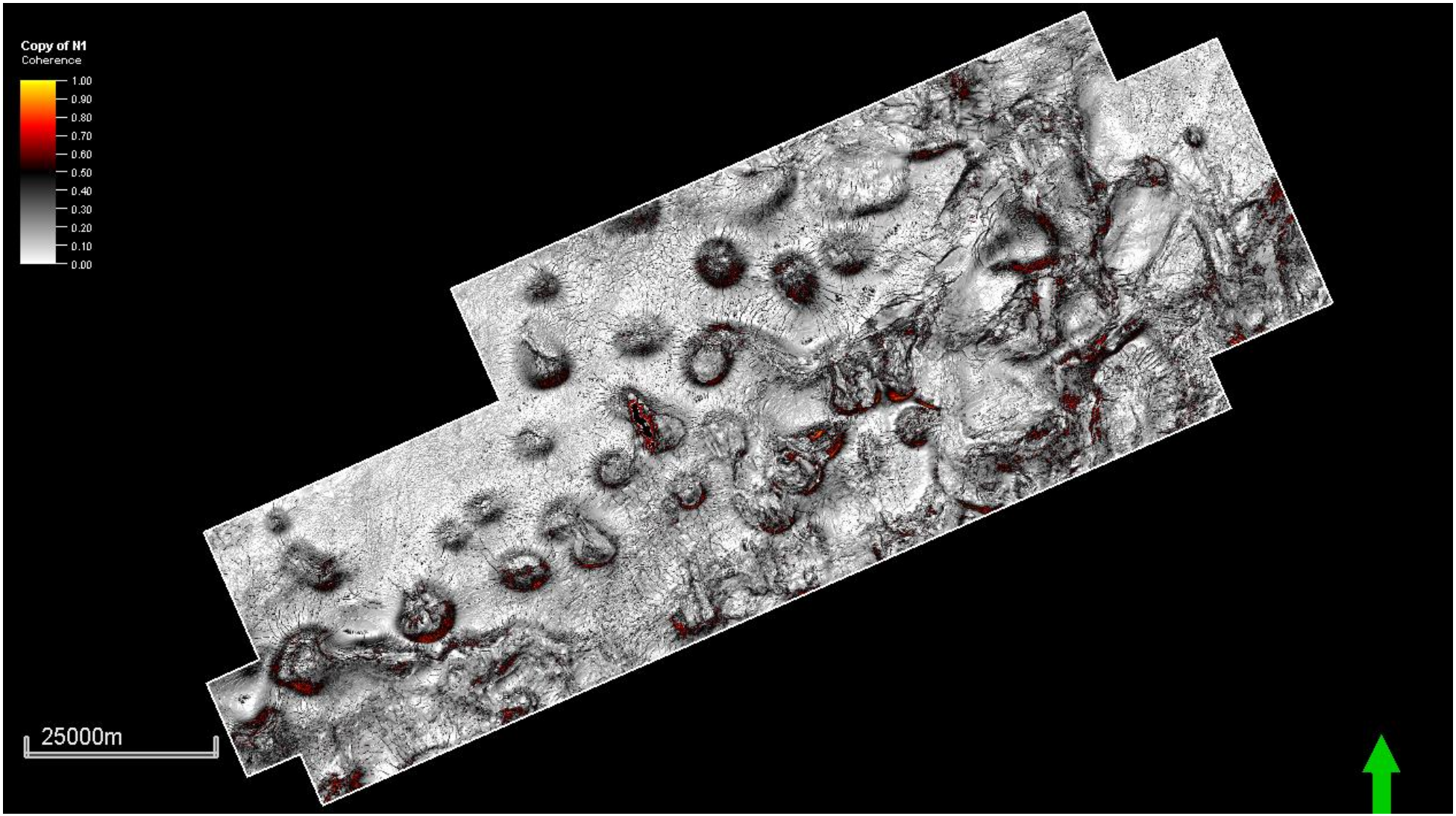
Copy of N1
Coherence
1.00
0.90
0.80
0.70
0.60
0.50
0.40
0.30
0.20
0.10
0.00
25000m

N3 horizon

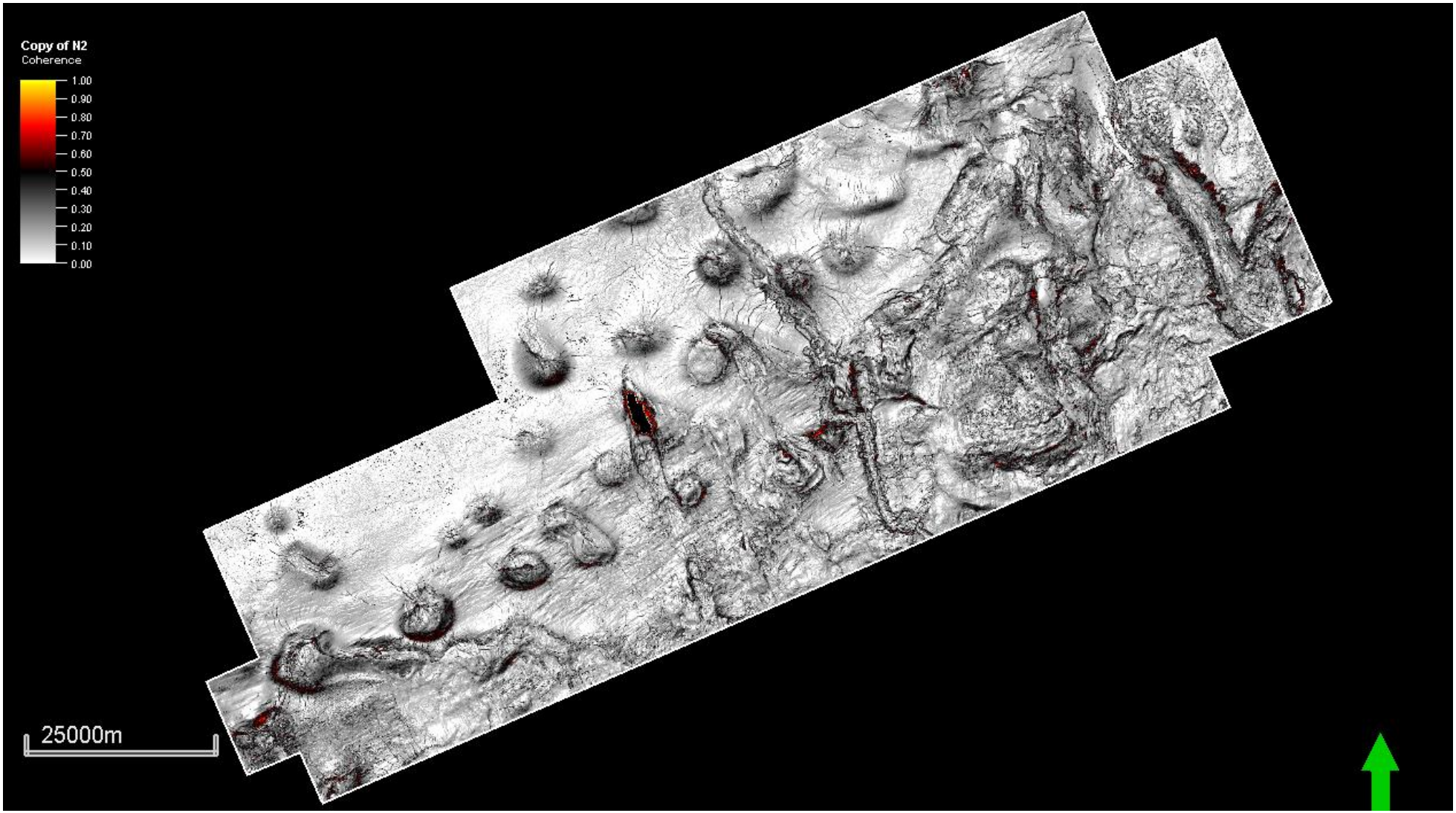
Copy of N2
Coherence
1.00
0.90
0.80
0.70
0.60
0.50
0.40
0.30
0.20
0.10
0.00
25000m

N4 horizon

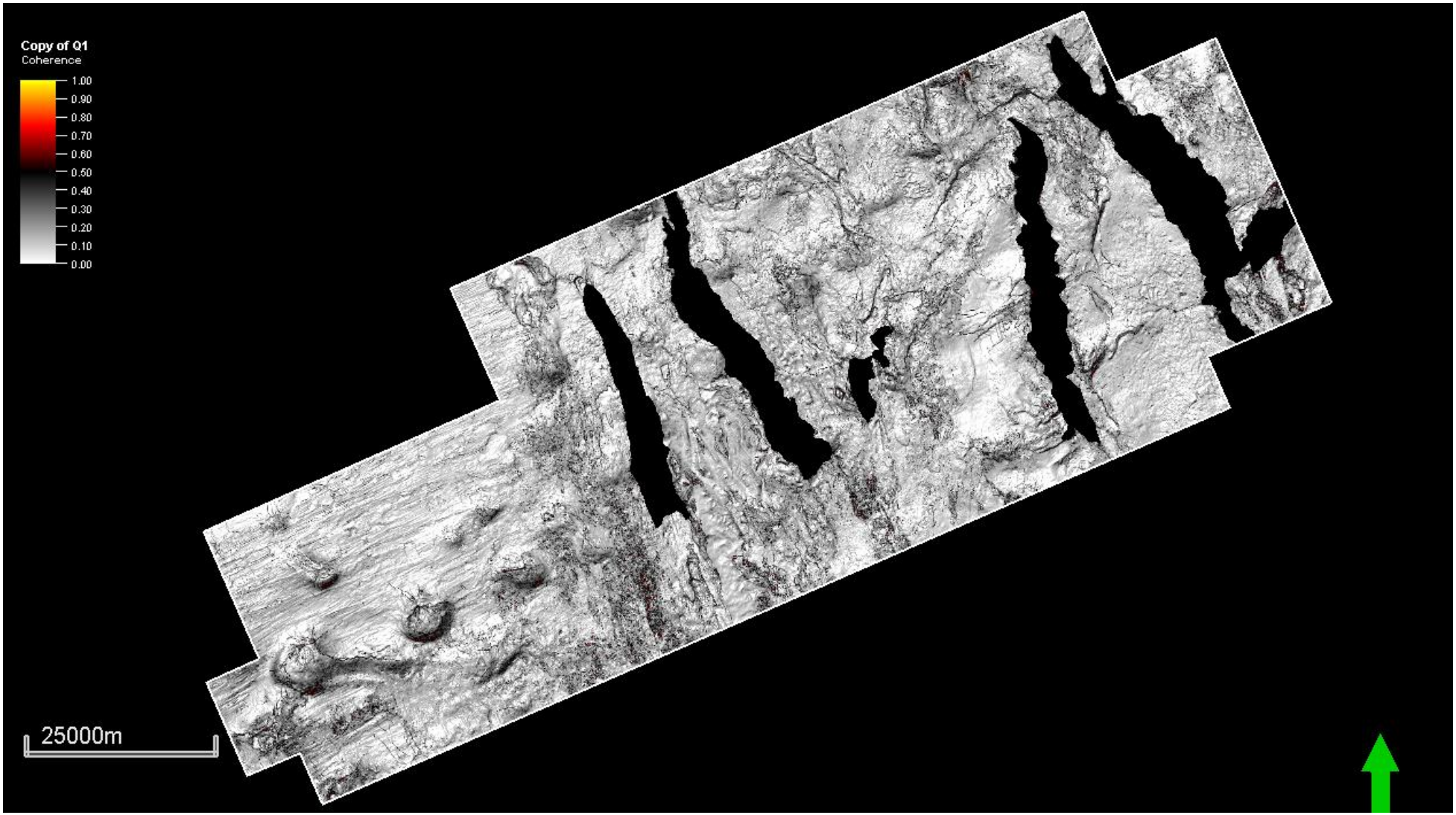
Copy of Q1
Coherence
1.00
0.90
0.80
0.70
0.60
0.50
0.40
0.30
0.20
0.10
0.00
25000m

N5 horizon

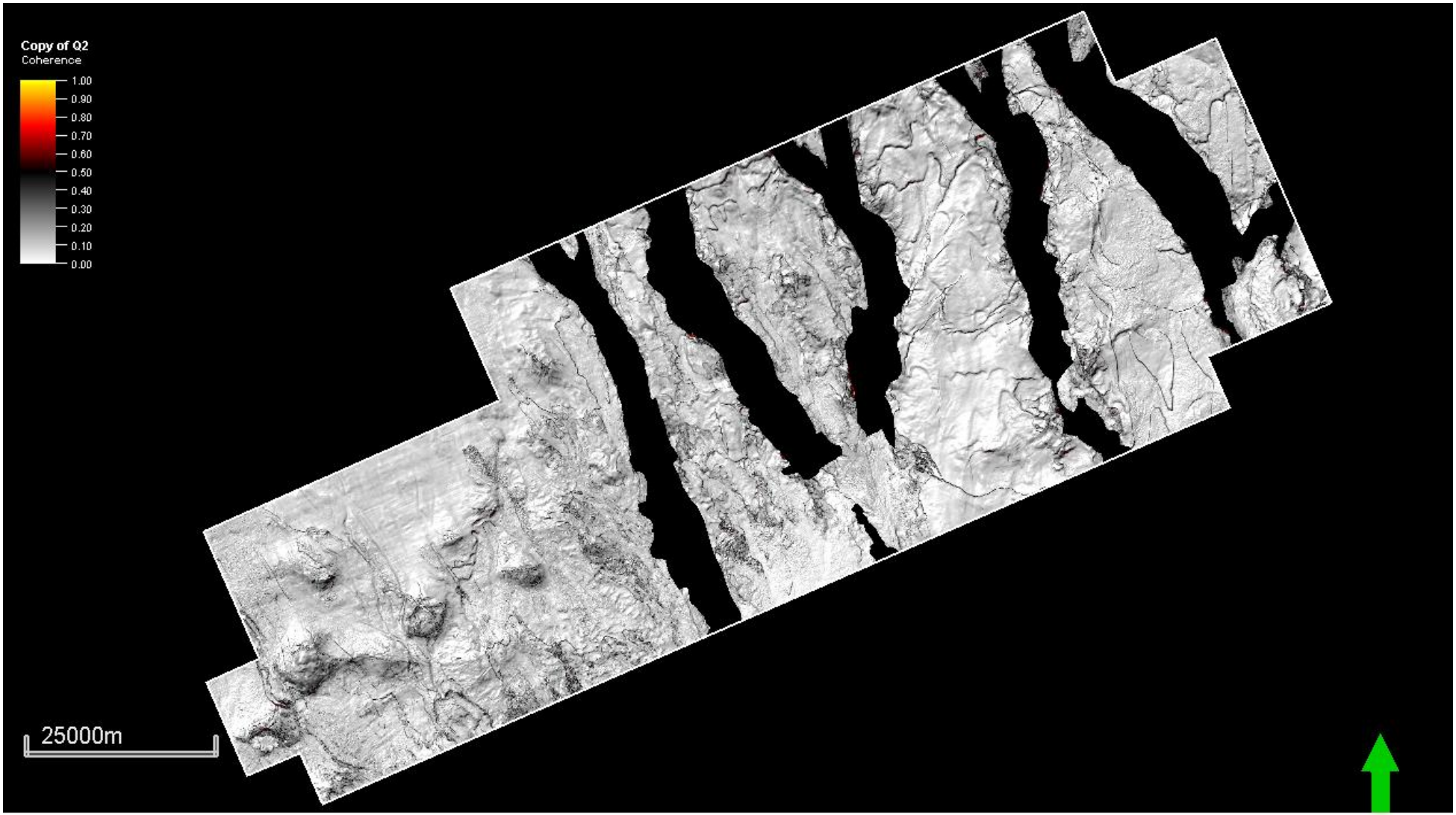
Copy of Q2
Coherence
1.00
0.90
0.80
0.70
0.60
0.50
0.40
0.30
0.20
0.10
0.00
25000m

N6 horizon

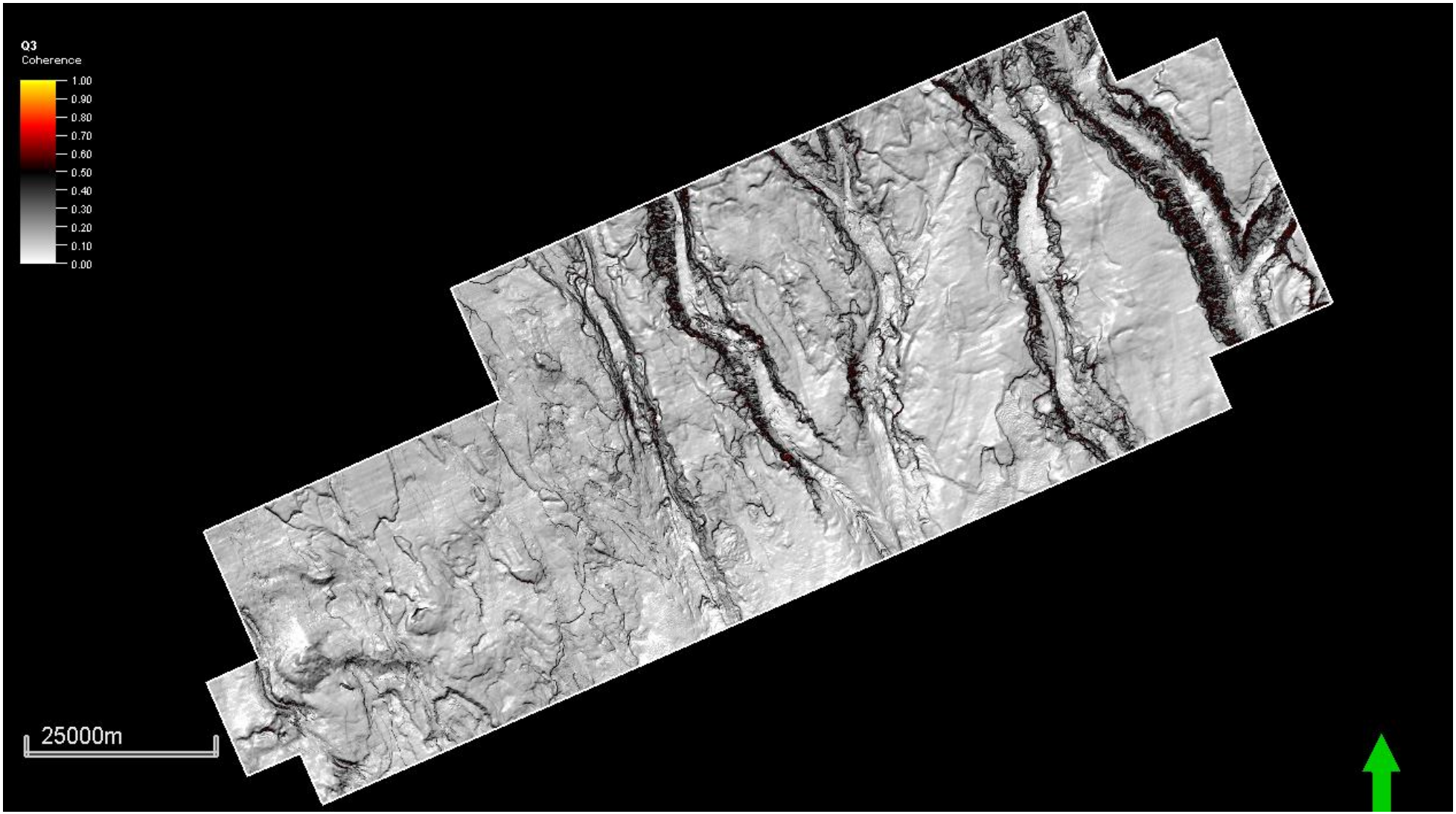
Q3
Coherence
1.00
0.90
0.80
0.70
0.60
0.50
0.40
0.30
0.20
0.10
0.00
25000m

V. Raw and unannotated versions of isochore maps

Unit 1

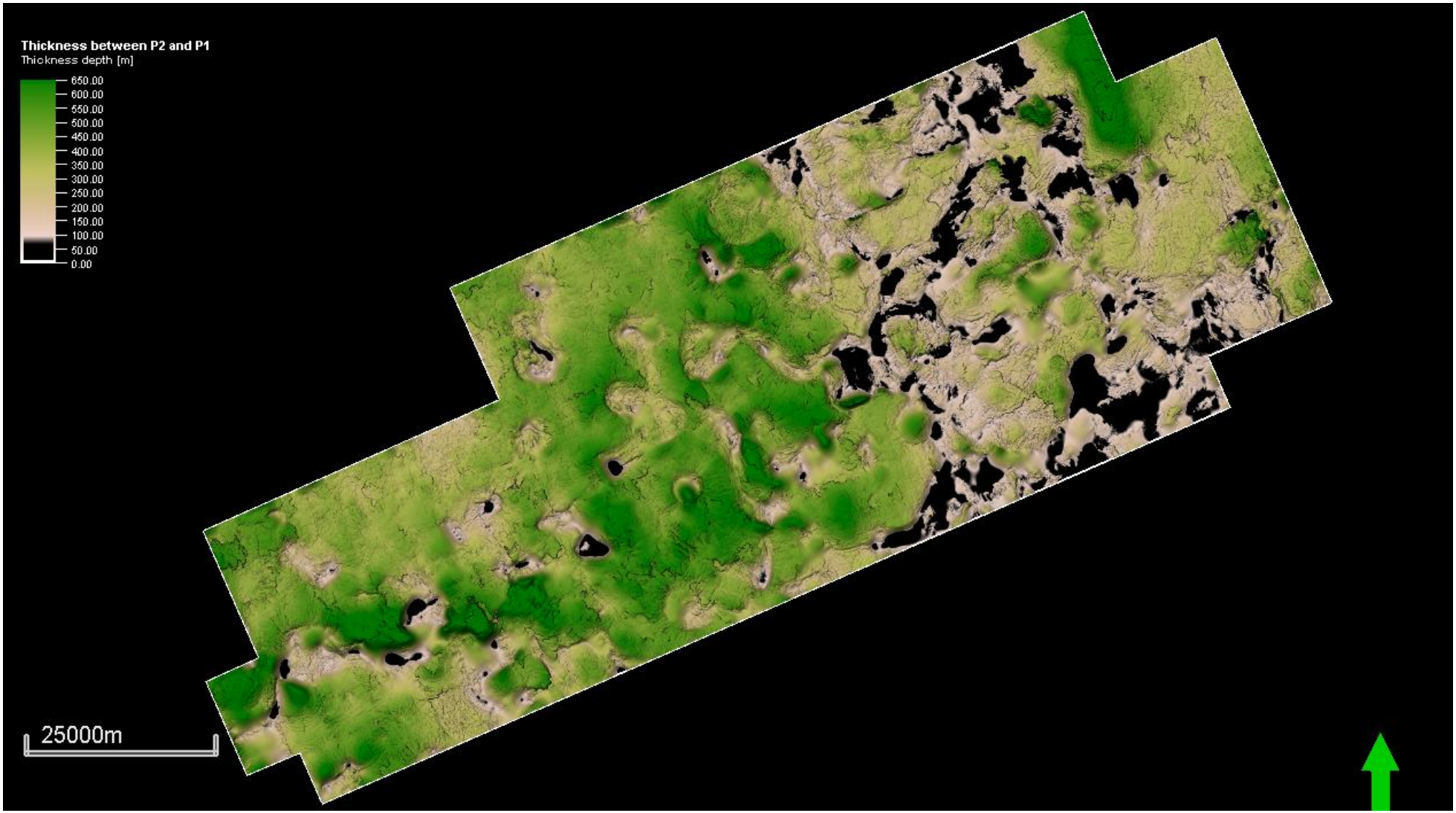

Unit 2

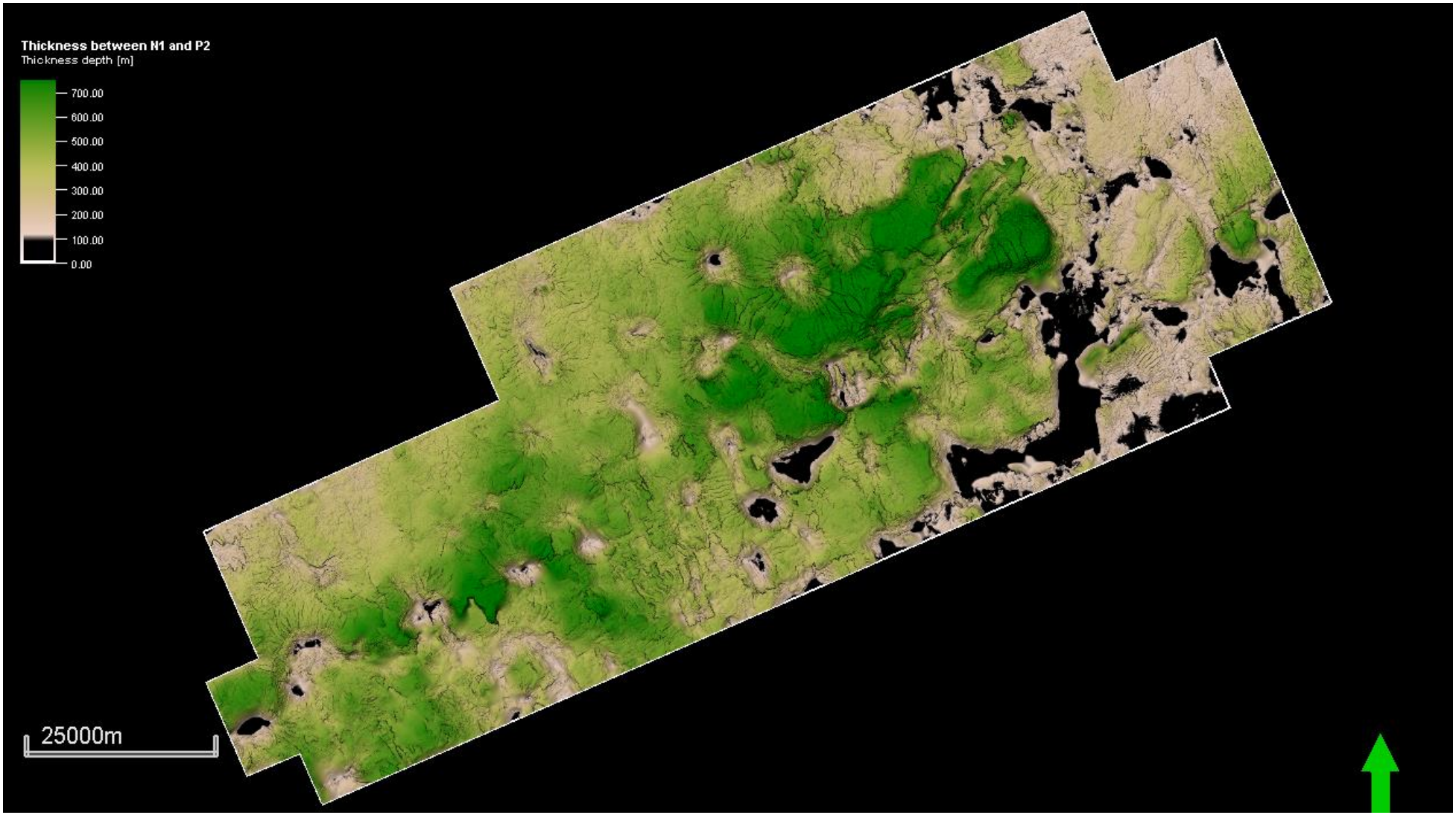
Thickness between N1 and P2
Thickness depth [m]
700.00
600.00
500.00
400.00
300.00
200.00
100.00
0.00
25000m

Unit 3

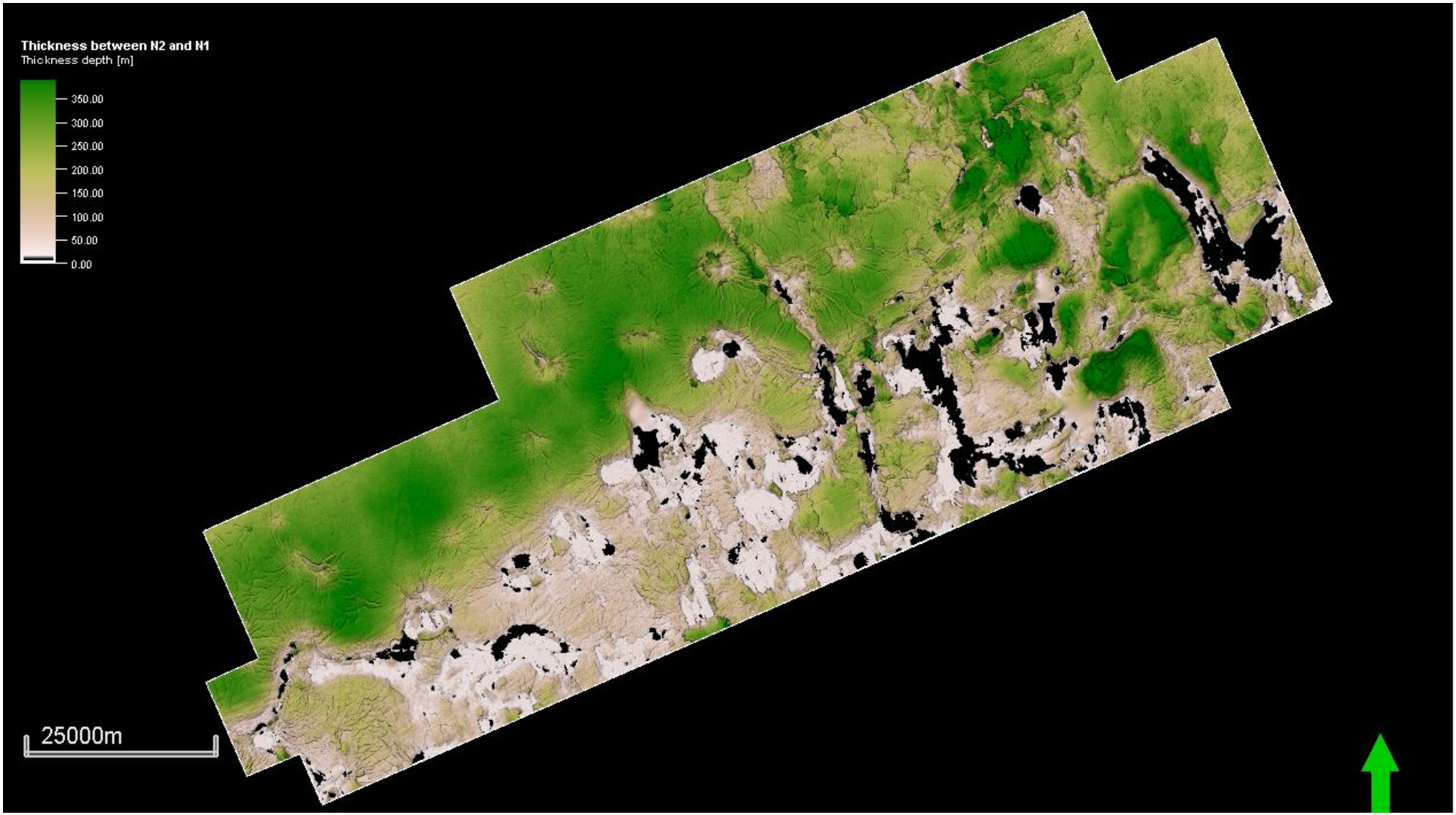
Thickness between N2 and N1
Thickness depth [m]
350.00
300.00
250.00
200.00
150.00
100.00
50.00
0.00
25000m

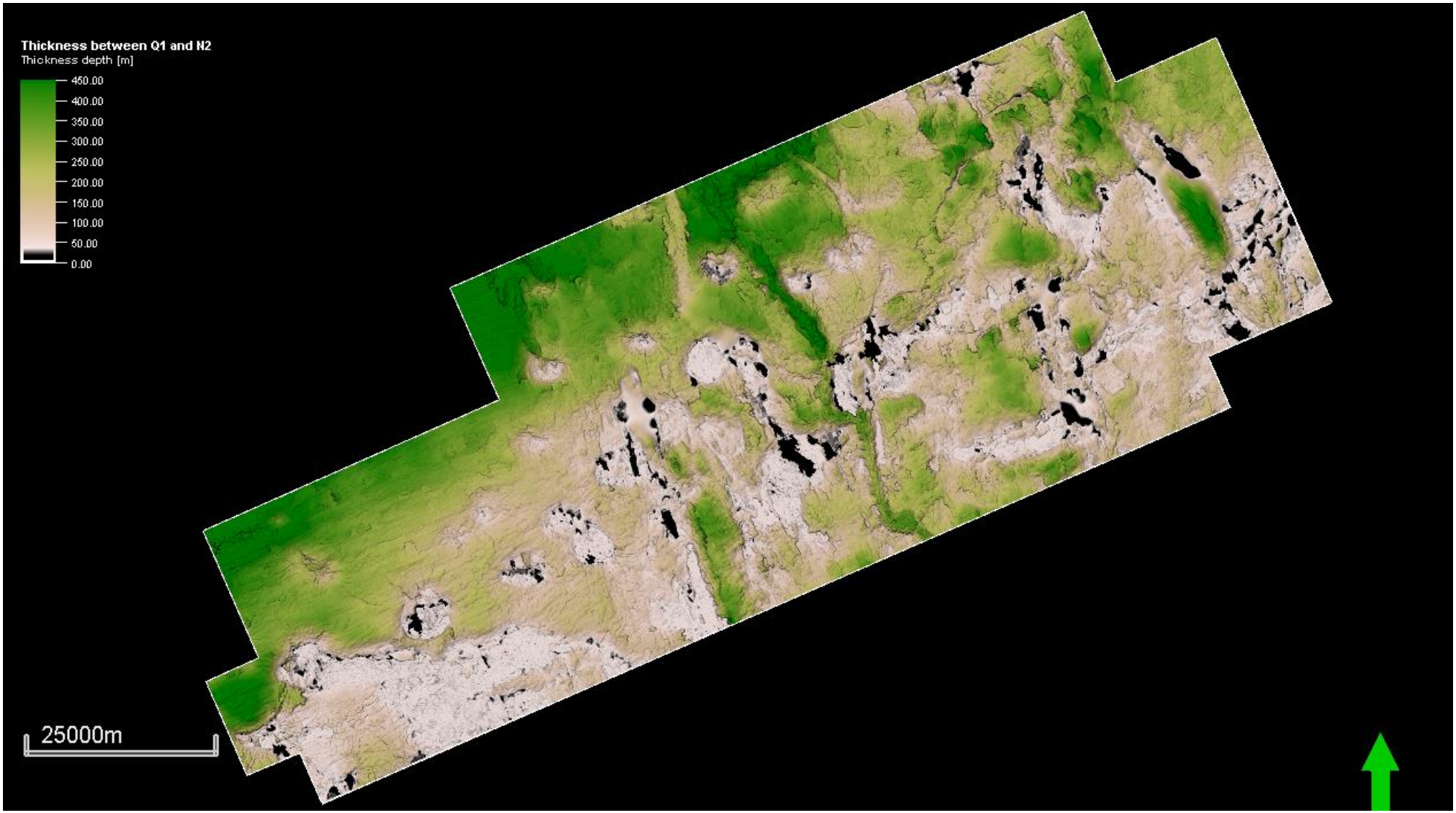
Thickness between Q1 and N2
Thickness depth [m]
450.00
400.00
350.00
300.00
250.00
200.00
150.00
100.00
50.00
0.00
25000m

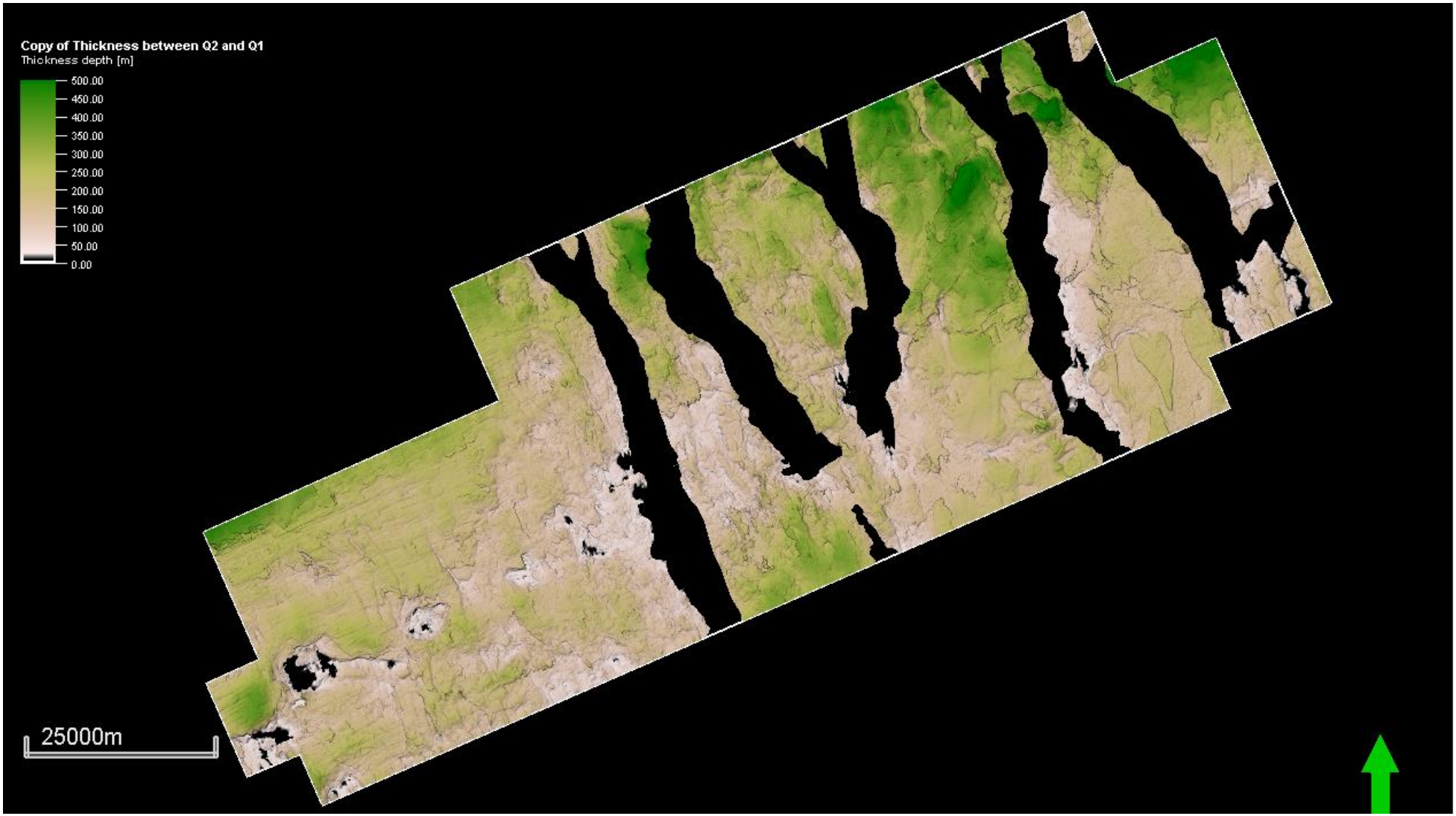
Copy of Thickness between Q2 and Q1
Thickness depth [m]
500.00
450.00
400.00
350.00
300.00
250.00
200.00
150.00
100.00
50.00
0.00
25000m

Unit 6

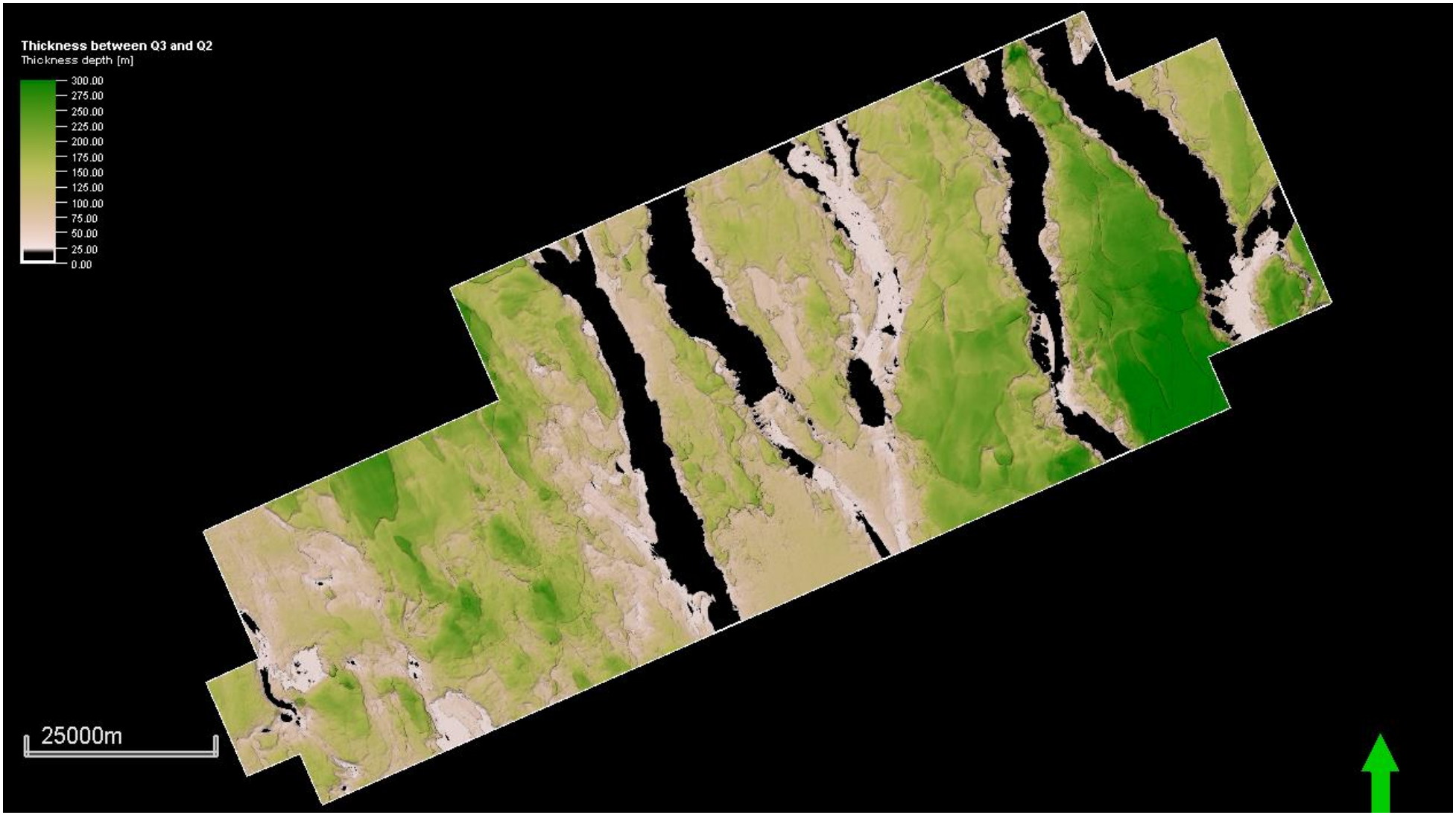
Thickness between Q3 and Q2
Thickness depth [m]
300.00
275.00
250.00
225.00
200.00
175.00
150.00
125.00
100.00
75.00
50.00
25.00
0.00
25000m

VI. Raw and unannotated versions of seismic profiles

A-A’ (dip-oriented)

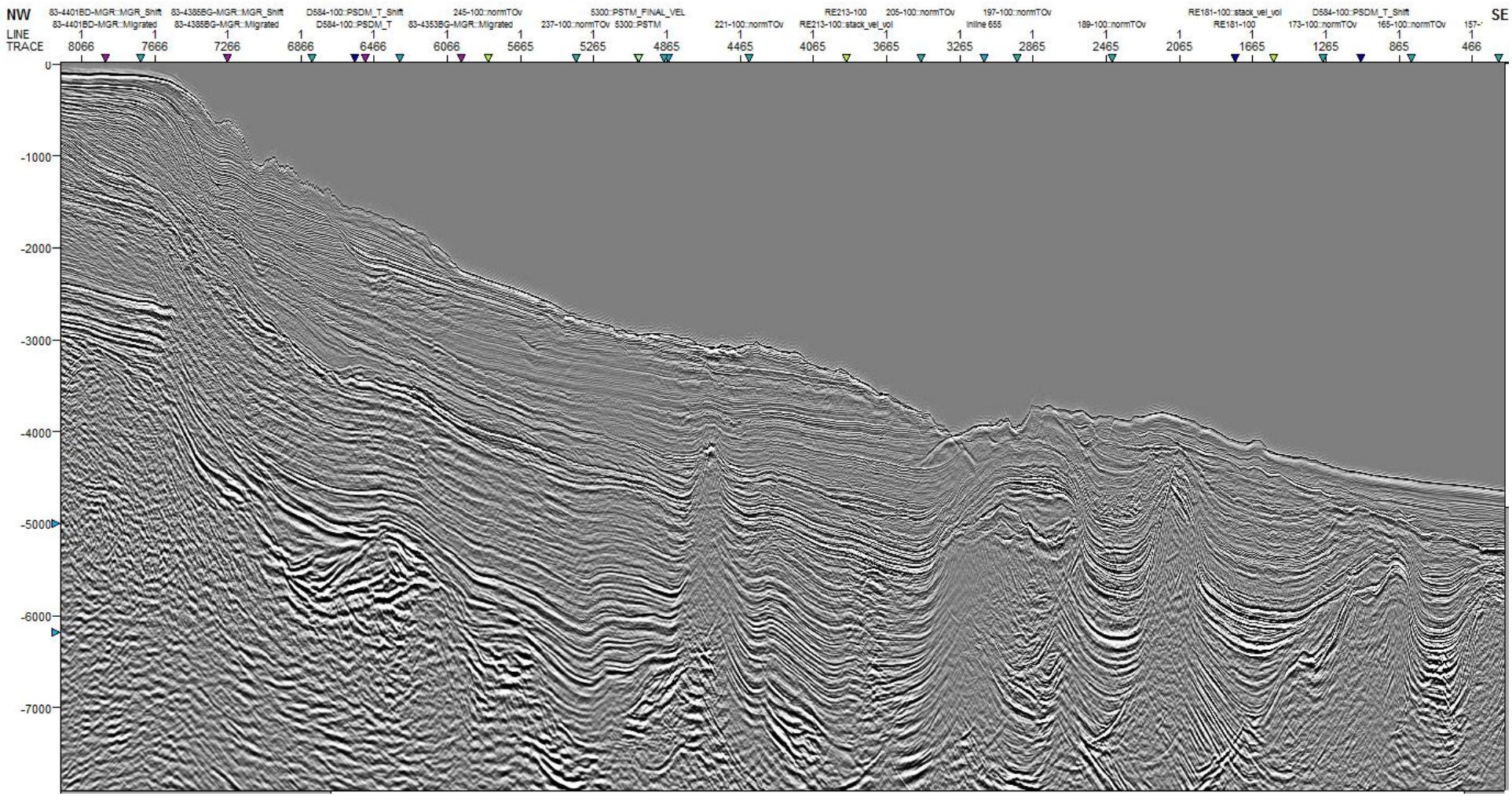

B-B’ (strike-oriented)

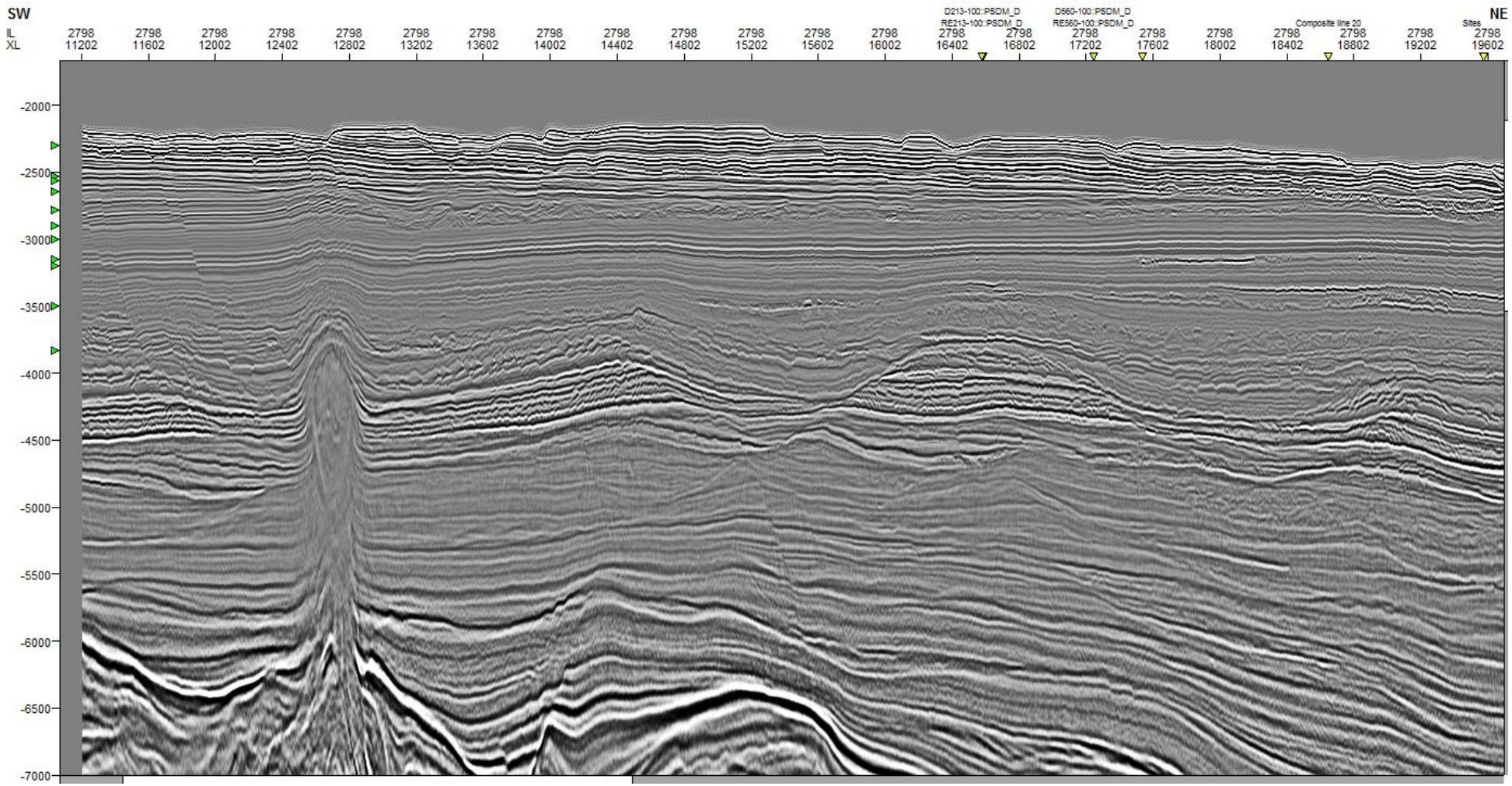

C-C’ (strike-oriented)

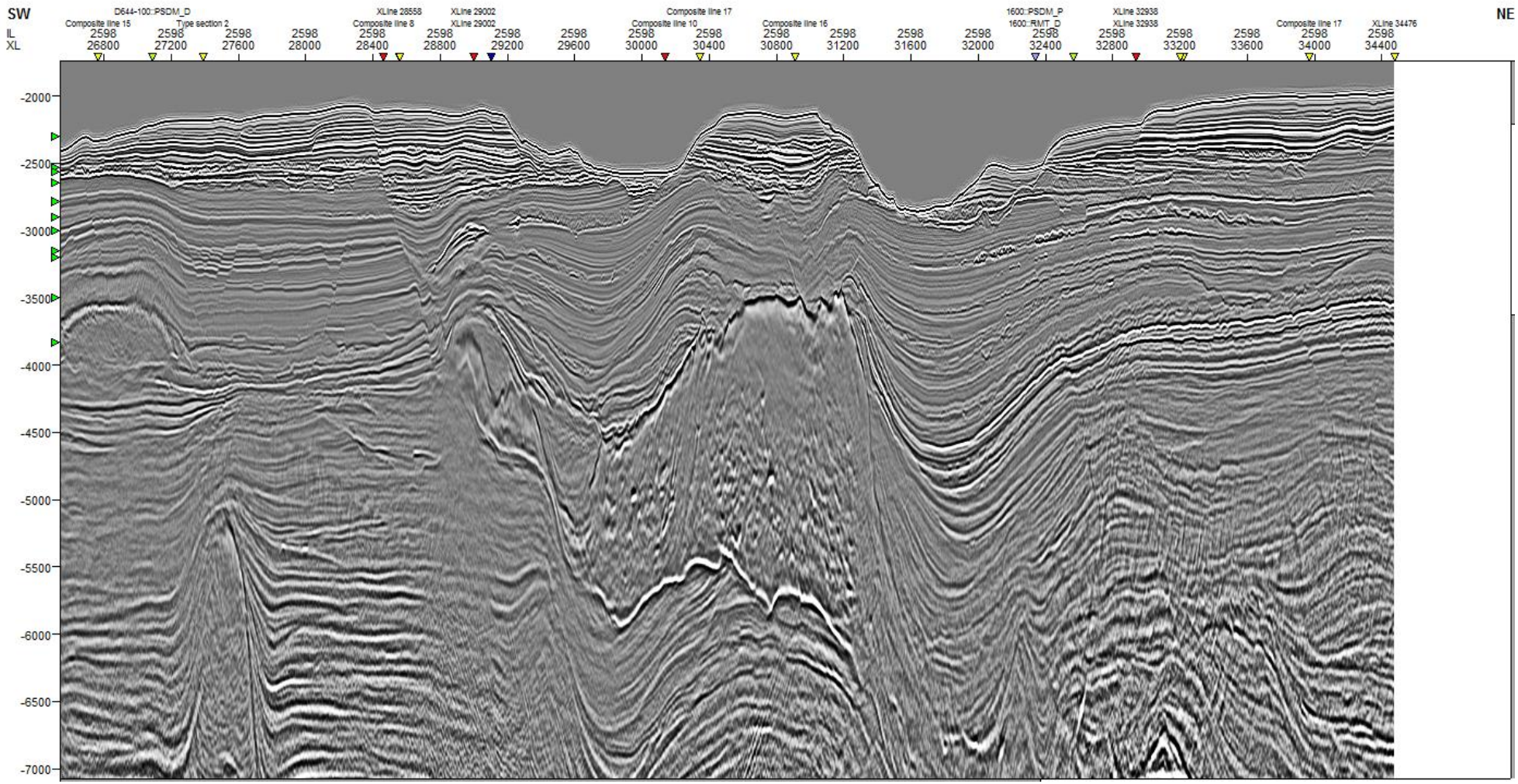

D-D’ (strike-oriented)

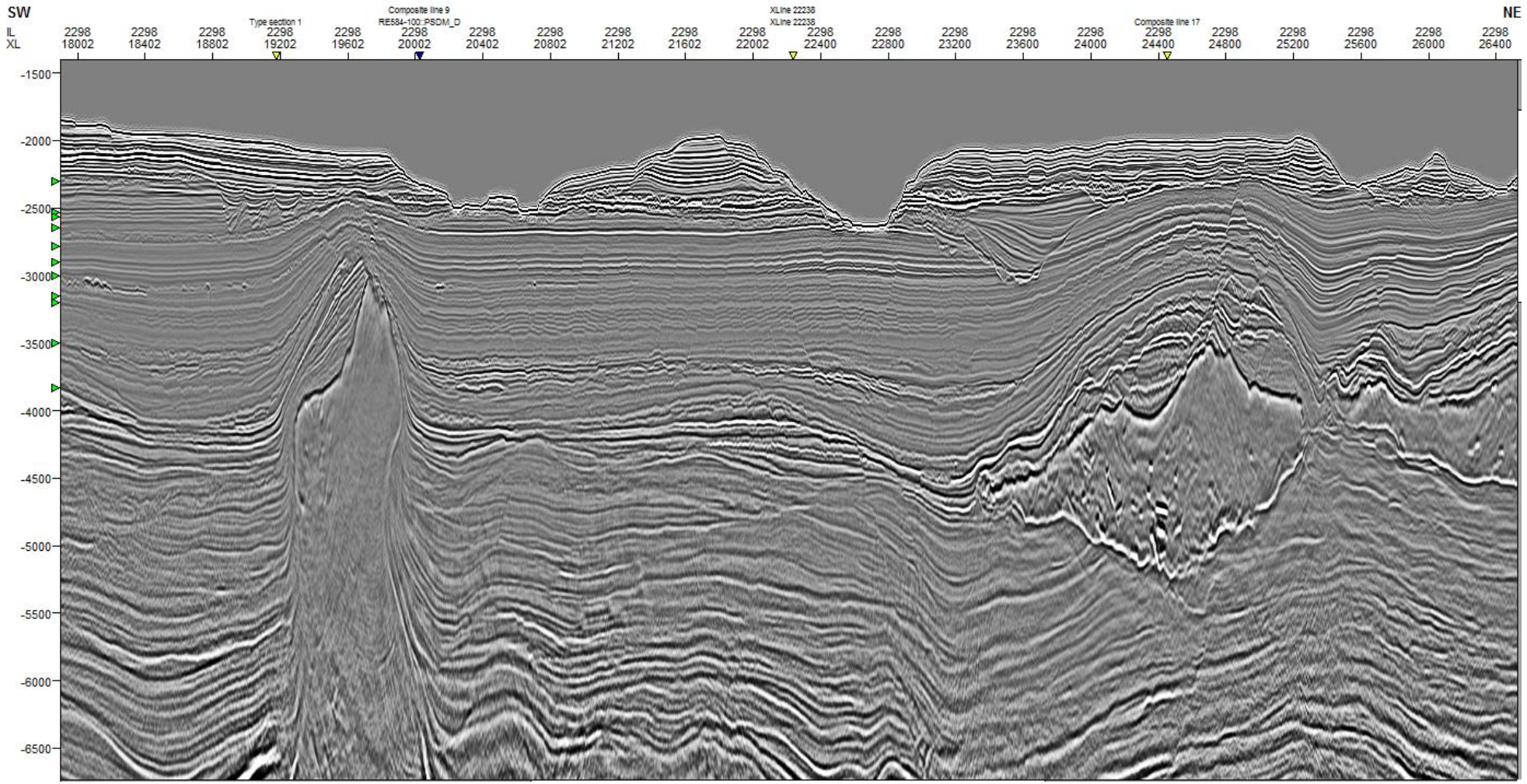

E-E’ (dip-oriented)

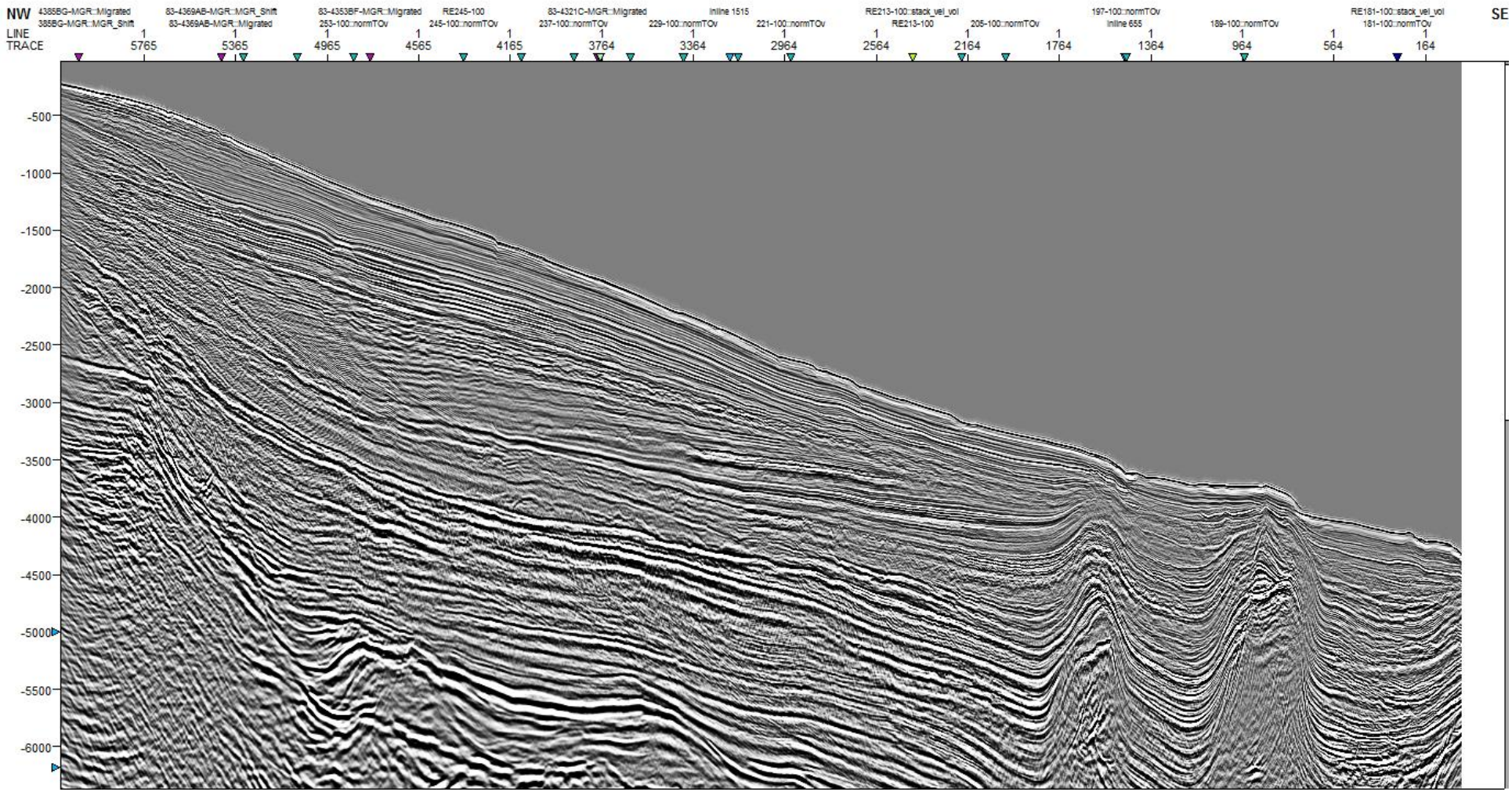

F-F’ (dip-oriented)

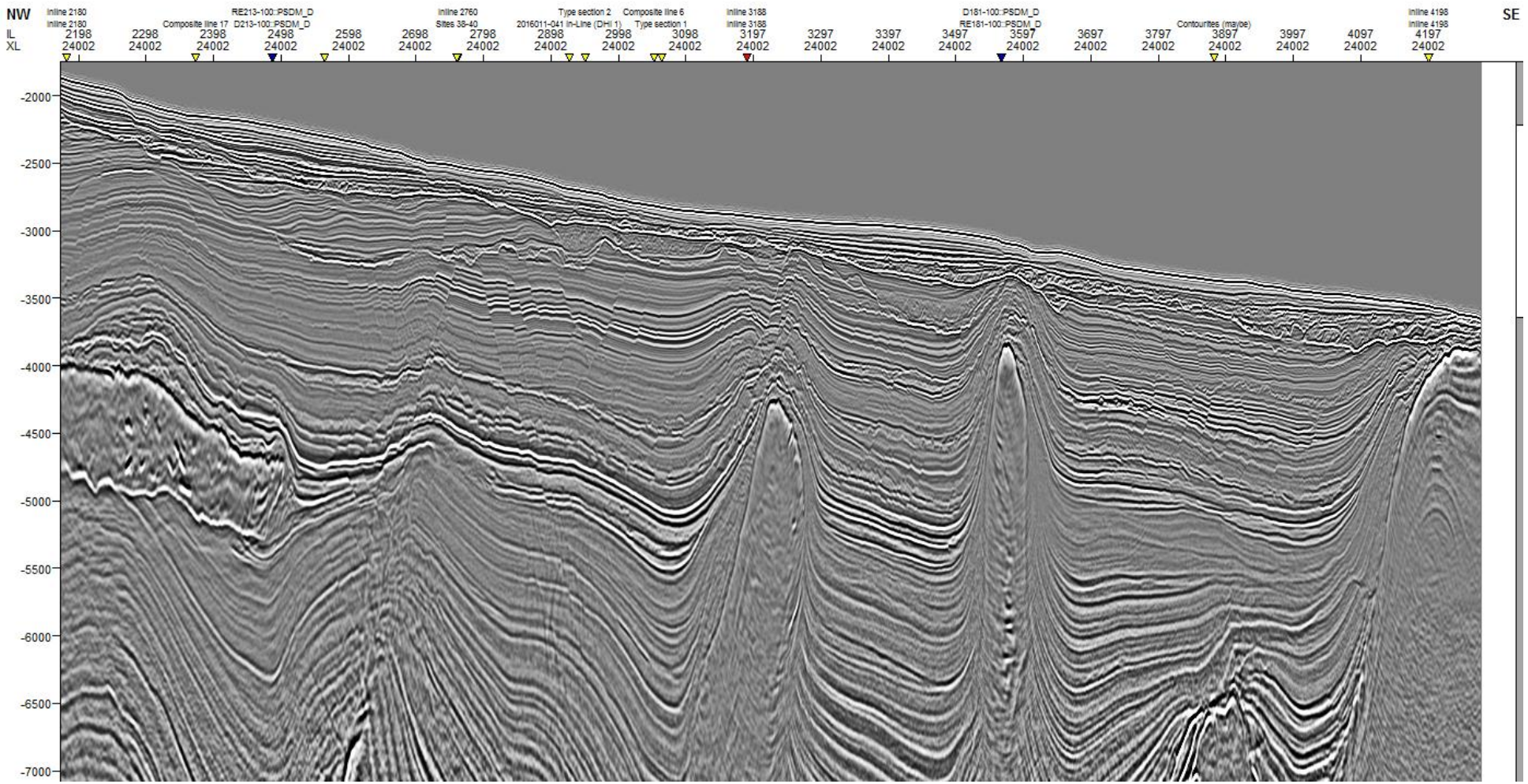

G-G’ (dip-oriented)

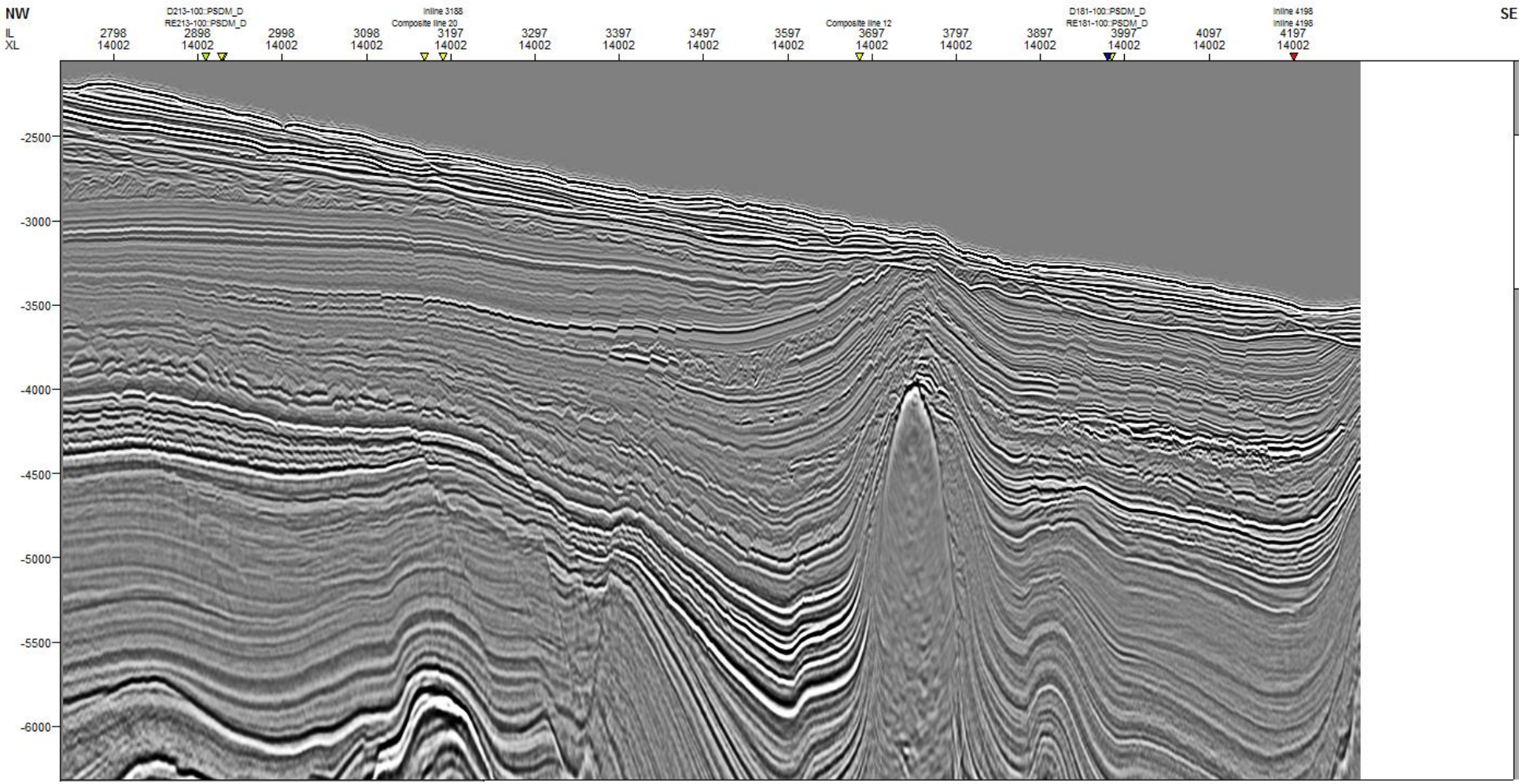

H-H’ (dip-oriented)

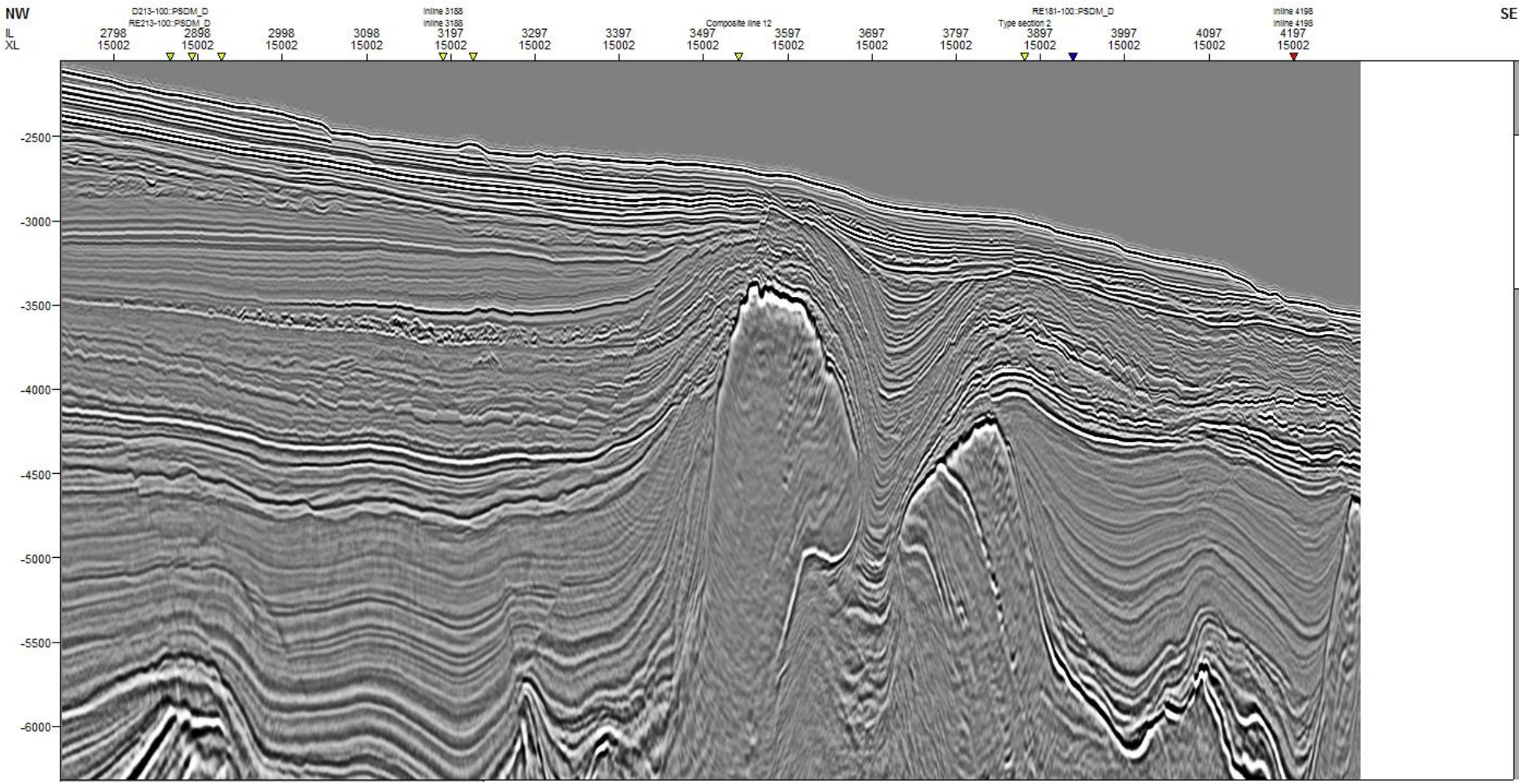

I-I’ (composite line)

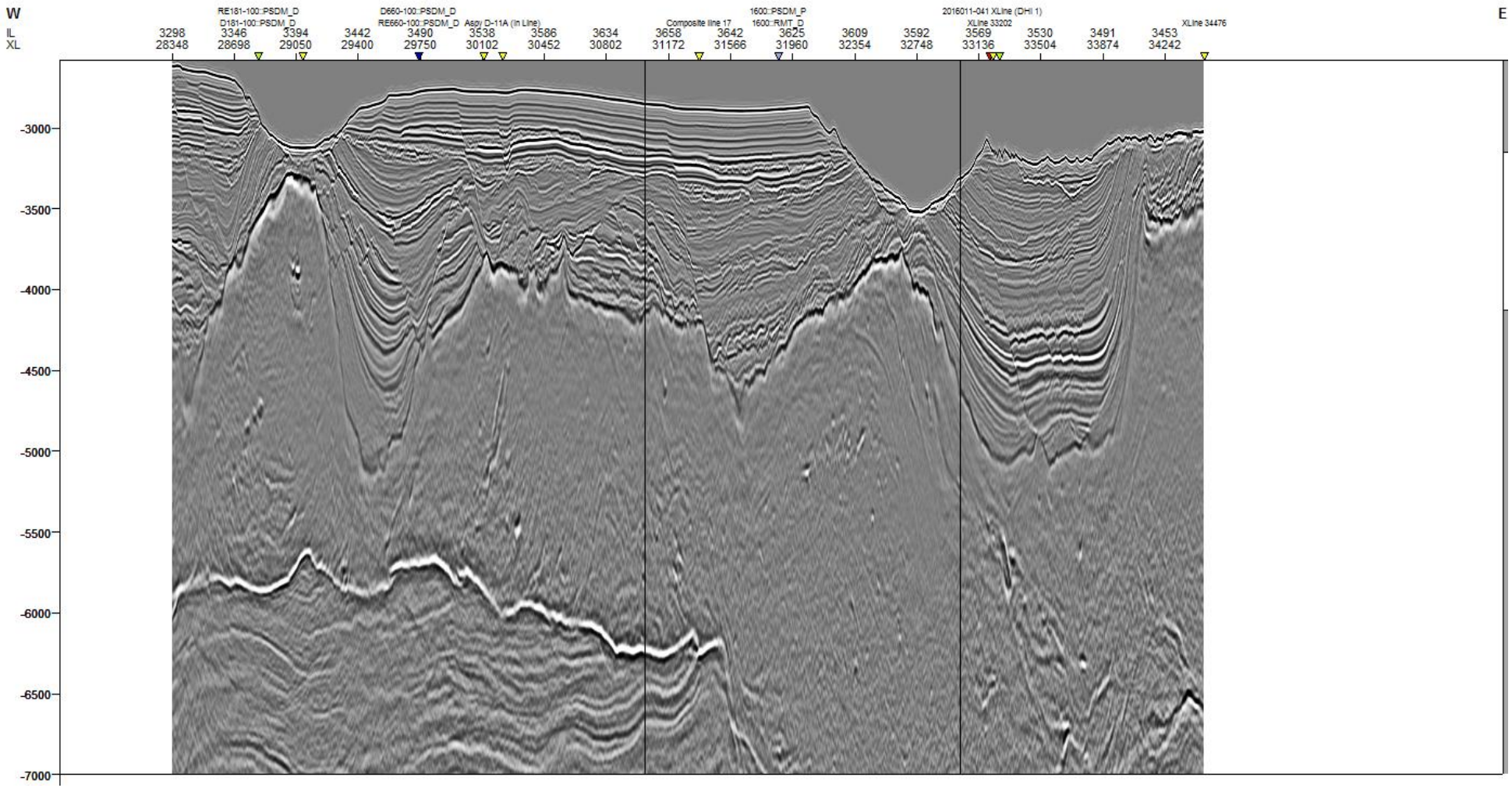

J-J’ (composite line)

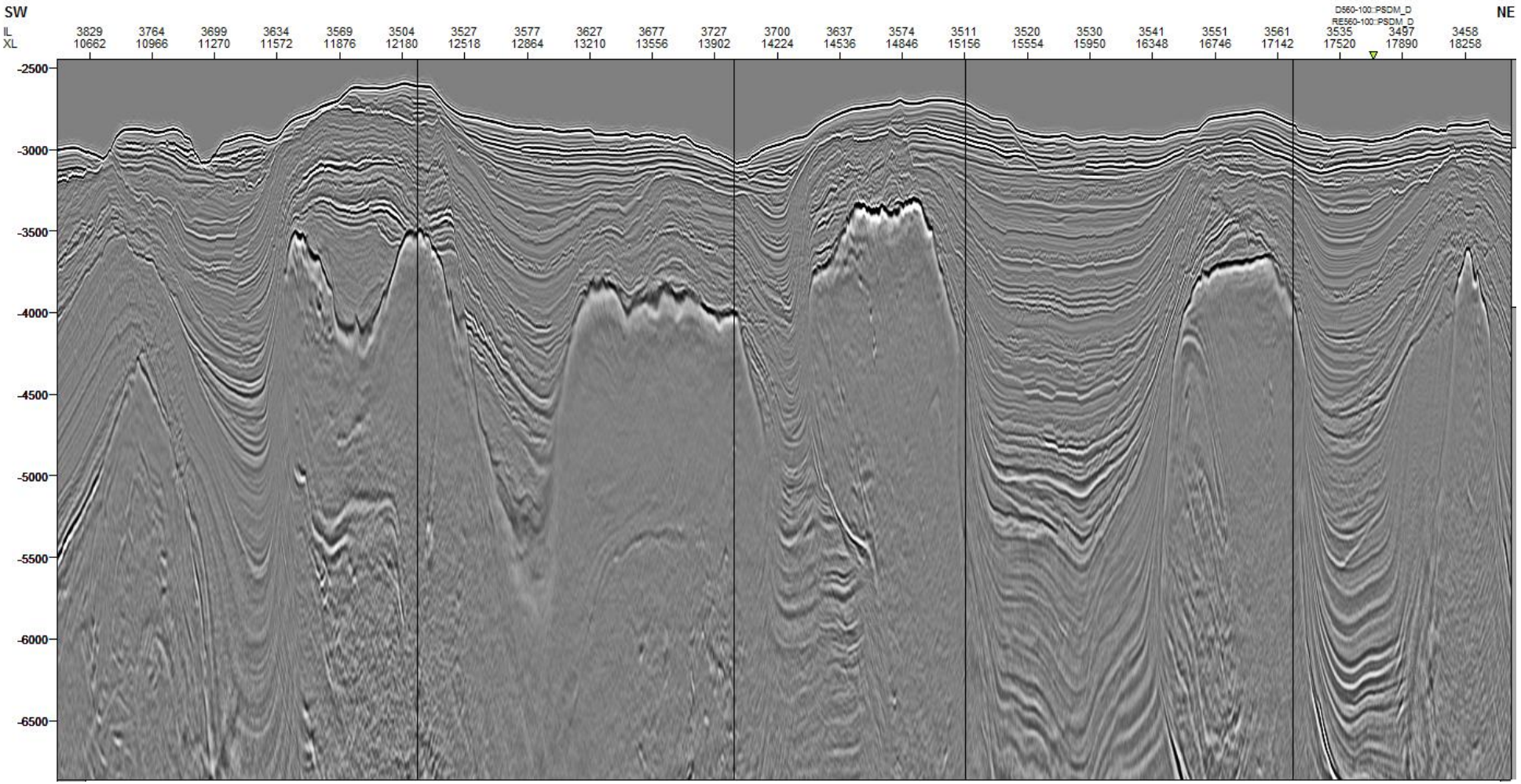

K-K’ (composite line)

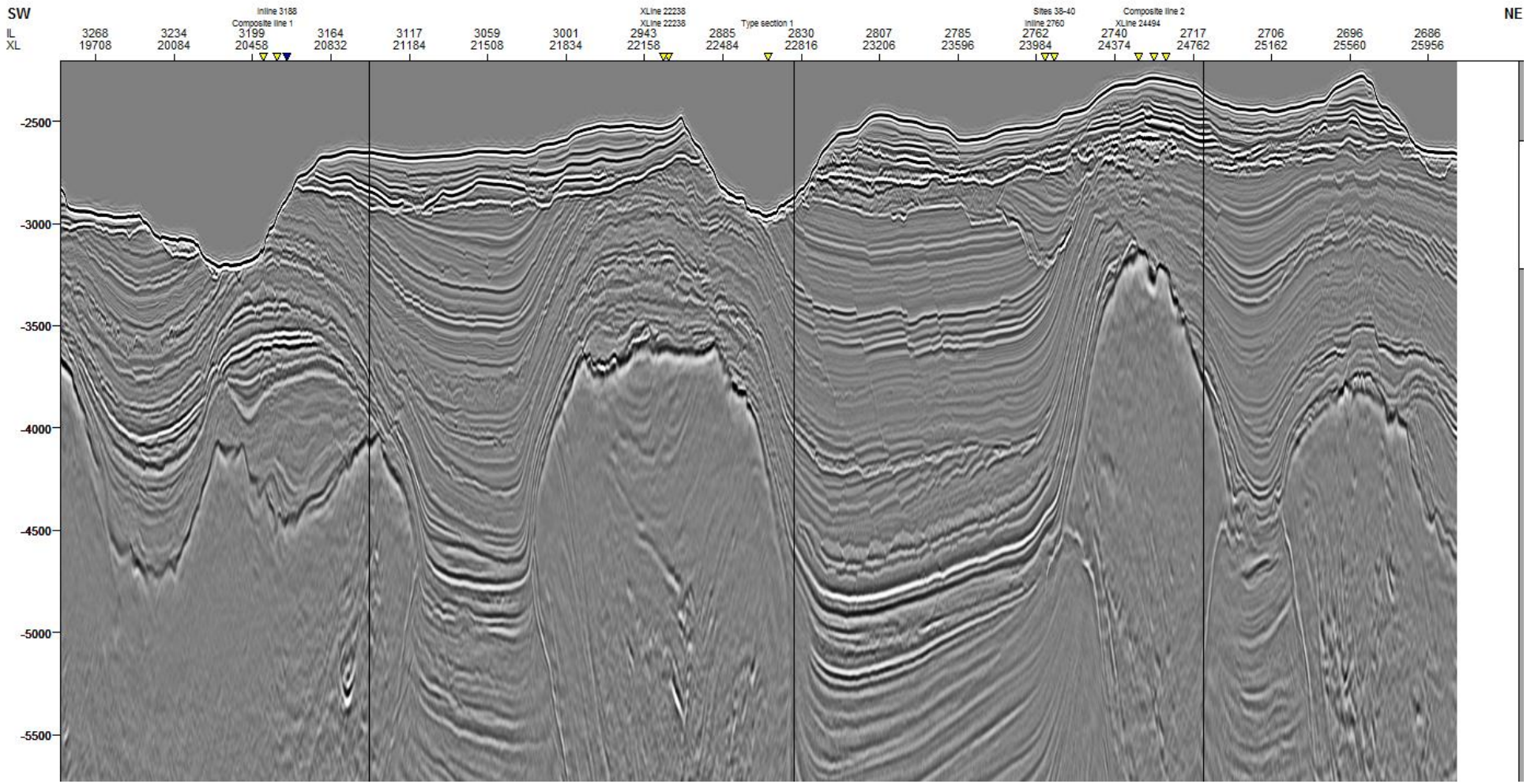

L-L’ (composite line)

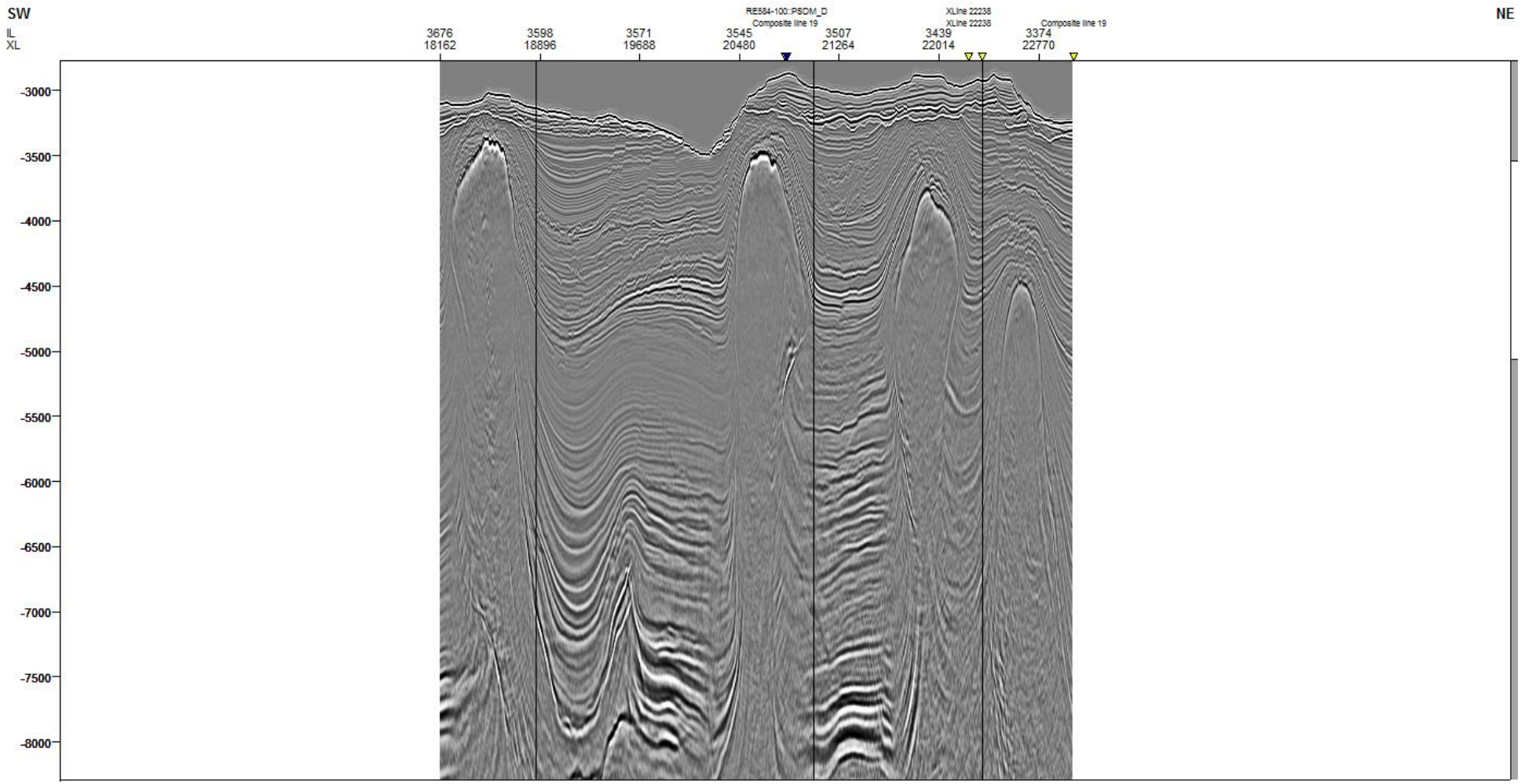

M-M’ (composite line)

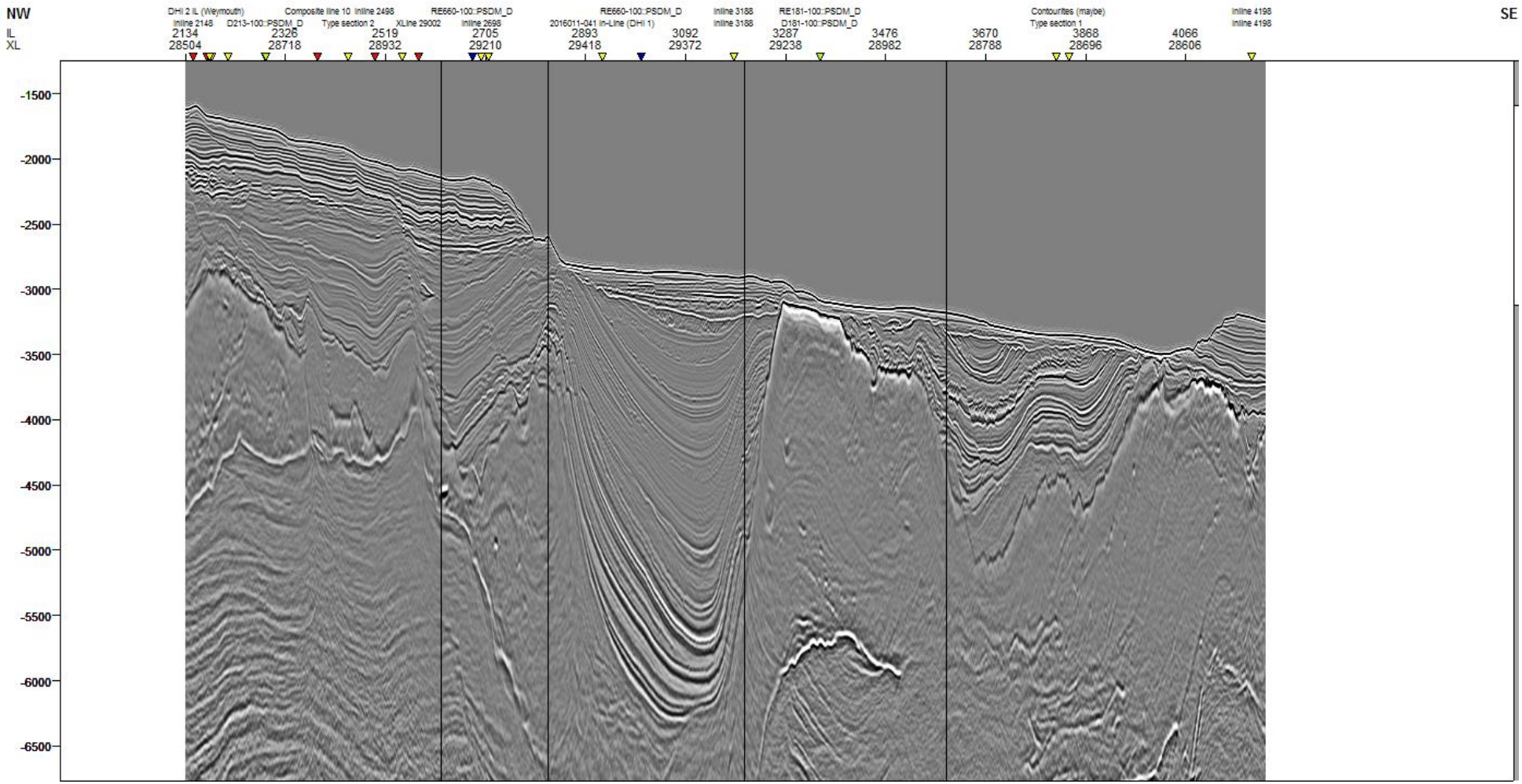

N-N’ (composite line)

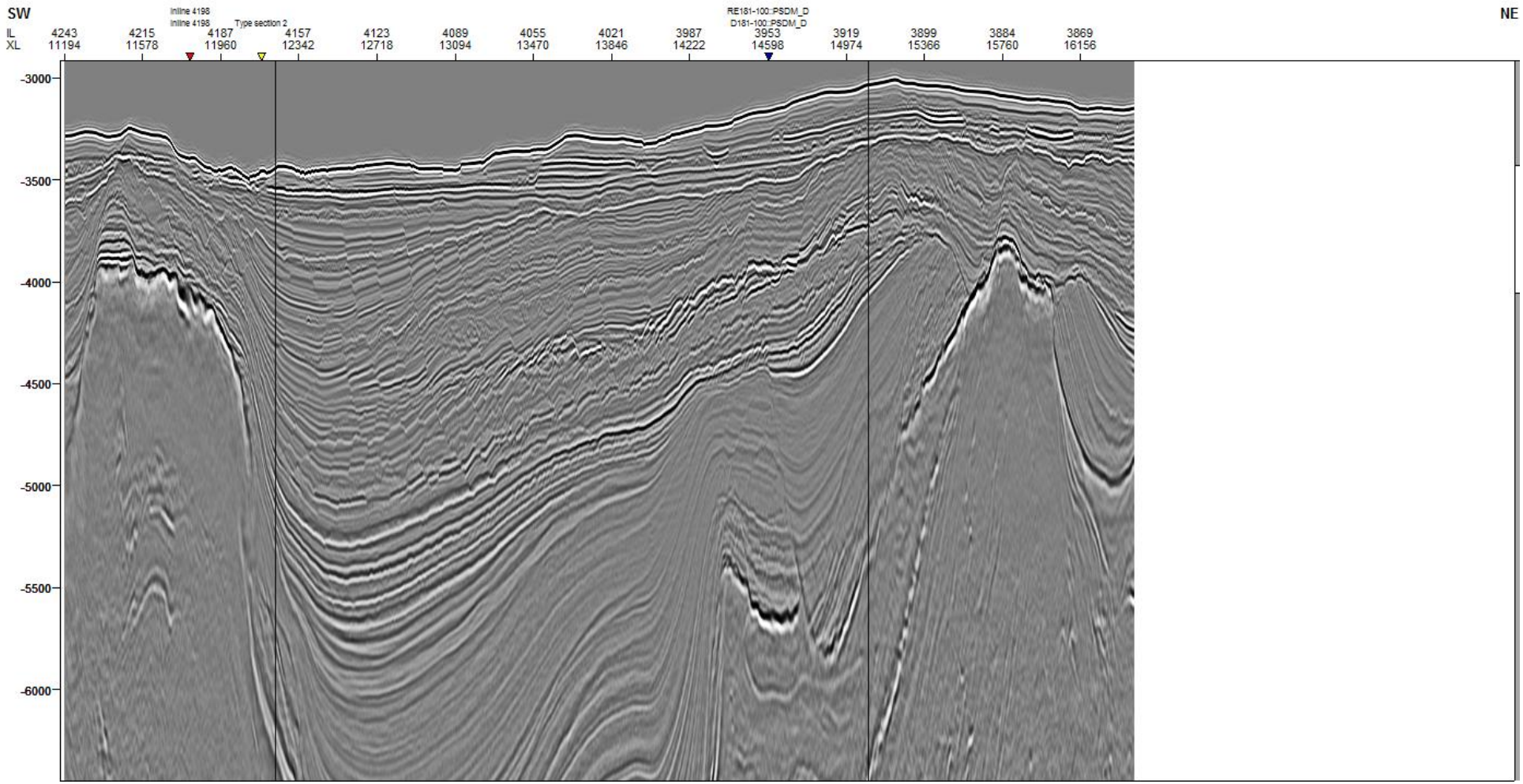

O-O’ (shallow; strike-oriented)

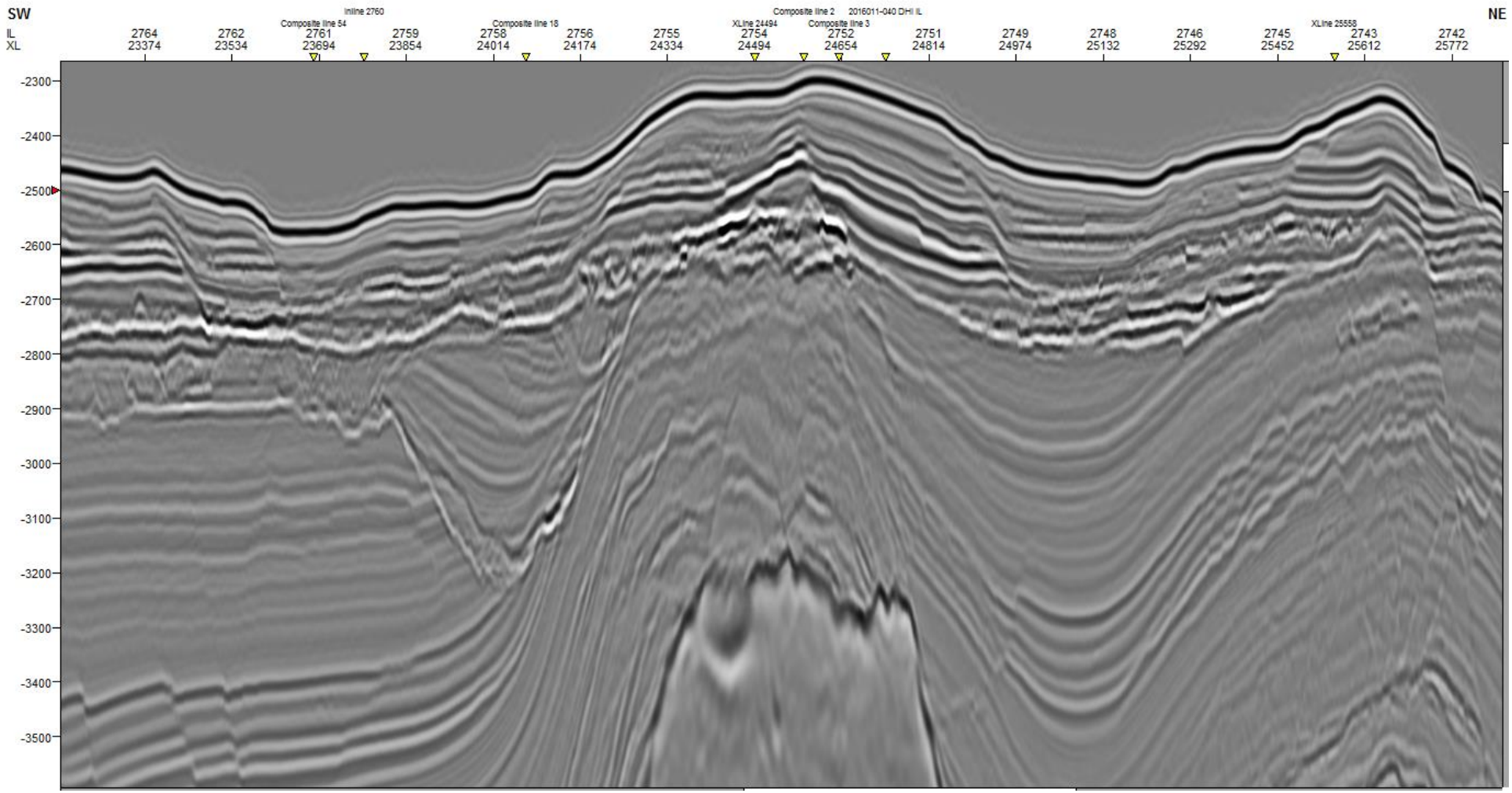

O-O’ (deeper; strike-oriented)

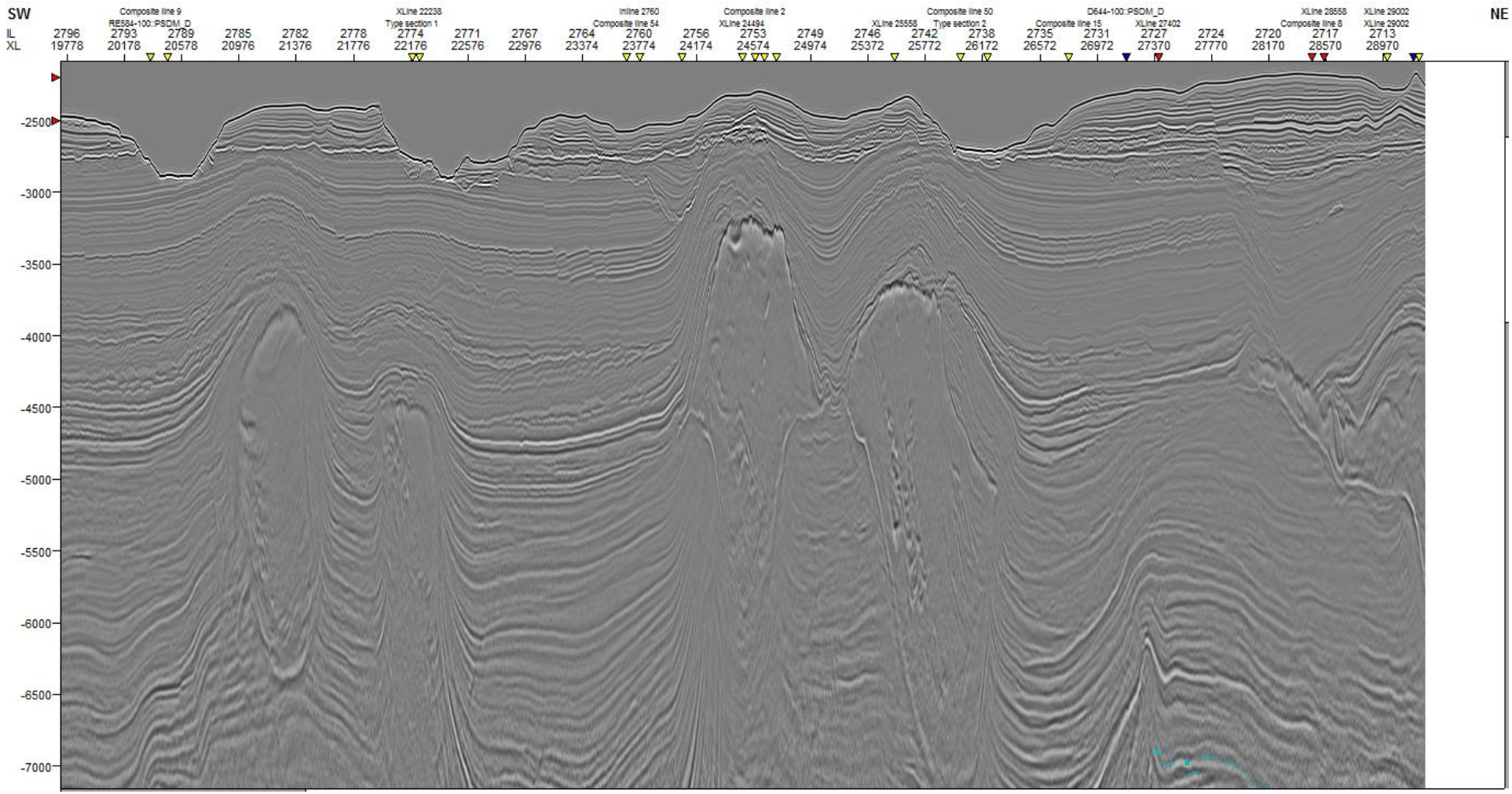

P-P’ (dip-oriented)

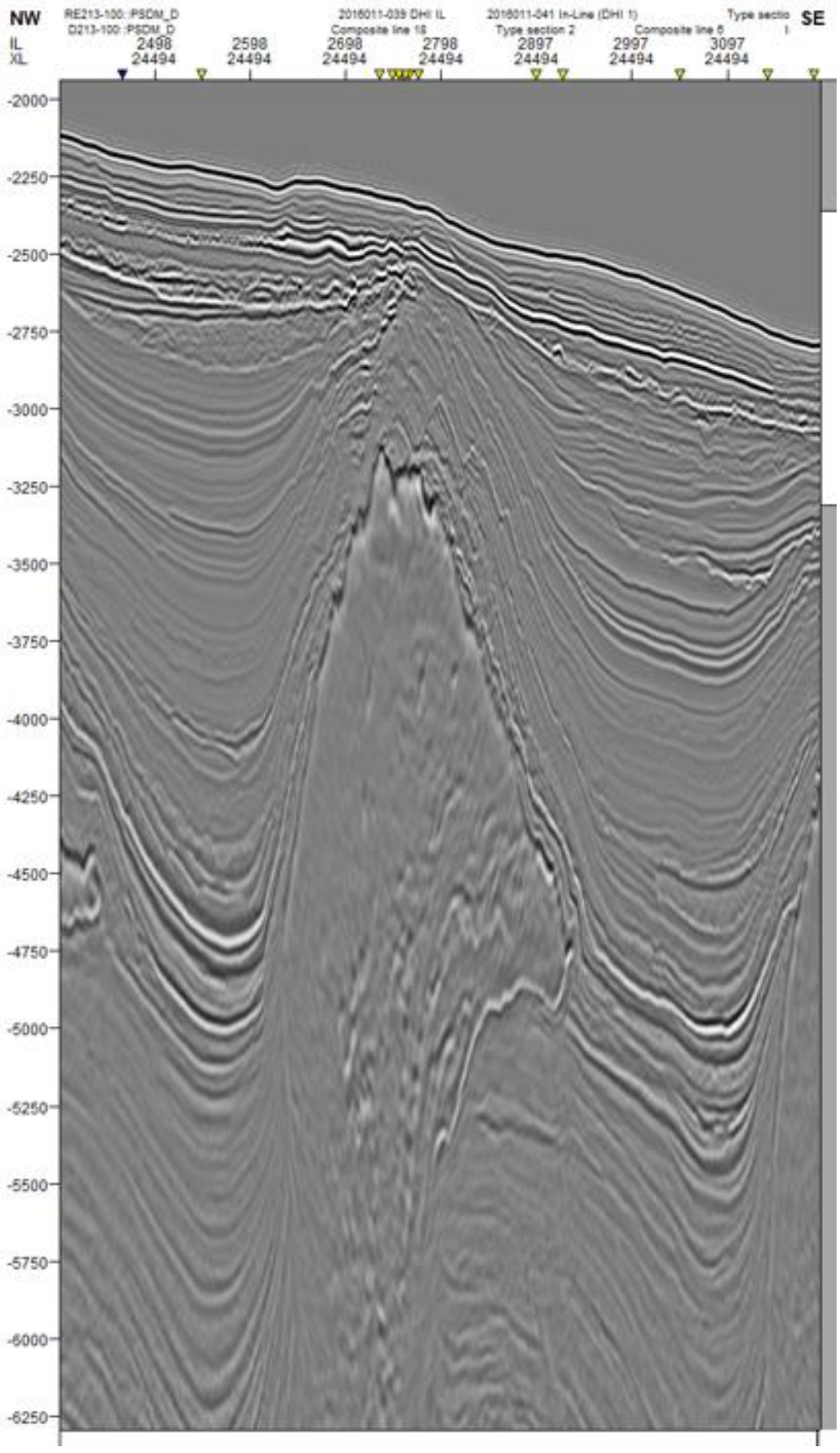

Q-Q' (strike-oriented)

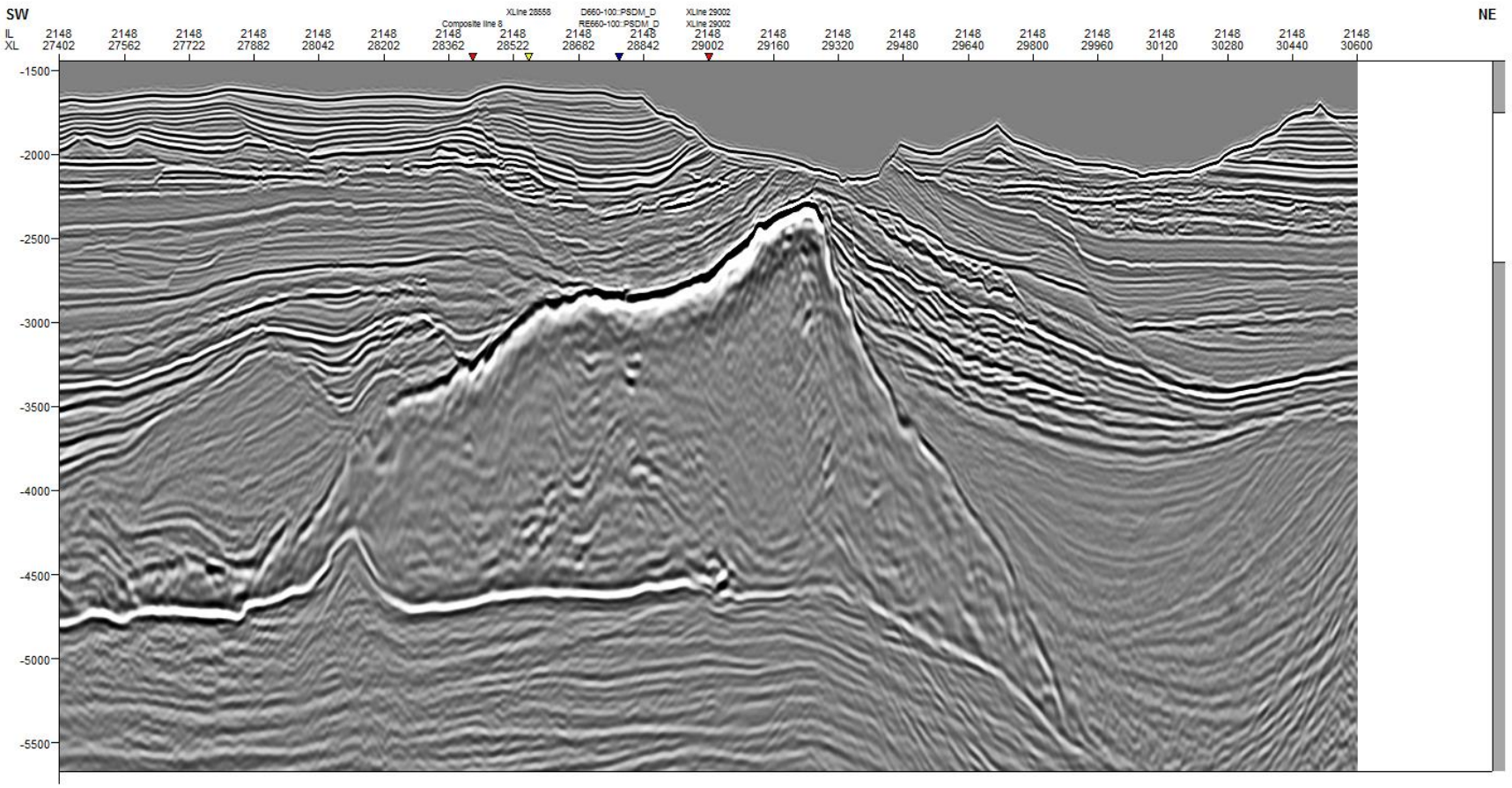

R-R’ (shallow; dip-oriented)

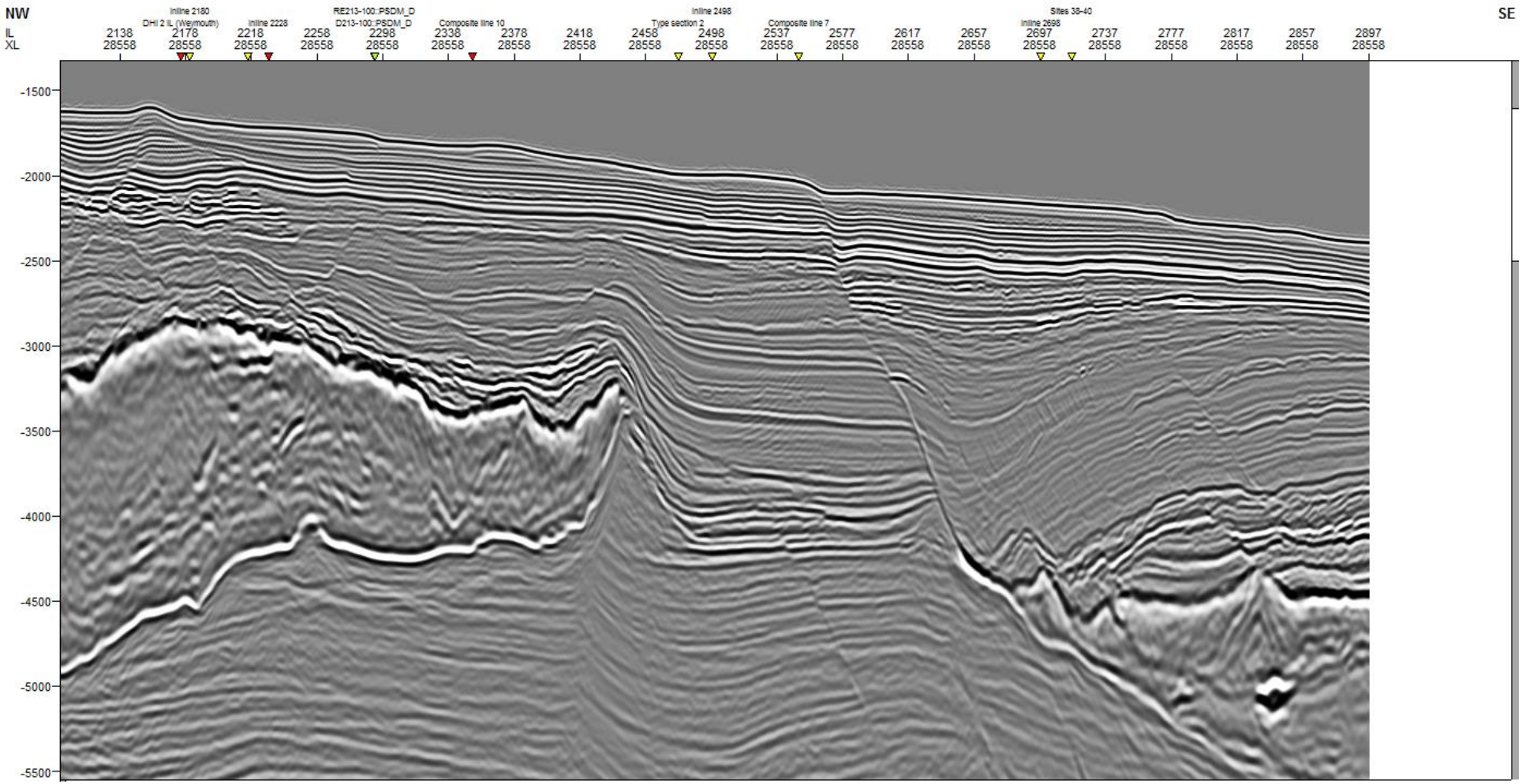

R-R’ (deeper; dip-oriented)

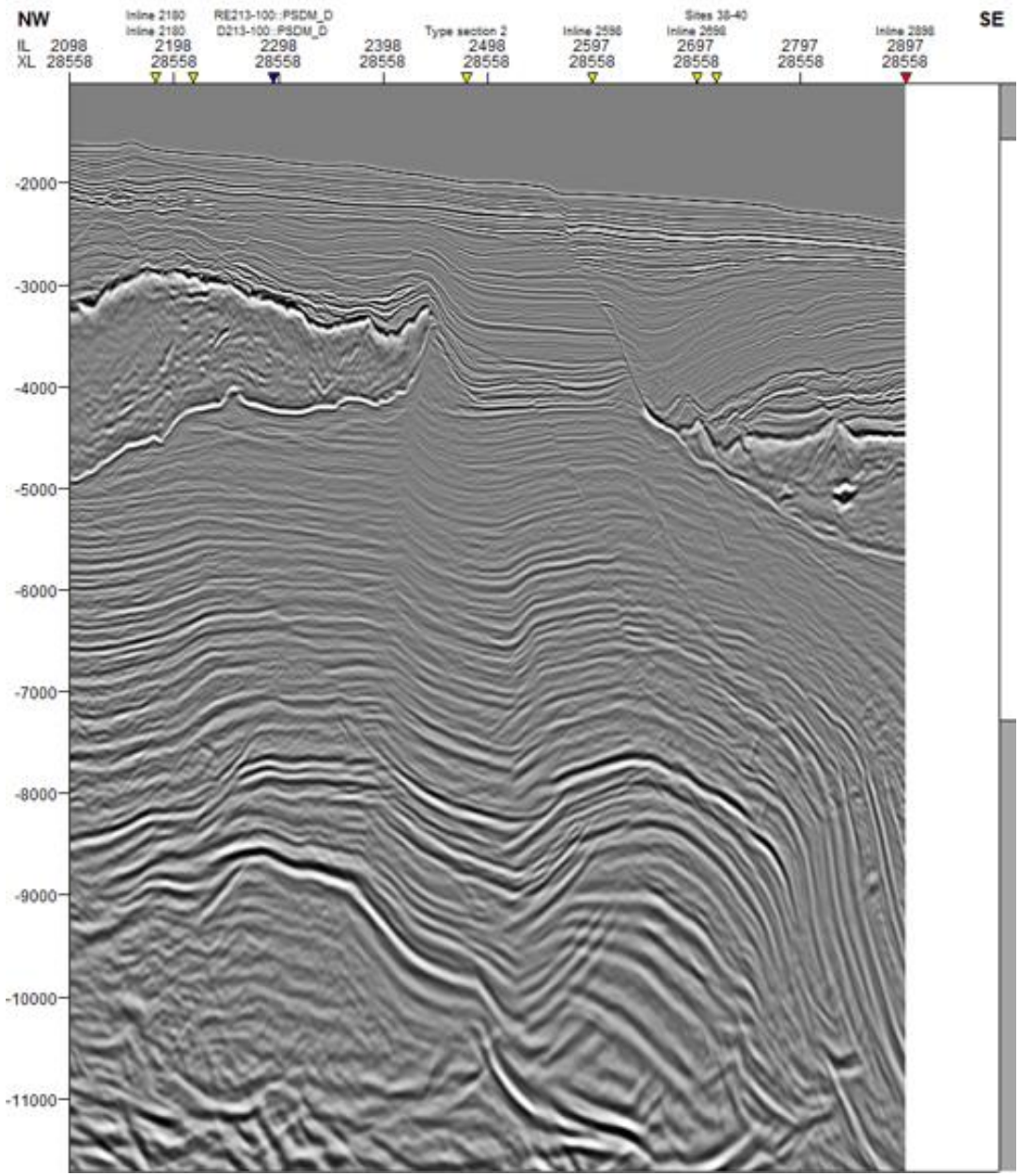

S-S’ (dip-oriented)

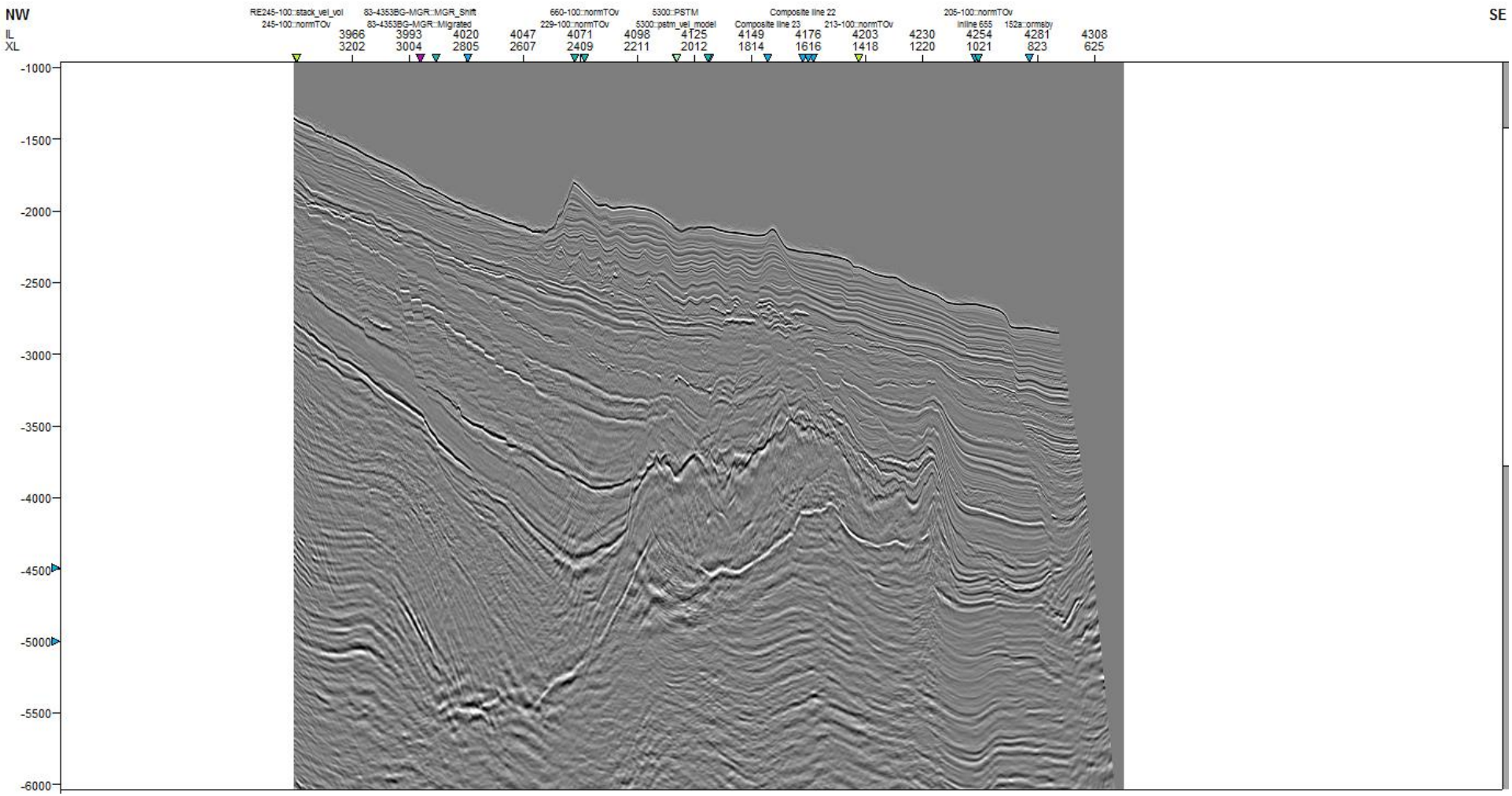

T-T’ (strike-oriented)

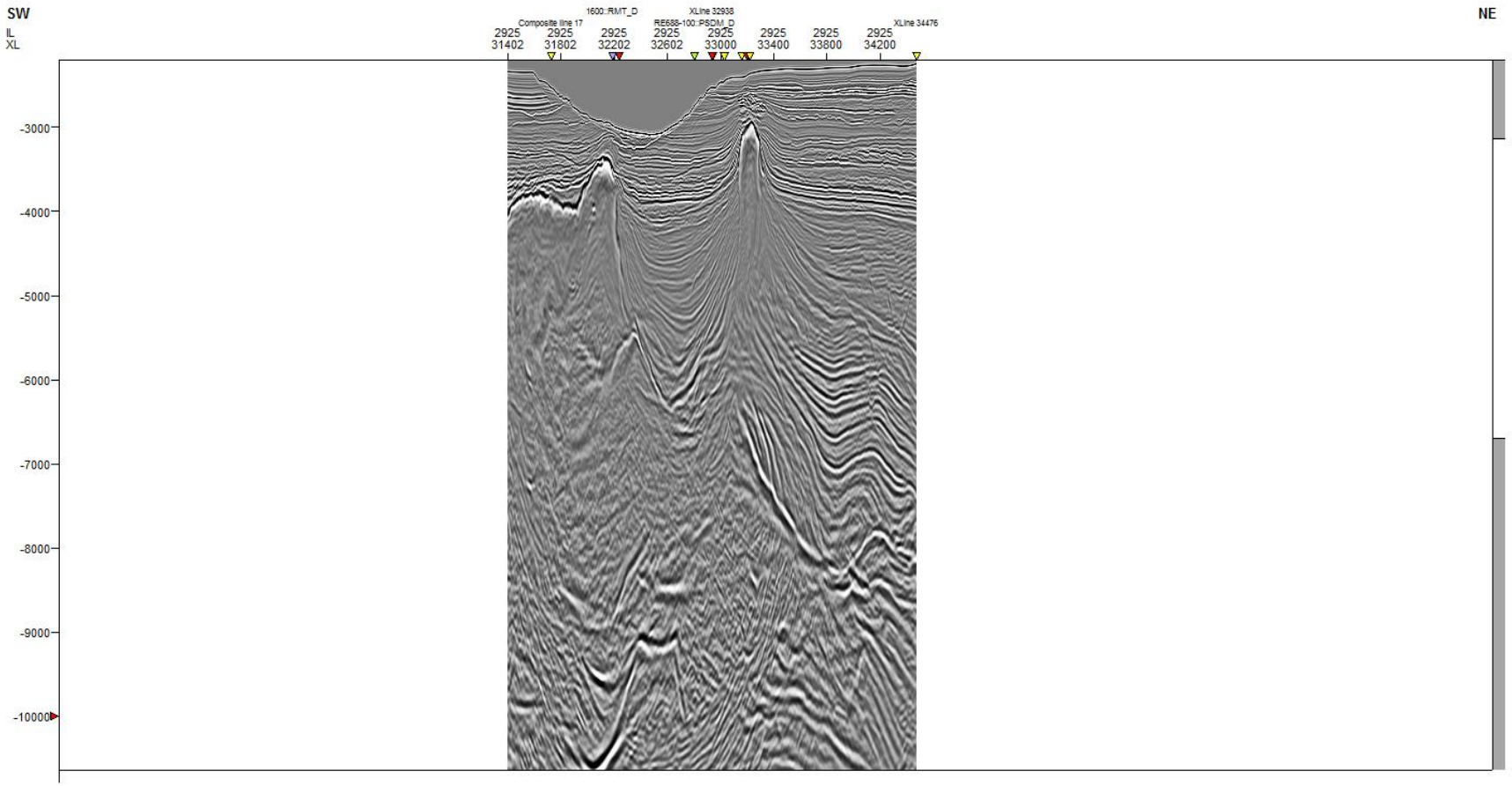

U-U’ (shallow; dip-oriented)

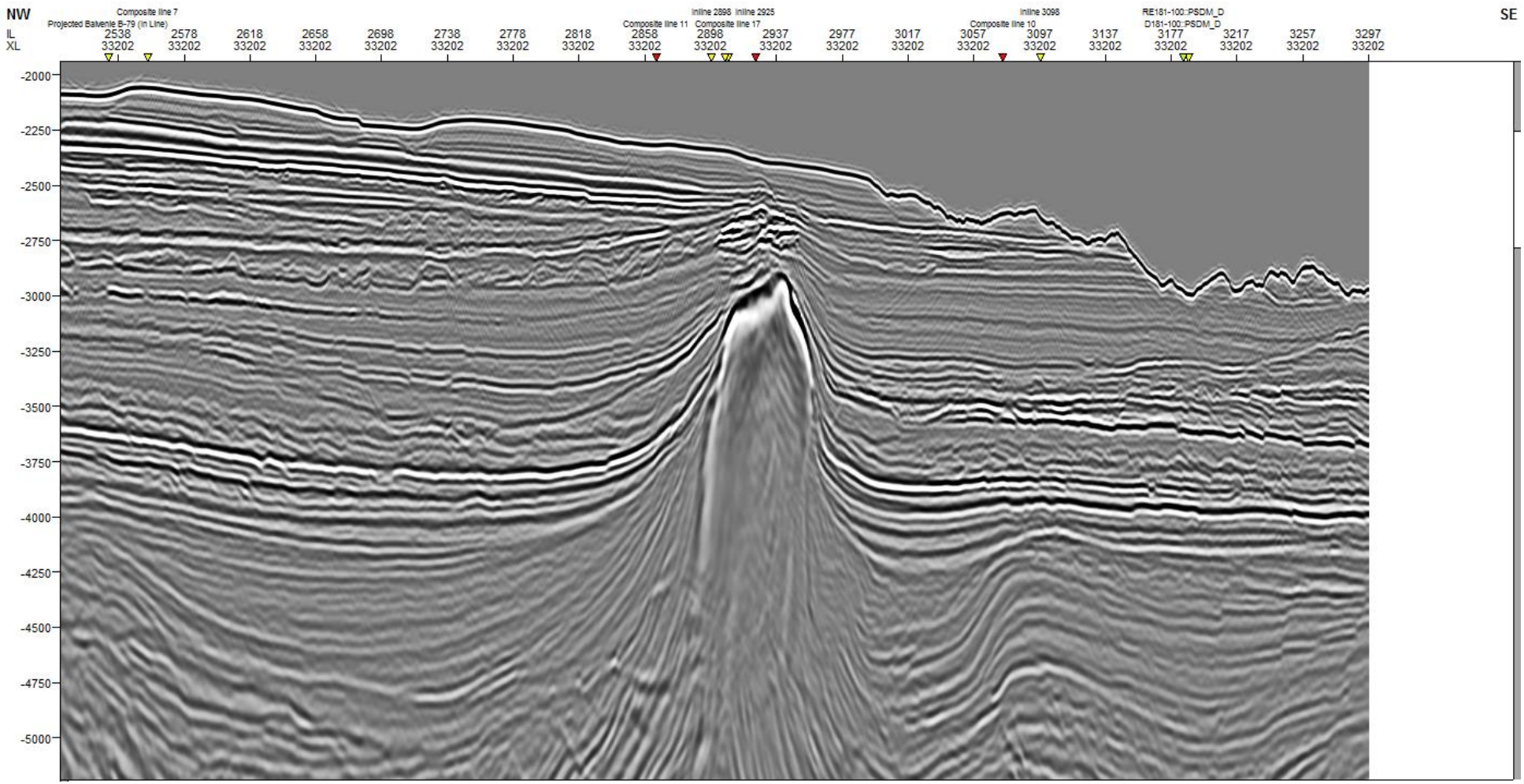

U-U’ (deeper; dip-oriented)